Paternal epigenetic inheritance of small RNA-mediated gene silencing in *Caenorhabditis elegans*

Dissertation

Zur Erlangung des Grades

Doktor der Naturwissenschaften

Am Fachbereich Biologie

Der Johannes Gutenberg-Universität Mainz

Jan Schreier

geboren am 12 Juli 1989 in Bad Saarow

Mainz, 2020

Table of contents

List of abbreviations

aa	amino acid
ALG	Argonaute (plant)-like gene
BACK	BTB and C-terminal Kelch
BFP	blue fluorescent protein
bp	base pair
BTB	broad-complex, tramtrack and bric à brac
BTBD	BTB domain containing
Cas9	CRISPR associated protein 9
CRISPR	clustered regularly interspaced short palindromic repeats
CSR	chromosome-segregation and RNAi deficient
DEPS	defective P granules and sterile
DNA	deoxyribonucleic acid
DPF	dipeptidyl peptidase four family
DPY	dumpy
dsDNA	double-stranded deoxyribonucleic acid
EGO	enhancer of *glp*-one
EMS	ethyl methanesulfonate
ENRI	enhanced nuclear RNAi
ER	endoplasmic reticulum
ERGO	endogenous-RNAi deficient Argonaute
Exon	expressed region
FB-MO	fibrous body-membranous organelle
FRAP	fluorescence recovery after photobleaching
Gb	gigabase
GFP	green fluorescent protein
GMCL	germ cell-less
H3K27	histone H3 lysine 27
H3K36	histone H3 lysine 36
H4K4	histone H3 lysine 4
H3K9	histone H3 lysine 9

hAgo2	human Argonaute RISC catalytic component 2
Him	high incidence of males
HOPS	homotypic fusion and protein sorting
HRDE	heritable RNAi deficient
IDR	intrinsically disordered region
Intron	intragenic/intervening region
IP	immunoprecipitation
IP-MS/MS	immunoprecipitation followed by mass spectrometry
kDa	kilodalton
LDS	lithium dodecyl sulfate
lincRNA	long intergenic non-coding RNA
LINE	long interspersed nuclear element
LTR	long terminal repeat
ncRNA	non-coding RNA
NMY	non-muscle myosin
NRDE	nuclear RNAi defective
nt	nucleotide
MAPK	mitogen-activated protein kinase
Mb	megabase
MEG	maternal effect germ-cell defective
MID	middle domain of Argonaute proteins
miRNA	microRNA
Mis	*Mutator*-induced sterility
mRNA	messenger RNA
Mrt	mortal germline
MosSCI	mos1-mediated single copy insertion
MSP	major sperm protein
MUT	*Mutator*
ORF	open reading frame
PAZ	PIWI/Argonaute/Zwille
PEI	paternal epigenetic inheritance defective
PGC	primordial germ cell
PGL	P Granule abnormality
piRNA	Piwi-interacting RNA

PIWI	P-element-induced whimpy testes
PME	paternal mitochondria elimination
POZ	poxvirus and zinc finger
PRG	Piwi (fruitfly) related gene
RC	rolling-circle
RDE	RNAi defective
RdRP	RNA-dependent RNA polymerase
RFP	red fluorescent protein
RIP	RNA immunoprecipitation
RISC	RNA-induced silencing complex
RNA	ribonucleic acid
RNAe	RNA-induced epigenetic silencing
RNAi	RNA interference
RPM	reads per million
RRF	RNA-dependent RNA polymerase family
rRNA	ribosomal RNA
SEC	self-excising cassette
SDS-PAGE	sodium dodecyl sulfate–polyacrylamide gel electrophoresis
siRNA	short-interfering RNA
SINE	short interspersed nuclear element
snoRNA	small nucleolar RNA
snRNA	small nuclear RNA
SPE	defective spermatogenesis
ssDNA	single-stranded deoxyribonucleic acid
ssODN	single-stranded oligodeoxynucleotide
TE	transposable element
TEI	transgenerational epigenetic inheritance
TIR	terminal inverted repeat
tRNA	transfer RNA
UNC	uncoordinated
UTR	untranslated region
WAGO	worm-specific Argonaute

List of figures

List of tables

Summary

Transgenerational epigenetic inheritance (TEI) describes the transmission of gene-regulatory information across generations without altering DNA sequences. This regulates the expression of transposons and protein-coding genes to preserve fertility and to prepare future generations for altered environmental conditions. Germ cell-resident mechanisms that drive TEI are often associated to RNA interference (RNAi) related pathways. Small non-coding RNAs, most notably short-interfering RNAs (siRNAs) and Piwi-interacting RNAs (piRNAs) are well-described to function in TEI via both nuclear and cytoplasmic pathways, with latter being often organized in phase-separated condensates.

In *C. elegans*, 22G RNAs are endogenous siRNAs with an established role in TEI. They are generated by the *Mutator* complex and associate to members of a highly diversified, worm-specific Argonaute family (WAGO), which mediates both transcriptional and post-transcriptional gene silencing. It has been shown that WAGO-mediated gene silencing can be inherited via both male and female gametes. While the maternal contribution gained much knowledge in recent years, molecular mechanisms ensuring paternal epigenetic inheritance remain largely unknown, with recent studies giving a first insight into histone-based mechanisms. However, the existence of a cytoplasmic pathway in paternal epigenetic inheritance remains enigmatic, especially since sperm maturation is accompanied by a massive reduction of the intracellular content.

In this work, I identify WAGO-3 as a germline-specific Argonaute protein and describe how a defective *Mutator* complex affects WAGO-3 loading and subcellular localization. I provide evidence that WAGO-3 is required for proper germ cell development and transgenerational maintenance of RNAi-driven gene silencing. In particular, I demonstrate that WAGO-3 is crucial for paternal epigenetic inheritance and describe a novel, sperm-specific condensate, the PEI granule, which ensures the paternal inheritance of cytoplasmic WAGO-3. Based on proteomic data, I identify the BTB domain-containing protein PEI-1, which specifically marks PEI granules and I dissect its requirement for PEI granule formation and WAGO-3 segregation during sperm maturation. Moreover, I provide first results indicating that PEI granules display liquid-like properties and retain WAGO-3 via hydrophobic interactions. Finally, my results link the localization of this phase-separated structure to S-palmitoylation and myosin-driven segregation of membranous organelles.

Zusammenfassung

Transgenerationale, epigenetische Vererbung beschreibt die generationsübergreifende Weitergabe von genregulatorischen Informationen, die nicht auf Änderungen der DNA-Sequenz beruhen. Dieser Prozess sorgt für die Aufrechterhaltung der Fruchtbarkeit und die Vorbereitung zukünftiger Generationen auf veränderte Umweltbedingungen, indem es die Genexpression von codierenden Genen und Transposons gezielt reguliert. Die spezifischen Mechanismen der epigenetischen Vererbung finden in den Keimzellen statt und sind oft mit den Signalwegen der RNA Interferenz (RNAi) verknüpft. Kurze, nichtcodierende RNA Moleküle, insbesondere short-interfering RNAs (siRNAs) und Piwi-interacting RNAs (piRNAs), sind an Regulationsmechanismen beteiligt, die sowohl im Zellkern als auch im Zytoplasma stattfinden. Letztere sind häufig in Kondensaten organisiert, welche durch Phasenseparation entstehen.

In *C. elegans* haben 22G RNAs, eine Gruppe der siRNAs, eine etablierte Funktion in transgenerationaler, epigenetischer Vererbung. Sie werden von dem sogenannten *Mutator* Komplex generiert und fungieren als Liganden für Mitglieder der wurmspezifischen Argonautenproteine (WAGO). Zusammen vermittlen sie Gen-Silencing auf transkriptionaler und post-transcriptionaler Ebene. Es ist bekannt, dass dieses WAGO-vermittelte Gen-Silencing sowohl über männliche als auch über weibliche Gameten vererbt werden kann. Während in den letzten Jahren neue Erkenntnisse zum mütterlichen Beitrag gewonnen wurden, bleiben die molekularen Mechanismen des väterlichen Beitrags weitgehend unbekannt. Obwohl neueste Studien einen ersten Einblick in nukleare Vorgänge geben, ist die Existenz eines zytoplasmatischen Signalweges der väterlichen, epigenetischen Vererbung bisher nicht erwiesen und bleibt fragwürdig. Dieser ist insbesondere rätselhaft, da die Bildung von Spermien mit einer massiven Verringerung des intrazellulären Materials einhergeht.

In dieser Arbeit identifiziere ich WAGO-3 als keimbahnspezifisches Argonautenprotein und beschreibe wie ein defekter *Mutator* Komplex die Beladung und die subzelluläre Lokalisation von WAGO-3 beeinflusst. Ich lege Beweise dafür vor, dass WAGO-3 für die ordnungsgemäße Entwicklung von Keimzellen und die generationsübergreifende Aufrechterhaltung des RNAi-gesteuerten Gen-Silencing erforderlich ist. Insbesondere zeige ich, dass WAGO-3 für die väterliche, epigenetische Vererbung von entscheidender Bedeutung ist, und beschreibe ein neues phasensepariertes, spermienspezifisches Kondensat, das PEI Granule, das die väterliche Vererbung von zytoplasmatischem

WAGO-3 sicherstellt. Basierend auf proteomischen Daten identifiziere ich ein bisher uncharakterisiertes Protein, das ich PEI-1 nenne, welches spezifisch PEI Granules kennzeichnet, und zeige dessen Voraussetzung für die Bildung von PEI Granules und die korrekte Segregation von WAGO-3 während der Spermatogenese. Darüber hinaus stelle ich erste Ergebnisse zur Verfügung, die darauf hinweisen, dass PEI Granules Eigenschaften einer Flüssigkeit besitzen und WAGO-3 über hydrophobe Wechselwirkungen aufnehmen. Zudem legen meine Ergebnisse nahe, dass die Lokalisation von PEI Granules von Palmitoylierung und der myosinabhängigen Segregation von membranumschlossenen Organellen abhängig ist.

Introduction

GERM CELLS

All sexually reproducing organisms contain germ cells, which are uniquely capable of a process called meiosis. This specialized cell division generates both male and female gametes: sperm and oocytes. Fusion of these haploid cells enables the development of an entirely new organism, with all its different organs, tissues and cell types, including a new set of germ cells. In order to maintain an unbroken chain, from generation to generation, germ cell fate must be properly specified and protected during development.

Animal research revealed two general modes of germ cell specification with are often referred to as preformation and induction, respectively (Seydoux and Braun, 2006). On the one hand, preformation describes a continuous germline identity, where maternally supplied determinants specify primordial germ cells in embryos. This mode of germ cell specification has been observed in the nematode *Caenorhabditis elegans*, the fruitfly *Drosophila melanogaster*, the frog *Xenopus laevis* and the fish *Danio rerio*. On the other hand, the mammal *Mus musculus* and the cricket *Gryllus bimaculatus* display a discontinuous germline identity, as primordial germ cells are newly induced during embryonic development (Strome and Updike, 2015).

Germ cells transmit epigenetic information

The inheritance of traits from one generation to the next is primarily driven by the transmission of genomic DNA. However, gametes do not only transmit DNA, but also gene-regulatory information that is not encoded in the genome. The transmission of this non-DNA sequence-based information is called epigenetic inheritance (Bošković and Rando, 2018; Perez and Lehner, 2019; Skvortsova et al., 2018), a phenomenon that was first reported more than 60 years ago (Brink, 1956). Without changing DNA sequences, epigenetic inheritance is capable of priming future generations towards changing physiological and environmental conditions (Kishimoto et al., 2018; Klosin et al., 2017; Perez and Lehner, 2019; Rechavi et al., 2014), thereby regulating, for instance, metabolism (Benyshek et al., 2006; Kaspar et al., 2020; King and Skinner, 2020), behavior (Dias and Ressler, 2014; Tyebji et al., 2020) and longevity (Greer et al., 2011, 2016; Rechavi et al., 2014). Moreover, epigenetic inheritance also preserves fertility, as it plays an important role in the maintenance of gene silencing of selfish genetic elements like transposons (Berrens et al., 2017; Goodier, 2016; Molaro and Malik, 2016; Ozata et al., 2019; Perez and Lehner, 2019). Studies on *Caenorhabditis elegans*, *Drosophila*

melanogaster and rodents showed that epigenetic information can be inherited via both male and female gametes (Alcazar et al., 2008; Brennecke et al., 2008; Öst et al., 2014; Perez and Lehner, 2019; Rassoulzadegan et al., 2006; Skvortsova et al., 2018).

Multiple mechanisms of epigenetic inheritance have been identified, with most of them being based on DNA methylation, histone modifications or transfer of small RNA species (Bošković and Rando, 2018; Perez and Lehner, 2019; Skvortsova et al., 2018). One of the best-studied mechanisms is RNA interference (RNAi). Since the discovery that RNAi-mediated gene regulation can be heritable (Grishok et al., 2000), pioneering research on *C. elegans* unveiled many aspects and molecular details that significantly shaped our current understanding of small RNA-mediated epigenetic inheritance (Ozata et al., 2019; Rechavi and Lev, 2017; Skvortsova et al., 2018). In *C. elegans*, RNAi-mediated gene regulation is transmitted to the next generation through the inheritance of distinct small RNA populations and histone modifications. The transmission via the oocyte has been thoroughly studied, and distinct nuclear and cytoplasmic pathways have been identified (Wan et al., 2018; Woodhouse and Ashe, 2020). In contrast, only chromatin-based mechanisms of RNAi inheritance via sperm have been reported so far (Kaneshiro et al., 2019; Tabuchi et al., 2018). Even though a significant amount of sperm-derived, small RNAs are indeed transferred to the embryo (Stoeckius et al., 2014), molecular details and functional aspects remain unknown. Emerging studies on rodents, however, support a model in which paternally inherited small RNA populations have functional impact (Rassoulzadegan et al., 2006; Sharma, 2019). For instance, sperm-derived miRNAs and tRNA fragments play an important role in the transmission of metabolic (Chen et al., 2016; Cropley et al., 2016; Sharma et al., 2016) and pathological phenotypes in mice and rats (Ben Maamar et al., 2018; Schuster et al., 2016; Skinner et al., 2018; Tyebji et al., 2020).

Germline development in *C. elegans*

After fertilization, a series of asymmetric divisions defines the P cell lineage with the P4 cell being generated at the 24-cell stage of embryogenesis. This cell is the sole founder of the germline and symmetrically divides at the 88-cell stage to generate the primordial germ cells Z2 and Z3 (**Figure 1**) (Sulston et al., 1983). Both cells do not divide further during embryogenesis, but resume mitotic activity in the first larval stage.

In contrast to somatic blastomeres, transcription by RNA polymerase II is blocked in P blastomeres, with the primordial germ cells Z2 and Z3 starting to express several

germline genes including *pgl-1* and *glh-1*, which are required for P granule assembly (Marnik and Updike, 2019; Seydoux and Dunn, 1997; Seydoux et al., 1996; Spencer et al., 2011). P granules are phase-separated condensates that are maternally supplied and exclusively inherited within the P cell lineage (**Figure 1**) (Updike and Strome, 2010). Although the asymmetric segregation of P granules during embryogenesis is not sufficient to specify germ cell fate (Gallo et al., 2010), P granules play an important role in germ cell proliferation and the maintenance of germ cell identity (Gallo et al., 2010; Kawasaki et al., 1998, 2004; Knutson et al., 2017; Spike et al., 2008; Updike et al., 2014).

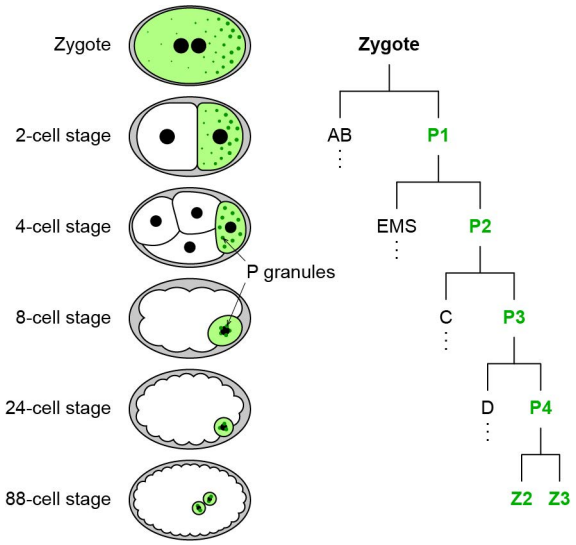

Figure 1 | Schematic representation of early embryogenesis in *C. elegans*. Maternally-provided P granules accumulate at the posterior of the zygote before the first cell division. This event ensures cytoplasmic partitioning of P granules with the P cell lineage. After four asymmetric cell divisons, P granules localize to the nuclear periphery in the P4 cell. This cell is the sole founder of the germline, and symmetrically divides at the 88-cell stage to generate the primordial germ cells Z2 and Z3.

The post-embryonic development of *C. elegans* comprises four larval stages (L1-L4) and adulthood. The two primordial germ cells Z2 and Z3 initiate germline proliferation in the mid-L1 stage. Continued mitoses during the first two larval stages generate an increasing population of germ cells, whose divisions follow a variable pattern. While the primordial germ cells are cellular, the growing germ cell population is organized in a syncytium by the second larval stage. Cells within this syncytium are partially enclosed by a plasma membrane, but divide autonomously. The central canal that connects syncytial germ cells is called rachis. In the transition between L2 and L3 stage, germ cells are displaced from the central region and two gonad arms are formed. During L3 stage, the most proximal germ cells cease proliferation and enter meiotic prophase I. This establishes a

distal-proximal polarization of the developing germline, which extends in the L4 stage and adulthood. Mitotically active germ cells are located at the distal end and are responsible for a four-fold amplification in total germ cell numbers during L4 stage. This mitotic region serves as place for self-renewal and production of naïve germ cells that undergo gametogenesis in the proximal germline (**Figure 2**) (Hall et al., 1999; Hirsh et al., 1976; Kimble and Hirsh, 1979; Kimble and White, 1981).

C. elegans has two natural sexes: hermaphrodite and male (Brenner, 1974; Nigon, 1949). Hermaphrodites are self-fertile females, whose sole male characteristic is the production of a limited amount of sperm during L4 stage. Following a switch to oogenesis in adulthood, the production of oocytes continues through adult life. Brood size is only limited by the number of available sperm. The gonad of adult hermaphrodites is symmetric and consists of two reflexed gonad arms that share a common uterus and vulva. Each gonad arm contains around 1000 germ cells and is connected to the uterus by the spermatheca, a tubular structure where mature sperm is stored and oocytes are fertilized. In contrast, the gonad of an adult male is asymmetric. A single gonad arm produces male gametes, which are stored in the seminal vesicle and remain inactive until ejaculation into the hermaphrodite (**Figure 2**) (Hirsh et al., 1976; Kimble and Hirsh, 1979; Kimble and White, 1981; Klass et al., 1976).

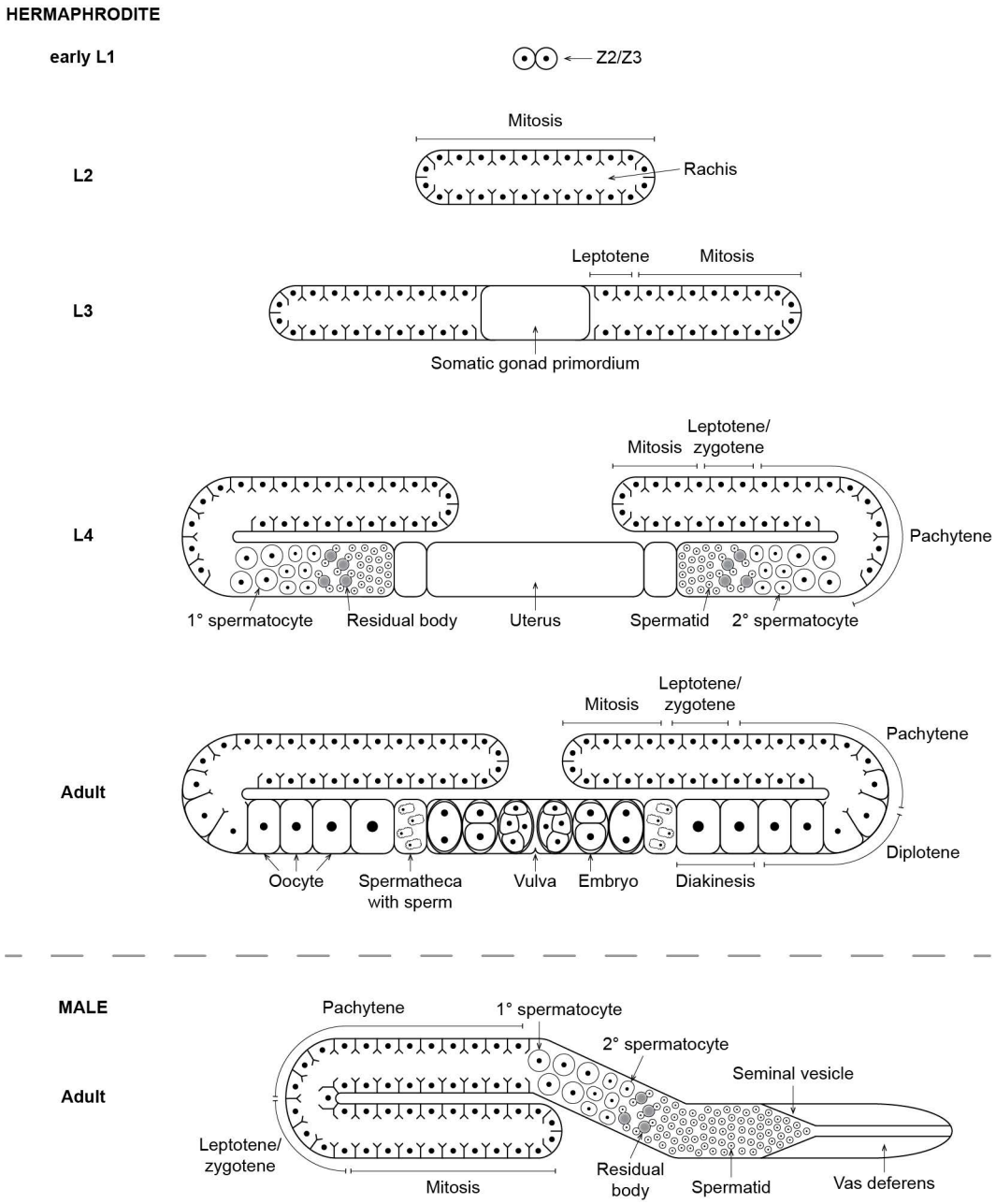

Figure 2 | Schematic representation of germline development in *C. elegans*. Early L1 larvae contain two primordial germ cells that resume mitotic activity in mid-L1 stage. Continued mitotic divisions generate a pool of naïve germ cells that start meiosis I in L3 larvae. The established distal-proximal polarization is extended during L4 stage and adulthood, which are characterized by spermatogenesis and oogenesis, respectively. Hermaphrodites contain a symmetric gonad, which consists of two reflexed gonad arms that are connected by two spermathecae and a shared uterus. The male gonad is asymmetric and comprises only one gonad arm that exclusively produces spermatids.

Spermatogenesis

Spermatogenesis describes the process of male gamete production. Since this work mainly places emphasis on mechanisms during sperm maturation, this process will be introduced a bit more extensively. Spermatogenesis begins in the L4 stage and continues throughout the adult stage in males. In contrast, it is restricted to the L4 stage in the hermaphroditic germline, where the first approximately 40 germ cells that enter meiosis differentiate into about 160 spermatids in each gonad arm (Schedl, 1997). Although the germline anatomy differs between males and hermaphrodites, the production of male gametes is similar at the cellular level (**Figure 3A**). Primary spermatocytes bud off the rachis and undergo the first meiotic division without the requirement for any accessory cell. Notably, the first meiotic division can have two results. Either the primary spermatocyte divides completely, resulting in two individual daughter cells, or cytokinesis is incomplete, leading to two daughter cells that remain connected. In both cases, the generated daughter cells, called secondary spermatocytes, continue with the second meiotic division, resulting in the formation of spermatids. This division is characterized by the concomitant formation of the residual body that forms between the two developing spermatids. The residual body is a so-called cytoplast, which describes an enucleated cell. During meiosis II, many cellular components are asymmetrically segregated into either the budding spermatids or the residual body, dependent on their requirement in mature sperm. In particular, the nucleus, the centriole, mitochondria and Golgi-derived membranous organelles are exclusively sorted in spermatids. In contrast, free ribosomes, the endoplasmic reticulum and the Golgi apparatus itself are removed from spermatids and sorted into the residual body (L'Hernault, 2009; Roberts et al., 1986; Ward et al., 1981; Wolf et al., 1978). Two myosin proteins, NMY-2 and SPE-15, govern these processes during meiosis II. While both motor proteins are required for the asymmetric segregation of the cellular content, they play distinct roles in spermatid formation. By migrating towards the spermatid poles, NMY-2 drives incomplete cytokinesis and promotes residual body expansion. Meanwhile, SPE-15 mediates spermatid budding and is eventually required to complete cytokinesis (Hu et al., 2019; Kelleher et al., 2000). Finally, residual bodies are phagocytosed by gonadal sheath cells and spermatids accumulate at the proximal end of each gonad arm (Huang et al., 2012b).

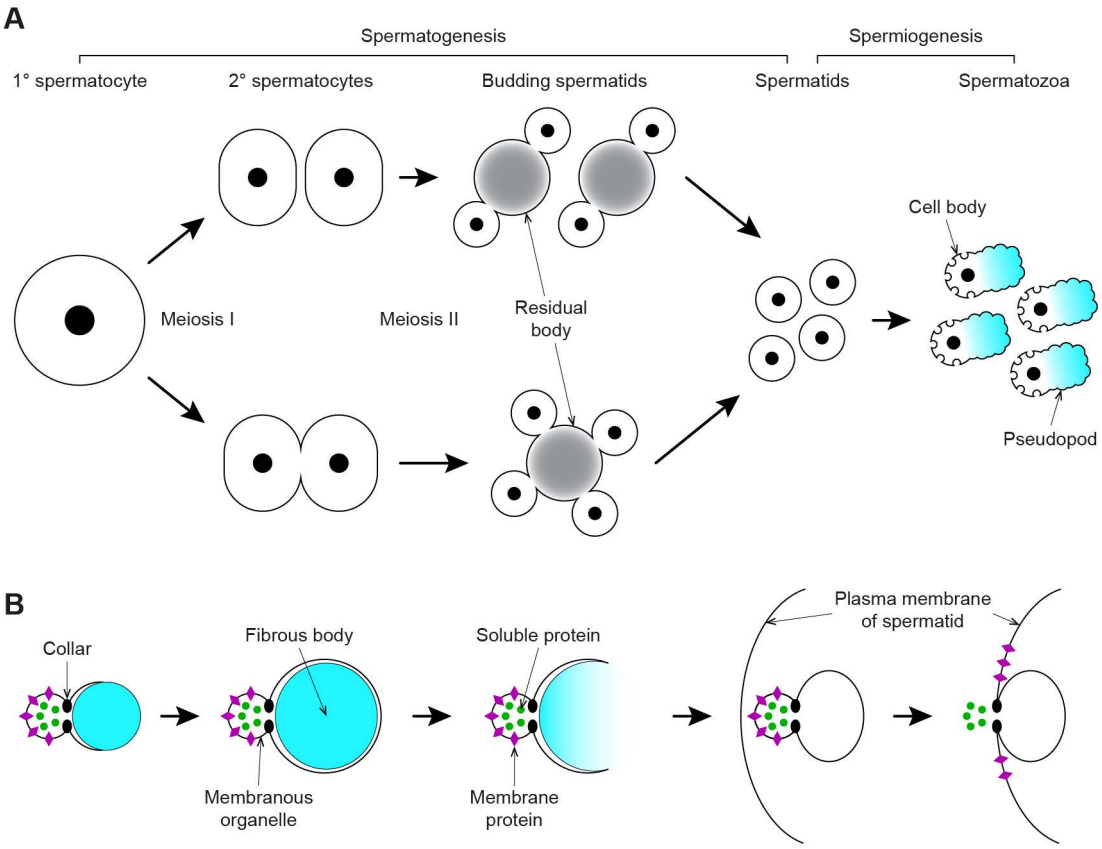

Figure 3 | Schematic representation of spermatogenesis and spermiogenesis in *C. elegans*. A, Approximately 40 pachytene-stage germ cells become primary spermatocytes, which symmetrically devide to produce seconday spermatocytes. Independent on the completion of cytokinesis, secondary spermatocytes undergo meiosis II to generate spermatids. In this process, developing spermatids are connected to a so-called residual body. This enucleated structure receives all cellular material that is not needed in mature sperm. Once the spermatids bud off, the residual body is phagocytized by gonadal sheath cells. After the first ovulation, spermatids undergo rapid activation to motile spermatozoa, which are capable of fertilizing oocytes. B, FB-MO morphogenesis is coordinated with sperm maturation. In primary spermatocytes, the Golgi-derived membranous organelle (MO) associates with a growing fibrous body (FB), which contains polymerized major sperm protein (MSP) fibers. Both structures are connected via a collar region. FM-MOs reach their maximum size in secondary spermatocytes. During meiosis II, FB-MOs are asymmetrically segregated into spermatids, where they release depolymerized MSP monomers and dimers in the cytoplasm. During spermiogenesis, MOs fuse with the plasma membrane, which results in the deposition of transmembrane proteins on the cell surface and the release of soluble proteins in the extracellular space. Finally, MSP polymerizes to fibers in the developing pseudopod.

The process of spermatogenesis is characterized by the formation of a sperm-specific organelle: the fibrous body-membranous organelle (FB-MO) (**Figure 3B**). This structure plays an important role in sperm maturation and activation, as it ensures correct localization of various proteins within the developing gamete. It starts to form in primary spermatocytes, by association of a Golgi-derived membranous organelle with a growing fibrous body. The membranous organelle is a specialized lysosome and its formation

requires SPE-39-mediated interaction with the HOPS complex (Zhu and L'Hernault, 2003; Zhu et al., 2009). The fibrous body contains bundled major sperm protein (MSP) filaments, whose assembly is dependent on the serine/threonine kinase SPE-6 (Varkey et al., 1993). After initial association, a membranous organelle-derived lipid bilayer starts to envelope the fibrous body, with a collar region keeping both structures separated. Several proteins have been identified to stabilize the association between the membranous organelle and the fibrous body. For instance, loss of the transmembrane proteins SPE-4 or SPE-10 results in premature dissociation of the fibrous body and thus defects in sperm maturation (Arduengo et al., 1998; Gleason et al., 2006; L'Hernault and Arduengo, 1992; Shakes and Ward, 1989). After reaching its maximum size in secondary spermatocytes, FB-MOs are asymmetrically segregated into budding spermatids during the second meiotic division. As spermatids bud off the residual body, the surrounding membrane of the fibrous body retracts and depolymerized MSP monomers and dimers disperse throughout the cytoplasm. The remaining membranous organelles adopt a peripheral distribution near the plasma membrane until sperm activation (L'Hernault, 2009; Roberts et al., 1986; Ward and Klass, 1982; Ward et al., 1981; Wolf et al., 1978).

Spermiogenesis

Spermiogenesis describes the differentiation of inactive spermatids into motile spermatozoa, which are capable of fertilizing oocytes. In young adult hermaphrodites, the first ovulations displace spermatids from the proximal gonad into the spermatheca, where they are rapidly activated. In contrast, male-derived spermatids differentiate into spermatozoa in the uterus after ejaculation into the hermaphrodite (Ward and Carrel, 1979). The resulting spermatozoa subsequently migrate into the spermatheca, where male-derived sperm outcompetes the smaller hermaphrodite-derived sperm, thereby ensuring the generation of male-sired offspring (LaMunyon and Ward, 1995, 1998). While the molecular mechanism that triggers spermiogenesis is unknown, morphological rearrangements during sperm activation are well described (**Figure 3, A and B**). First, FB-MO-derived membranous organelles permanently fuse with the plasma membrane (Nelson and Ward, 1980; Wolf et al., 1978). This calcium-dependent process is regulated by multiple proteins including FER-1, SPE-10 and SPE-17 (L'Hernault et al., 1993; Shakes and Ward, 1989; Washington and Ward, 2006). Upon fusion, membranous organelle-provided transmembrane proteins are deposited on the plasma membrane and soluble proteins are released into the spermatheca. Defects in this process are often associated with sterility, as the deposited

proteins are required for fertilization and oocyte maturation, respectively (Chatterjee et al., 2005; Kroft et al., 2005; Miller et al., 2001, 2003; Putiri et al., 2004; Xu and Sternberg, 2003). Second, the sperm extends a single pseudopod, in which MSP polymerizes to a filamentous network that enables cell locomotion in an actin-independent manner (Nelson and Ward, 1980; Roberts, 1983; Roberts and Stewart, 1997; Ward and Klass, 1982). This locomotion is typically used by displaced sperm to crawl back into the spermatheca. Third, laminar membranes separate the pseudopod from the cell body, which contains the highly condensed genome. Interestingly, the genome is not surrounded by a membranous nuclear envelope, but by an electron-dense ribonucleoprotein halo and mitochondria (Ellis and Stanfield, 2014; L'Hernault, 2009; Nelson and Ward, 1980; Ward et al., 1981; Wolf et al., 1978).

Oogenesis

The differentiation of naïve germ cells into oocytes occurs in adult hermaphrodites. During the entire process of oogenesis, the MAPK pathway plays a central role, as it regulates multiple steps including pachytene progression, apoptosis, oocyte growth and meiotic maturation (Arur et al., 2009; Church et al., 1995; Kim et al., 2013; Lee et al., 2007b). Once syncytial germ cells exit pachytene, a significant number of cells undergo apoptosis and possibly function as nurse cells by donating cellular content to maturing oocytes (Gumienny et al., 1999). Oocyte growth is mainly based on actin-dependent cytoplasmic streaming from the rachis. While the exact mechanism remains unknown, oocytes are seemingly the driving force for this process, as gonadal sheaths cells and germ cell apoptosis are dispensable to generate the cytoplasmic flow (Wolke et al., 2007). At later stages, the most proximal oocytes additionally increase in size by yolk uptake (Grant and Hirsh, 1999).

Next to enabling sperm motility, MSP also functions as a hormone that positively regulates final stages of oocyte development. After spermiogenesis, extracellular MSP activates signaling pathways in the gonadal sheath cells that promote oocyte growth (Govindan et al., 2009). This proximal MSP signaling works in opposition to the distal GLP-1 signaling, which promotes germ cell proliferation and inhibits meiotic entry. Thus, both pathways function in concert with each other to regulate oogenesis until mature oocytes complete cellularization and arrest at diakinesis (Govindan et al., 2009; Nadarajan et al., 2009). In addition, proximal MSP signaling is also required for oocyte maturation (Govindan et al., 2009; Huelgas-Morales and Greenstein, 2018; Miller et al., 2001). This process describes the transition from diakinesis to metaphase I, a crucial

step that prepares oocytes for fertilization. MSP-dependent activation of distinct signaling pathways induces both nuclear and cytoplasmic events, including meiotic spindle assembly, chromosome segregation, nuclear envelope breakdown and reorganization of cytoplasmic organelles. In absence of sperm, arrested oocytes become endomitotic and lose their competence for fertilization (Kim et al., 2013).

Genome organization and transposable elements

As mentioned above, gene silencing information that regulates transposon expression is known to be epigenetically inherited (Ozata et al., 2019). In this section, the genome of *C. elegans* and its transposable elements are introduced.

General information on the *C. elegans* genome

The genome of *C. elegans* is organized in five autosomes (I-V) and one sex chromosome (X) (Brenner, 1974; Nigon, 1949; Waterston and Sulston, 1995). Instead of having a single centromere, *C. elegans* chromosomes are holocentric, as they possess multiple kinetochores that are distributed along the entire chromosome length (Albertson and Thomson, 1982, 1993). Each chromosome contains a gene-rich central region, which is flanked by gene-poor regions of high repeat density and high recombination rate (Barnes et al., 1995; Rockman and Kruglyak, 2009). The sex of offspring is determined by the number of sex chromosomes, resulting in either hermaphrodite (XX) or male (X0) development (Brenner, 1974; Nigon, 1949). While oocytes always transmit one sex chromosome, sperm can be devoid of the sex chromosome and thus govern the sexual dimorphism. In nature, males typically occur from rare nondisjunction events with a frequency of up to 0.002 %, although the adaption of laboratory strains led to an increased male frequency (0.1 %) (Anderson et al., 2010; Chasnov and Chow, 2002; Hodgkin, 1983).

The 100 Mb genome comprises 49,189 genes, including 19,999 protein-coding genes, 27,658 genes that are classified as pseudogenes or non-coding RNAs, and 1,532 so far unclassified genes. Due to alternative splicing events, the 19,999 annotated protein-coding genes produce 28,350 different coding sequences, of which the vast majority (95.4 %) has been experimentally confirmed. In addition, 3,684 genes are organized in 1,385 individual operons (genome assembly WBcel235; Wormbase version WS276) (Spieth et al., 1993; The *C. elegans* Sequencing Consortium, 1998; Waterston and Sulston, 1995; Zorio et al., 1994).

Transposable elements

Transposable elements (TEs) are DNA sequences that are capable of moving or multiplying themselves to new positions within the genome. With a few exceptions, all studied genomes contain a highly variable fraction that is transposon-derived: 2.7 % in *Takifugu rubripes* (365 Mb genome), 12 % in *Caenorhabditis elegans* (100 Mb genome), 46 % in *Homo sapiens* (2.9 Gb genome) and 85 % in *Zea mays* (2.3 Gb genome) (Huang et al., 2012a). Their genomic distribution is not random and guided by selective forces. In fact, many TE insertions are found in specific regions that favor their propagation without greatly compromising the host genome function (Sultana et al., 2017). Because transposition events rarely prove beneficial for the host genome, many TE insertions accumulate inactivating mutations over time and consequently lose the ability to transpose (Bourque et al., 2018).

Most identified TEs can be grouped in two major classes based on their transposition intermediate and mechanism. Both of these classes can be divided in subclasses, with each member sharing a common genetic organization and strategy for chromosomal integration. Further classification in superfamilies, families and subfamilies is based on phylogeny with the aim to group closely related TEs that originate from a common ancestral element. Due to the continuous discovery of novel transposons, this classification system is constantly changing (Arkhipova, 2017; Wicker et al., 2007). Given the plethora of transposable elements, this chapter will only cover TEs found in *C. elegans*.

Retrotransposons

Class 1 elements, also called retrotransposons, use a so-called 'copy-and-paste' transposition mechanism and rely on an RNA intermediate (Boeke et al., 1985). Upon transcription, a TE-encoded reverse transcriptase generates a complementary DNA, which integrates elsewhere in the genome. As each transposition event generates a new copy, retrotransposons significantly drive genome expansion and generate repetitive regions. Retrotransposons can be divided into long terminal repeat (LTR) and non-LTR elements, with later including both long and short interspersed nuclear elements (LINEs and SINEs) (Bourque et al., 2018; Wicker et al., 2007).

LTR retrotransposons contain two open reading frames (ORFs), *gag* and *pol*, that are flanked by long terminal repeats, whose length can range from a few hundred to a few thousand basepairs. The *gag* ORF encodes a single capsid protein that can form

intracellular virus-like particles. The *pol* ORF encodes four proteins: a reverse transcriptase, an aspartic proteinase, a DDE integrase and an RNase H enzyme. This genetic organization is closely related to retroviruses, which represent a superfamily of LTR retrotransposons and additionally encode an envelope protein to produce virus particles that can leave the cell (Wicker et al., 2007).

LINEs lack long terminal repeats and typically contain a single ORF encoding an endonuclease and a reverse transcriptase (Luan et al., 1993). Occasionally, they also have a *gag*-like ORF upstream of the *pol* ORF. Their termini are characterized by a tandem repeat or an A-rich sequence (Dewannieux et al., 2003). In contrast to LTR retrotransposons and LINEs, SINEs are non-autonomous TEs that originate from retrotransposition events of various RNA polymerase III transcribed genes. While all SINEs contain an internal RNA polymerase III promoter that drives expression, the remaining sequence is short and highly variable, causing SINEs to be dependent on the enzymatic machinery of LINEs (Kajikawa and Okada, 2002; Kramerov and Vassetzky, 2005; Wicker et al., 2007).

DNA Transposons

Class II elements, also known as DNA transposons, are characterized by a transposition mechanism that lacks an RNA intermediate. More than 80 % of all TEs found in *C. elegans* belong to this transposon class, of which the majority is likely inactive (Feschotte and Pritham, 2007; Laricchia et al., 2017). DNA transposons are divided in two subclasses based on the number of DNA strands that are cut during transposition.

The genetic organization of subclass I DNA transposons comprises terminal inverted repeats (TIRs) of variable length and an open reading frame encoding a transposase. Upon expression, this enzyme recognizes both TIRs, generates double-strand breaks at each end and catalyzes the insertion of the excised DNA in a different genomic location. Although they transpose via a 'cut-and-paste' mechanism, subclass I DNA transposons can increase their copy number within the genome by exploiting the host machinery. For instance, a transposition event during DNA replication can generate a new copy when the TE transposes from a newly replicated site to an unreplicated site (Engels et al., 1990; Feschotte and Pritham, 2007; Greenblatt and Alexander Brink, 1963; Greenblatt and Brink, 1962; Nassif et al., 1994; Ros and Kunze, 2001; Wicker et al., 2007).

Subclass II DNA transposons follow a 'copy-and-paste' strategy without generating double-strand breaks. Their transposition involves the displacement and replication of

a single-stranded DNA sequence that inserts elsewhere in the genome. The only members of subclass II DNA transposons found in *C. elegans* are Helitrons, which replicate via a rolling-circle (RC) mechanism and account for approximately 2 % of the *C. elegans* genome. While all Helitrons contain short, conserved, terminal motifs that are distinct from TIRs, only a subset of Helitrons is autonomous and encodes an Y2-type tyrosine recombinase, which possesses both helicase and replication initiator activity (Feschotte and Pritham, 2007; Kapitonov and Jurka, 2001; Wicker et al., 2007).

Transposons: threat and benefactor

Excessive TE activity most commonly poses a threat to the genome, as transposition events can cause a variety of deleterious effects. Spreading of mobile elements can influence host gene expression at both the transcriptional and post-transcriptional level. For instance, transposition events can disrupt existing exons or cis-regulatory elements, which in turn alters transcript length, alternative splicing, polyadenylation and miRNA binding. Such effects lead to novel allelic variants that can display altered expression patterns, localizations and molecular functions (Daniel et al., 2015; Elbarbary et al., 2016; Feschotte, 2008; Huang et al., 2012a). In addition, TE activity can also promote genomic rearrangements and genome instability. Even when they lost the capability to mobilize, closely related TE copies possess highly homologous regions that can trigger recombination events leading to replication errors, inversions, translocations, duplications or large-scale deletions (Ade et al., 2013; Bennetzen and Wang, 2014; Carvalho and Lupski, 2016; Deininger et al., 2003; Han et al., 2008; Lee et al., 2007a). Finally, more than 120 transposition events have been reported to be associated with genetic diseases and cancer in humans, demonstrating that TE activity is relevant to human health (Hancks and Kazazian, 2016).

However, a growing body of evidence supports the idea that transposition events can also be beneficial for the host genome and seemingly drive genome evolution (Bennetzen and Wang, 2014; Chuong et al., 2017; Deininger et al., 2003; Feschotte, 2008; Feschotte and Pritham, 2007; McClintock, 1951, 1956). Spreading of mobile elements and the sequence variations triggered by TE activity can contribute to a genetic diversity that evolves genome architecture and generates genetic innovations. Especially under stress conditions, TE activity might prove beneficial for adaptive evolution (Horváth et al., 2017; Lanciano and Mirouze, 2018). While mutagen-induced or TE-mediated deletions remove genomic DNA, transposition events promote genome expansion over time. These processes significantly drive the evolution of genome size and composition (Gregory and

Johnston, 2008; Kapusta et al., 2017; Pellicer et al., 2014; Thybert et al., 2018). Furthermore, TEs are a source of both protein-coding and non-coding material that has the potential to generate genetic novelties (Joly-Lopez and Bureau, 2018; Naville et al., 2016). Indeed, a number of protein-coding genes, non-coding RNAs, and cis-regulatory elements are TE-derived (Chuong et al., 2017; Feschotte, 2008; Jangam et al., 2017; McCue and Slotkin, 2012; Piriyapongsa et al., 2007). For instance, RAG1 and RAG2 proteins are subunits of the V(D)J recombinase in jawed vertebrates. Both proteins are encoded by genes that are derived from an ancestral DNA transposon (Huang et al., 2016; Kapitonov and Koonin, 2015). Similarly, TE insertions within long non-coding RNAs and untranslated regions of mRNAs can affect transcript stability, localization, processing and translation efficiency (Gong and Maquat, 2011; Hu et al., 2015; Shen et al., 2011).

TE activity is a major drive for adaptive genome evolution, while simultaneously posing a threat to genome stability and function. Thus, regulatory mechanisms have been evolving to regulate TE expression in a way that transposition events occur at low rate without creating a fitness disadvantage for the host genome. Multiple host-derived and self-regulatory mechanisms have been identified to control this balance. First, transposase enzymes are seemingly inefficient and their low enzymatic activities directly restrict transposition rates (Bourque et al., 2018). This becomes apparent from genetic screens that yielded highly hyperactive transposases that showed an up to 100-fold increase in efficiency (Lampe et al., 1999; Mátés et al., 2009). Second, some TEs control their own propagation by expressing truncated or mutated proteins that reduce TE activity (Lohe and Hartl, 1996; Saha et al., 2015). Third, the host machinery has evolved a variety of mechanisms to control TE expression on both the transcriptional and the post-transcriptional level. Next to transcription factors of the KRAB zinc-finger family (Imbeault et al., 2017; Yang et al., 2017), DNA methylation, histone modifications and RNAi represent potent defense strategies against vigorous TE activity in germ cells and embryonic stem cells (Berrens et al., 2017; Goodier, 2016; Molaro and Malik, 2016; Ozata et al., 2019).

RNA interference

RNA interference is a conserved mechanism that regulates eukaryotic gene expression (Ghildiyal and Zamore, 2009; Ketting, 2011). It is based on a ribonucleoprotein complex called RNAi-induced silencing complex (RISC). Among other proteins, the RISC comprises a specific RNA-binding protein, the Argonaute protein, which binds to a small regulatory RNA molecule. While the small RNA guides target transcript recognition via base-pairing interactions, the Argonaute protein mediates distinct downstream processes that regulate gene expression. Depending on the Argonaute protein, RISCs can inhibit translation and trigger transcript degradation via cleavage, deadenylation or decapping (Höck and Meister, 2008; Hutvagner and Simard, 2008). Besides cytoplasmic functions, some RISCs are reported to translocate into the nucleus, where they can trigger the deposition of repressive chromatin marks, inhibition of RNA polymerase elongation and DNA methylation (Buckley et al., 2012; Castel and Martienssen, 2013; Guang et al., 2008, 2010; Mao et al., 2015; Meister, 2013). Since its discovery, a number of RNAi-related pathways have been identified and their classification is largely based on the small regulatory RNA that is incorporated in the RISC. Based on their biogenesis and association with distinct Argonaute clades, small regulatory RNAs are most commonly divided in three classes: microRNAs (miRNAs), short-interfering RNAs (siRNAs) and Piwi-interacting RNAs (piRNAs) (Ghildiyal and Zamore, 2009; Hutvagner and Simard, 2008; Peters and Meister, 2007).

Next to composition, the subcellular localization of RISCs significantly contributes to their individual function. The first compartments that were described to contain RISCs are processing bodies and stress granules. Both condensates represent major compartments for RISCs in somatic cells and are implicated in RNA turnover and translational regulation (Anderson and Kedersha, 2009; Balagopal and Parker, 2009). However, recent findings challenged this view, as RISC was identified to also localize to epithelial adherens junctions (Kourtidis and Anastasiadis, 2018; Kourtidis et al., 2015, 2017). Moreover, the increasing knowledge about phase separation revealed a more complex level of RISC regulation and novel membrane-less organelles continue to be discovered, especially in germ cells (Ketting, 2011; Phillips et al., 2012; Updike and Strome, 2010; Voronina et al., 2011; Wan et al., 2018). Their identification provides a new insight into the spatiotemporal organization of RNAi-related pathways that control gene expression during gamete development. Notably, phase separation does not only drive the assembly of subcellular compartments for RISCs to function, but also affects

RISC assembly and facilitates gene regulatory mechanisms (Sheu-Gruttadauria and MacRae, 2018).

Argonaute proteins: key players in RNA interference

Argonaute proteins play the most central role in RNAi-related pathways, as they define RISC composition and function. Except of *Saccharomyces cerevisiae*, which has lost its RNAi machinery, Argonaute proteins are found in all eukaryotic genomes that have been studied so far. Most of them encode multiple Argonaute proteins and their number ranges from one in *Schizosaccharomyces pombe* to 20 in *C. elegans* (Höck and Meister, 2008). In addition, Argonaute proteins have also been identified in several prokaryotes. Although their structure is highly similar to eukaryotic Argonaute proteins, their function is seemingly restricted to host defense against mobile genetic elements, similarly to CRISPR (Kuzmenko et al., 2020; Makarova et al., 2009; Olovnikov et al., 2013; Sasaki and Tomari, 2012; Swarts et al., 2014b, 2014a).

Argonaute protein classification

Eukaryotic Argonaute proteins can be divided in three clades. First, the AGO clade groups proteins that are most homologous to *Arabidopsis thaliana* AGO1. Members of this clade are often ubiquitously expressed and associate with either miRNAs or siRNAs. Second, the PIWI clade comprises Argonaute proteins that are similar to *Drosophila melanogaster* Piwi. These proteins are mainly expressed in germ cells and associate with piRNAs in order to function in RNA surveillance and transposon silencing. Third, the worm-specific Argonaute (WAGO) clade comprises a highly diversified set of Argonaute proteins that is unique to nematodes and bind a specific subspecies of endogenous siRNAs (Hutvagner and Simard, 2008; Meister, 2013; Swarts et al., 2014a).

Argonaute protein architecture

Independent on the clade, all eukaryotic Argonaute proteins share a conserved domain composition that consists of two lobes. The first lobe comprises the Argonaute N domain and PAZ domain, whereas the MID domain and PIWI domain form the second lobe. Both lobes are connected via a hinge region that creates a binding channel for the interacting small RNA molecule (Hutvagner and Simard, 2008; Meister, 2013; Sheu-Gruttadauria and MacRae, 2017; Swarts et al., 2014a). While not directly involved in small RNA

binding, the Argonaute N domain plays an important role in RISC assembly, as it assists the unwinding of RNA duplexes (Kwak and Tomari, 2012). Moreover, it is also involved in target RNA cleavage and dissociation (Faehnle et al., 2013; Hauptmann et al., 2013). The PAZ domain contains a specific pocket that is responsible for binding the 3' end of the associated small RNA in a sequence-independent manner (Lingel et al., 2004; Ma et al., 2004). Notably, members of the PIWI clade have evolved a PAZ domain that specifically binds methylated 3' ends (Simon et al., 2011). Similarly, the MID domain is required for interaction with the 5' end of the bound small RNA. The basic pocket of the MID domain contains two binding sites that recognize the 5' phosphate and the first nucleobase, respectively. Many Argonaute proteins indeed show a higher affinity for a specific nucleobase or 5' phosphate group, which can be either a mono- or triphosphate (Boland et al., 2010; Frank et al., 2010, 2012; Ketting, 2011; Nakanishi, 2016). Thus, the MID domain significantly contributes to the preferential binding of Argonaute proteins to distinct small RNA classes. The PIWI domain adopts an RNaseH-like fold. While most Argonaute proteins do not show endonucleolytic activity, some still contain the catalytic DED(D/H) tetrad that enables cleavage when the target transcript is extensively base-paired to the bound small RNA (Jinek and Doudna, 2009; Nakanishi et al., 2012; Parker, 2010; Parker et al., 2004; Song et al., 2004).

RNAi-related pathways in *C. elegans*

From the seminal discovery of RNAi to the first mechanistic insight into RNAi inheritance, *C. elegans* research has been greatly contributing to our current understanding of both molecular mechanisms and cellular organization of RNAi-related pathways (Alcazar et al., 2008; Fire et al., 1998; Grishok et al., 2000; Ozata et al., 2019; Wan et al., 2018; Weiser and Kim, 2019). In fact, the RNAi machinery of *C. elegans* is highly diversified. It comprises up to 20 Argonaute proteins and a variety of small RNA classes (**Table 1 and Figure 4**). Except the miRNA pathway, small RNA pathways in *C. elegans* function sequentially to regulate gene expression. RDE-1, PRG-1, ALG-3, ALG-4 and ERGO-1 are so-called primary Argonaute proteins of various small RNA pathways that are responsible for target transcript recognition. Upon binding, they trigger the activity of RNA-dependent RNA polymerases (RdRPs) in order to amplify the initial response (Sijen et al., 2001). Using the target transcript as template, RdRPs produce a specific subclass of endogenous siRNAs, called 22G RNAs (Sijen et al., 2007). These small regulatory RNAs have an average size of 22 nucleotides and a strong preference for a triphosphorylated guanine as their most 5' nucleobase. 22G RNAs specifically associate

with members of the WAGO clade, which function as secondary Argonaute proteins and ultimately mediate transcriptional and post-transcriptional gene silencing. Strikingly, WAGO-mediated gene silencing can be transgenerationally inherited via both nuclear and cytoplasmic pathways (**Figure 5**) (Ketting, 2011; Ozata et al., 2019; Xu et al., 2018a).

Table 1 | Argonaute proteins of *C. elegans*. Members of each Argonaute clade are listed with their respective gene status, tissue expression, subcellular localization and interacting small non-coding RNA.

Argonaute protein	Gene status	Tissue expression	Subcellular localization	Small RNA	5' end	1st nt bias	3' end
ALG-1	pc	ubiquitous	cytoplasm; P body	miRNA	mono-P	-	hydroxyl
ALG-2	pc	ubiquitous	cytoplasm; P body?	miRNA	mono-P	-	hydroxyl
ALG-5	pc	germline	P granules	miRNA	mono-P	-	hydroxyl
RDE-1	pc	ubiquitous	cytoplasm	exo-siRNA	mono-P	-	O-methyl
PRG-1	pc	germline	P granule	piRNA	mono-P	U	O-methyl
PRG-2	pseudo						
ALG-3	pc	spermatocytes	P granule	26G RNA	mono-P	G	hydroxyl
ALG-4	pc	spermatocytes	P granule	26G RNA	mono-P	G	hydroxyl
ERGO-1	pc	germline / soma	P granule?	26G RNA	mono-P	G	O-methyl
WAGO-1	pc	germline	P granule	22G RNA	tri-P	G	hydroxyl
WAGO-2	pseudo						
WAGO-3 (PPW-2)	pc	germline?	?	22G RNA	tri-P	G	hydroxyl
WAGO-4	pc	germline	P granule, Z granule	22G RNA	tri-P	G	hydroxyl
WAGO-5	pc	?	?	22G RNA	tri-P	G	hydroxyl
WAGO-6 (SAGO-2)	pc	soma?	?	22G RNA	tri-P	G	hydroxyl
WAGO-7 (PPW-1)	pc	germline?	?	22G RNA	tri-P	G	hydroxyl
WAGO-8 (SAGO-1)	pc	soma?	?	22G RNA	tri-P	G	hydroxyl
WAGO-9 (HRDE-1)	pc	germline	nucleus	22G RNA	tri-P	G	hydroxyl
WAGO-10	pc	?	?	22G RNA	tri-P	G	hydroxyl
WAGO-11	pseudo						
WAGO-12 (NRDE-3)	pc	soma	nucleus	22G RNA	tri-P	G	hydroxyl
CSR-1	pc	germline	P granule	22G RNA	tri-P	G	hydroxyl
C04F12.1	pc	?	?	?			
C14B1.7	pseudo						
H10D12.2	pseudo						
C06A1.4	pseudo						

pc – protein-coding, pseudo – pseudogene, P – phosphate, U – uracil, G – guanine

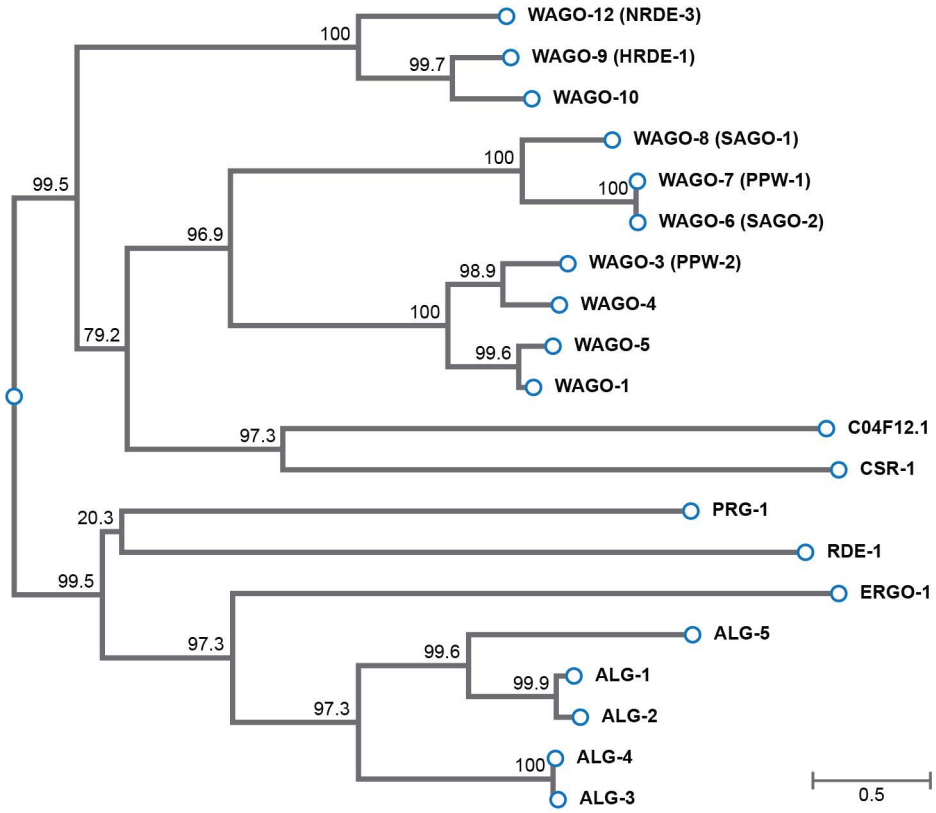

Figure 4 | Phylogenetic tree of the 20 Argonaute proteins of *C. elegans*. Alignment and phylogenetic reconstructions were performed using the function "build" of ETE 3 v3.1.1 as implemented on the GenomeNet (Huerta-Cepas et al., 2016a). The tree was constructed using FastTree with slow NNI and MLACC=3 (Price et al., 2009).

The RDE-1 pathway

RDE-1 plays a crucial role in the RNAi response to exogenous double-stranded RNA, which, for instance, can originate from natural Orsay virus infections (**Figure 5**) (Félix and Wang, 2019; Félix et al., 2011; Tabara et al., 1999). Exogenous RNAs are processed by the double-stranded RNA-binding protein RDE-4 and the ribonuclease-III-related enzyme DCR-1 into 23 nucleotide long siRNA duplexes (Duchaine et al., 2006; Ketting, 2001; Parker et al., 2006; Tabara et al., 2002). Upon binding RDE-1, the catalytically active PIWI domain removes the passenger-strand and the 3′ end of the remaining guide-strand is 2′ O-methylated by HENN-1 (Steiner et al., 2009; Svendsen et al., 2019). Instead of cleaving target RNAs, RDE-1 triggers 22G RNA biogenesis by recruiting RDE-8 (Tsai et al., 2015). This endonuclease catalyzes target RNA cleavage. The generated RNA fragments, however, are not fully degraded but serve as template for 22G RNA biogenesis, which is promoted by RDE-10, RDE-11, RDE-12 and the RdRP RRF-1 (Shirayama et al., 2014; Yang et al., 2012, 2014; Zhang et al., 2012).

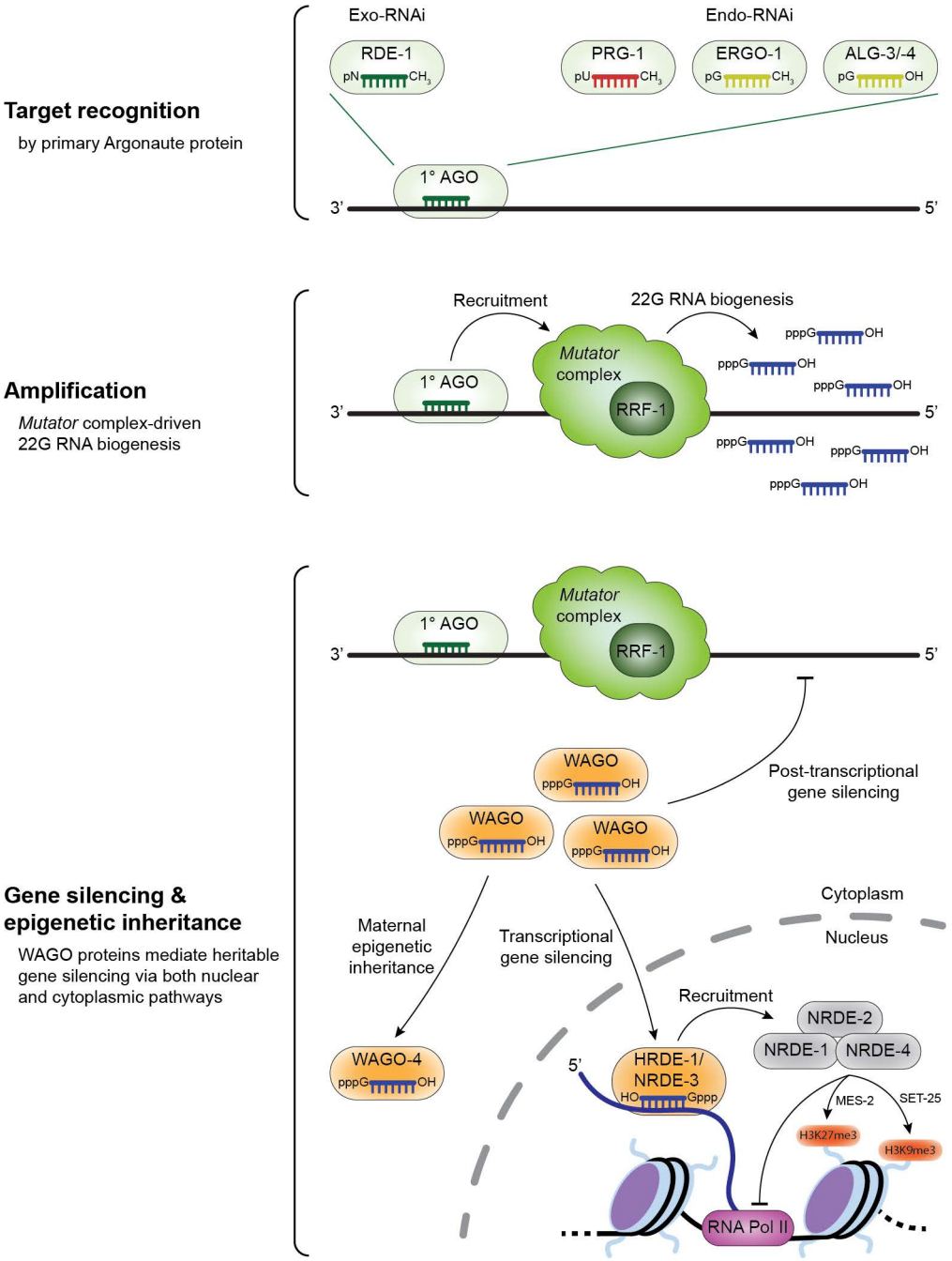

Figure 5 | Small RNA pathways of *C. elegans* function sequentially to regulate gene expression. Exogenous and endogenous target transcripts are identified by primary Argonaute proteins. Upon recognition, they recruit the *Mutator* complex, which contains the RNA-dependent RNA polymerase (RdRP) RRF-1. Using the target transcript as template, the *Mutator* complex produces secondary endo-siRNAs, called 22G RNAs. These small non-coding RNAs serve as cofactors for secondary Argonaute proteins of the WAGOs clade. Upon association with target-derived 22G RNAs, WAGO proteins both localize to the nucleus or cytoplasm and mediate heritable gene silencing through multiple RNAi-related pathways. In the nucleus, HRDE-1 (germline) or NRDE-3 (soma) binds to the nascent target transcript and recruits the NRDE complex, which triggers deposition of repressive chromatin marks and inhibition of RNA polymerase II elongation. In the cytoplasm, other members of the WAGO clade mediate post-transcriptional gene silencing. WAGO-4 is specifically expressed in the germline and required for maternal inheritance of 22G RNA-mediated gene silencing information.

The ALG-3/-4 and ERGO-1 pathway

Next to exogenous siRNAs, *C. elegans* also produces certain subclasses of endogenous siRNAs, and one of them is called 26G RNAs. They have a characteristic length of 26 nucleotides and a 5' bias for a monophosphorylated guanine (Ruby et al., 2006). A recent study shed light on the assembly of the ERI complex, which is responsible for 26G RNA biogenesis. The zinc-finger protein GTSF-1 forms a premature complex with the TUDOR domain-containing protein ERI-5 and the RdRP RRF-3. This pre-ERI complex regulates the assembly of the ERI complex by controlling the incorporation of RRF-3 (Almeida et al., 2018). While principles of recognition remain unknown, target transcripts serve as template for RRF-3, which functions together with DCR-1 to produce 26G RNAs (Duchaine et al., 2006; Gent et al., 2010; Han et al., 2009; Pavelec et al., 2009; Thivierge et al., 2012; Vasale et al., 2010; Welker et al., 2011). Interestingly, two distinct 26G RNA subpopulations can be distinguished, as 26G RNAs can either be loaded into ALG-3/-4 or ERGO-1 (**Table 1**) (Han et al., 2009). Mechanistic details of both pathways, however, are poorly understood.

ALG-3 and ALG-4 are functionally redundant, primary Argonaute proteins that are specifically expressed during spermatogenesis, but absent in mature sperm. They are required for proper sperm maturation and activation, as they positively regulate the expression of many spermatogenesis-specific genes, including *msp* paralogs. It is proposed that ALG-3/-4 act with CSR-1 to promote the expression of these genes, but mechanistic details are clearly lacking. In contrast, a subset of ALG-3/-4 target genes is negatively regulated and initial experiments pointed to an involvement of the WAGO pathway (Conine et al., 2010, 2013; Han et al., 2009).

ERGO-1 shows a mutually exclusive expression pattern compared to ALG-3/-4: it is expressed in the oogenic germline, embryos and somatic tissues (Gent et al., 2010; Han et al., 2009; Vasale et al., 2010). In addition, ERGO-1 associated 26G RNAs are stabilized by HENN-1, which catalyzes the 2' O-methylation of their 3' end (Billi et al., 2012; Kamminga et al., 2012; Montgomery et al., 2012). ERGO-1 regulates gene expression of pseudogenes, long non-coding RNAs, recently duplicates genes and repetitive intergenic loci by triggering 22G RNA biogenesis (**Figure 5**) (Fischer et al., 2011; Gent et al., 2010; Newman et al., 2018; Vasale et al., 2010; Zhang et al., 2011; Zhou et al., 2014). One WAGO protein that could be linked to ERGO-1 activity is the somatically-expressed, nuclear Argonaute proteins NRDE-3 (Gent et al., 2010; Zhou et al., 2014).

The PRG-1 pathway

The genome of *C. elegans* encodes two Argonaute proteins that are attributed to the Piwi clade: PRG-1 and PRG-2. Since *prg-2* is classified as pseudogene, PRG-1 is likely the only functional member of the PIWI clade. It is specifically expressed in the germline and binds 21U RNAs, which are classified as piRNAs of *C. elegans* (Batista et al., 2008; Das et al., 2008; Wang and Reinke, 2008). In contrast to exo-siRNAs and 26G RNAs, 21U RNAs are individually transcribed from more than 15,000 monocistronic loci. Almost all of these loci are clustered on chromosome IV in two genomic regions of 2.5 Mb and 3.7 Mb, respectively (Batista et al., 2008; Ruby et al., 2006). Their transcription is regulated by a dedicated machinery, which may has evolved from molecular mechanisms that govern small nuclear RNA biogenesis (Beltran et al., 2019). Each 21U RNA producing locus contains a preceding consensus motif, also known as Ruby motif (Billi et al., 2013; Ruby et al., 2006). This sequence specifies 21U RNA expression by presenting the binding site for the so-called upstream sequence transcription complex (USTC). This multi-protein complex comprises PRDE-1, SNPC-4, TOFU-4 and TOFU-5. Collectively, they recruit RNA polymerase II, whose pausing determines the characteristic 21U RNA precursor length of 28 nucleotides (Beltran et al., 2019; Gu et al., 2012b; Kasper et al., 2014; Weick et al., 2014; Weng et al., 2019). The downstream processing of precursors into mature 21U RNAs is governed by the PETISCO complex and likely involves additional thus far uncharacterized TOFU proteins (de Albuquerque et al., 2014; Cordeiro Rodrigues et al., 2019; Goh et al., 2014). Following removal of the first two nucleotides, 21U RNA intermediates are trimmed by the 3'-5' exonuclease PARN-1 and loaded into PRG-1 (Tang et al., 2016). Finally, HENN-1 completes 21U RNA processing by catalyzing 2' O-methylation of the 3' end (Billi et al., 2012; Kamminga et al., 2012; Montgomery et al., 2012).

PRG-1 plays an important role in germ cell development, as it prevents transcriptional dysregulation by controlling gene expression of both transposable elements and endogenous genes, especially histone genes (Barucci et al., 2020; Batista et al., 2008; Cox et al., 1998; Reed et al., 2019; Tang et al., 2018; Wang and Reinke, 2008). Similar to the miRNA paradigm, PRG-1/21U RNA complexes recognize most target transcripts via imperfect base-paring interactions, which may explain why PRG-1 does not show endonuclease activity *in vivo*, although it contains the catalytic tetrad. While tolerating up to four mismatches, the seed region, ranging from position 2 to position 7, requires perfect pairing (Bagijn et al., 2012; Shen et al., 2018; Zhang et al., 2018). Upon recognition, PRG-1 initiates gene silencing by inducing the production of 22G RNAs (**Figure 5**). Thereby PRG-1 continuously directs WAGO activity and significantly shapes

the 22G RNA population in the germline (Batista et al., 2008; Das et al., 2008; Lee et al., 2012; Reed et al., 2019).

The WAGO pathway

As described above, several primary Argonaute proteins can initiate gene silencing by inducing the production of 22G RNAs. Upon target recognition, they recruit the so-called *Mutator* complex, which is responsible for 22G RNA biogenesis. While many components of this multi-protein complex have been identified, their molecular functions and the exact mode of operation remain elusive. However, it is proposed that endoribonuclease activity, possibly mediated by NYN-1, NYN-2 or RDE-8, stimulates 22G RNA biogenesis. The generated target RNA fragments are substrates for the ribonucleotidyltransferase RDE-3. This enzyme catalyzes the non-templated addition of alternating uracil and guanine. Once this sequence reaches a length of at least 17 nucleotides, it can recruit the RdRP RRF-1, which uses the RNA fragments as templates to generate 22G RNAs via a thus far unknown mechanism (**Figure 5**) (Phillips et al., 2012, 2014; Shukla et al., 2020; Tsai et al., 2015; Uebel et al., 2018; Zhang et al., 2011).

Mutator-dependent 22G RNAs are loaded into members of the highly diversified WAGO clade (**Table 1 and Figure 4**). Upon binding, they act as secondary Argonaute proteins and mediate both transcriptional and post-transcriptional gene silencing in a presumably semi-redundant manner (**Figure 5**) (Gu et al., 2009; Pak and Fire, 2007; Yigit et al., 2006). Interestingly, two distinct *Mutator*-dependent 22G RNA populations can be distinguished. The first population is called secondary 22G RNAs and they map close to the recognition site of the primary Argonaute protein that initiated gene silencing. The second population, called tertiary 22G RNA, covers the whole gene body and their biogenesis is triggered by WAGO activity (Sapetschnig et al., 2015). Thus, WAGO-mediated amplification of the gene silencing response may represent a major contribution to post-transcriptional gene silencing, as target transcripts are continuously cleaved to produce more 22G RNAs. In addition to cytoplasmic functions, the WAGO protein HRDE-1 shuttles into the nucleus and mediates transcriptional gene silencing. Similar to its somatically expressed homolog NRDE-3, HRDE-1 binds nascent transcripts and recruits a nuclear complex, including NRDE-1, NRDE-2 and NRDE-4, which mediates the deposition of repressive chromatin marks and the inhibition of RNA polymerase II elongation (**Figure 5**) (Buckley et al., 2012; Burkhart et al., 2011; Burton et al., 2011; Gu et al., 2012a; Guang et al., 2008, 2010; Mao et al., 2015).

Although the WAGO clade comprises many members, only a few have been characterized in detail. Next to the two WAGO proteins mentioned above, WAGO-1, WAGO-3, WAGO-4 and WAGO-7 are involved in germline RNAi, although molecular details for WAGO-1, WAGO-3 and WAGO-7 are largely lacking (Gu et al., 2009; Robert et al., 2005; Tijsterman et al., 2002; Vastenhouw et al., 2003; Wan et al., 2018; Xu et al., 2018b). In contrast, WAGO-6 and WAGO-8 may play a role in somatic RNAi (Yigit et al., 2006). Overall, the dissection of the WAGO clade in terms of functional specificity and redundancy currently remains an unsolved problem.

The CSR-1 pathways

Among all encoded Argonaute proteins, CSR-1 is the only member that is required for viability (Claycomb et al., 2009; Yigit et al., 2006). It is specifically expressed in the germline and in primordial germ cells, where it targets numerous germline expressed genes and seemingly promotes their gene expression rather than gene silencing (Claycomb et al., 2009; Conine et al., 2013; Seth et al., 2013, 2018; Wedeles et al., 2013). The target repertoire of CSR-1 is based on the association with a distinct subpopulation of 22G RNAs that is produced by the RdRP EGO-1 in a *Mutator* complex-independent manner (Claycomb et al., 2009; Maniar and Fire, 2011; Phillips et al., 2014; Smardon et al., 2000). Since PRG-1 can tolerate up to four mismatches during target transcript recognition, theoretically it is able to initiate WAGO-dependent gene silencing for any given transcript in the cell (Bagijn et al., 2012). According to a current model, CSR-1 is proposed to counteract PRG-1-mediated RNA surveillance by licensing genes for expression. Thereby, the balance between PRG-1 and CSR-1 on a target transcript is hypothesized to direct its expression (Seth et al., 2013, 2018; Wedeles et al., 2014, 2013). Impairment of this balance causes transcriptional dysregulation, which in turn results in defects during germline development (de Albuquerque et al., 2015; Phillips et al., 2015). Another intriguing aspect of the CSR-1 pathway is the involvement of the nucleotidyltransferase CDE-1. This enzyme catalyzes non-templated 3' uridylation of CSR-1-bound 22G RNAs, an RNA modification that is associated with RNA decay in multiple organisms (Song et al., 2015). Thereby, CDE-1 restricts EGO-1-produced 22G RNAs to the CSR-1 pathway by preventing their accumulation and possible misrouting into the WAGO pathway (van Wolfswinkel et al., 2009).

RNAi inheritance in *C. elegans*

Collectively, WAGO-mediated gene silencing can be very stable and heritable across generations. Once established, this gene silencing can stochastically become independent on the primary Argonaute protein. This phenomenon is best studied for PRG-1-initiated gene silencing and referred to as RNA-induced epigenetic silencing (RNAe). While PRG-1 becomes dispensable, the maintenance of RNAe requires both the *Mutator* complex and WAGO activity (Ashe et al., 2012; Bagijn et al., 2012; Lee et al., 2012; Luteijn et al., 2012; Shirayama et al., 2012). While HRDE-1, together with its interacting protein EMB-4, clearly plays a critical role in the nuclear pathway of RNAi inheritance (**Figure 5**) (Akay et al., 2017; Buckley et al., 2012; Tyc et al., 2017), the cytoplasmic contribution is less well understood. A recent study, however, gave a first insight by the characterization of WAGO-4, a cytoplasmic Argonaute protein that is required for RNAi inheritance via female gametes (**Figure 5**) (Wan et al., 2018; Xu et al., 2018b). Moreover, genetic experiments demonstrated that either a paternally active or a maternally active 22G RNA pathways is sufficient to properly direct the embryonic re-establishment of gene silencing after *de novo* production of 22G RNAs (de Albuquerque et al., 2015; Phillips et al., 2015). However, whether this parental contribution reflects the combination of nuclear and cytoplasmic pathways, or only one of them, remains unknown.

In addition, PRG-1 also contributes to the inheritance of RNAi. PRG-1/21U RNA complexes are inherited via the oocyte and a maternally active 21U RNA pathway is necessary to guide embryonic WAGO activity, thereby ensuring proper germ cell development (de Albuquerque et al., 2015; Phillips et al., 2015).

Cell organization by phase separation

Cells are highly compartmentalized in order to organize their numerous molecular processes and to facilitate rapid adaptation to changing environmental conditions. While many organelles like the nucleus, the endoplasmic reticulum (ER), the Golgi apparatus or mitochondria are membrane-bound, a variety of membrane-less compartments, like the nucleolus or processing bodies, have been found to contribute to cellular organization. Emerging evidence supports the idea that membrane-less compartments are involved in a plethora of cellular processes, of which some are specific to certain cell types. They spatiotemporally concentrate certain molecules and thereby create a dynamic microenvironment for distinct biochemical reactions. Moreover, they further separate biological processes that share a common compartment, and potentially play a major role in stress adaptation due to their sensitivity to physiochemical changes (Alberti, 2017; Banani et al., 2017; Hyman et al., 2014; Shin and Brangwynne, 2017; Wu et al., 2020).

Principles of condensate formation

Membrane-less compartments are also referred to as biomolecular condensates. They are formed by a process called liquid-liquid phase separation, which is a special form of phase transition, a physicochemical process that describes the change from one physical state to another. Liquid-liquid phase separation describes the 'demixing' of a homogenous solution of molecules in two distinct phases. While both phases maintain liquid properties, molecules are enriched in one phase, whereas they are depleted in the second phase. The interface forms independently of a lipid bilayer and allows certain exchange dynamics of some molecules between both phases. Upon formation, liquid condensates can be homogenous, develop multiple sub-territories (Feric et al., 2016; Putnam et al., 2019), or undergo further phase transition via hardening to adopt physical properties of gel-like or glass-like states. In fact, hardening of biomolecular condensates can even promote solid-like states like crystals or amyloid aggregates, which are often associated with cell pathology and disease. These transitions can be solely time-dependent or mediated via changes of the condensate composition (Alberti, 2017; Banani et al., 2017; Hyman et al., 2014; Shin and Brangwynne, 2017).

Liquid-liquid phase separation is driven by weak interactions involving both proteins and nucleic acids, most commonly RNA. In particular, the ability to interact with multiple

molecules, called multivalency, is a crucial parameter that determines phase separation behavior. Multivalency can be achieved in different ways, for instance by a modular domain composition. Each module mediates weak interactions with ligands and thus drives the formation of an interaction network. Such network can be homogenous or based on interactions between different kinds of domains. Dependent on the availability of ligands and their respective contribution to the interaction network, each multivalent protein has a critical concentration threshold for phase separation. Increasing the number of interacting modules, multivalent proteins or ligands directly correlates with condensate formation (Alberti, 2017; Banani et al., 2017; Hyman et al., 2014; Shin and Brangwynne, 2017). Next to modular domain organisation, multivalency can also be achieved by intrinsically disordered regions (Cho et al., 2018; Chong et al., 2018; Sabari et al., 2018; Wang et al., 2018a). Such regions lack any fixed tertiary structure due to their sequence composition, which often displays low complexity or a prevalence of certain amino acids (Habchi et al., 2014; Wang et al., 2018a). These two characteristics together with the charge pattern have been shown to affect phase separation by lowering the critical concentration threshold and modulating physical properties (Alberti, 2017; Banani et al., 2017; Hyman et al., 2014; Shin and Brangwynne, 2017; Wang et al., 2018a).

Independent on how multivalency is achieved, various factors can further effect phase separation behavior. First, post-translational modifications, especially phosphorylation, methylation and ADP-ribosylation are shown to modulate the interaction network to either favor or disfavor phase separation (Hofweber and Dormann, 2019). Second, flexible linker sequences between interacting modules often have poor solubility and contribute to phase separation by forming weak interactions among each other (Hyman et al., 2014).

While molecules of a single type can undergo phase separation, condensate formation can also require multi-protein complexes or ribonucleoproteins. Based on *in vitro* experiments, proteins with the lowest critical concentration may initiate condensate formation, which in turn enables recruitment of interacting molecules of higher critical concentration (Alberti, 2017). In addition, RNA is a polyvalent molecule that has been shown to promote phase separation of RNA-binding proteins, and active transcription is indeed required for the formation of the nucleolus (Berry et al., 2015; Lin et al., 2015). Upon assembly, liquid condensates can change in size. One underlying principle is called coalescence, which describes the fusion of condensates upon contact, if they can freely move by Brownian motion. Another principle is called Ostwald ripening, which describes the growth of large condensates at the expense of small condensates. This process is driven by different Laplace pressures between condensates of various sizes. The Laplace

pressure describes the pressure difference between the inside and the outside of a condensate, with the inside pressure being larger than the outside pressure. This pressure difference is higher in smaller condensates compared to larger condensates, which causes a diffusive transport of molecules along this gradient, resulting in smaller condensates to shrink and larger condensates to grow (Alberti, 2017; Hyman et al., 2014).

Biomolecular condensates: an expanding universe of cell organization

Numerous biomolecular condensates have been identified and our knowledge about their biological relevance is rapidly advancing. Most astonishingly, membrane-less organelles display a variety of localization patterns and their diversity and number is highly variable between different cell types. Both features make it difficult to grasp the extent of their contribution to cell organization.

While biomolecular condensates are described in both cytoplasm and nucleoplasm, some are seemingly associated to membranous structures like the ER, the nuclear envelope, the plasma membrane or mitochondria (Banani et al., 2017; Wang et al., 2020; Zhao and Zhang, 2020). In fact, membranes affect condensates in multiple ways. In addition to providing a platform for condensate formation, the association of biomolecular condensates with membranous structures limits intracellular mobility and influences condensate growth by preventing coalescence. Furthermore, it enables controlled translocation of molecules across membranes and contributes to condensate trafficking and storage. While many studies highlight the importance of membranes for condensate localization and function, mechanisms that ensure their membrane association remain largely unknown, with just a few chases linking membrane association to protein-protein interactions with transmembrane complexes. (Marnik and Updike, 2019; Wu et al., 2020; Zhao and Zhang, 2020).

Some biomolecular condensates, like the nucleolus and processing bodies, are found in most cells. In contrast, several membrane-less organelles are specific to certain cell types (Banani et al., 2017; Wu et al., 2020). In particular, a number of specialized condensates can be found in germ cells (Voronina et al., 2011). Depending on the organism, they can be involved various processes including germ cell specification, maintenance of germ cell identity, small RNA biogenesis, RNAi-pathways, mRNA localization and storage, translation or epigenetic inheritance (**Table 2**) (Gallo et al., 2010; King and Zhou, 2004; N. Kotaja, 2007; Phillips et al., 2012; Strome and Updike, 2015; Updike and Strome, 2010;

Voronina et al., 2011; Wan et al., 2018; Wang et al., 2020). Strikingly, the repertoire of membrane-less compartments significantly changes during gametogenesis and while cytoplasmic condensates have been described in mature oocytes, no germ-cell specific structure has been reported in mature sperm of any organism studied so far (Lehtiniemi and Kotaja, 2018; Voronina et al., 2011).

Table 2 | List of best-studied biomolecular condensates of germ cells.

Name	Cell type	Subcellular localization	Function
Balbiani body	Young oocytes (insects and vertebrates)	Cytoplasm	Germ cell specification, epigenetic inheritance
Sponge body	Oocytes and nurse cells (*D. melanogaster*)	Cytoplasm, ER-associated	Transport of material from nurse cell to oocyte
Perinuclear nuage	Naïve germ cells and differentiating gametes (insects and vertebrates)	Nuclear periphery	mRNA regulation, piRNA biogenesis
pi-body	Gonocytes, spermatogonia, spermatocytes (*M. musculus*)	Cytoplasm, mitochondria-associated	mRNA regulation, piRNA biogenesis, control of RNA translation
piP-body	Gonocytes, spermatogonia, spermatocytes (*M. musculus*)	Cytoplasm, mitochondria-associated	mRNA regulation, piRNA biogenesis, control of RNA translation
Chromatoid body	Spermatocytes, spermatids (*M. musculus*)	Cytoplasm, mitochondria-associated	mRNA storage and translational repression, piRNA pathway
P granule	Naïve germ cells and differentiating gametes (*C. elegans*)	Nuclear periphery	mRNA regulation, piRNA biogenesis, RNAi inheritance
Mutator focus	Naïve germ cells (*C. elegans*)	Nuclear periphery	Endo-siRNA biogenesis
Z granule	Naïve germ cells and oocytes (*C. elegans*)	Nuclear periphery	Maternal RNAi inheritance

Biomolecular condensates organize RNAi-related pathways

In *C. elegans*, three germ cell-specific, biomolecular condensates contribute to the organization of the RNAi machinery: P granules, *Mutator* foci and Z granules. All three compartments show liquid-like properties and localize in juxtaposition with each other at the nuclear periphery (**Figure 6A**) (Brangwynne et al., 2009; Marnik and Updike, 2019; Phillips et al., 2012; Uebel et al., 2018; Wan et al., 2018). While clearly separating molecular processes, their close localization ensures certain exchange dynamics between these condensates.

P granules can be found throughout germ cell development and gametogenesis, with the exception of spermatids and spermatozoa (**Figure 6B**) (Updike and Strome, 2010). Their assembly is governed by a complex interaction network between many intrinsically disordered proteins, including PGL-1 and PGL-3 (Marnik and Updike, 2019). P granules are home to several Argonaute proteins like PRG-1, CSR-1, WAGO-1, WAGO-4, ALG-3 and ALG-5 (Batista et al., 2008; Brown et al., 2017; Claycomb et al., 2009; Conine et al., 2010; Gu et al., 2009; Wan et al., 2018), as well as the 21U RNA and EGO-1-dependent 22G RNA biogenesis machinery (Claycomb et al., 2009; Cordeiro Rodrigues et al., 2019). P granules are seemingly associated with clusters of nuclear pore complexes, thereby extending their size exclusion properties (**Figure 6A**) (Pitt et al., 2000). Indeed, P granules are shown to retard mRNA export into the cytoplasm (Sheth et al., 2010). This allows multiple RNAi-related pathways to scan the transcriptome and mediate gene regulatory functions. At least in embryonic P blastomeres, P granules have an additional sub-territory, the MEG phase, whose formation is dependent on the intrinsically disordered proteins MEG-3 and MEG-4. This gel-like structure is required for embryonic P granule condensation and enables mRNA storage within P granules, which in turn ensures their expression and segregation with the P cell lineage (Dodson and Kennedy, 2019; Lee et al., 2020; Ouyang et al., 2019; Putnam et al., 2019).

Mutator foci are predominately found in the distal gonad covering a region that ranges from mitotically active to pachytene-stage germ cells. Their formation is independent on P granules and triggered by the intrinsically disordered protein MUT-16, whose phase separation serves as platform for the recruitment of additional components like MUT-7, MUT-14, MUT-15, RDE-2, RDE-3, NYN-1, NYN-2, RDE-8 and RRF-1. Together, these proteins, and likely others, form the *Muta*tor complex that is required for the biogenesis of a subpopulation of 22G RNAs that specifically associates with WAGO proteins (Ketting et al., 1999; Phillips et al., 2012, 2014; Shukla et al., 2020; Tsai et al., 2015; Uebel et al., 2018; Zhang et al., 2011).

The assembly of Z granules is poorly understood, but it clearly depends on P granules. Z granules can be found in both the adult germline and the embryo, where they start to form during pachytene and in primordial germ cells, respectively. The only two proteins that are known to localize to Z granules are the Argonaute protein WAGO-4 and the zinc-finger protein ZNFX-1. While initially localizing to P granules, WAGO-4 and ZNFX-1 segregate to newly formed Z granules. Although mechanistic details are missing, Z granules are maternally inherited to the next generation and play an important role in RNAi inheritance (Ishidate et al., 2018; Wan et al., 2018; Xu et al., 2018b).

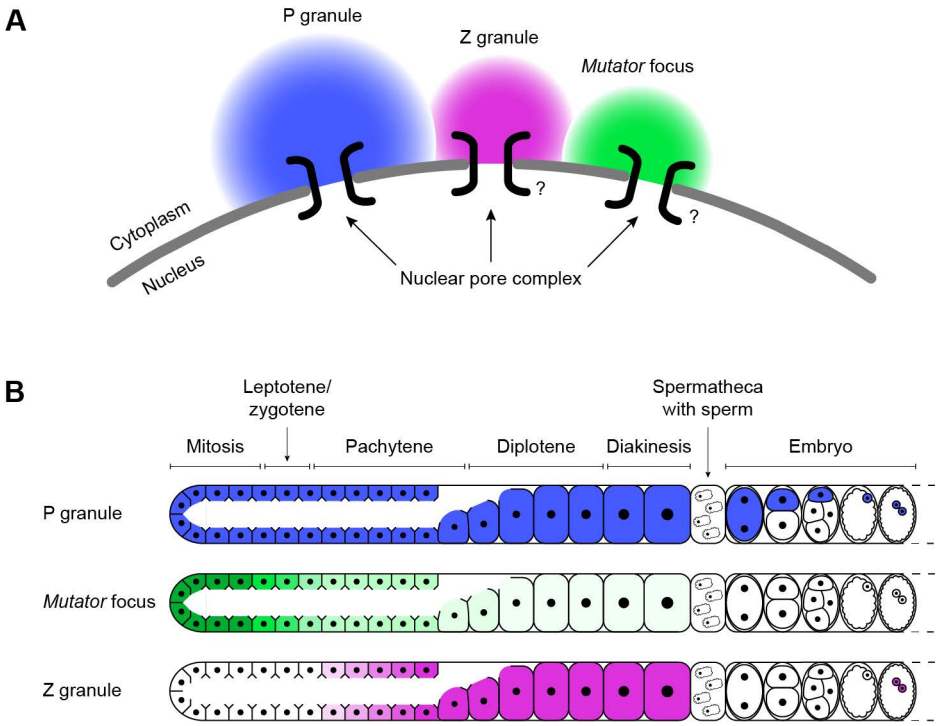

Figure 6 | Three perinuclear condensates organize RNAi-related pathways in germ cells of *C. elegans*. A, Schematic representation of a pachytene-stage germ cell, which contains all three biomolecular condensates at the nuclear periphery. The orientation of the Z granule and the *Mutator* focus relative to the nucleus is not yet known. B, Schematic representation of the distribution of P granules, *Mutator* foci and Z granules in the gonad of an adult hermaphrodite. Except sperm, P granules are present throughout germ cell development. In contrast, *Mutator* foci are predominantly found in the distal gonad, and Z granules start to appear in pachytene and primordial germ cells.

Aim of the thesis

Gene regulation via RNAi plays a central role during development and counteracts excessive transposon activity in germ cells. Especially the transgenerational inheritance of RNAi effects is a remarkable process that preserves fertility by preventing transcriptional dysregulation in the next generation. In this work, we aimed to further dissect the WAGO clade, while turning our attention to the paternal contribution during RNAi inheritance. Since some Argonaute proteins are maternally inherited, we wondered whether some of the uncharacterized WAGO proteins are responsible for the paternal inheritance of 22G RNAs. In particular, we were intrigued by the absence of germ cell specific condensates in mature sperm. Do they indeed not exist, or have they simply not been identified yet? Since spermatogenesis is accompanied by a massive reorganization of the intracellular content, paternal inheritance of small RNAs possibly requires a dedicated condensate that secures Argonaute proteins in maturing sperm. In addition to providing key insights into epigenetic inheritance, the identification of such a process could provide new insights into the shuttling of molecules between biomolecular condensates as well as the asymmetric segregation of membrane-less compartments during cell differentiation.

Materials and Methods

C. elegans culture and strains

Unless otherwise stated, all worm strains were cultured according to standard laboratory conditions at 20°C on Nematode Growth Medium (NGM) plates seeded with *Escherichia coli* OP50 (Brenner, 1974). Animals for IP-MS/MS experiments were grown on egg plates (90 mm diameter) (Schweinsberg and Grant, 2013) for one generation, synchronized by bleaching, and then grown on standard NGM plates (90 mm diameter) for one generation before harvest. Egg plates were generated by thoroughly mixing egg yolk with 50 ml LB media/egg. Following incubation at 65°C for 2-3 hours, the mixture was allowed to cool to room temperature before adding 10 ml OP50 culture/egg. Approximately 10 ml was put on top of standard NGM plates (90 mm diameter) and incubated at room temperature. Next day, excess liquid was decanted and egg plates were incubated at room temperature for another two days. All strains are in the N2 Bristol background. The strains USC988, USC1092 and USC1137 were kindly provided by Carolyn M. Phillips from the University of Southern California. The laboratory of Steven W. L'Hernault at the Emory University generated and provided the SL1697 strain. Helge Grosshans from the Friedrich Miescher Institute in Basel kindly provided the strains HW1867 and HW2915. Every other non-'RFK' strain was provided by the *Caenorhabditis* Genetics Center (CGC), which is funded by NIH Office of Research Infrastructure Programs (P40 OD010440). Strains used in this study are listed in Table 3.

Table 3 | Stains used in this study

Strain	Genotype
N2	*C. elegans* wild isolate var Bristol
USC1092	*alg-3(cmp155[gfp + loxP + 3xflag::alg-3]) IV.*
RFK956	*alg-3(cmp155[gfp + loxP + 3xflag::alg-3]) IV; pei-1(xf193[pei-1::mTagRfp-t]) IV.*
USC1137	*csr-1(cmp173[gfp + loxP + 3xflag::csr-1b]) IV.*
RFK1252	*csr-1(cmp173[gfp + loxP + 3xflag::csr-1b]) IV; pei-1(xf193[pei-1::mTagRfp-t]) IV.*
DG3226	*deps-1(bn124) I.*
HW2915	*dpf-3(xe246[dpf-3::3xflag::tev::gfp::hibit]) I.*
RFK1182	*dpf-3(xe246[dpf-3::3xflag::tev::gfp::hibit]) I; pei-1(ok1050) IV.*
RFK1147	*dpf-3(xe246[dpf-3::3xflag::tev::gfp::hibit]) I; pei-1(xf193[pei-1::mTagRfp-t]) IV.*
HW1867	*dpf-3(xe68) I.*
RFK1150	*dpf-3(xe68) I; otIs45[unc-119p::gfp] V.*
YY538	*hrde-1(tm1200) III.*
RFK1230	*hrde-1(tm1200) III; otIs45[unc-119p::gfp] V.*
RFK1231	*hrde-1(tm1200) III; pei-1(ok1050) IV; otIs45[unc-119p::gfp] V.*
RFK1246	*mjSi22[mex-5p::mCherry::his-58 + 21UR-1_as + tbb-2(3'UTR)] (on) I; mut-7(xf125) III; unc-119(ed3) III.*
RFK316	*mjSi22[mex-5p::mCherry::his-58 + 21UR-1_as + tbb-2(3'UTR)] (RNAe) I; prg-1(n4357) I; unc-119(ed3) III.*
RFK1253	*mjSi22[mex-5p::mCherry::his-58 + 21UR-1_as + tbb-2(3'UTR)] (on) I; prg-1(n4357) I; wago-3(pk1673) I; unc-119(ed3) III.*
SX2078	*mjSi22[mex-5p::mCherry::his-58 + 21UR-1_as + tbb-2(3'UTR)] (off) I; unc-119(ed3) III.*
RFK1247	*mjSi22[mex-5p::mCherry::his-58 + 21UR-1_as + tbb-2(3'UTR)] (off) I; wago-3(pk1673) I; unc-119(ed3) III.*
NL1810	*mut-16(pk710) I.*
RFK691	*mut-16(xf142) I.*
RFK1031	*mut-16(xf142) I; otIs45[unc-119p::gfp] V.*
RFK1063	*mut-16(xf142) I; pei-1(ok1050) IV; otIs45[unc-119p::gfp] V.*
RFK936	*mut-16(xf142) I; pei-1(xf193[pei-1::mTagRfp-t]) IV.*
RFK1037	*mut-16(xf142) I; wago-3(pk1673) I; otIs45[unc-119p::gfp] V.*
NL917	*mut-7(pk204) III.*
RFK652	*mut-7(xf125) III.*
YY186	*nrde-2(gg91) II.*
RFK1232	*nrde-2(gg91) II; otIs45[unc-119p::gfp] V.*
RFK1233	*nrde-2(gg91) II; pei-1(ok1050) IV; otIs45[unc-119p::gfp] V.*
OH441	*otIs45[unc-119p::gfp] V.*
RB1083	*pei-1(ok1050) IV.*
RFK1016	*pei-1(ok1050) IV; otIs45[unc-119p::gfp] V.*
RFK750	*pei-1(xf166[pei-1::3xmyc]) IV.*
RFK848	*pei-1(xf190[pei-1::d10]) IV.*
RFK921	*pei-1(xf193[pei-1::mTagRfp-t]) IV.*
RFK963	*pei-1(xf205[pei-1_Δidr::mTagRfp-t]) IV.*
RFK962	*pei-1(xf216[pei-1_Δbtb+back::mTagRfp-t]) IV.*
RFK1032	*pei-1(xf223[pei-1_Δbtb+back+idr::mTagRfp-t]) IV.*
RFK1065	*pei-1(xf227[pei-1_Δbtb::mTagRfp-t]) IV.*

RFK1027	*pei-1(xf228[pei-1_Δback+idr::mTagRfp-t]) IV.*
RFK1132	*pei-1(xf237[pei-1_Δback::mTagRfp-t]) IV.*
RFK926	*pgl-1(xf203[pgl-1::d10]) IV.*
RFK1086	*pgl-1(xf233[pgl-1::mTagRfp-t]) IV.*
SX922	*prg-1(n4357) I.*
RFK233	*prg-1(n4357) I; mut-16(pk710) I; otIs45[unc-119p::gfp] V.*
RFK237	*prg-1(n4357) I; mut-7(pk204) III.*
RFK1033	*prg-1(n4357) I; mut-7(xf125) III.*
RFK1038	*prg-1(n4357) I; mut-7(xf125) III; pei-1(ok1050) IV.*
RFK1245	*prg-1(n4357) I; nrde-2(gg91) II; otIs45[unc-119p::gfp] V.*
RFK832	*prg-1(n4357) I; otIs45[unc-119p::gfp] V.*
RFK1064	*prg-1(n4357) I; pei-1(ok1050) IV.*
RFK870	*prg-1(n4357) I; pei-1(ok1050) IV; otIs45[unc-119p::gfp] V.*
RFK1127	*prg-1(n4357) I; pei-1(xf193[pei-1::mTagRfp-t]) IV; otIs45[unc-119p::gfp] V.*
RFK788	*prg-1(n4357) I; wago-3(pk1673) I.*
RFK1036	*prg-1(n4357) I; wago-3(pk1673) I; mut-7(xf125) III.*
RFK820	*prg-1(n4357) I; wago-3(pk1673) I; otIs45[unc-119p::gfp] V.*
RFK1073	*prg-1(n4357) I; wago-4(tm1019) II.*
BA782	*spe-10(hc104) V; him-5(e1490) V.*
DU23	*spe-15(ok153) I; dpy-5(e61) I; him-8(e1489) IV; sDp2 (I;f).*
SL1697	*spe-45(eb39[spe-45::mCherry]) IV; him-5(e1490) V.*
EG6699	*ttTi5605 II; unc-119(ed3) III; oxEx1578[eft-3p::gfp + Cbr-unc-119(+)].*
EG6703	*unc-119(ed3) III; cxTi10816 IV; oxEx1582[eft-3p::gfp + Cbr-unc-119(+)].*
RFK823	*unc-119(ed3) III;* *xfSi187[mut-14p::mut-14::mTagBfp::mut-14 3'UTR + Cbr-unc-119(+)] IV.*
USC988	*wago-1(cmp92[gfp + loxP + 3xflag::wago-1]) I;* *mut-16(cmp41[mut-16::mCherry + loxP + 2xha]) I.*
RFK945	*wago-1(cmp92[gfp + loxP + 3xflag::wago-1]) I; pei-1(xf193[pei-1::mTagRfp-t]) IV.*
NL5117	*wago-3(pk1673) I.*
RFK1015	*wago-3(pk1673) I; otIs45[unc-119p::gfp] V.*
RFK935	*wago-3(pk1673) I; pei-1(xf193[pei-1::mTagRfp-t]) IV.*
RFK561	*wago-3(xf118[gfp + loxP SEC loxP + 3xflag::wago-3]) I.*
RFK560	*wago-3(xf119[gfp + loxP + 3xflag::wago-3]) I.*
RFK1148	*wago-3(xf119[gfp + loxP + 3xflag::wago-3]) I; deps-1(bn124) I;* *pei-1(xf193[pei-1::mTagRfp-t]) IV.*
RFK563	*wago-3(xf119[gfp + loxP + 3xflag::wago-3]) I; mut-16(pk710) I.*
RFK668	*wago-3(xf119[gfp + loxP + 3xflag::wago-3]) I; mut-16(pk710) I;* *xfSi139[pgl-1p::pgl-1::mTagBfp::pgl-1 3'UTR + Cbr-unc-119(+)] II;* *unc-119(ed3) III.*
RFK754	*wago-3(xf119[gfp + loxP + 3xflag::wago-3]) I; mut-16(xf142) I.*
RFK784	*wago-3(xf119[gfp + loxP + 3xflag::wago-3]) I; mut-16(xf142) I; pei-1(ok1050) IV.*
RFK588	*wago-3(xf119[gfp + loxP + 3xflag::wago-3]) I; mut-7(pk204) III.*
RFK872	*wago-3(xf119[gfp + loxP + 3xflag::wago-3]) I; mut-7(pk204) III; unc-119(ed3) III;* *xfSi187[mut-14p::mut-14::mTagBfp::mut-14 3'UTR + Cbr-unc-119(+)] IV.*
RFK812	*wago-3(xf119[gfp + loxP + 3xflag::wago-3]) I; mut-7(xf125) III.*
RFK779	*wago-3(xf119[gfp + loxP + 3xflag::wago-3]) I; mut-7(xf125) III; pei-1(ok1050) IV.*
RFK1034	*wago-3(xf119[gfp + loxP + 3xflag::wago-3]) I; otIs45[unc-119p::gfp] V.*
RFK778	*wago-3(xf119[gfp + loxP + 3xflag::wago-3]) I; pei-1(ok1050) IV.*

RFK817	*wago-3(xf119[gfp + loxP + 3xflag::wago-3]) I; pei-1(xf166[pei-1::3xmyc]) IV.*
RFK933	*wago-3(xf119[gfp + loxP + 3xflag::wago-3]) I; pei-1(xf193[pei-1::mTagRfp-t]) IV.*
RFK1209	*wago-3(xf119[gfp + loxP + 3xflag::wago-3]) I; pei-1(xf193[pei-1::mTagRfp-t]) IV; him-5(e1490) V.*
RFK1149	*wago-3(xf119[gfp + loxP + 3xflag::wago-3]) I; pei-1(xf193[pei-1::mTagRfp-t]) IV; spe-10(hc104) V; him-5(e1490) V.*
RFK1017	*wago-3(xf119[gfp + loxP + 3xflag::wago-3]) I; pei-1(xf205[pei-1_Δidr::mTagRfp-t]) IV.*
RFK1018	*wago-3(xf119[gfp + loxP + 3xflag::wago-3]) I; pei-1(xf216[pei-1_Δbtb+back::mTagRfp-t]) IV.*
RFK1030	*wago-3(xf119[gfp + loxP + 3xflag::wago-3]) I; pei-1(xf223[pei-1_Δbtb+back+idr::mTagRfp-t]) IV.*
RFK1062	*wago-3(xf119[gfp + loxP + 3xflag::wago-3]) I; pei-1(xf227[pei-1_Δbtb::mTagRfp-t]) IV.*
RFK1066	*wago-3(xf119[gfp + loxP + 3xflag::wago-3]) I; pei-1(xf228[pei-1_Δback+idr::mTagRfp-t]) IV.*
RFK1131	*wago-3(xf119[gfp + loxP + 3xflag::wago-3]) I; pei-1(xf237[pei-1_Δback::mTagRfp-t]) IV.*
RFK1080	*wago-3(xf119[gfp + loxP + 3xflag::wago-3]) I; pgl-1(xf233[pgl-1::mTagRfp-t]) IV.*
RFK1081	*wago-3(xf119[gfp + loxP + 3xflag::wago-3]) I; pgl-1(xf233[pgl-1::mTagRpf-t]) IV; pei-1(ok1050) IV.*
RFK1226	*wago-3(xf119[gfp + loxP + 3xflag::wago-3]) I; prg-1(n4357) I; pgl-1(xf233[pgl-1::mTagRpf-t]) IV.*
RFK1228	*wago-3(xf119[gfp + loxP + 3xflag::wago-3]) I; spe-15(ok153) I; pei-1(xf193[pei-1::mTagRfp-t]) IV; him-8(e1489) IV.*
RFK589	*wago-3(xf119[gfp + loxP + 3xflag::wago-3]) I; rrf-1(pk1417) I.*
RFK590	*wago-3(xf119[gfp + loxP + 3xflag::wago-3]) I; rrf-2(pk2040) I.*
RFK591	*wago-3(xf119[gfp + loxP + 3xflag::wago-3]) I; rrf-3(pk1426) II.*
RFK1210	*wago-3(xf119[gfp + loxP + 3xflag::wago-3]) I; spe-45(eb39[spe-45::mCherry]) IV; him-5(e1490) V.*
RFK674	*wago-3(xf119[gfp + loxP + 3xflag::wago-3]) I; xfSi139[pgl-1p::pgl-1::mTagBfp::pgl-1 3'UTR + Cbr-unc-119(+)] II; unc-119(ed3) III.*
RFK673	*wago-3(xf119[gfp + loxP + 3xflag::wago-3]) I; xfSi139[pgl-1p::pgl-1::mTagBfp::pgl-1 3'UTR + Cbr-unc-119(+)] II; unc-119(ed3) III; mut-7(pk204) III.*
RFK816	*wago-3(xf119[gfp + loxP + 3xflag::wago-3]) I; xfSi139[pgl-1p::pgl-1::mTagBfp::pgl-1 3'UTR + Cbr-unc-119(+)] II; unc-119(ed3) III; pei-1(ok1050) IV.*
RFK843	*wago-3(xf178[gfp + loxP + 3xflag::wago-3(replacement of S1099 – S1120 with 'AGAGAG')]) I.*
RFK1084	*wago-3(xf232[gfp + loxP + 3xflag]) I.*
RFK626	*xfSi139[pgl-1p::pgl-1::mTagBfp::pgl-1 3'UTR + Cbr-unc-119(+)] II; unc-119(ed3) III.*

MosSCI transgenesis

The MosSCI system was used to insert transgenes for ectopic expression (Frøkjær-Jensen et al., 2008, 2012). The *pgl-1::mTagBfp* and *mut-14::mTagBfp* transgene were targeted to the locus *ttTi5605* on chromosome II and *cxTi10816* on chromosome IV, respectively. The endogenous promoter and 3'UTR sequences were used to express both transgenes (Lamesch et al., 2004). The *mTagBfp* coding sequence including three introns was amplified from pUA97, which was a gift from Oliver Hobert (Addgene plasmid # 69340; http://n2t.net/addgene:69340; RRID:Addgene_69340). All plasmids used for microinjection were purified from 4 ml bacterial culture using PureLink™ HiPure Plasmid Miniprep Kit (Art. No. K210011, Invitrogen™), eluted in sterile water and confirmed by enzymatic digestion and sequencing. To generate transgenic lines, DNA mixes containing 50 ng/µl pCFJ601, 10 ng/µl pMA122, 10 ng/µl pGH8, 5 ng/µl pCFJ104, 2.5 ng/µl pCFJ90 and 50 ng/µl of either pRFK2564 (*pgl-1::mTagBfp*) or pRFK2597 (*mut-14::mTagBfp)* were injected in both gonads of 20 young adults of either the EG6699 (insertion on chromosome II) or EG6703 (insertion on chromosome IV) strain. The progeny was screened as previously described (Frøkjær-Jensen et al., 2008, 2012). Successful insertion events were confirmed by Sanger sequencing. All generated strains were out-crossed at least two times prior to any further cross or analysis.

pCFJ601, pMA122, pGH8, pCFJ90 and pCFJ104 were gifts from Erik Jorgensen (Addgene plasmid # 34874; http://n2t.net/addgene:34874; RRID:Addgene_34874, Addgene plasmid # 34873; http://n2t.net/addgene:34873; RRID:Addgene_34873, Addgene plasmid # 19359; http://n2t.net/addgene:19359; RRID:Addgene_19359, Addgene plasmid # 19327; http://n2t.net/addgene:19327; RRID:Addgene_19327, Addgene plasmid # 19328; http://n2t.net/addgene:19328; RRID:Addgene_19328) (Frøkjær-Jensen et al., 2008, 2012)

CRISPR/Cas9-mediated genome editing

All protospacer sequences were chosen using CRISPOR (http://crispor.tefor.net) (Haeussler et al., 2016) and cloned in either pRK2411 (plasmid expressing Cas9 + sgRNA(F+E) (Chen et al., 2013); derived from pDD162) or pRK2412 (plasmid expressing sgRNA(F+E) (Chen et al., 2013) with Cas9 deleted; derived from pRK2411) via site-directed, ligase-independent mutagenesis (SLIM) (Chiu et al., 2004, 2008). pDD162 (Peft-3::Cas9 + Empty sgRNA) was a gift from Bob Goldstein (Addgene plasmid # 47549; http://n2t.net/addgene:47549; RRID:Addgene_47549) (Dickinson et al., 2013). SLIM

reactions were transformed in Subcloning Efficiency™ DH5α™ Competent Cells (Art. No. 18265017, Invitrogen™) and plated on LB agar plates supplemented with 100 µg/ml ampicillin. All protospacer sequences are listed in Table 4.

Table 4 | Protospacer sequences used for CRISPR/Cas9-mediated genome editing

Gene	Allele	Sequence (5' to 3')
dpy-10	*cn64*	GCT ACC ATA GGC ACC ACG AG
mut-7	*xf125*	AAC ATC GGG ACA AAG TTT GG TTT GGC GGT TTG GTA TCT GG GTG TGG AGA ATG CGG TAC GG AAG GAA ATT GAA CGA GTT GG
mut-16	*xf142*	GGA TAA TCA TCA TCA CTT T GAT CGG AGA TGT CTA ATT C ATC AGT TTC CGT ATA CGA GG TTG TCC GGT ATC GTT TCT GG
pei-1	*xf166*	GAT TTC GTA AAC TGC CTA GT
	xf190	GAT TTC GTA AAC TGC CTA GT
	xf205	GGG TAC AAA TAC TGG GAT TG CAA CTG ACG ATC TCT CCA AG
	xf216	GCA ATA CGC TCG AAA TGC TG CAA CTG ACG ATC TCT CCA AG
	xf223	GCA ATA CGC TCG AAA TGC TG GGG TAC AAA TAC TGG GAT TG
	xf227	GCA ATA CGC TCG AAA TGC TG CCA TAA TTG GTG ATC CAT TG
	xf228	GGG TAC AAA TAC TGG GAT TG CCA TAA TTG GTG ATC CAT TG
	xf237	CAA CTG ACG ATC TCT CCA AG CCA TAA TTG GTG ATC CAT TG
pgl-1	*xf203*	GGG GGT CGT GGT GGA CGC GG
unc-58	*e665*	ATC CAC GCA CAT GGT CAC TA
wago-3	*xf119*	ATT CAC AAT GCC TGC TAC AC
	xf178	TGA TTA TTA TTT CAG TCT GG
	xf232	GTG CTT AAG CAT TGA CAC GG GAT GAC AAG AGA GGA TCC GG

Insertion of a *gfp::3flag* sequence was based on a plasmid DNA donor template containing a self-excising drug selection casseste (SEC), which was designed and cloned as previously described (Dickinson et al., 2015). pDD282 was a gift from Bob Goldstein (Addgene plasmid # 66823; http://n2t.net/addgene:66823; RRID:Addgene_66823) (Dickinson et al., 2015). pJW1259 was used as Cas9 plasmid and was a gift from Jordan Ward (Addgene plasmid # 61251; http://n2t.net/addgene:61251; RRID:Addgene_61251) (Ward, 2014). All plasmids were purified from 4 ml bacterial culture using either NucleoSpin® Plasmid (Art. No. 740588.50, Macherey-Nagel®) or PureLink™ HiPure Plasmid Miniprep Kit (Art. No. K210011, Invitrogen™), eluted in sterile water and confirmed by enzymatic digestion and sequencing.

PCR products served as linear, double-stranded DNA donor templates for the insertion of *mTagRfp-t* sequences. The *mTagRfp-t* coding sequence including three introns and flanking homology regions was amplified from pDD286, which was a gift from Bob Goldstein (Addgene plasmid # 70684; http://n2t.net/addgene:70684; RRID:Addgene_70684). All PCR products were purified using the QIAquick® PCR Purification Kit (Art. No. 28106, QIAGEN®), eluted in sterile water and confirmed by agarose gel electrophoresis. For all epitope tag insertions, co-conversions and precise deletions, we ordered 4 nmole Ultramer® DNA oligodeoxynucleotides from Integrated DNA Technologies™, which served as linear, single-stranded DNA (ssODN) donor templates. All Ultramer® DNA oligodeoxynucleotides were resuspended in sterile water. All linear DNA donor templates contained ~35 bp homology regions (Paix et al., 2014, 2016) and are listed in Table 5 and Table 6.

Table 5 | Linear ssDNA donor templates used for CRISPR/Cas9-mediated genome editing.

Gene	Allele	Sequence (5' to 3')
dpy-10	*cn64*	CACTTGAACTTCAATACGGCAAGATGAGAATGACTGGAAACCGTACCGCATG CGGTGCCTATGGTAGCGGAGCTTCACATGGCTTCAGACCAACAGCCTAT
pei-1	*xf166*	GAA ACC AAT TCC ACA ATC CCA GTA TTT GTA CCC CAA CGG ATC CGG AGG TGG AGG TGA ACA AAA ACT TAT TTC TGA AGA GGA TCT TGA GCA AAA GCT CAT CTC CGA GGA GGA CCT CGA GCA GAA GTT GAT CAG CGA GGA AGA CTT GTA GGC AGT TTA CGA AAT CAA ACA ATC AAT CAA TCT G
	xf190	GAA ACC AAT TCC ACA ATC CCA GTA TTT GTA CCC CAA CGC TAC CAT AGG CAC CAC GAG CGG TAG GCA GTT TAC GAA ATC AAA CAA TCA ATC AAT CTG
	xf205	CCC TTG GAG ACA CCT CCA CCT CCG GAT CCG TTG GGG TAC AAA TAC TGG GAT GGA GAG ATC GTC AGT TGG GAT TTC GAG GCG ATT TCC GAA TTT GTG AGG
	xf216	CTT TTT TGG GTA CAA TCT TAA TTT CAA TAG TGC CAC TCT GTG GAG CAG CGT TAG CGT GTA ACG AGT TTC TG
	xf223	CCC TTG GAG ACA CCT CCA CCT CCG GAT CCG TTG GGG TAC AAA TAC TGG GAC TGT GGA GCA GCG TTA GCG TGT AAC GAG TTT CTG
	xf227	GAA CCG AAA AAG CAC GCG CCG ATG CAA TAT TGA GAG CCA TAA TTG GTG ATC CCT GTG GAG CAG CGT TAG CGT GTA ACG AGT TTC TG
	xf228	CCC TTG GAG ACA CCT CCA CCT CCG GAT CCG TTG GGG TAC AAA TAC TGG GAA TTG TGG TTT AGA ATC TTT TGT TCA ATT TGA CGT TGC AAC ATG GTC ACC TG
	xf237	CTT TTT TGG GTA CAA TCT TAA TTT CAA TAG TGC CAC TAT TGT GGT TTA GAA TCT TTT GTT CAA TTT GAC GTT GCA AC
pgl-1	*xf203*	CTT AAA AAA CAA ATT AAA CAT TCA ATA GTT GGA GTT TAC CGC TCG TGG TGC CTA TGG TAG CCG AAA CCT CCT CTA CCT CCG CGT CCA CCG TAA CCA CCA CGT CCA CGA TCT CCG CCG TAT CC
unc-58	*e665*	ATT TTG TGG TAT AAA ATA GCC GAG TTA GGA AAC AAA TTT TTC TTT CAG GTT TCT CAG TAG TGA CCA TGT GCG TGG ATC TTG CGT CCA CAC ATC TCA AGG CGT ACT T
wago-3	*xf178*	GGA CCA ATA TTG AGC TCC CAT GGT TTT GGC GGT GCA CCA GCT CCT GCG CCA GCC TGA AAT AAT AAT CAA CAT TAA ACG TCA AGA CTT C
	xf232	GGA CGA CGA CGA CAA GCG TGA TTA CAA GGA TGA CGA TGA CAA GAG ATA AGC ACT CAC CCG AAG ATC AAG TTG TAC CAT TTT TTA ATC C

Table 6 | Linear dsDNA donor templates used for CRISPR/Cas9-mediated genome editing.

Gene	Allele	Sequence (5' to 3')
pei-1	*xf193*	GAA ACC AAT TCC ACA ATC CCA GTA TTT GTA CCC CAA CGG ATC CGG AGG TGG AGG TGT CTC CAA GGG AGA GGA GCT CAT CAA GGA GAA CAT GCA CAT GAA GCT CTA CAT GGA GGG AAC CGT CAA CAA CCA CCA CTT CAA GTG CAC CTC CGA GGG AGA GGG AAA GCC ATA CGA GGG AAC CCA AAC CAT GCG TAT CAA GGT AAG TTT AAA CAT ATA TAT ACT AAC TAA CCC TGA TTA TTT AAA TTT TCA GGT CGT CGA GGG AGG ACC ACT CCC ATT CGC CTT CGA CAT CCT CGC CAC CTC CTT CAT GTA CGG ATC CCG TAC CTT CAT CAA CCA CAC CCA AGG AAT CCC AGA CTT CTT CAA GCA ATC CTT CCC AGA GGG ATT CAC CTG GGA GCG TGT CAC CAC CTA CGA GGA CGG AGG AGT CCT CAC CGC CAC CCA AGA CAC CTC CCT CCA AGA CGG ATG CCT CAT CTA CAA CGT CAA GGT AAG TTT AAA CAG TTC GGT ACT AAC TAA CCA TAC ATA TTT AAA TTT TCA GAT CCG TGG AGT CAA CTT CCC ATC CAA CGG ACC AGT CAT GCA AAA GAA GAC CCT CGG ATG GGA GGC CAA CAC CGA GAT GCT CTA CCC AGC CGA CGG AGG ACT CGA GGG ACG TAC CGA CAT GGC CCT CAA GCT CGT CGG AGG AGG ACA CCT CAT CTG CAA CTT CAA GAC CAC CTA CCG TTC CAA GGT AAG TTT AAA CAT GAT TTT ACT AAC TAA CTA ATC TGA TTT AAA TTT TCA GAA GCC AGC CAA GAA CCT CAA GAT GCC AGG AGT CTA CTA CGT CGA CCA CCG TCT CGA GCG TAT CAA GGA GGC CGA CAA GGA GAC CTA CGT CGA GCA ACA CGA GGT CGC CGT CGC CCG TTA CTG CGA CCT CCC ATC CAA GCT CGG ACA CAA GCT CAA CGG AAT GGA CGA GCT CTA CAA GTA GGC AGT TTA CGA AAT CAA ACA ATC AAT CAA TCT G
pgl-1	*xf233*	GGA TAC GGC GGA GAT CGT GGA CGT GGT GGT TAC GGT GGA CGC GGA GGT AGA GGA GGT TTC GGA TCC GGA GGT GGA GGT GTC TCC AAG GGA GAG GAG CTC ATC AAG GAG AAC ATG CAC ATG AAG CTC TAC ATG GAG GGA ACC GTC AAC AAC CAC CAC TTC AAG TGC ACC TCC GAG GGA GAG GGA AAG CCA TAC GAG GGA ACC CAA ACC ATG CGT ATC AAG GTA AGT TTA AAC ATA TAT ATA CTA ACT AAC CCT GAT TAT TTA AAT TTT CAG GTC GTC GAG GGA GGA CCA CTC CCA TTC GCC TTC GAC ATC CTC GCC ACC TCC TTC ATG TAC GGA TCC CGT ACC TTC ATC AAC CAC ACC CAA GGA ATC CCA GAC TTC TTC AAG CAA TCC TTC CCA GAG GGA TTC ACC TGG GAG CGT GTC ACC ACC TAC GAG GAC GGA GGA GTC CTC ACC GCC ACC CAA GAC ACC TCC CTC CAA GAC GGA TGC CTC ATC TAC AAC GTC AAG GTA AGT TTA AAC AGT TCG GTA CTA ACT AAC CAT ACA TAT TTA AAT TTT CAG ATC CGT GGA GTC AAC TTC CCA TCC AAC GGA CCA GTC ATG CAA AAG AAG ACC CTC GGA TGG GAG GCC AAC ACC GAG ATG CTC TAC CCA GCC GAC GGA GGA CTC GAG GGA CGT ACC GAC ATG GCC CTC AAG CTC GTC GGA GGA GGA CAC CTC ATC TGC AAC TTC AAG ACC ACC TAC CGT TCC AAG GTA AGT TTA AAC ATG ATT TTA CTA ACT AAC TAA TCT GAT TTA AAT TTT CAG AAG CCA GCC AAG AAC CTC AAG ATG CCA GGA GTC TAC TAC GTC GAC CAC CGT CTC GAG CGT ATC AAG GAG GCC GAC AAG GAG ACC TAC GTC GAG CAA CAC GAG GTC GCC GTC GCC CGT TAC TGC GAC CTC CCA TCC AAG CTC GGA CAC AAG CTC AAC GGA ATG GAC GAG CTC TAC AAG TAA ACT CCA ACT ATT GAA TGT TTA ATT TGT TTT TTA AG

To generate the *mut-16* and *mut-7* deletion alleles, we injected animals with 50 ng/µl pJW1259, 30 ng/µl of each sgRNA(F+E), 10 ng/µl pGH8, 5 ng/µl pCFJ104, and 2.5 ng/µl pCFJ90. F1 animals expressing all three co-injection markers were selected for subsequent screening of *mut-16* or *mut-7* deletion alleles. To insert a *gfp::3xflag* sequence in *wago-3*, the injection mix included 50 ng/µl pJW1259, 50 ng/µl pRFK2505, 10 ng/µl pRFK2485, 10 ng/µl pGH8, 5 ng/µl pCFJ104, and 2.5 ng/µl pCFJ90. Screening of F1 animals was performed as previously described (Dickinson et al., 2015). Every other CRISPR/Cas9-mediated genome editing was performed using either *dpy-10(cn64)* or *unc-58(e665)* co-conversion strategies (Arribere et al., 2014). To insert epitope tag or protospacer sequences, we injected 50 ng/µl Cas9 + sgRNA(F+E) (co-conversion), 50 ng/µl sgRNA(F+E) (gene of interest), 750 nM ssODN donor1 (co-conversion), and 750 nM ssODN donor2 (gene of interest). To insert a *mTagRfp-t* sequence in *pei-1* and *pgl-1*, we first transplanted the protospacer sequence used for the *dpy-10* co-conversion directly upstream of the respective stop codon to generate *d10*-entry strains (El Mouridi et al., 2017). These strains served as reference strains for the insertion of a *mTagRfp-t* sequence by injecting 50 ng/µl Cas9 + sgRNA(F+E) (*dpy-10* co-conversion), 1000 nM ssODN donor (*dpy-10* co-conversion), and 300 ng/µl linear, double-stranded DNA donor. Precise deletions in *pei-1* and *wago-3* were generated by injecting 50 ng/µl Cas9 + sgRNA(F+E) (co-conversion), 50 ng/µl of each sgRNA(F+E) (gene of interest), 750 nM ssODN donor1 (co-conversion), and 750 nM ssODN donor2 (gene of interest). Unless otherwise stated, DNA injection mixes were injected in both gonad arms of one to 20 young adult N2 hermaphrodites maintained at 20°C. Selected F1 progeny were screened for insertion or deletion by PCR. Successful editing events were confirmed by Sanger sequencing. All generated mutant strains were out-crossed at least two times prior to any further cross or analysis. All CRISPR/Cas9-generated alleles are listed in Table 7.

Table 7 | Alleles generated by CRISPR/Cas9-mediated genome editing.

Allele	Selection approach	Details
mut-16(xf142) I.	Co-injection marker	3990 bp deletion & 6 bp insertion (ATTCAGAATGACAATATGGA - Indel[CAATAT] - ATTCAGAACAACCCTCAACA). First 85 amino acids are *mut-16* followed by 33 altered amino acids and premature stop codon
mut-7(xf125) III.	Co-injection marker	2734 bp deletion (GCGATGCCGGATAGAGGAAA - Deletion – ATGGTCGTGGCAATCAAGCG). First 82 amino acids are *mut-7* followed by 50 altered amino acids and postmature stop codon
pei-1(xf166[pei-1::3xmyc]) IV.	*dpy-10* co-conversion	C-terminal *3xmyc* insertion
pei-1(xf190[pei-1::d10]) IV.	*unc-58* co-conversion	C-terminal *d10* insertion
pei-1(xf193[pei-1::mTagRfp-t]) IV.	*dpy-10* co-conversion	C-terminal *mTagRfp-t* insertion
pei-1(xf205[pei-1_Δidr::mTagRfp-t]) IV.	*dpy-10* co-conversion	1160 bp in-frame deletion ranging from S257 to Q558 of *pei-1(xf193) IV.*
pei-1(xf216[pei-1_Δbtb+back::mTagRfp-t]) IV.	*dpy-10* co-conversion	1321 bp in-frame deletion ranging from H15 to P256 of *pei-1(xf193) IV.*
pei-1(xf223[pei-1_Δbtb+back+idr::mTagRfp-t]) IV.	*dpy-10* co-conversion	2481 bp in-frame deletion ranging from H15 to Q558 of *pei-1(xf193) IV.*
pei-1(xf227[pei-1_Δbtb::mTagRfp-t]) IV.	*dpy-10* co-conversion	701 bp in-frame deletion ranging from H15 to N130 of *pei-1(xf193) IV.*
pei-1(xf228[pei-1_Δback+idr::mTagRfp-t]) IV.	*dpy-10* co-conversion	1780 bp in-frame deletion ranging from G131 to Q558 of *pei-1(xf193) IV.*
pei-1(xf237[pei-1_Δback::mTagRfp-t]) IV.	*dpy-10* co-conversion	620 bp in-frame deletion ranging from G131 to P256 of *pei-1(xf193) IV.*
pgl-1(xf203[pgl-1::d10]) IV.	*unc-58* co-conversion	C-terminal *d10* insertion
pgl-1(xf233[pgl-1::mTagRfp-t]) IV.	*unc-58* co-conversion	C-terminal *mTagRfp-t* insertion
wago-3(xf119[gfp + loxP + 3xflag::wago-3]) I.	SEC	N-terminal *gfp::3xflag* insertion
wago-3(xf178[gfp + loxP + 3xflag(replacement of S1099 - S1120 with 'AGAGAG')]) I.	*dpy-10* co-conversion	66 bp in-frame deletion ranging from S1099 to S1120 of *wago-3(xf119) I.*
wago-3(xf232[gfp + loxP + 3xflag]) I.	*dpy-10* co-conversion	3405 bp in-frame deletion ranging from G279 to A1259 of *wago-3(xf119) I.*

Mortal germline assay

All mutant strains were confirmed and out-crossed four times before starting the experiment. For each strain, 90 L2 or L3 animals were distributed to 15 NGM plates (90 mm diameter), resulting in six larvae per plate. Animals were grown at 25°C. Worms were picked onto fresh plates every second generation. The experiment was stopped after 17 generations.

Mutator-induced sterility crosses

All strains were confirmed and out-crossed two times before setting up crosses. We note that out-crossing ensured comparable results as an enhanced Mis phenotype was observed when using non-out-crossed animals. The transgenic allele *otIs45[unc-119p::gfp] V.* was always present in paternal strains and served as mating control to avoid picking self-fertilized offspring. Only L2 stage F1 animals were picked onto individual plates to avoid any biased selection. After three days, male or dead F1 animals were excluded from the analysis. Fertility of F1 animals was determined by the presence of F2 animals after another two to four days.

Immunoprecipitation experiments

Unless otherwise stated, synchronized animals were cultured at 20°C until late-L4 stage, harvested with M9 buffer and frozen on dry ice in sterile water and 200 µl aliquots. Aliquots were thawed on ice, mixed with same volume of 2x lysis buffer (50 mM Tris HCl pH 7.5, 300 mM NaCl, 3 mM $MgCl_2$, 2 mM DTT, 0.2 % Triton™ X-100, cOmplete™ Mini EDTA-free Protease Inhibitor Cocktail (Art. No. 11836170001, Roche)) and sonicated using a Bioruptor® Plus device (Art. No. B01020001, Diagenode) (4°C, 10 cycles à 30 seconds ON and 30 seconds OFF). Following centrifugation for 10 min at 4°C and 21,000 xg, supernatants were carefully transferred into a fresh tube without taking any material from the pellet or lipid phase. Pellet fractions were washed three times in 1x lysis buffer and resuspended in 1x Novex™ NuPAGE™ LDS sample buffer (Art. No. NP0007, Invitrogen™) supplemented with 100 mM DTT. Total protein concentrations of soluble worm extracts were determined using the Pierce™ BCA™ Protein-Assay (Art. No. 23225, Thermo Scientific™) and an Infinite® M200 Pro plate reader (Tecan). Extracts were diluted with 1x lysis buffer to reach 550 µl and a total protein concentration of 3 µg/µl. For each sample, 50 µl of this extract was added to 50 µl 1x Novex™ NuPAGE™ LDS sample buffer supplemented with 100 mM DTT and served as input control sample.

For each immunoprecipitation (IP) experiment, 30 µl Novex™ DYNAL™ Dynabeads™ Protein G (Art. No. 10004D, Invitrogen™) were washed three times with 500 µl 1x wash buffer (25 mM Tris HCl pH 7.5, 150 mM NaCl, 1.5 mM $MgCl_2$, 1 mM DTT, cOmplete™ Mini EDTA-free Protease Inhibitor Cocktail), combined with the remaining 500 µl extract and incubated with rotation for 1 h at 4°C. In the meantime, 8 µg antibody (Monoclonal ANTI-FLAG® M2, Art. No. F3165, Sigma-Aldrich® / Myc-Tag (9B11) Mouse mAb, Art. No. 2276, Cell Signaling Technology®) was conjugated to another 30 µl Novex™ DYNAL™ Dynabeads™ Protein G according to the manufacturer's instructions. Extracts were separated from non-conjugated Dynabeads™, combined with antibody-conjugated Dynabeads™ and incubated with rotation for 2 h at 4°C. Following three washes with 500 µl 1x wash buffer, antibody-conjugated Dynabeads™ were resuspended in 25 µl 1.2x Novex™ NuPAGE™ LDS sample buffer supplemented with 120 mM DTT.

For RIP experiments, immunoprecipitations were performed as described above with the following modifications: i) adult animals were harvested, ii) soluble worm extract was diluted to 650 µl and a total protein concentration of 7 µg/µl, of which 150 µl served as input sample for later RNA extraction, iii) antibody-conjugated Dynabeads™ were resuspended in 50 µl nuclease-free water.

Immunoprecipitation experiments associated with mass spectrometry and small RNA sequencing were performed in quadruplicates and triplicates, respectively.

Western Blot

Whole-worm extracts were obtained and normalized to total protein concentration like described above. Alternatively, 50 L4 stage hermaphrodites were hand-picked in 1x Novex™ NuPAGE™ LDS sample buffer (Art. No. NP0007, Invitrogen™) supplemented with 100 mM DTT and incubated for 10 min at 95°C. Following thorough mixing and centrifugation for 10 min at 21,000 xg, supernatants were transferred into fresh tubes.

For immunoprecipitation experiments, equal amounts of input samples (2 %) and IP samples (10 %) were adjusted to same volume with 1x Novex™ NuPAGE™ LDS sample buffer (Art. No. NP0007, Invitrogen™) supplemented with 100 mM DTT and incubated for 10 min at 95°C.

Together with PageRuler™ Prestained Protein Ladder (10 to 180 kDa, Art. No. 26616, Thermo Scientific™), samples were separated on a Novex™ NuPAGE™ 4-12 % Bis-Tris Mini Protein Gel (Art. No. NP0323, Invitrogen™) in 1x Novex™ NuPAGE™ MOPS SDS Running Buffer (Art. No. NP0001, Invitrogen™) at 50 mA. Afterwards, proteins were

transferred on an Immobilon™-P Membran (PVDF, 0.45 µm, Art. No. IPVH00010, Merck Millipore) for 16 h at 15 V using a Mini Trans-Blot® Cell (Art. No. 1703930, Bio-Rad) and 1x NuPAGE™ Transfer Buffer (Art. No NP0006, Invitrogen™) supplemented with 20 % methanol. Following incubation in 1x PBS supplemented with 5 % skim milk and 0.05 % Tween®20 for 1 h, the PVDF membrane was occasionally cut according to the molecular weight of the proteins of interest. Each part was incubated in 1x PBS supplemented with 0.5 % skim milk, 0.05 % Tween®20 and the primary antibody (1:5,000 Monoclonal ANTI-FLAG® M2, Art. No. F3165, Sigma-Aldrich® / 1:1,000 Myc-Tag (9B11) Mouse mAb, Art. No. 2276, Cell Signaling Technology® / 1:5,000 anti-Histone H3, Art. No. H0164, Sigma-Aldrich® / 1:1,000 GFP (B-2), Art. No. sc-9996, Santa Cruz Biotechnology® / 1:5,000 β-Actin (D6A8), Art. No. 8457, Cell Signaling Technology® / 1:10,000 Monoclonal Anti-α-Tubulin, Art. No. T6074, Sigma-Aldrich®) for 1 h, followed by three washes with 1x PBS supplemented with 0.05 % Tween®20 (hereinafter referred to as 0.05 % PBS-T) for 10 min each, one hour incubation in 0.05 % PBS-T supplemented with the secondary antibody (1:10,000 anti-mouse IgG, HRP-linked antibody, Art. No. 7076, Cell Signaling Technology® / 1:10,000 anti-rabbit IgG, HRP-linked antibody, Art. No. 7074, Cell Signaling Technology®) and three final washes with 0.05 % PBS-T for 10 min each. Chemiluminescence detection was performed using Amersham™ ECL Select™ Western Blotting Detection Reagent (Art. No. RPN2235, GE Healthcare) and a ChemiDoc™ XRS+ System (Art. No. 1708265, Bio-Rad).

Mass spectrometry and proteome comparison

IP samples resuspended in Novex™ NuPAGE™ LDS sample buffer (Art. No. NP0007, Invitrogen™) were incubated at 70°C for 10 min and separated on a Novex™ NuPAGE™ 4-12 % Bis-Tris Mini Protein Gel (Art. No. NP0321, Invitrogen™) in 1x Novex™ NuPAGE™ MOPS SDS Running Buffer (Art. No. NP0001, Invitrogen™) at 180 V for 10 min. After separation the samples were processed by in-gel digest as previously described (Kappei et al., 2013; Shevchenko et al., 2007). Following protein digest, the peptides were desalted using a C18 StageTip (Rappsilber et al., 2007). For measurement the digested peptides were separated on a 25 cm reverse-phase capillary (75 µm inner diameter) packed with Reprosil C18 material (Dr. Maisch GmbH). Elution was carried out along a two hour gradient of 2 to 40 % of a mixture of 80 % acetonitrile/0.5 % formic acid with the EASY-nLC 1000 system (Art. No. LC120, Thermo Scientific™). A Q Exactive™ Plus mass spectrometer (Thermo Scientific™) operated with a Top10 data-dependent MS/MS acquisition method per full scan was used for measurement (Bluhm et al., 2016).

Processing of the obtained results was performed with the MaxQuant software, version 1.5.2.8 against the Wormbase protein database (version WS263) for quantitation (Cox and Mann, 2008). The processed data was visualized with R® and R-Studio® using in-house scripts. The mass spectrometry proteomics data have been deposited to the ProteomeXchange Consortium via the PRIDE (Perez-Riverol et al., 2019) partner repository with the dataset identifier PXD019099. Mitochondrial and spermatid proteins were described in previous proteomic studies (Jing et al., 2009; Ma et al., 2014). Genes encoding ribosomal proteins were obtained from Wormbase (version WS275). Comparison of protein lists was visualized with Intervene (Khan and Mathelier, 2017).

RNA extraction, library preparation and sequencing

RNA of input and GFP::3xFLAG::WAGO-3 immunoprecipitation samples was extracted using TRIzol™ LS Reagenz (Art. No. 10296010, Invitrogen™) according to the manufacturer's instructions, and resuspended in nuclease-free water. RNA quality and quantity was assessed using the Bioanalyzer RNA 6000 Nano Kit (Art. No. 5067-1511, Agilent Technologies) and Qubit™ RNA BR Assay Kit (Art. No. Q10210, Invitrogen™), respectively.

RNA 5' Pyrophosphohydrolase (RppH) (Art. No. M0356S, New England BioLabs®) treatment was performed with a starting amount of 690 ng. After purification samples were quantified using the Qubit™ RNA HS Assay Kit (Art. No. Q32852, Invitrogen™). NGS library preparation was performed with NEXTFLEX® Small RNA-Seq Kit v3 (Bioo Scientific®) following Step A to Step G of the manufacturer's standard protocol (v16.06). Libraries were prepared with a starting amount ranging between 426 ng – 896 ng and amplified in 16 PCR cycles. Amplified libraries were purified by running an 8 % TBE gel and size-selected for 15 – 50 bp. Libraries were profiled in a High Sensitivity DNA Chip on a 2100 Bioanalyzer Instrument (Agilent Technologies) and quantified using the Qubit™ dsDNA HS Assay Kit (Art. No. Q32851, Invitrogen™), in a Qubit™ 2.0 Fluorometer (Invitrogen™). All samples were pooled in equimolar ratio and sequenced on one NextSeq 500/550 Flowcell, SR for 1x 84 cycles plus seven cycles for the index read.

Read processing and mapping

Raw sequenced reads from high quality samples as assessed by FastQC were fed to Cutadapt (Martin, 2011) for adapter removal (-a TGGAATTCTCGGGTGCCAAGG -O 5 -m 26 -M 48) and low-quality reads were filtered out using the FASTX-Toolkit

(fastq_quality_filter, -q 20 -p 100 -Q 33). Unique molecule identifiers (UMIs) were used to remove PCR duplicates via an in-house script and were subsequently removed using seqtk (trimfq-l 4 – b 4). Finally, reads shorter than 15 nt were removed with seqtk (seq -L 15). Reads were aligned to the *C. elegans* genome assembly WBcel235 using bowtie v1.2.2 (Langmead et al., 2009) (–phred33-quals –tryhard –best –strata –chunkmbs 256 -v 2 -M 1).

Small RNA classification and target identification

A custom GTF-file was created by adding transposons retrieved from Wormbase (PRJNA13758.WS264) to the Ensembl reference WBcel235.84. Small RNAs classes were then defined as: 21U-RNAs, 21 nucleotide long mapped reads that map sense to annotated piRNA loci; 22G-RNAs, mapped reads of lengths 20-23 nucleotides, with no 5' bias, and map antisense to protein-coding/pseudogenes/lincRNA/transposons; 26G-RNAs, mapped reads 26 nucleotides long and map antisense to annotated protein-coding/pseudogenes/lincRNA; miRNAs are 20-24 nt reads mapping sense to annotated miRNA loci; finally all mapped reads longer than 26 nucleotides were classed in a separate group. Read filtering was done with a python script (https://github.com/adomingues/filterReads/blob/master/filterReads/filterSmallRNAclasses.py) based on pysam v0.8.1 / htslib (Li et al., 2009), in combination with BEDTools intersect (Quinlan and Hall, 2010).

22G reads mapping to features in the custom annotation were counted using htseq-count v0.9.0 (Anders et al., 2015) (-s no -m intersection-nonempty). Differential targeting analysis was carried out in R® using DESeq2 (Love et al., 2014) with a strict cut-off for the adjusted p-value of 0.01. A cut-off for fold-change (IP versus input) was determined by fitting a Gaussian to the fold-change-distribution of reads mapping to miRNA, which are known not to bind WAGOs, and choosing the value that corresponds to a false discovery rate (FDR) of 5% for this RNA species; here log2-fold-change > 1.3.

Protein-coding target genes of WAGO-3 were compared to: i) protein-coding target genes of CSR-1 (Claycomb et al., 2009), ii) protein-coding target genes of siRNAs downregulated in *mut-16* mutant animals (Phillips et al., 2014), and iii) protein-coding target genes of sperm-derived 22G RNAs (Stoeckius et al., 2014). To determine germline expression, protein-coding target genes of WAGO-3 were compared to lists of genes expressed in the *C. elegans* germline of either *fem-3* or *fog-2* mutant animals (Ortiz et al.,

2014). Comparison of gene lists was visualized with Intervene (Khan and Mathelier, 2017).

22G RNA coverage on protein-coding genes

Coverage of 22Gs along targeted protein coding genes was visualized by i) creating bigwig tracks normalized to mapped non-structural reads (rRNA/tRNA/snoRNA/snRNA) * 1 million (RPM) using a combination of BEDTools (genomeCoverageBed -bg -scale -split) (Quinlan and Hall, 2010) followed by bedGraphToBigWig; ii) $\log_2$(IP/input) normalized tracks were created with deepTools v2.4.2 (Ramírez et al., 2014) (bigwigCompare –binSize 10 –ratio log2); iii) coverage for each gene was determine with deepTools (computeMatrix scale-regions --metagene --missingDataAsZero -b 250 -a 250 --regionBodyLength 2000 --binSize 50 --averageTypeBins median); and plots generated with plotProfile (--plotType se --averageType mean --perGroup) to scale and visualize 22G abundance along targeted genes.

Reads mapping to intronic, exonic, or untranslated regions were counted using a custom Python script. Reads mapping at exon-intron junctions were counted as 0.5 intronic and 0.5 exonic regardless of the spanned region.

Microscopy

For L4 larvae, adults and males, 20 – 30 animals were washed in a drop of 100 µl M9 buffer and subsequently transferred to a drop of 50 µl M9 buffer supplemented with 40 mM sodium azide on a coverslip. After 15 to 30 min, excess buffer was removed and a glass slide containing a freshly made agarose pad (2 % (w/v) in water) was placed on top of the coverslip. For imaging embryos, adult hermaphrodites were washed and dissected in M9 buffer before mounting. To image sperm, L4 males were singled from hermaphrodites, grown over night, washed and dissected in SMG buffer (50 mM HEPES pH 7.5, 50 mM NaCl, 25 mM KCl, 5 mM $CaCl_2$, and 1 mM $MgSO_4$, 10 mM glucose) by cutting near the vas deferens. Animals and sperm were immediately imaged using a TCS SP5 Leica confocal microscope equipped with a HCX PL APO 63x water objective (NA 1.2) or HCX PL APO CS 40x oil objective (NA 1.3). Fluorescence emission was detected by either photomultiplier tubes (PMTs) or hybrid detectors (HyDs). Depending on the experiment, SMG buffer was supplemented with 1:2,000 Hoechst33342 (Art. No. H1399, Invitrogen™), 200 nM MitoTracker® Green FM (Art. No. M7514, Invitrogen™) or

1,6-hexanediol (Art. No. 240117, Sigma-Aldrich®), and sperm were imaged after 30 min incubation. To score the expression of a germline-specific mCherry::H2B transgene (*mjSi22*), we used a Leica DM6000 B research microscope equipped with a HC PL Fluotar 20x dry objective (NA 0.5). Images were processed using Fiji and the following figures were deconvolved using the Huygens Remote Manager v3.6: Fig. 2, A-C, Fig. 11, A-B, Fig. 12, A-D, Fig. 13, A-C, Fig. 19, A-B, Fig. 22D, Fig. 23, Fig. 29, A-B and D, Fig. 30A, Fig. 31A and C-D.

Live imaging

Time series of spermatocytes expressing GFP::3xFLAG::WAGO-3 were acquired with a fluorescence spinning disk confocal microscope from Visitron Systems (VisiSope 5Elements) based on a Nikon Ti-2E stand and a spinning disk from Yokogawa (CSU-W, 50 µm pinhole) controlled by the VisiView® software. The microscope was equipped with a 60x plan apochromatic water immersion objective (CFI Plan Apo VC, NA 1.2), a twofold magnification lens in front of the sCMOS camera (BSI, Photometrics), and a stage-top incubation chamber for live imaging (20°C, ambient CO_2). The sample was excited by an argon laser at λ_{ex} = 488 nm (200 mW, power set to 20 %) and the emission was detected in a range of λ_{em} = 500 - 550 nm (ET525/50m, Chroma).

FRAP

FRAP measurements were performed on a TCS SP5 Leica confocal microscope equipped with a FRAP-booster and a HCX PL APO 63x water objective (NA 1.2). An entire granule was bleached in a fixed region of interest (ROI) (0.9 µm diameter), while two additional control ROIs of same size were used to detect fluorescence emission of an unbleached granule and background signal, respectively. Five pre-bleach frames were recorded (5x 0.374 s/frame), followed by two bleach frames (2x 0.374 s/frame), and 3 sets of post-bleach frames (10x 0.5 s/frame, 10x 5 s/frame, 15x 10 s/frame). Data analysis including full scale normalization and curve fitting using a double term exponential equation was performed using easyFRAP-web (Koulouras et al., 2018).

Online resources

All databases, predictors and other online resources are listed in Table 8.

Table 8 | List of online resources used in this study.

Name	URL	Reference
BLAST®	https://blast.ncbi.nlm.nih.gov/Blast.cgi	(Camacho et al., 2009)
Clustal Omega	https://www.ebi.ac.uk/Tools/msa/clustalo/	(Madeira et al., 2019)
CRISPOR	http://crispor.tefor.net/	(Haeussler et al., 2016)
CSS-Palm 2.0	http://www.csspalm.biocuckoo.org/online.php	(Ren et al., 2008)
easyFRAP-web	https://easyfrap.vmnet.upatras.gr/	(Koulouras et al., 2018)
EggNOG 4.5.1	http://eggnog45.embl.de/#/app/home	(Huerta-Cepas et al., 2016b)
Ensembl GeneTree	http://www.ensembl.org/index.html	(Yates et al., 2019)
ETE 3	https://www.genome.jp/tools-bin/ete	(Huerta-Cepas et al., 2016a)
FastTree	http://microbesonline.org/fasttree/	(Price et al., 2009)
GPS-Lipid	http://lipid.biocuckoo.org/webserver.php	(Xie et al., 2016)
HHpred	https://toolkit.tuebingen.mpg.de/tools/hhpred	(Zimmermann et al., 2018)
HRM v3.6	https://huygens.imb.uni-mainz.de/login.php	-
IDT™ OligoAnalyzer	https://eu.idtdna.com/calc/analyzer	-
InParaniod 8	http://inparanoid.sbc.su.se/cgi-bin/index.cgi	(Sonnhammer and Östlund, 2015)
InterPro	https://www.ebi.ac.uk/interpro/	(Mitchell et al., 2019)
Intervene	https://asntech.shinyapps.io/intervene/	(Khan and Mathelier, 2017)
Jpred4	https://www.compbio.dundee.ac.uk/jpred/index.html	(Drozdetskiy et al., 2015)
MobiDB 3.0	https://mobidb.bio.unipd.it/	(Piovesan et al., 2018)
NetPhos 3.1	http://www.cbs.dtu.dk/services/NetPhos/	(Blom et al., 1999)
OMA Browser	https://omabrowser.org/oma/home/	(Altenhoff et al., 2018)

OrthoDB v10.1	https://www.orthodb.org/	(Kriventseva et al., 2019)
Pfam 33.1	https://pfam.xfam.org/	(El-Gebali et al., 2019)
PONDR®	http://www.pondr.com/	-
Primer3web v4.1.0	http://primer3.ut.ee/	(Untergasser et al., 2012)
SMART	http://smart.embl-heidelberg.de/	(Letunic and Bork, 2018)
SWISS-MODEL Repository	https://swissmodel.expasy.org/	(Bienert et al., 2017)
UniProt	https://www.uniprot.org/	(Bateman, 2019)
WatCut	http://watcut.uwaterloo.ca/	-
Worm ORFeome v3.1	http://worfdb.dfci.harvard.edu/	(Lamesch et al., 2004)
Wormatlas	https://www.wormatlas.org/	-
Wormbase	https://wormbase.org/	-
Wormbook	http://wormbook.org/	-
Wormbuilder	http://www.wormbuilder.org/	-

Results

WAGO-3 is a germline-specific Argonaute protein of *C. elegans*

Although WAGO-3 was the first Argonaute protein of *C. elegans* that has been shown to be involved in transposon silencing (Robert et al., 2005; Vastenhouw et al., 2003), its molecular function and biological relevance among the semi-redundant WAGO clade remains largely unknown. In order to investigate this particular member of the Argonaute family, we inserted a *gfp::3xflag* encoding sequence directly downstream of the endogenous start codon of *wago-3* using CRISPR/Cas9-mediated genome editing. At first, we performed fluorescence microscopy to determine the expression pattern of GFP::3xFLAG::WAGO-3. We imaged *C. elegans* hermaphrodites of different developmental stages and found that GFP::3xFLAG::WAGO-3 is specifically and globally expressed throughout germline development. In early L1 larvae, GFP::3xFLAG::WAGO-3 was detected in the two primordial germ cells Z2 and Z3 (**Figure 7A**). After germline proliferation, GFP::3xFLAG::WAGO-3 was evenly detected in both gonads of L4 larvae (**Figure 7B**). Thus, we conclude that WAGO-3 is a germ cell-specific Argonaute protein of *C. elegans*.

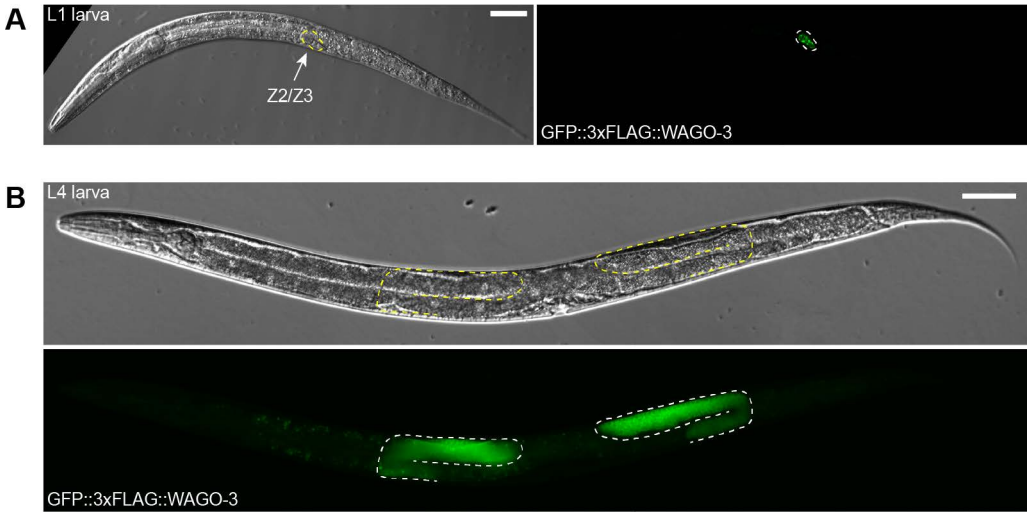

Figure 7 | WAGO-3 is globally expressed throughout germline development. A-B, Fluorescence micrographs of a L1 (A) and L4 (B) larva expressing GFP::3xFLAG::WAGO-3. Primordial germ cells (A) and gonads (B) are outlined by dashed lines. Scale bars: 20 µm (A), 50 µm (B)

WAGO-3 localizes to P granules and is present in mature sperm

The subcellular localization of proteins is crucial for their molecular function and provides context to understand dynamics between subcellular compartments. In *C. elegans* germ cells, the perinuclear, non-membranous organelle called P granule is home to RNAi–related pathways responsible for mRNA surveillance, transposon silencing and fertility (Marnik and Updike, 2019). PGL-1 has been identified to play a crucial role in P granule assembly and was frequently used as general marker protein for microscopic analyses (Kawasaki et al., 1998, 2004). Thus, we inserted an *mTagRfp-t* encoding sequence directly upstream of the endogenous stop codon of *pgl-1* using CRISPR/Cas9-mediated genome editing. Additionally, we also inserted a single-copy *pgl-1::mTagBfp* transgene on chromosome II using MosSCI transgenesis. To minimize potential artefacts arising from ectopic expression, we used promoter and 3'UTR sequences of the endogenous *pgl-1* gene to control the expression of the MosSCI transgene (Lamesch et al., 2004).

We found that GFP::3xFLAG::WAGO-3 co-localized with PGL-1::mTagRFP-T to perinuclear P granules in naïve germ cells and early oocytes, before P granules become progressively more cytoplasmic during oogenesis (**Figure 8A**) (Wang and Seydoux, 2014). Notably, we also found strong GFP::3xFLAG::WAGO-3 signal within the spermatheca, where spermatozoa are stored (**Figure 8A**). This finding indicates that WAGO-3 is expressed during spermatogenesis and maintained in mature sperm, revealing the presence of WAGO-3 in both male and female gametes.

In addition to the described larval and adult stages, we also detected parentally deposited GFP::3xFLAG::WAGO-3 in embryos. GFP::3xFLAG::WAGO-3 always co-localized with either PGL-1::mTagBFP or PGL-1::mTagRFP-T within the transcriptionally quiescent P cell lineage, starting with the P1 cell in 2-cell stage embryos (**Figure 8B**) and eventually reaching the primordial germ cells Z2 and Z3 in gastrula-stage embryos (**Figure 8C**). This observation indicates an inheritance of WAGO-3 via parental gametes. Notably, GFP::3xFLAG::WAGO-3 showed a rather complete co-localization with PGL-1::mTagRFP-T at the nuclear periphery of primordial germ cells, suggesting that WAGO-3 does not likely localize to Z granules during embryogenesis.

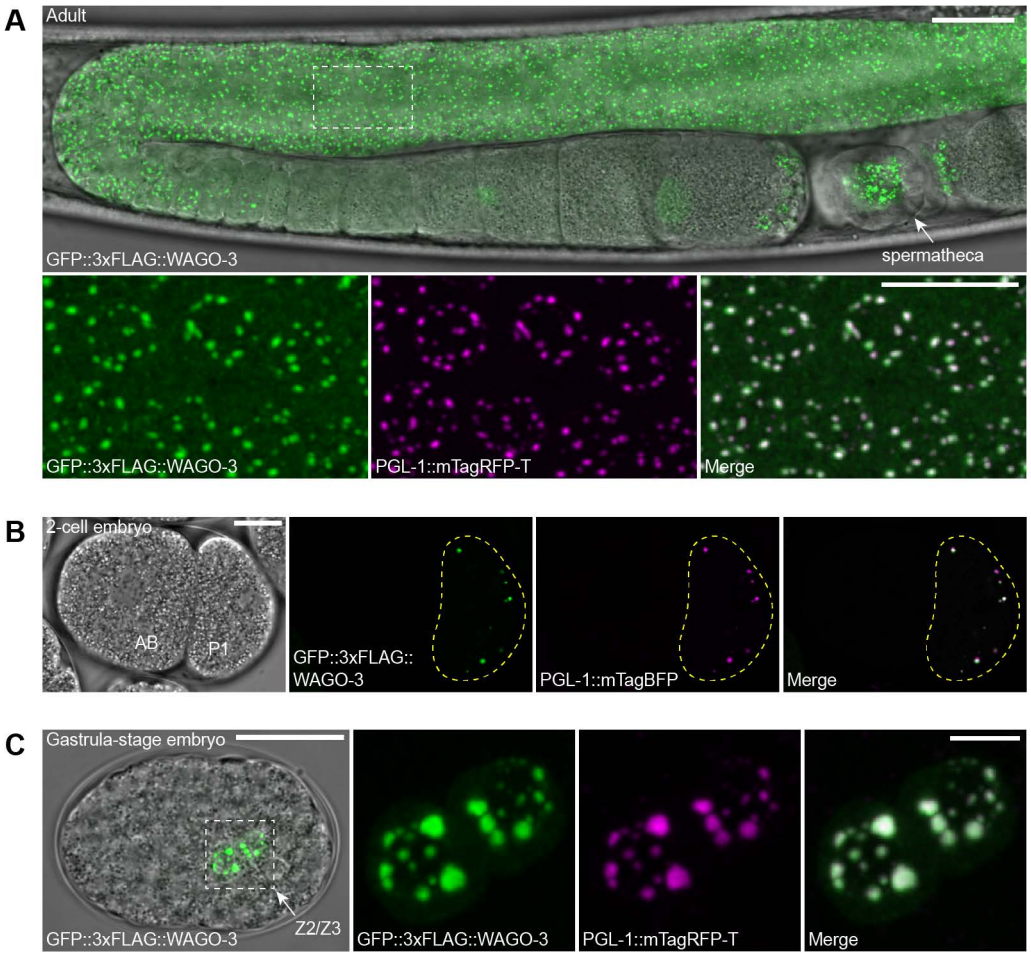

Figure 8 | WAGO-3 co-localizes with PGL-1 to perinuclear condensates and is detectable within the spermatheca. A, Confocal maximum intensity projections showing the gonad of an adult hermaphrodite expressing GFP::3xFLAG::WAGO-3 and PGL-1::mTagRFP-T. Zoom shows perinuclear co-localization of GFP::3xFLAG::WAGO-3 and PGL-1::mTagRFP-T in meiotic germ cells. B-C, Confocal micrographs (B) and maximum intensity projections (C) of parentally deposited GFP::3xFLAG::WAGO-3 in a 2-cell stage (B) and gastrula-stage (C) embryo. The P1 cell is outlined by a yellow dashed line. Zoom shows perinuclear co-localization of GFP::3xFLAG::WAGO-3 and PGL-1::mTagRFP-T in the primordial germ cells (C). Scale bars: 20 µm (A, gonad), 10 µm (A, zoom), 10 µm (B, 2-cell embryo), 20 µm (C, gastrula-stage embryo), 4 µm (C, zoom)

The *Mutator* complex affects the stability and perinuclear localization of WAGO-3

Several classes of small, non-coding RNAs can act as co-factors of Argonaute proteins to guide target transcript recognition via base-pairing interactions(Ghildiyal and Zamore, 2009). Next to target recognition, the association of Argonaute proteins with their cognate small, non-coding RNAs was shown to universally promote Argonaute stability (Derrien et al., 2012; Johnston et al., 2010; Kobayashi et al., 2019a, 2019b; Martinez and Gregory, 2013; Smibert et al., 2013; Suzuki et al., 2009). Given that WAGO proteins are

believed to be associated with *Mutator*-dependent 22G RNAs, we addressed the effect of various RNAi-related factors on GFP::3xFLAG::WAGO-3 stability. To achieve this, we introduced selected mutant alleles into our genome-edited strain. These alleles comprised the primary Argonaute protein PRG-1, the *Mutator* complex components MUT-7 and MUT-16, and three RNA-dependent RNA polymerases (RdRPs) named RRF-1, RRF-2 and RRF-3. Given that the fourth RdRP, called EGO-1, is essential for viability (Smardon et al., 2000), we excluded this gene in our analysis. While PRG-1 is required for 21U RNA biogenesis and function (Bagijn et al., 2012; Batista et al., 2008; Das et al., 2008; Lee et al., 2012), loss of MUT-7 or MUT-16 causes global depletion of *Mutator*-dependent 22G RNAs (Phillips et al., 2012; Zhang et al., 2011). RRF-1 has a partially redundant role in *Mutator*-dependent 22G RNA biogenesis, as EGO-1 can compensate loss of RRF-1 (Gu et al., 2009). RRF-3 is required for 26G RNA biogenesis, a class of primary siRNAs, which was shown to trigger *Mutator*-dependent 22G RNA production (Conine et al., 2010; Gent et al., 2009, 2010; Han et al., 2009; Vasale et al., 2010). In contrast, the molecular function of RRF-2 remains elusive. However, its gene annotation as 'pseudogene' was recently changed to 'protein-coding' (Wormbase version WS276), suggesting a role of RRF-2 in RNAi-related pathways. We collected late-L4 stage hermaphrodites expressing GFP::3xFLAG::WAGO-3 in the individual mutant backgrounds and probed for the FLAG tag via Western detection. First, loss of PRG-1 does not globally affect GFP::3xFLAG::WAGO-3 stability within the first three homozygous generations (**Figure 9A**), suggesting a 21U RNA independent loading of WAGO-3. Similarly, loss of any of the RRF proteins did not show any apparent effect on GFP::3xFLAG::WAGO-3 stability (**Figure 9B**), indicating a (semi-)redundant role of RRF proteins in WAGO-3 loading, consistent with previous studies (Gu et al., 2009). In contrast, both MUT-7 and MUT-16 were found to be required for GFP::3xFLAG::WAGO-3 stability, as Western detection showed a dramatically reduced protein abundance of GFP::3xFLAG::WAGO-3, substantiating that *Mutator*-dependent 22G RNA biogenesis is required for WAGO-3 stability. During our Western detections of GFP::3xFLAG::WAGO-3, we noticed a second band of lower molecular weight when probing with anti-FLAG antibodies, but not when probing with anti-GFP antibodies (**Figure 9B**). Hypothesized that this observation was due to proteolytic cleavage of the fusion-protein between the GFP and the 3xFLAG tag, animals were directly picked and boiled in LDS loading buffer. This procedure resulted in the absence of the second, lower molecular weight band (**Figure 9A**), confirming the idea that proteolysis in the extracts is responsible for the additional band seen in **Figure 9B**.

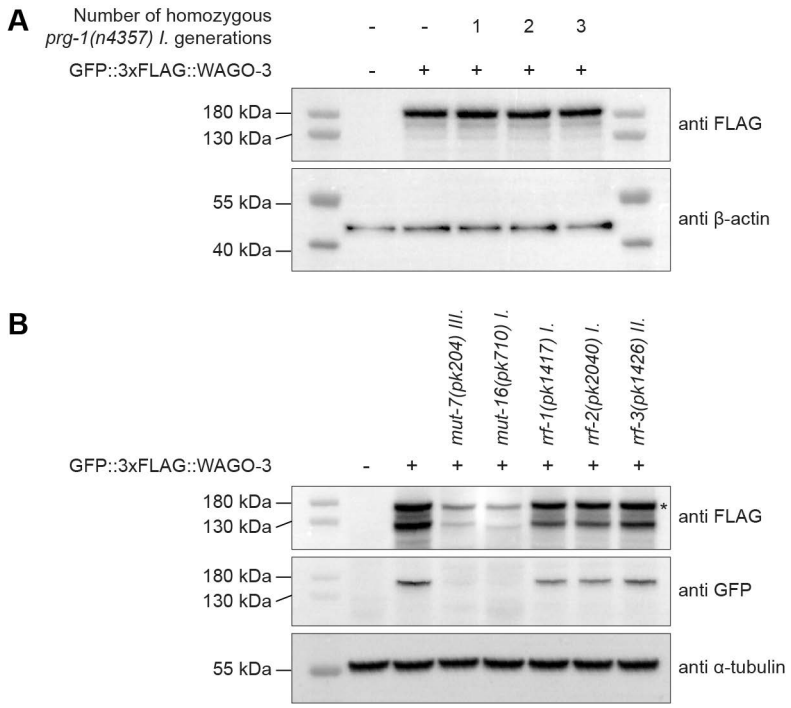

Figure 9 | *Mutator* genes affect WAGO-3 stability. A-B, Whole-worm extracts of late-L4 stage hermaphrodites were separated via SDS-PAGE, followed by Western transfer and chemiluminescence detection of GFP::3xFLAG::WAGO-3. Extracts were obtained by boiling 50 hermaphrodites per strain in LDS sample buffer (A), or by collecting synchronized animals and subsequent normalization of extracts to total protein concentration (B). The asterisk marks the predicted full-length GFP::3xFLAG::WAGO-3 fusion-protein (B). α-tubulin (A) and β-actin (B) were used a loading control.

MUT-7 and MUT-16 were shown to be components of the *Mutator* complex, which is responsible for *Mutator*-dependent 22G RNA biogenesis (Phillips et al., 2012; Uebel et al., 2018). Although loss of MUT-7 causes global depletion of *Mutator*-dependent 22G RNAs, the *Mutator* complex was shown to partially assemble at the nuclear periphery (Uebel et al., 2018; Zhang et al., 2011). In contrast, absence of the nucleating protein MUT-16 results in both lack of *Mutator*-dependent 22G RNAs as well as any detectable *Mutator* complex assembly (Phillips et al., 2012). So far, it remains elusive how P granule-localized WAGO proteins are loaded with their 22G RNA co-factors, as their biogenesis is spatially separated from P granules.

Given the destabilization of GFP::3xFLAG::WAGO-3 in absence of a fully functional *Mutator* complex, we performed confocal microscopy in order to identify changes in the subcellular localization of GFP::3xFLAG::WAGO-3. Loss of either MUT-7 or MUT-16 causes absence of GFP::3xFLAG::WAGO-3 during meiosis and gametogenesis. The only cytoplasmic signals could still be detected in the distal region of the gonad containing mitotically active germ cells (**Figure 10A**). Closer investigation of mitotic germ cells revealed striking differences in the subcellular localization of GFP::3xFLAG::WAGO-3.

While no perinuclear localization of GFP::3xFLAG::WAGO-3 was detected in absence of MUT-16 (**Figure 10B**), a few perinuclear foci could still be identified in *mut-7* mutant hermaphrodites. The remaining GFP::3xFLAG::WAGO-3 foci were reduced in number and co-localized with some, but not all PGL-1::mTagBFP foci (**Figure 10B**). The observed pattern, however, resembled the described localization of the *Mutator* complex, which is most concentrated in the mitotic region of the germline (Phillips et al., 2012). In order to visualize the *Mutator* complex, we inserted an *mut-14::mTagBfp* transgene on chromosome IV using MosSCI transgenesis. Strikingly, we found that perinuclear GFP::3xFLAG::WAGO-3 foci co-localized with all MUT-14::mTagBFP foci in *mut-7* mutant animals. This finding suggests that WAGO-3 stays in the *Mutator* complex when 22G RNAs are absent.

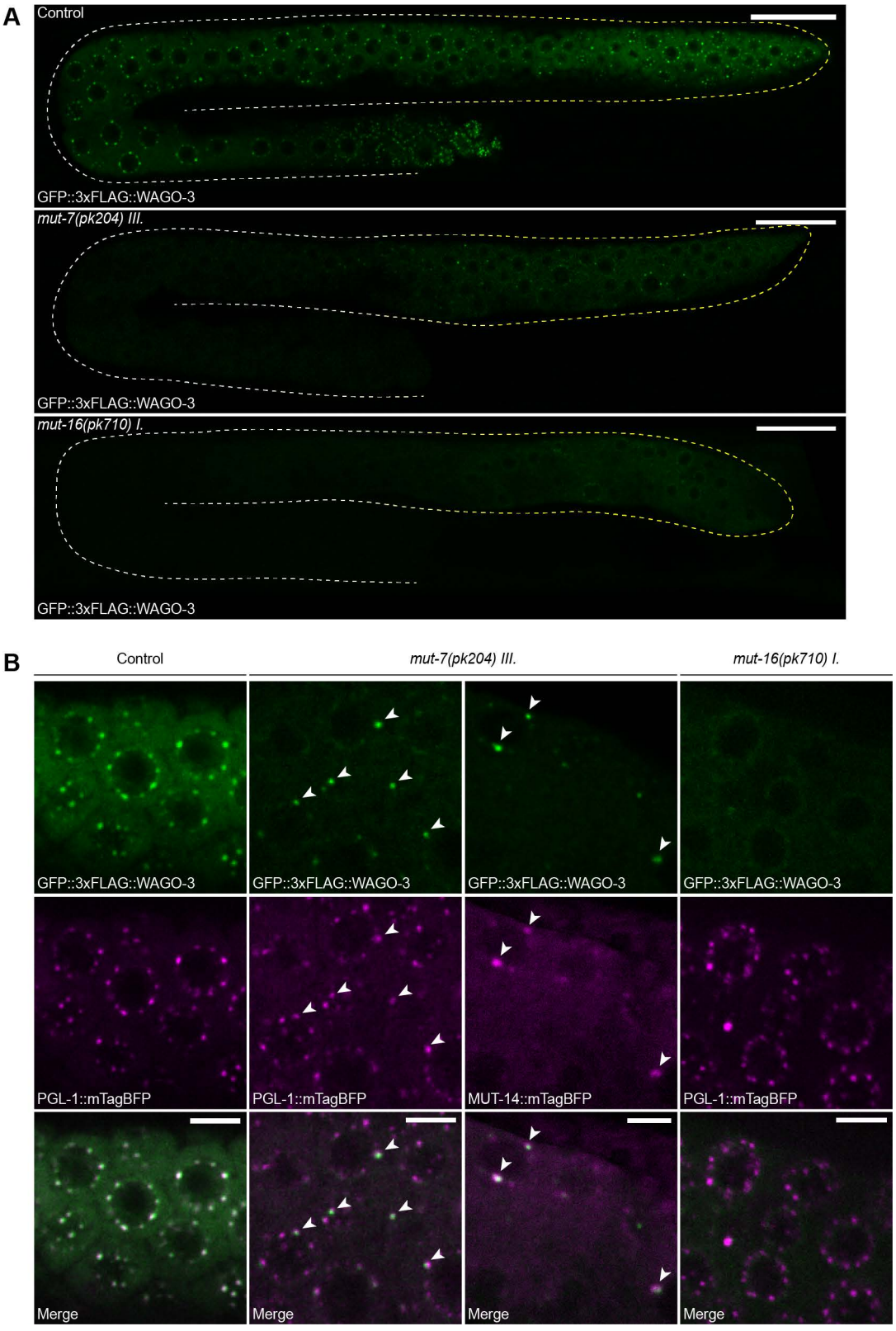

Figure 10 | *Mutator* genes are required for perinuclear distribution of WAGO-3. A, Confocal micrographs showing gonads of L4 larvae expressing GFP::3xFLAG::WAGO-3 in absence of either MUT-7 or MUT-16. Gonads are outlined by a dashed line, with the yellow part highlighting the mitotic region. B, Confocal micrographs showing localization of GFP::3xFLAG::WAGO-3 to P granules or *Mutator* foci in mitotic germ cells of indicated mutants. PGL-1::mTagBFP and MUT-14::mTagBFP fusion-proteins serve as P granule and *Mutator* foci marker, respectively. Scale bars: 20 µm (A), 4 µm (B)

The *Mutator* complex ensures proper WAGO-3 loading

Intrigued by our microscopy results, we next sought out to determine the endogenous target genes of WAGO-3 by identifying WAGO-3 associated small RNAs. Following immunoprecipitation of GFP::3xFLAG::WAGO-3 from adult animals, we cloned and sequences small RNAs from both input and anti-FLAG immunoprecipitation samples. We performed this experiment in five different genetic backgrounds to assess the small RNA association of WAGO-3 in absence of either MUT-7 or any of the three RRF proteins.

We found no obvious differences in the global small RNA profile of individual *rrf* mutants (**Figure 11, A and B**). As expected, however, a global depletion of 22G RNAs was observed in *mut-7* mutant animals (**Figure 11, A and B**), confirming previous studies (de Albuquerque et al., 2015; Zhang et al., 2011). Independently of the genetic background, we found that GFP::3xFLAG::WAGO-3 is predominantly associated with small RNAs that have characteristics of 22G RNAs. None of the selected mutants caused GFP::3xFLAG::WAGO-3 to be associated with any other small RNA class than 22G RNAs (**Figure 11, A and B**).

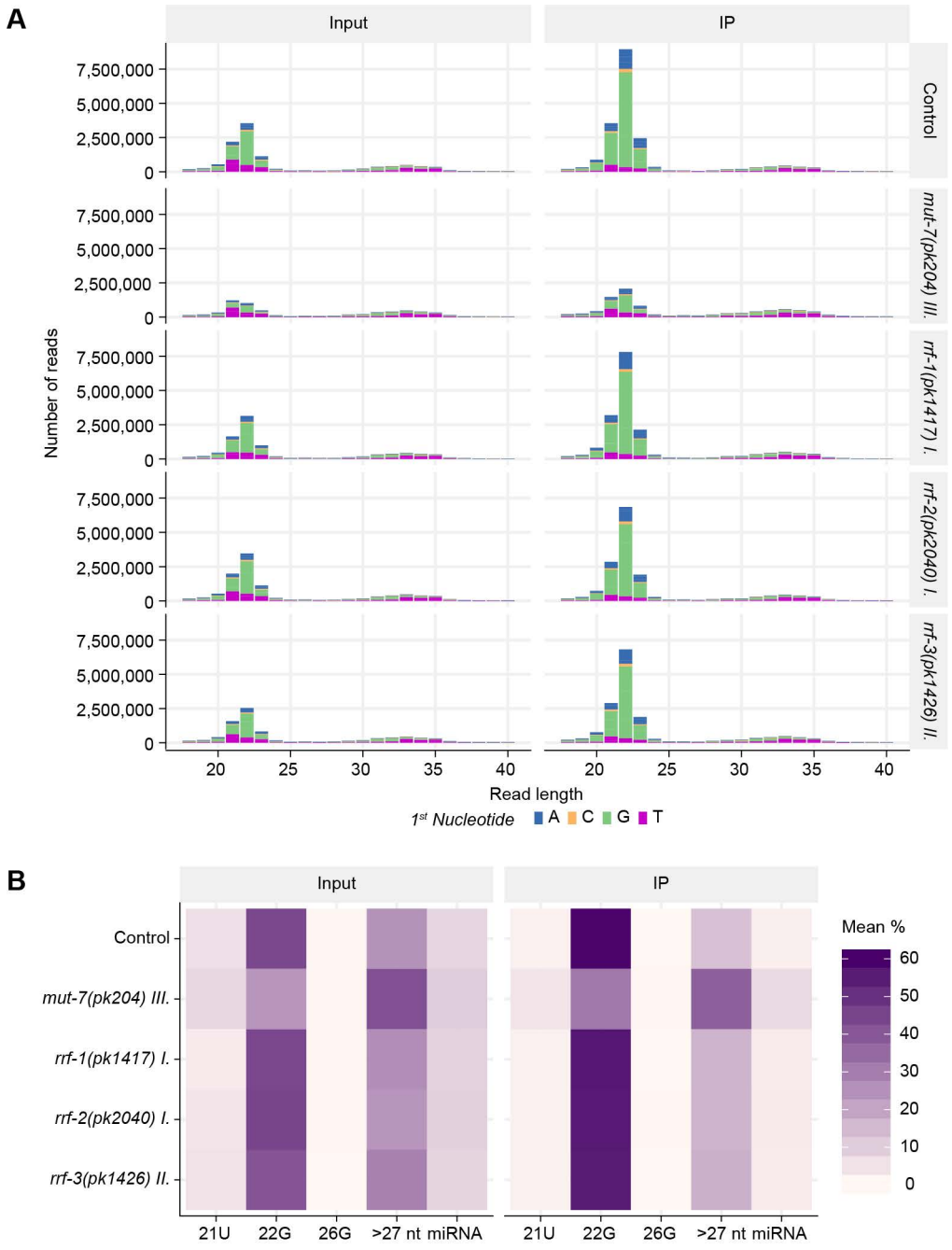

Figure 11 | WAGO-3 is associated to 22G RNAs. A, Read length distribution and first nucleotide bias of indicated small RNA libraries of GFP::3xFLAG::WAGO-3 RIP experiments. B, Mean abundance of defined small RNA populations in the indicated small RNA libraries.

Based on sequence complementary and defined thresholds ($\log_2$(fold change) > 1.3, FDR ≤ 0.01), we identified 2166 WAGO-3 target genes, which were grouped in four categories: non-coding RNA (ncRNA), pseudogene, transposon and protein-coding. Notably, WAGO-3 mostly targeted protein-coding genes (**Figure 12A**), although their genomic coverage is rather low (9 %; 1794/19999). The number of WAGO target genes was significantly reduced when compared to any of the selected mutants (**Figure 12A**).

Although *mut-7* mutant animals lack the majority of *Mutator*-dependent 22G RNAs, immunoprecipitation of GFP::3xFLAG::WAGO-3 still enriched a population of remaining 22G RNAs targeting a set of genes, which is comparable to the other examined mutants in terms of total number (**Figure 12A**). Next, we compared the distribution of our four categories between the mutant backgrounds and the control. We found that loss of MUT-7 caused a significantly changed distribution, as WAGO-3 targeted more protein-coding genes. In contrast, all of the *rrf* mutants displayed a similar distribution of WAGO-3 target genes between the four categories **(Figure 12A**). Finally, we compared the individual WAGO-3 target genes between the five genetic conditions. This revealed minor changes with regard to the RdRP mutants. About 500 WAGO-3 target genes were missing in each *rrf* mutant, of which 248 genes were mutually absent (**Figure 12, B-D**). In contrast, loss of MUT-7 clearly altered the target repertoire of WAGO-3 (**Figure 12E**).

We analyzed the differences in *mut-7* mutant animals in more detail. First, we focused on protein-coding genes. WAGO-3 was found to target both germline-expressed and soma-expressed genes with a slight, but significant bias towards germline-expressed genes (**Figure 12F**). Interestingly, loss of MUT-7 further shifted the target repertoire towards germline-expressed genes (**Figure 12F**). Among those, WAGO-3 displayed a small, but significant preference for spermatogenic transcripts over oogenic transcripts, with *mut-7* mutants altering this bias towards gender-neutrally expressed genes (**Figure 12G**).

Next, we compared the protein-coding target genes of WAGO-3 with CSR-1 and the *Mutator* complex. As expected, WAGO-3 covered the vast majority of known *Mutator* complex targets (**Figure 12H**), which were identified by small RNA sequencing of *mut-16* mutant animals (Phillips et al., 2014). In contrast, and consistent with the proposed model of CSR-1, we found that WAGO-3 and CSR-1 target genes were almost mutually exclusive (**Figure 12H**) (Claycomb et al., 2009). Notably, loss of MUT-7 caused WAGO-3 to be associated with more 22G RNAs from CSR-1 targets. Although statistically significant, the increase in number was found to be rather mild, as the vast majority of WAGO-3 and CSR-1 targeted protein-coding genes were still mutually exclusive (**Figure 12H**). This observation clearly indicates a separation of the WAGO and CSR pathway in terms of small RNA association, even in 22G RNA-defective animals.

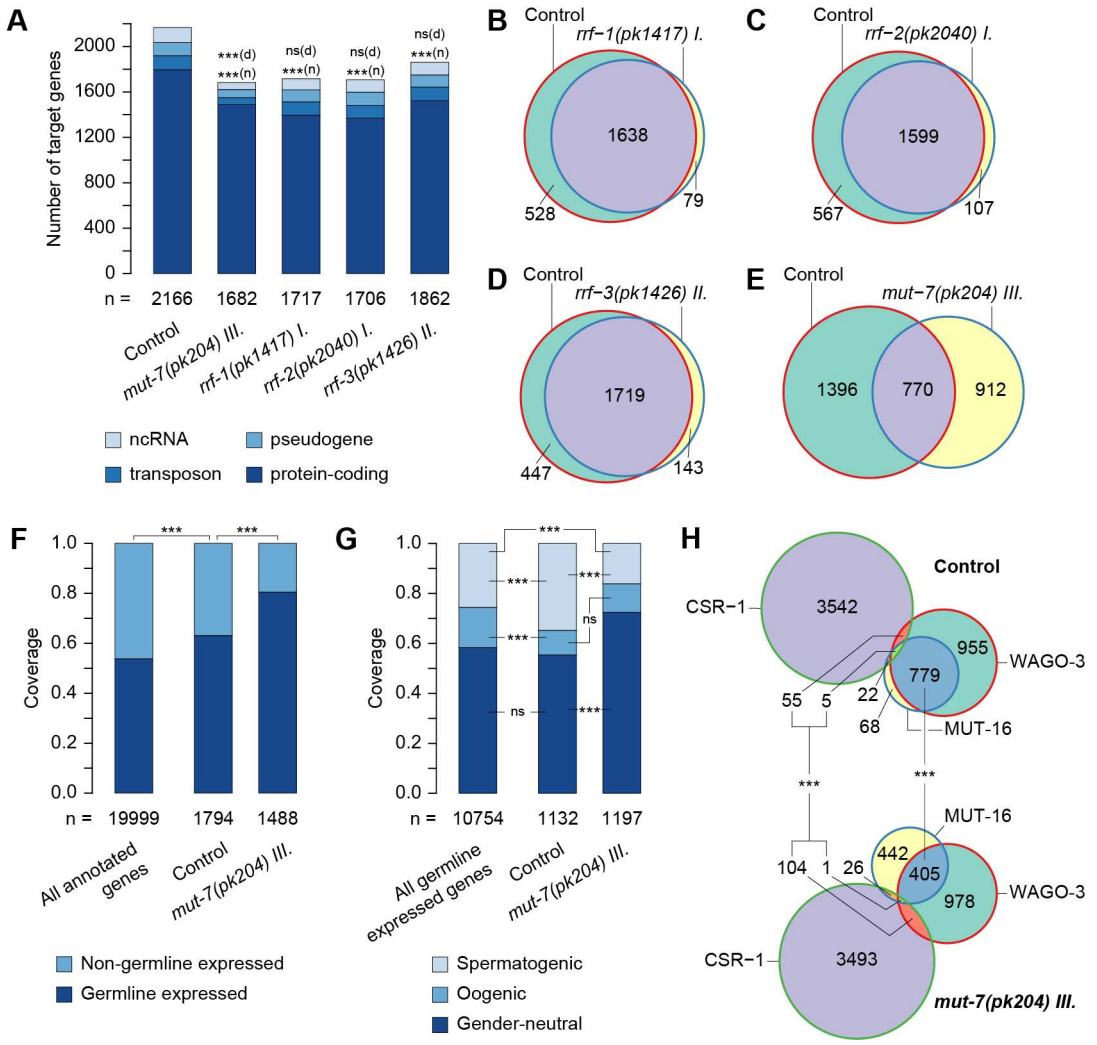

Figure 12 | Loss of MUT-7 alters the spectrum of WAGO-3 associated 22G RNAs. A, Total number (n) and distribution (d) of GFP::3xFLAG::WAGO-3 target genes in indicated mutants. Target genes were grouped in the following categories: non-coding RNA (ncRNA), pseudogene, transposon, protein-coding. B-E, Venn diagrams showing overlap of GFP::3xFLAG::WAGO-3 target genes in absence of RRF-1 (B), RRF-2 (C), RRF-3 (D) and MUT-7(E). F-G, Classification of GFP::3xFLAG::WAGO-3 targeted protein-coding genes according to germline expression (F) and gamete-specific expression (G). H, Venn diagrams showing overlap of protein-coding target genes between WAGO-3, CSR-1 and the *Mutator* complex in either presence or absence of MUT-7. P-values were calculated with a chi-square test (A, F, G, H). ***: $p \leq 0.001$, ns: $p > 0.05$

We also determined the 22G RNA targeting profile of WAGO-3 targeted protein-coding genes. When analyzing the 22G RNA coverage on gene features, we found that the vast majority of WAGO-3 associated 22G RNAs targeted exonic sequences in both wild-type and *mut-7* mutant animals (**Figure 13, A and B**). While we found a minor fraction of 22G RNAs targeting 5' UTRs and introns in both data sets, we noticed an increased targeting of 3' UTRs in absence of MUT-7. Since GFP::3xFLAG::WAGO-3 was not detected in the

nucleus, the low intron coverage may be due to alternative splicing events rather than targeting precursor transcripts.

A recent study characterized the 22G RNA distribution along the gene length of both WAGO and CSR-1 targets (Ishidate et al., 2018). While WAGO proteins cover the whole gene body, CSR-1 was found to display a preference for the 3' end of target genes. Consistently, we found that WAGO-3 associated 22G RNA covered the whole target gene body (**Figure 13C**), even in absence of MUT-7 (**Figure 13D**). The 22G RNA distribution in *mut-7* mutants, however, displayed on intermediate profile between the previously reported 22G RNA distributions on WAGO and CSR-1 targets.

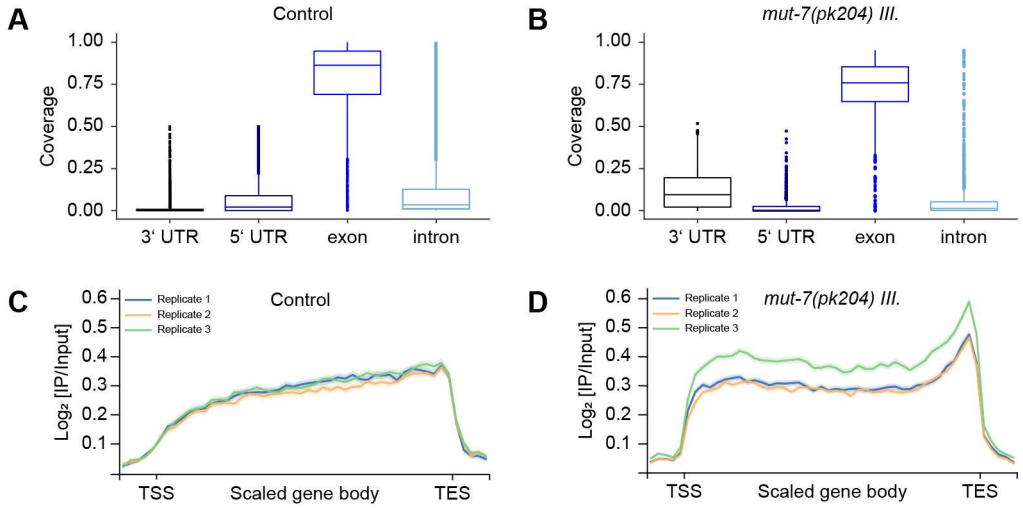

Figure 13 | WAGO-3 associated 22G RNAs target exonic sequences along the whole target body. A-D, Feature coverage (A-B) and metagene analysis (C-D) of 22G RNA reads mapping to protein-coding target genes of GFP::3xFLAG::WAGO-3 in either presence (A, C) or absence (B, D) of MUT-7. For the metagene analysis, gene body lengths were scaled between transcription start site (TSS) and transcription end site (TES). 200 nucleotide regions upstream of the TSS and downstream of the TES were included in the analyses. Shading around each line represents the standard error of each bin.

Finally, we focused on WAGO-3 targeted transposons. Notably, nearly 70 % of all annotated transposable elements covering every transposon class were represented in WAGO-3 associated 22G RNAs (69 %; 124/179) (**Figure 14, A and B**), consistent with its role in TE silencing (Robert et al., 2005; Vastenhouw et al., 2003). Loss of MUT-7, however, resulted in a significantly decreased transposon coverage of WAGO-3 (**Figure 14A**), without displaying a bias towards a specific transposon class (**Figure 14B**). Transposable elements that were still targeted by WAGO-3 represent a subset of transposable elements typically targeted by WAGO-3 (**Figure 14C**). In contrast,

loss of either RRF-1, RRF-2 or RRF-3 did not cause a significant change in the transposon coverage or targeting preference of WAGO-3 (**Figure 14, A and D-F**).

Taken together, none of the individual RdRPs was specifically required for WAGO-3 loading, but is likely acting in a (semi-)redundant manner with other RdRPs. MUT-7, however, was found to be required to ensure proper WAGO-3 association with *Mutator*-dependent 22G RNAs. Although WAGO-3 still covered a subset of its typical target genes, loss of MUT-7 significantly altered the WAGO-3 associated 22G RNA population.

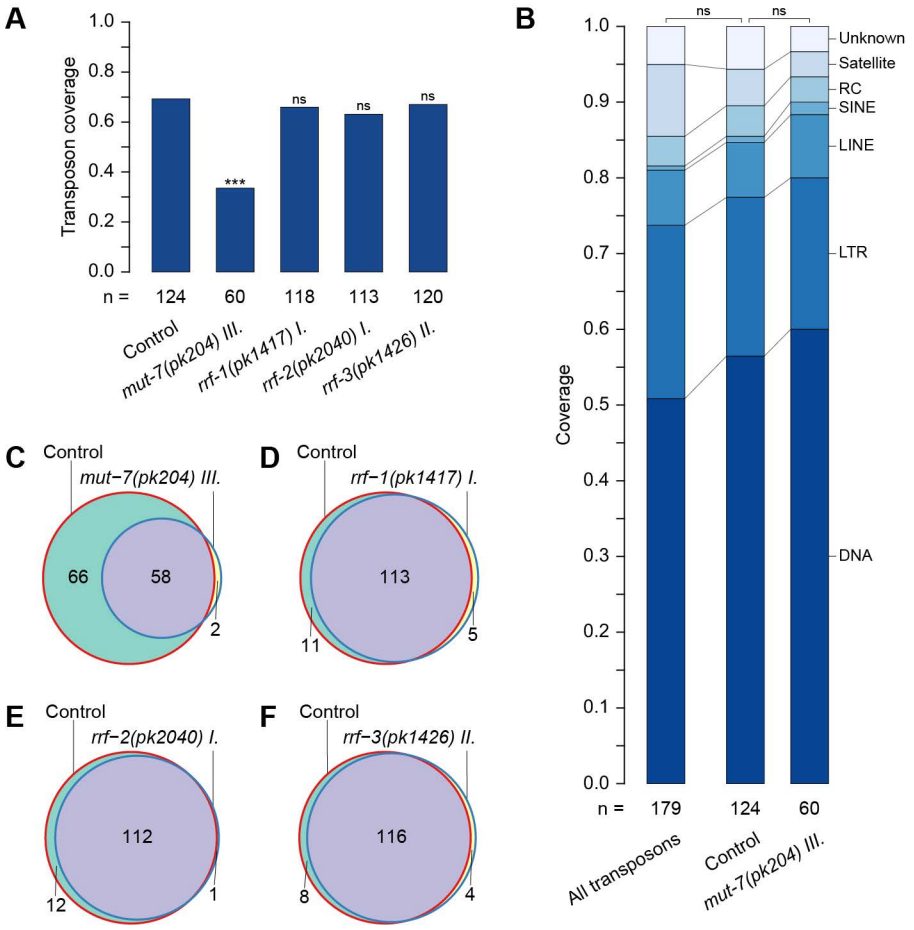

Figure 14 | WAGO-3 targets the majority of transposable elements in a *Mutator* complex-dependent manner. A, Number and coverage of transposons targeted by GFP::3xFLAG::WAGO-3 in indicated mutants. B, Distribution of GFP::3xFLAG::WAGO-3 targeted transposons based on transposons classes. C-F, Venn diagrams showing overlap of GFP::3xFLAG::WAGO-3 targeted transposons in absence of MUT-7 (C), RRF-1 (D), RRF-2 (E) and RRF-3 (F). P-values were calculated with a chi-square test (A, B). ***: $p \leq 0.001$, ns: $p > 0.05$

Quantitative proteomics identified the WAGO-3 interacting protein PEI-1

Intrigued by the presence of WAGO-3 in mature sperm, we performed immunoprecipitation experiments of GFP::3xFLAG::WAGO-3 using whole-worm extracts from late-L4 stage hermaphrodites, followed by label-free quantitative mass spectrometry. We specifically chose late-L4 stage larvae in order to cover the whole process of spermatogenesis. This experiment identified a number of WAGO-3 co-enriched proteins (**Figure 15A**). Among them, known P granule components like DEPS-1, PRG-1 and WAGO-1 were identified (Batista et al., 2008; Gu et al., 2009; Spike et al., 2008). Additionally, we detected four VIT proteins, which were commonly found to be co-enriched in IP-MS/MS experiments of germline-localized proteins (Almeida et al., 2018; Cordeiro Rodrigues et al., 2019). We also identified SET-27, a predicted H3K36 or H3K4 specific histone methyltransferase as well as four uncharacterized proteins: Y111B2A.3, W09B7.2, F40A3.6 and F27C8.5.

The gene *Y111B2A.3* encodes a protein of 83 kDa with no assigned domain, but two predicted intrinsically disordered regions. Although the molecular function of *Y111B2A.3* has not been described so far, a paralogous gene named *edg-1* (Enlarged Deps-1 Granule phenotype) may indicate an involvement in the assembly of biomolecular condensates. In fact, publically available RNA sequencing data suggest a germline-specific expression in embryos, larvae and adults. A recent RNAi screen revealed the requirement of *Y111B2A.3* for proper embryonic development (Fernandez, 2005).

W09B7.2 and *F40A3.6* encode small proteins of 35 kDa and 30 kDa, respectively. While both proteins do not contain any discernible domain, an extensive intrinsically disordered region was predicted to cover the first 103 amino acids of W09B7.2, and almost the whole F40A3.6 protein. According to transcriptomic data, *W09B7.2* and *F40A3.6* are expressed in the germline (Ortiz et al., 2014). We also generated a *W09B7.2* deletion allele using the CRISPR/Cas9-mediated genome editing system. This deletion allele was not studied in detail, but we found that loss of W09B7.2 does not affect GFP::3xFLAG::WAGO-3 localization, neither in sperm nor in naïve germ cells (data not shown).

Eventually, we focused on the fourth uncharacterized gene named *F27C8.5*. Interestingly, both transcriptomic and proteomic data indicated presence of F27C8.5 in sperm (Ma et al., 2014; Ortiz et al., 2014). In accordance with the observed *F27C8.5* mutant phenotype, which will be presented in a later chapter, we named this gene *pei-1* (Paternal Epigenetic Inheritance defective-1). In order to validate the mass spectrometry result, we inserted a *3xmyc* encoding sequence directly upstream of the endogenous stop codon of *pei-1*,

enabling immuno-based approaches. In accordance with the mass spectrometry data, we could successfully detect the co-enrichment of PEI-1::3xMYC in GFP::3xFLAG::WAGO-3 immunoprecipitation experiments via Western detection (**Figure 15B**).

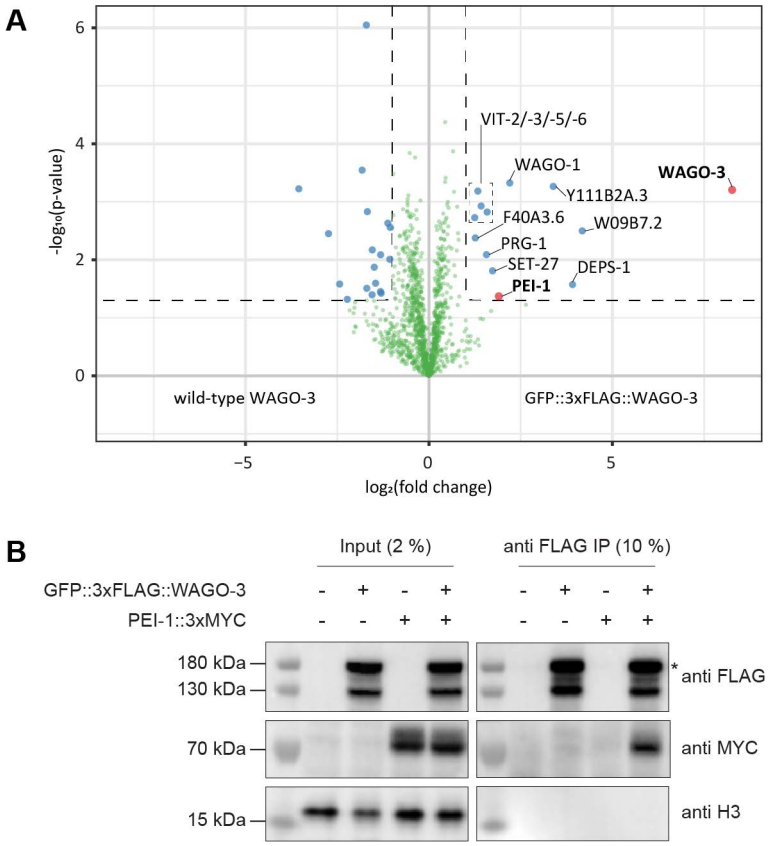

Figure 15 | Identification of the WAGO-3 interacting protein PEI-1. A, Volcano plot representing label-free proteomic quantification of GFP::3xFLAG::WAGO-3 immunoprecipitation experiments from late-L4 stage hermaphrodite extracts. The *X*-axis indicates the mean fold enrichment of individual proteins in the control (wild-type WAGO-3) versus the genome-edited strain (GFP::3xFLAG::WAGO-3). The *Y*-axis represents $-\log_{10}$(p-value) of observed enrichments. Dashed lines show thresholds at P = 0.05 and twofold enrichment. Blue and green data points represent above and below threshold, respectively. WAGO-3 and PEI-1 are highlighted with red data points. B, Co-immunoprecipitation experiments using whole-worm extracts of late-L4 stage hermaphrodites. Input and immunoprecipitation (IP) samples were separated via SDS-PAGE, followed by Western transfer and chemiluminescence detection of GFP::3xFLAG::WAGO-3, PEI-1::3xMYC and histone H3. The asterisk marks the predicted full-length GFP::3xFLAG::WAGO-3 fusion-protein.

PEI-1 secures WAGO-3 during spermatogenesis

First, we examined the loss of PEI-1 on global WAGO-3 abundance. Therefore, we created deletion alleles for both *mut-7* and *mut-16* using CRISPR/Cas9-mediated genome editing, since we cannot guarantee that the previously described point mutations result in null mutants (**Figure 16A**) (Ketting et al., 1999; Vastenhouw et al., 2003). Using the publicly available *pei-1(ok1050)* deletion allele, we then generated strains expressing GFP::3xFLAG::WAGO-3 in absence of either PEI-1, MUT-7, MUT-16, or selected combinations. We found that loss of PEI-1 alone does not destabilize GFP::3xFLAG::WAGO-3 when using whole-worm extracts of late-L4 stage hermaphrodites. Also, PEI-1 did not seem to further reduce GFP::3xFLAG::WAGO-3 abundance in simultaneous absence with either MUT-7 or MUT-16 (**Figure 16B**).

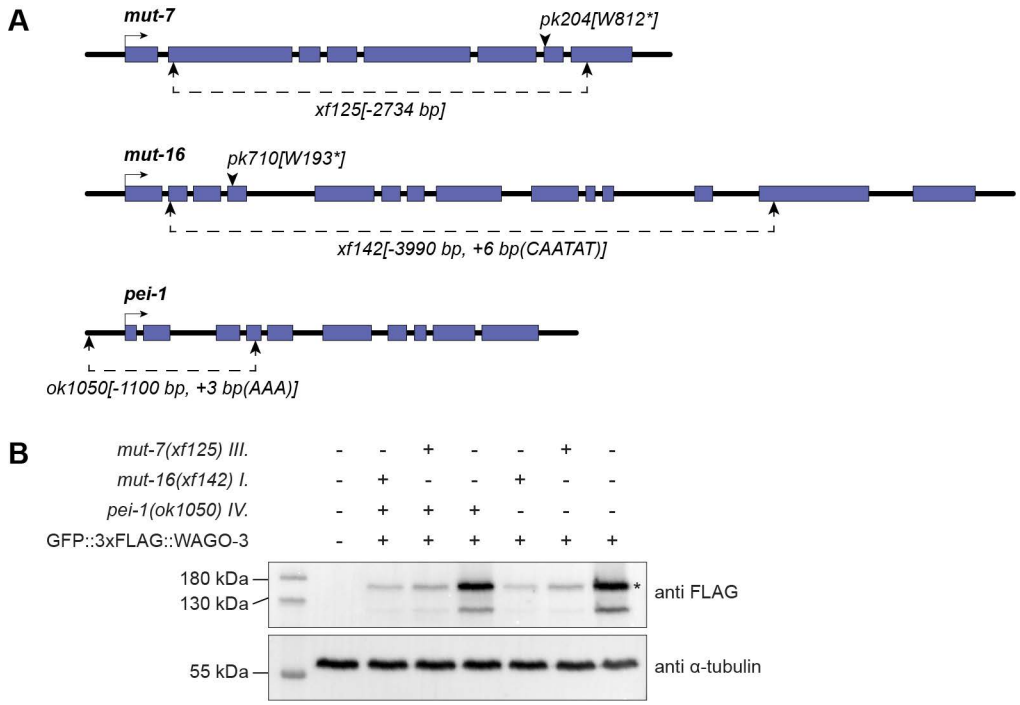

Figure 16 | PEI-1 does not globally affect WAGO-3 stability. A, Schematic representation of the *mut-7*, *mut-16* and *pei-1* locus. Arrowheads highlight point mutations, dashed arrows indicate deletions, solid arrows mark the transcription start sites and blue boxes represent exonic sequences. B, Whole-worm extracts of late-L4 stage hermaphrodites were separated via SDS-PAGE, followed by Western transfer and chemiluminescence detection of GFP::3xFLAG::WAGO-3. Extracts were obtained by collecting synchronized animals and normalized to total protein concentration. The asterisk marks the predicted full-length GFP::3xFLAG::WAGO-3 fusion-protein. α-tubulin was used a loading control.

In order to characterize PEI-1 in greater detail, we generated another endogenously tagged *pei-1* allele encoding a PEI-1::mTagRFP-T fusion-protein. Since we did not see any major, PEI-1-dependent changes in GFP::3xFLAG::WAGO-3 abundance, we used confocal microscopy to monitor GFP::3xFLAG::WAGO-3, PGL-1::mTagRFP-T and PEI-1::mTagRFP-T localization during spermatogenesis in late-L4 stage hermaphrodites. Like described earlier, GFP::3xFLAG::WAGO-3 co-localized with PGL-1::mTagRFP-T to perinuclear P granules in naïve, meiotic germ cells. However, subcellular alterations occurred from the primary spermatocyte stage onwards. First, GFP::3xFLAG::WAGO-3 was found to accumulate in distinct, non-perinuclear, cytoplasmic foci before P granules began to disappear (**Figure 17A**). Notably, these cytoplasmic GFP::3xFLAG::WAGO-3 foci could be detected throughout spermatogenesis (**Figure 17A**). Second, as previously reported, P granules, marked by PGL-1 or any other P granule marker protein, were absent in later stages of spermatogenesis (Updike and Strome, 2010). Third, PEI-1::mTagRFP-T displayed a spermatogenesis-specific expression pattern and started to be expressed right when GFP::3xFLAG::WAGO-3 started to accumulate in cytoplasmic foci. Strikingly, PEI-1::mTagRFP-T always co-localized with GFP::3xFLAG::WAGO-3 to the novel sperm foci (**Figure 17B and 19A**). Both protein were not detected in residual bodies, which contain cellular material that is discarded during sperm maturation (Ellis and Stanfield, 2014).

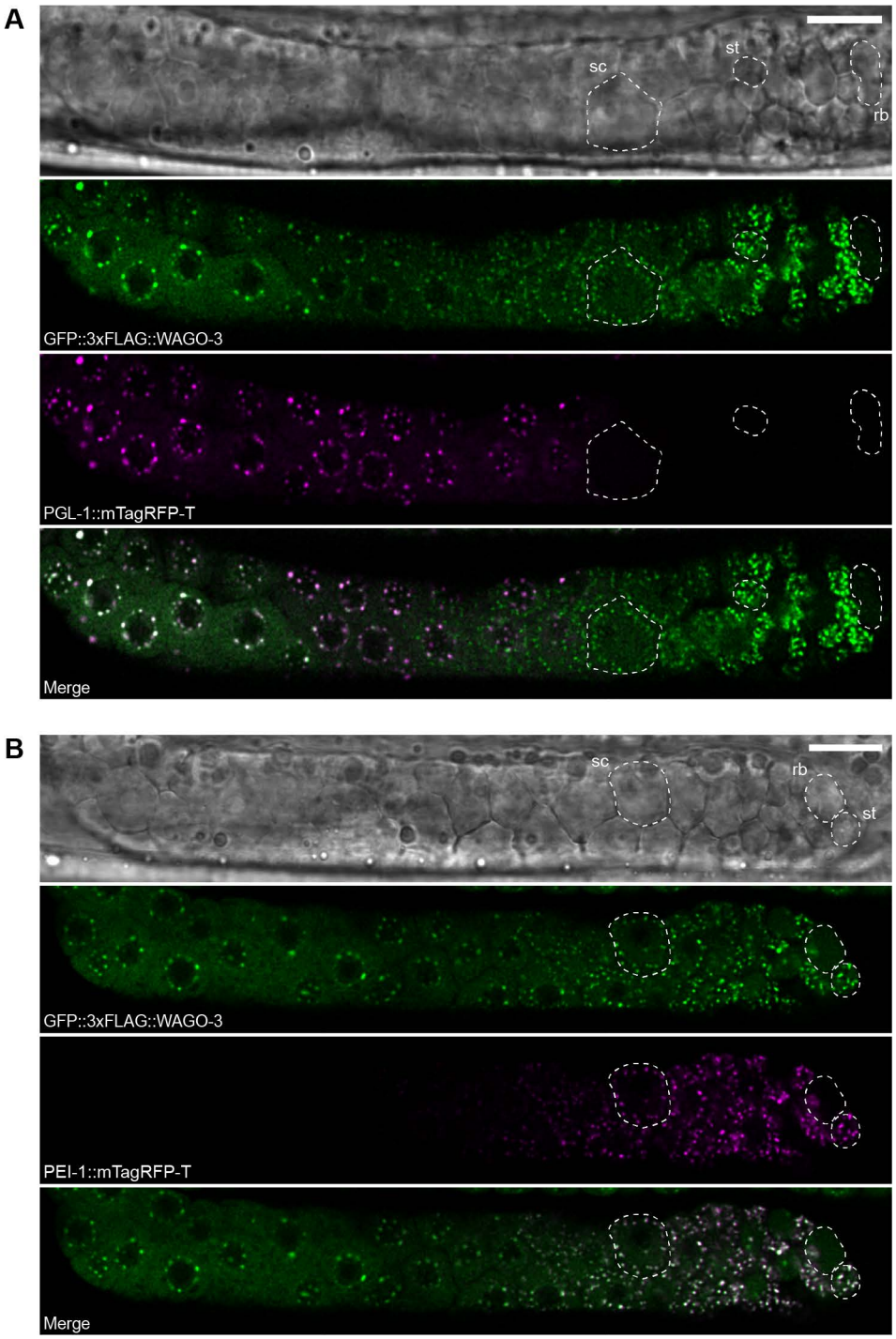

Figure 17 | PEI-1 is specifically expressed during spermatogenesis and always co-localizes with WAGO-3. A-B, Confocal micrographs showing the proximal region of spermatogenic gonads of late-L4 stage hermaphrodites expressing GFP::3xFLAG::WAGO-3 together with PGL-1::mTagRFP-T (A) or PEI-1::mTagRFP-T (B). Representative spermatocytes (sc), spermatids (st) and residual bodies (rb) are outlined by a dashed line. Scale bars: 10 µm (A-B)

Using the *pei-1(ok1050)* deletion allele, we next assessed the requirement of PEI-1 for the subcellular localization of GFP::3xFLAG::WAGO-3 and PGL-1::mTagRFP-T during sperm maturation. Even though *pei-1* mutants did not show any obvious defects in P granule formation, a remarkable change of the GFP::3xFLAG::WAGO-3 localization was detected (**Figure 18A**). While GFP::3xFLAG::WAGO-3 still localized to P granules in naïve germ cells, no localization to cytoplasmic sperm foci was detected in spermatocytes and spermatids in absence of PEI-1 (**Figure 18A)**. Instead, GFP::3xFLAG::WAGO-3 was found to stay within remaining P granules in early spermatocytes and to accumulate in residual bodies (**Figure 18A and 19B**). Notably, this altered subcellular localization in *pei-1* mutants resulted in complete absence of GFP::3xFLAG::WAGO-3 from mature sperm, as it exclusively localized to residual bodies. Thereby GFP::3xFLAG::WAGO-3 followed the same fate as other Argonaute proteins like WAGO-1 (**Figure 18B**), ALG-3 (**Figure 18C**) and CSR-1 (**Figure 18D**), which have been described to be expressed during early stages of spermatogenesis.

In contrast, maternal deposition of GFP::3xFLAG::WAGO-3 was still detectable within the P cell lineage of *pei-1* mutant embryos (**Figure 19C**), indicating that PEI-1 specifically affects WAGO-3 during spermatogenesis. We conclude that WAGO-3 is special amongst *C. elegans* Argonaute proteins, as it is maintained during spermatogenesis by re-localizing to cytoplasmic sperm foci before P granules disappear. Furthermore, PEI-1 is a novel protein that specifically marks these cytoplasmic sperm foci, and is additionally required for proper GFP::3xFLAG::WAGO-3 localization and segregation into mature sperm.

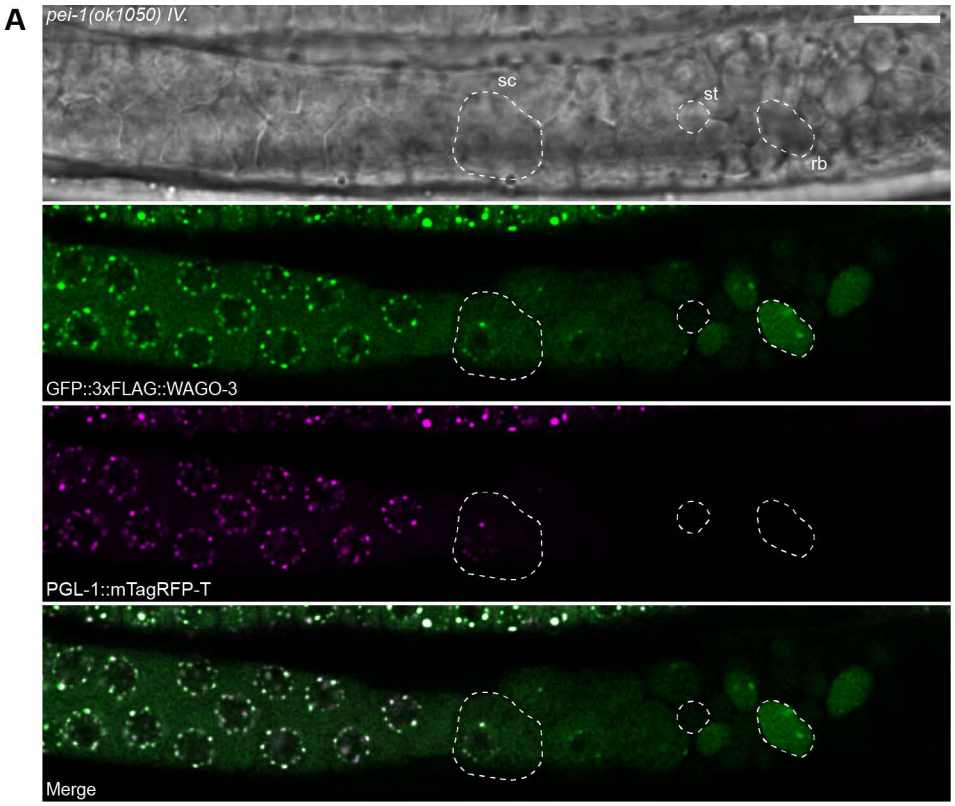
A
pei-1(ok1050) IV.
sc
st
rb
GFP::3xFLAG::WAGO-3
PGL-1::mTagRFP-T
Merge

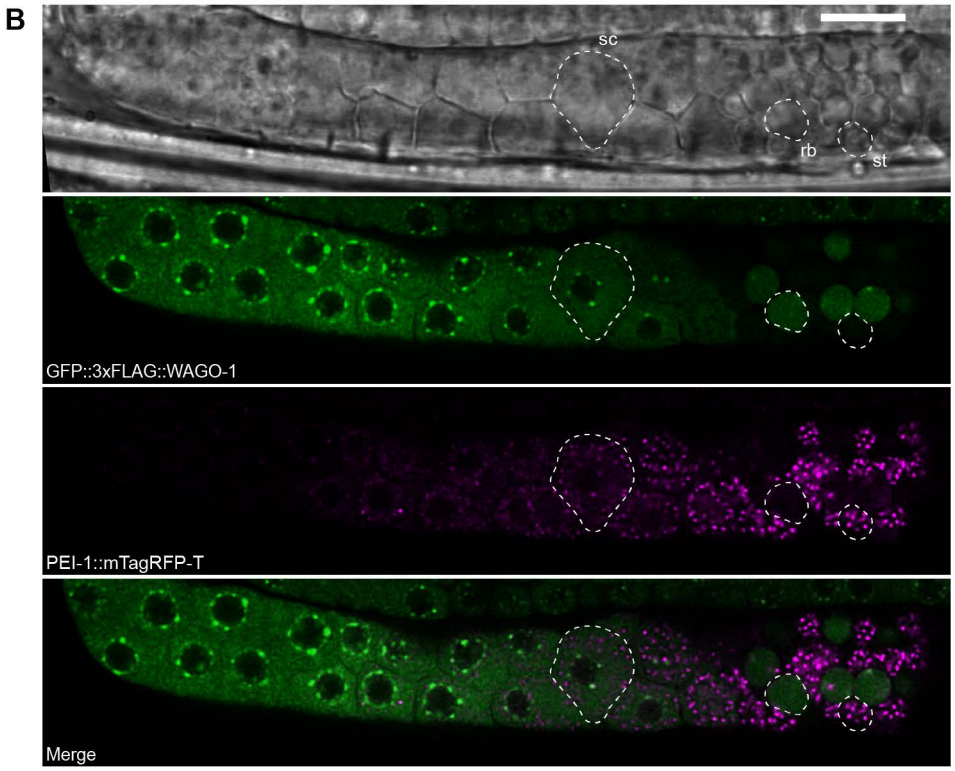
B
sc
rb
st
GFP::3xFLAG::WAGO-1
PEI-1::mTagRFP-T
Merge

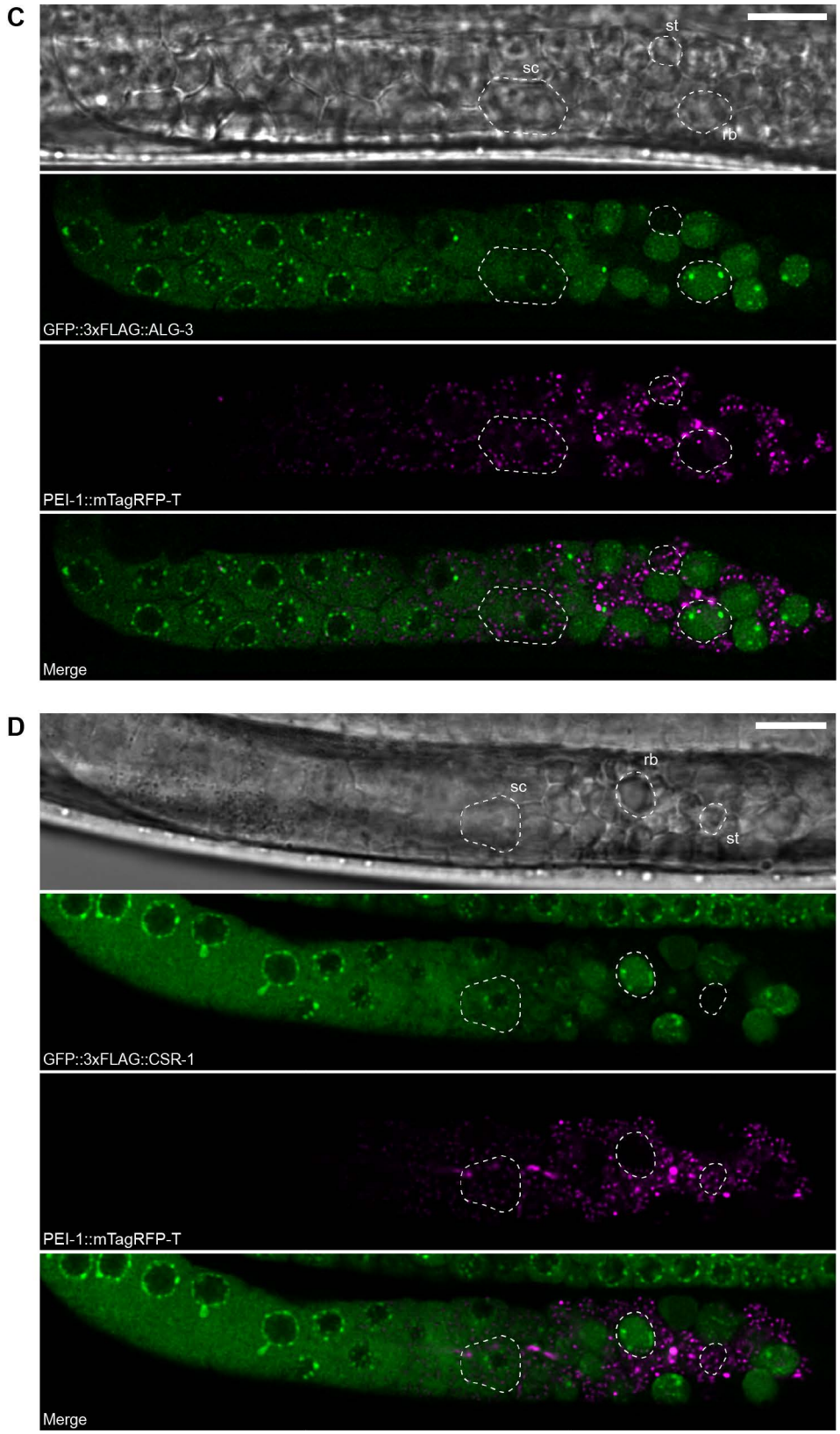

Figure 18 | PEI-1 secures WAGO-3 during spermatogenesis. A-D, Confocal micrographs showing the proximal region of spermatogenic gonads of late-L4 stage hermaphrodites expressing GFP::3xFLAG::WAGO-3 and PGL-1::mTagRFP-T in a *pei-1(ok1050)* mutant (A), or PEI-1::mTagRFP-T together with GFP::3xFLAG::WAGO-1 (B), GFP::3xFLAG::ALG-3 (C) or GFP::3xFLAG::CSR-1 (D). Representative spermatocytes (sc), spermatids (st) and residual bodies (rb) are outlined by a dashed line. Scale bars: 10 µm (A-D)

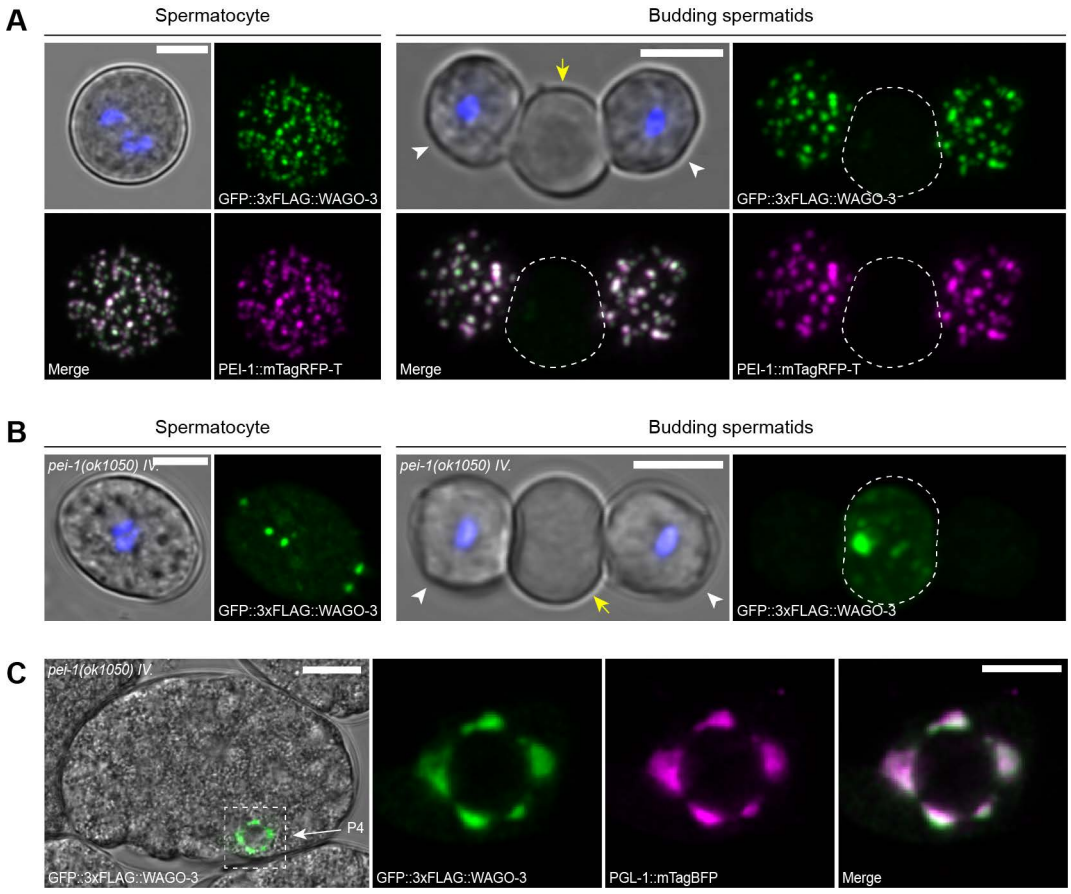

Figure 19 | PEI-1 ensures WAGO-3 localization to sperm foci. A-B, Confocal maximum intensity projections of male-derived spermatocytes and budding spermatids expressing GFP::3xFLAG::WAGO-3 either together with PEI-1::mTagRFP-T (A), or in absence of PEI-1 (B). White arrowheads mark budding spermatids, yellow arrows and dashed lines indicate residual bodies. Hoechst33342 was used to stain DNA. C, Confocal micrographs showing maternally deposited GFP::3xFLAG::WAGO-3 in a *pei-1(ok1050)* mutant, gastrula-stage embryo. Zoom shows perinuclear co-localization of GFP::3xFLAG::WAGO-3 and PGL-1::mTagBFP in the P4 blastomere. Scale bars: 4 µm (A-B), 10 µm (C, embryo), 4 µm (C, zoom)

WAGO-3 is involved in germ cell development and maintenance of RNAe

Unlike other model organisms, many *C. elegans* mutants of small RNA pathways that are involved in genome defense against transposable elements do not display acute sterility but rather a progressive reduction in fertility over generations (Buckley et al., 2012; Spracklin et al., 2017; Wan et al., 2018; Xiao et al., 2011). This phenotype is called mortal germline (Mrt) and eventually results in sterility (Greer et al., 2014; Katz et al., 2009; Lev et al., 2017; Sakaguchi et al., 2014; Simon et al., 2014). Since WAGO-3 was shown to be involved in transposon silencing (Robert et al., 2005; Vastenhouw et al., 2003), we tested whether WAGO-3 and PEI-1 are required for proper germ cell development across generations at elevated temperature. In fact, we found that WAGO-3 was required for

germline immortality, as out-crossed *wago-3* mutant animals became sterile after 13 generations at 25°C (**Figure 20A**). Likewise, *hrde-1* mutant animals displayed a mortal germline phenotype, which served as positive control (Buckley et al., 2012). Interestingly, no loss of reproductive ability was observed for *pei-1* mutants.

The Mrt phenotype usually results from transcriptional dysregulation, which in turn can be caused by defects in RNAi inheritance (Buckley et al., 2012; Perez and Lehner, 2019; Wan et al., 2018). Since WAGO-3 is present in both oocytes and sperm, and additionally inherited to the next generation via deposition into embryos, we sought to test the involvement of WAGO-3 in 22G RNA-mediated TEI. To achieve this, we made use of a so-called 21U RNA sensor. The 21U RNA sensor is a single-copy transgene (*mjSi22*), which encodes a germline-specific mCherry::H2B fusion-protein containing a targeting site for one of the most abundant 21U RNAs of *C. elegans* (*21ur-1*) (Bagijn et al., 2012). Consequently, the 21U RNA sensor is targeted by PRG-1, which initiates its silencing (Bagijn et al., 2012; Lee et al., 2012) (**Figure 20B**). Once established, this gene silencing can be maintained in absence of PRG-1 for many generations and is consequently referred to as RNAe (Ashe et al., 2012; Luteijn et al., 2012; Shirayama et al., 2012) (**Figure 20C**). Thus, the 21U RNA sensor can be used as reporter to monitor the maintenance of RNAe-driven gene silencing.

We introduced *prg-1*, *wago-3* or *mut-7* mutant alleles into a strain carrying a silenced, single-copy insertion of the 21U RNA sensor and scored its activity after seven generations of homozygosity. Since *mut-7* is crucial for 22G RNA-mediated TEI (de Albuquerque et al., 2015; Phillips et al., 2015), this gene served as positive control. We found that loss of WAGO-3 alone did not cause any activation of the 21U RNA sensor (**Figure 20D**). In contrast, about one third of all examined *prg-1; wago-3* double mutant animals showed 21U RNA sensor activity after seven generations (~38 %; n = ≥ 50) (**Figure 20E**), while no 21U RNA sensor expression was detected in the first double homozygous generation. As expected, loss of MUT-7 completely restored the 21U RNA sensor activity (100 %; n = ≥ 50) (**Figure 20F**). This finding reveals that WAGO-3 is required for the transgenerational maintenance of the RNAe-driven gene silencing targeting the 21 U RNA sensor. Hence, WAGO-3 most likely plays a role in 22G RNA-mediated TEI.

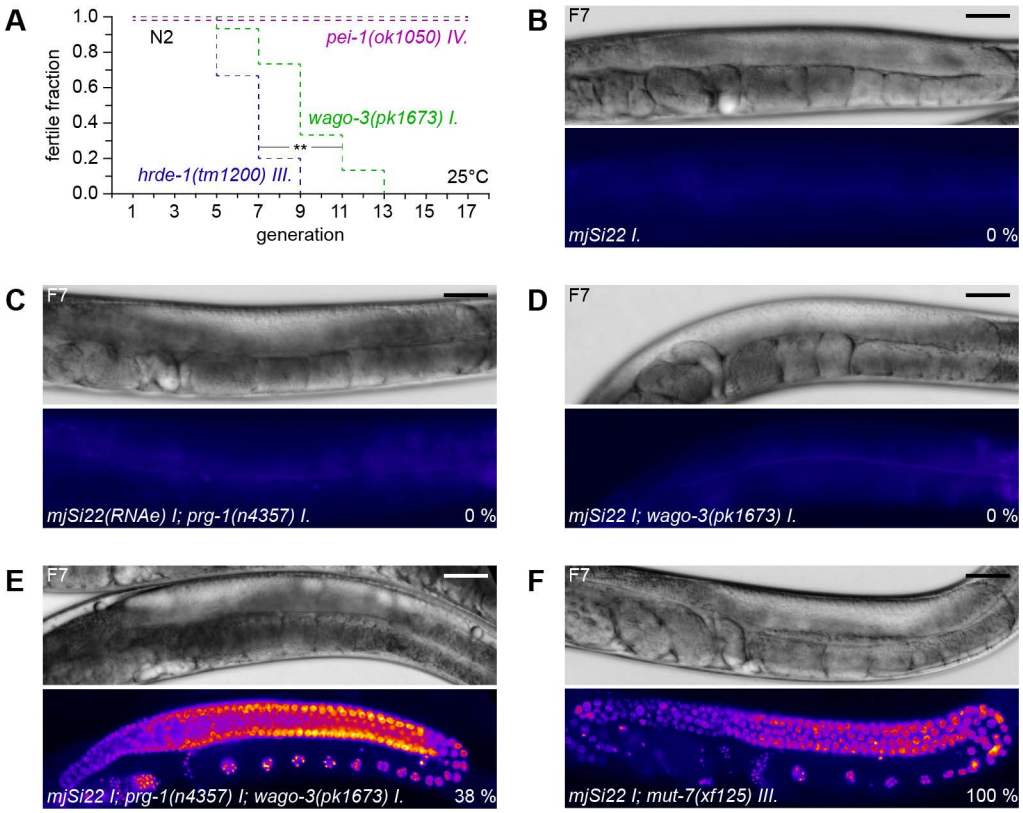

Figure 20 | WAGO-3 is involved in transgenerational epigenetic inheritance. A, Mortal germline assay representing loss of fertility of out-crossed strains with indicated genotype at 25°C. B-F, Fluorescence micrographs showing re-activation of a 21U RNA-targeted transgene (*mjSi22*) in absence of both PRG-1 and WAGO-3. Expression of the transgene was determined after seven generations of homozygosity. No activity was detected in the first double mutant generation. Percentage in lower right corner shows fraction of animals expressing the transgene (n ≥ 50). Scale bars: 30 µm (B-F). The p-value was calculated with a logrank test (A). **: p ≤ 0.01

WAGO-3 and PEI-1 are required for paternal epigenetic inheritance of 22G RNA-mediated gene silencing information

In order to get an idea about the parental contribution of WAGO-3 in TEI, we re-analyzed our WAGO-3 RIP-small RNA sequencing data in order to compare protein-coding target genes between GFP::3xFLAG::WAGO-3 and either sperm- or oocyte-derived 22G RNAs. Interestingly, the target repertoire of sperm- and oocyte-derived 22G RNAs highly overlaps, with just a minor set of genes being specifically targeted by any of these 22G RNA populations (Stoeckius et al., 2014). When we included WAGO-3 associated 22G RNAs in this analysis, we noticed a bias of WAGO-3 towards target genes that are mutually targeted by both gamete-derived 22G RNA populations (**Figure 21A**).

When comparing sorted gene lists ranked by RPM of mapped gamete-derived 22G RNAs with all identified WAGO-3 protein-coding target genes, we found that WAGO-3 has a

significant preference to cover genes that are highly targeted by sperm-derived 22G RNAs compared to oocyte-derived 22G RNAs (**Figure 21B**). The *vice versa* comparison did not show any major differences between both gamete-derived 22G RNA populations, but confirmed the high coverage of WAGO-3 associated and gamete-derived 22G RNA target genes (**Figure 21C**). However, we noticed that many of the top WAGO-3 targets were not covered by any of the gamete-derived 22G RNA populations (**Figure 21, A and C**), suggesting that WAGO-3 possibly targets a different set of genes in naïve germ cells compared to oocytes or sperm.

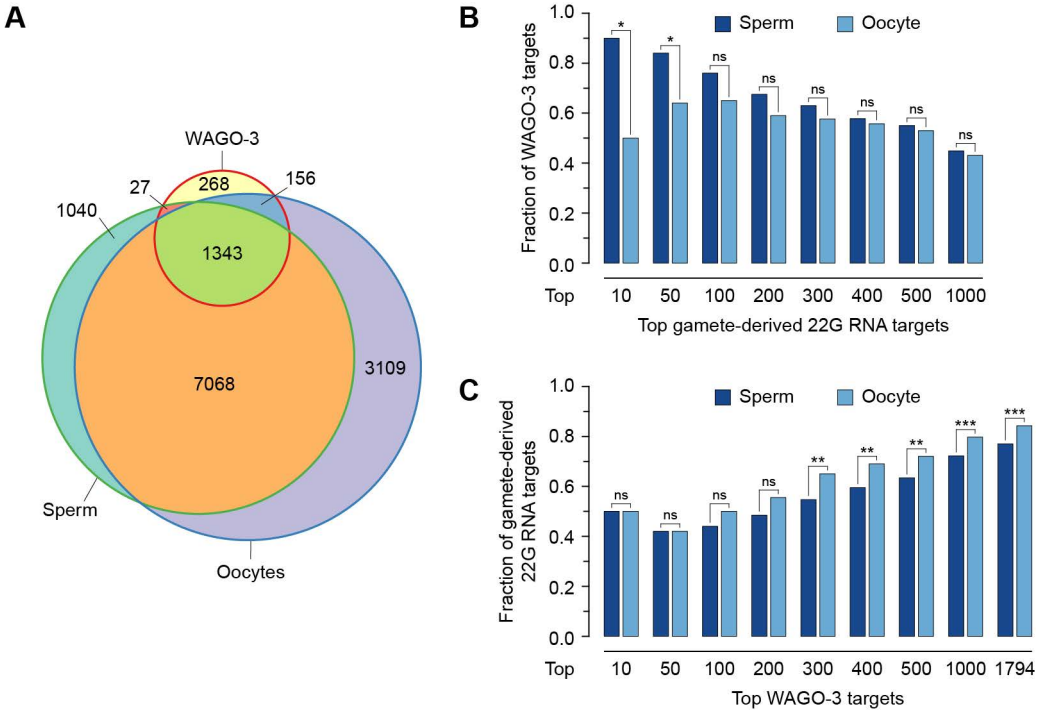

Figure 21 | WAGO-3 is mostly associated with 22G RNAs that are mutually found in sperm and oocytes. A, Venn diagram showing overlap of protein-coding target genes of sperm-derived, oocyte-derived and WAGO-3 associated 22G RNAs. B, Bar chart showing how many of the top gamete-derived 22G RNA targets genes (protein-coding) were also identified as WAGO-3 target genes. C, Bar chart showing how many of the top WAGO-3 targets genes (protein-coding) were also identified as gamete-derived 22G RNA target genes. P-values were calculated with a chi-square test (B, C). ***: $p \leq 0.001$, **: $p \leq 0.01$, *: $p \leq 0.051$, ns: $p > 0.051$

As we found WAGO-3 to be required for the transgenerational maintenance of RNAe-driven gene silencing, we decided to investigate whether WAGO-3 and PEI-1 are crucial for either maternal or paternal RNAi inheritance. Therefore, we implemented a genetic system to test the roles of various RNAi factors, including WAGO-3 and PEI-1, in the epigenetic inheritance of 22G RNA-mediated gene silencing information in an

endogenous setting. We, however, focused more on the paternal contribution as the sperm localization of WAGO-3, regulated by PEI-1, is a novel feature of WAGO proteins.

We and others have previously shown that certain small RNA populations are required for the epigenetic inheritance of gene silencing information (de Albuquerque et al., 2015; Phillips et al., 2015). First, RNAe memory is solely based on an active *Mutator*-dependent 22G RNA pathway, where either a paternal or a maternal contribution is sufficient to re-establish accurate gene silencing in the following generation (**Figure 22A**). Second, maternal 21U RNAs were also shown to be sufficient for the accurate zygotic re-establishment of endogenous RNAi. Loss of all of these three small RNA populations causes a high degree of sterility in filial animals that are proficient for 22G RNA biogenesis. This phenotype is called '*Mutator*-induced sterility' (Mis) and is based on the production of 22G RNAs, which target genes that are normally not targeted, resulting in stochastic, erroneous gene silencing, which finally prevents proper germ cell development. Since any of the above-described small RNA pathways is sufficient to rescue the Mis phenotype, this genetic system represents a reliable approach to assess the requirement of individual proteins for the epigenetic inheritance of gene silencing information.

To examine the paternal epigenetic inheritance, we crossed various mutant males with hermaphrodites that lack both 21U RNAs and 22G RNAs (**Figure 22B**). As published, 21U RNA-defective males, generated by loss of PRG-1, produced fertile offspring. In contrast, 22G RNA-defective males, generated by loss of the 22G RNA biogenesis factor MUT-16, sired predominantly sterile offspring. Notably, the offspring of *wago-3* mutant males showed the same degree of sterility, suggesting that WAGO-3 is sufficient for paternal rescue of the Mis phenotype. This finding highlights WAGO-3 as a key player in paternal epigenetic inheritance of 22G RNA-mediated gene silencing information.

Epigenetic inheritance involves distinct roles of both cytoplasmic and nuclear machineries (Xu et al., 2018a). On the one hand, small RNA inheritance occurs via Argonaute proteins localizing to heritable, biomolecular condensates (Wan et al., 2018). On the other hand, the nuclear RNAi pathways triggers the deposition of repressive chromatin marks (Buckley et al., 2012; Mao et al., 2015). In order to distinguish between both mediators, we made use of additional genes including *pei-1*, *hrde-1* and *nrde-2*. As described above, we found that WAGO-3 localizes to distinct sperm foci in a PEI-1 dependent manner. Thus, PEI-1 might be exclusively responsible for the paternal inheritance of WAGO-3 associated 22G RNAs. In contrast, HRDE-1 and NRDE-2 represent

two proteins that were shown to be involved in the nuclear RNAi pathway (Buckley et al., 2012; Mao et al., 2015).

We found that the offspring of *pei-1*, *hrde-1* and *nrde-2* single mutant males were fertile (**Figure 22B**), indicating that cytoplasmic WAGO-3, or nuclear RNAi alone is enough to establish a paternal gene silencing memory. Interestingly, *hrde-1; pei-1* and *nrde-2; pei-1* double mutant males sired significant numbers of sterile F1 animals, even though the penetrance was not as high as for *wago-3* mutant males (**Figure 22B**). This finding indicates that any paternal contribution, either the cytoplasmic or the nuclear pathway, is sufficient to rescue the Mis phenotype in the presence of an active, paternal 21U RNA pathway. Simultaneous loss of both epigenetic mediators suspended the paternal gene silencing memory, although not completely. Intriguingly, *nrde-2; pei-1* double mutant males caused a stronger Mis phenotype compared to *hrde-1; pei-1* double mutant males (**Figure 22B**), suggesting that HRDE-1 might not be the only germline-expressed Argonaute protein to trigger nuclear RNAi.

The so far described males were proficient for 21U RNA biogenesis. Thus, the paternal gene silencing memory comprised both 21U RNA-dependent and RNAe-driven gene silencing. Although PRG-1 alone was found to be insufficient to provide a paternal gene silencing memory, it was reported to affect the *Mutator*-dependent 22G RNA population. While the 22G RNA abundance was not affected in absence of PRG-1, the population of 22G RNA targeted genes was significantly altered, as approximately 66 % of annotated WAGO target genes were depleted of 22G RNAs (Reed et al., 2019). Thus, we repeated the analyses with *prg-1(n4357)* mutant males, in order to test the role of WAGO-3, PEI-1 and NRDE-2 in paternal RNAe memory (**Figure 22B**). Strikingly, we found that in absence of PRG-1, paternal RNAe memory is highly dependent on all three examined proteins. In absence of 21U RNAs, loss of either the cytoplasmic (PEI-1) or the nuclear (NRDE-2) pathway is sufficient to suspend the paternal RNAe memory. These results highlight the biological relevance of the observed localization of GFP::3xFLAG::WAGO-3 to sperm foci and its regulation by PEI-1, but also confirm a nuclear component in paternal 22G RNA-mediated TEI (Kaneshiro et al., 2019; Tabuchi et al., 2018).

We also tested our genome-edited alleles to assess the molecular functionality of the generated fusion-proteins (**Figure 22B**). Given that fluorescent protein tags are rather big, their interference with the underlying protein can result in perturbations to the overall fold and function (Crivat and Taraska, 2012). Since a N-terminal GFP::3xFLAG fusion was shown to partially interfere with WAGO-4 function (Wan et al., 2018), it may be expected that our GFP::3xFLAG::WAGO-3 fusion-protein also does not behave as a

wild-type WAGO-3. Indeed, it showed a partial Mis phenotype (**Figure 22B**). More surprisingly, the endogenously edited *pei-1(xf193)* allele, encoding the PEI-1::mTagRFP-T fusion-protein, also resulted in a Mis phenotype. Given that we did not observe any mislocalization of GFP::3xFLAG::WAGO-3 in *pei-1(xf193)* animals, compared to *pei-1* wild-type animals, we propose that the inability to rescue the Mis phenotype may hint towards defects in later stages, possibly during embryogenesis.

To examine the contribution of WAGO-3 and PEI-1 in maternal epigenetic inheritance, we crossed appropriate mutant hermaphrodites lacking 21U RNAs with *mut-16* mutant males. We found that neither WAGO-3 nor PEI-1 was required for maternal rescue of the Mis phenotype (**Figure 22C**). Interestingly, while WAGO-4 was recently shown to be required for the maternal epigenetic inheritance of exogenous RNAi effects (Wan et al., 2018), we found that WAGO-4, like WAGO-3, is also dispensable for 22G RNA-mediated inheritance of endogenous RNAi effects. Possibly, *wago-3; wago-4* double mutants may need to be analyzed to reveal the maternal Mis phenotype.

Finally, we were intrigued by one of our previous studies showing that *wago-1; wago-2; wago-3* triple mutants cannot establish the Mis phenotype (de Albuquerque et al., 2015). This was interpreted as WAGO-1, WAGO-2 and WAGO-3 being required to induce the erroneous gene silencing. Based on this observation, we set out to test the requirement of WAGO-3 and PEI-1 for the zygotic re-establishment of 22G RNA-mediated gene silencing. Therefore, we crosses 22G RNA-defective males with 21U RNA- and 22G RNA-defective hermaphrodites, while both parents were also mutant for either *wago-3* or *pei-1*. We found that neither loss of WAGO-3 nor of PEI-1 rescued the Mis phenotype in this setting (**Figure 22D**), indicating that WAGO-3 is not needed in the embryo to drive the Mis phenotype.

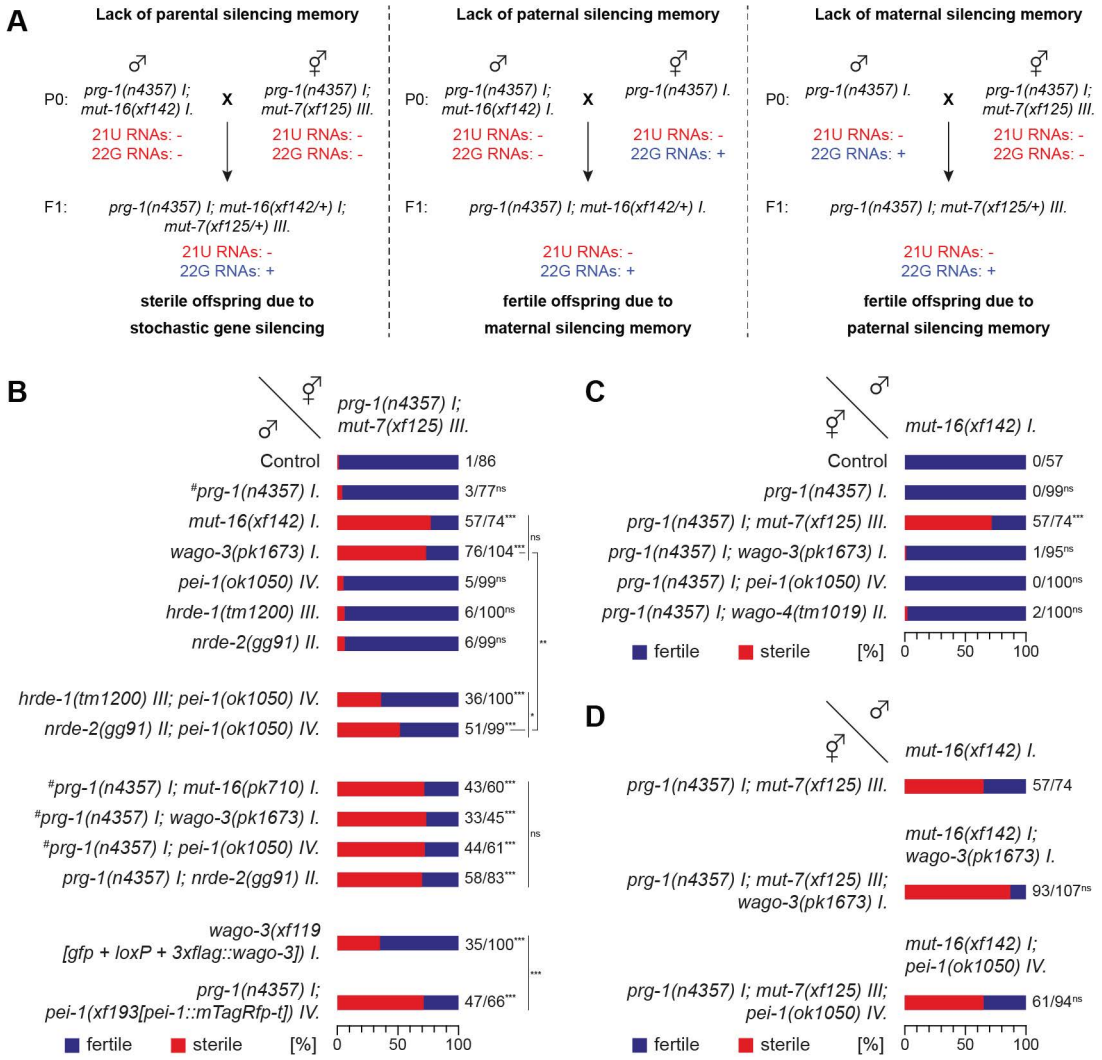

Figure 22 | WAGO-3 and PEI-1 are required for paternal epigenetic inheritance. A, Schematic illustrating the generation of animals that establish 22G RNA populations *de novo* in absence of 21U RNAs. Loss of MUT-7 or MUT-16 causes global depletion of *Mutator*-dependent 22G RNAs, whereas PRG-1 is required for 21U RNA biogenesis and function. B-C, Percentage of fertile F1 animals generated by indicated crosses attributing either paternal (B) or maternal (C) epigenetic silencing memory. Fertility indicates presence of paternal (B) or maternal (C) 22G RNA-mediated epigenetic inheritance. Sterility is caused by lack of every parental 22G RNA-mediated epigenetic inheritance, resulting in stochastic gene silencing in the F1 progeny. D, Percentage of fertile F1 animals generated by indicated crosses attributing the zygotic re-establishment of the 22G RNA pathway. Fertility indicates impaired zygotic re-establishment of endogenous RNAi, whereas sterility results from a properly functioning 22G RNA pathway. Octothorpes mark crosses where the *mut-7(pk204)* allele was used instead of the *mut-7(xf125)* allele. P-values were calculated with a chi-square test (B, C). ***: $p \leq 0.001$, **: $p \leq 0.01$, *: $p \leq 0.05$, ns: $p > 0.05$

Sperm foci formation and WAGO-3 interaction are mediated via different PEI-1 regions

To better understand the regulation of WAGO-3-mediated paternal epigenetic inheritance, we investigated PEI-1 in detail. We found that PEI-1 displays a bimodal composition in terms of intrinsically ordered and intrinsically disordered regions. The N-terminal half of PEI-1 predominately folds into alpha helical structures forming an annotated BTB domain (**Figure 23A**). The BTB domain, also known as POZ domain, is described to mediate protein-protein interactions resulting in either homomeric or heteromeric oligomerization (Ahmad et al., 1998, 2003; Bardwell and Treisman, 1994; Katsani, 1999; Li et al., 1999; Melnick et al., 2000; Takenaga et al., 2003). Using the MPI Bioinformatics Toolkit HHpred, which detects remote homologs based on Hidden Markov Models for both the query and the database (Zimmermann et al., 2018), we found that the remaining alpha helices likely adopt a BACK domain (**Figure 23A**). In contrast to the BTB domain, the molecular function of the BACK domain remains elusive, as nothing has been reported besides its helical composition and location following a BTB domain (Stogios and Privé, 2004).

Using two different PONDR® algorithms, namely VSL2 and VL3, we found that the C-terminal half of PEI-1 is predicted to be intrinsically disordered (**Figure 23B**), meaning that it lacks any fixed super-secondary and tertiary structure. VSL2, on the one hand, combines two predictors that were trained with short (< 31 residues) and long (> 30 residues) disordered regions, respectively. On the other hand, the VL3 predictor was optimized for long disordered regions.

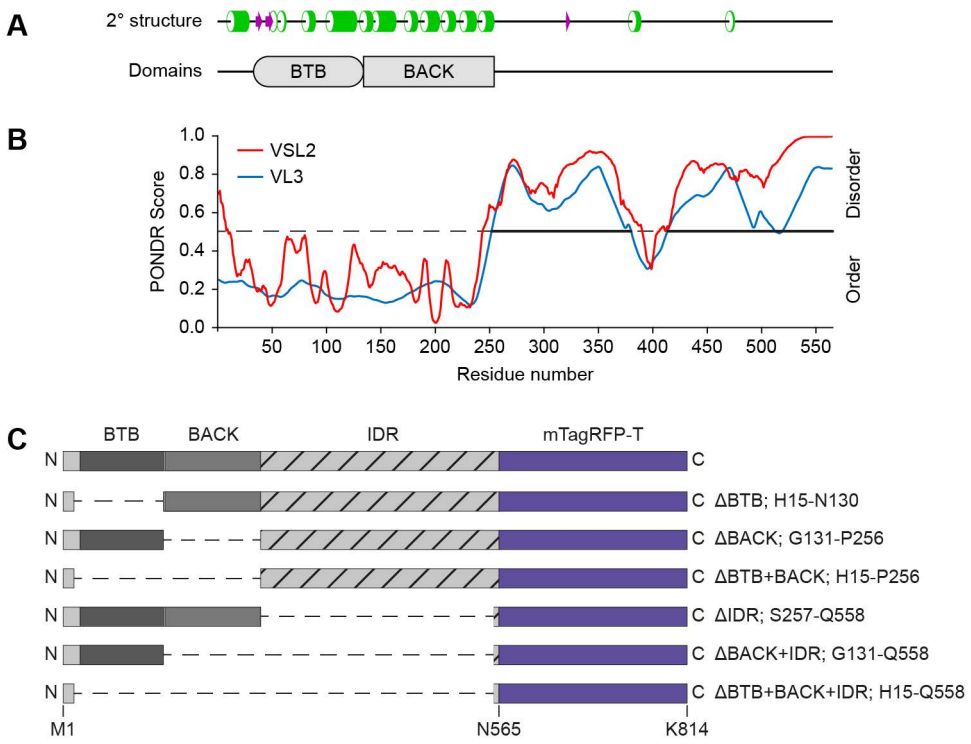

Figure 23 | PEI-1 is a BTB domain-containing protein comprising an extensive, intrinsically disordered region. A, PEI-1 protein composition in terms of secondary and fixed tertiary structure. Secondary structure elements were predicted using Jpred4 (Drozdetskiy et al., 2015). Helices are marked as green tubes, and sheets as magenta arrows. Domain annotations are based on InterPro (BTB) and HHpred (BACK) (Mitchell et al., 2019; Zimmermann et al., 2018). B, PONDR® predictions of intrinsically disordered regions in PEI-1 using VSL2 and VL3 algorithms. C, Schematic representation of truncated PEI-1::mTagRFP-T proteins generated by CRISPR/Cas9-mediated genome editing.

Following these annotations and predictions, we used the CRISPR/Cas9-mediated genome editing system to further edit the endogenous *pei-1* locus by introducing defined deletions. Thereby, we generated seven different PEI-1::mTagRFP-T variants (**Figure 23C**), which were used to perform co-localization studies with GFP::3xFLAG::WAGO-3 to determine individual effects on the subcellular localization and distribution of both WAGO-3 and PEI-1 during spermatogenesis (**Figure 24**). In order to clearly define specific cell types, we imaged isolated spermatocytes and budding spermatids derived from male animals. In addition, we focused on the spermatheca of adult hermaphrodites, as this tubular structure of the somatic gonad is the only place where spermatozoa can be found *in vivo*.

Like described above, full-length PEI-1::mTagRFP-T was always found to co-localize with GFP::3xFLAG::WAGO-3 to distinct, cytoplasmic foci of spherical shape during spermatogenesis and within the spermatheca. Deletion of the BTB domain resulted in normally appearing foci in spermatocytes and budding spermatids. However, we also

detected an accompanied, diffuse cytoplasmic signal of both GFP::3xFLAG::WAGO-3 and PEI-1::mTagRFP-T within the spermatheca. Loss of the BACK domain led to a similar phenotype, but in addition affected the number and homogeneity of detected foci throughout spermatogenesis and in mature sperm. Absence of both the BTB domain and BACK domain caused an even more severe phenotype. Although some foci were still present in spermatocytes and budding spermatids, no foci, but only diffuse cytoplasmic signals were detectable within the spermatheca. Albeit affecting number and homogeneity of sperm foci, none of these three *pei-1* deletions resulted in GFP::3xFLAG::WAGO-3 or PEI-1::mTagRFP-T accumulation in the residual body. Also, we found that both proteins always co-localized, independently on the presence or absence of sperm foci.

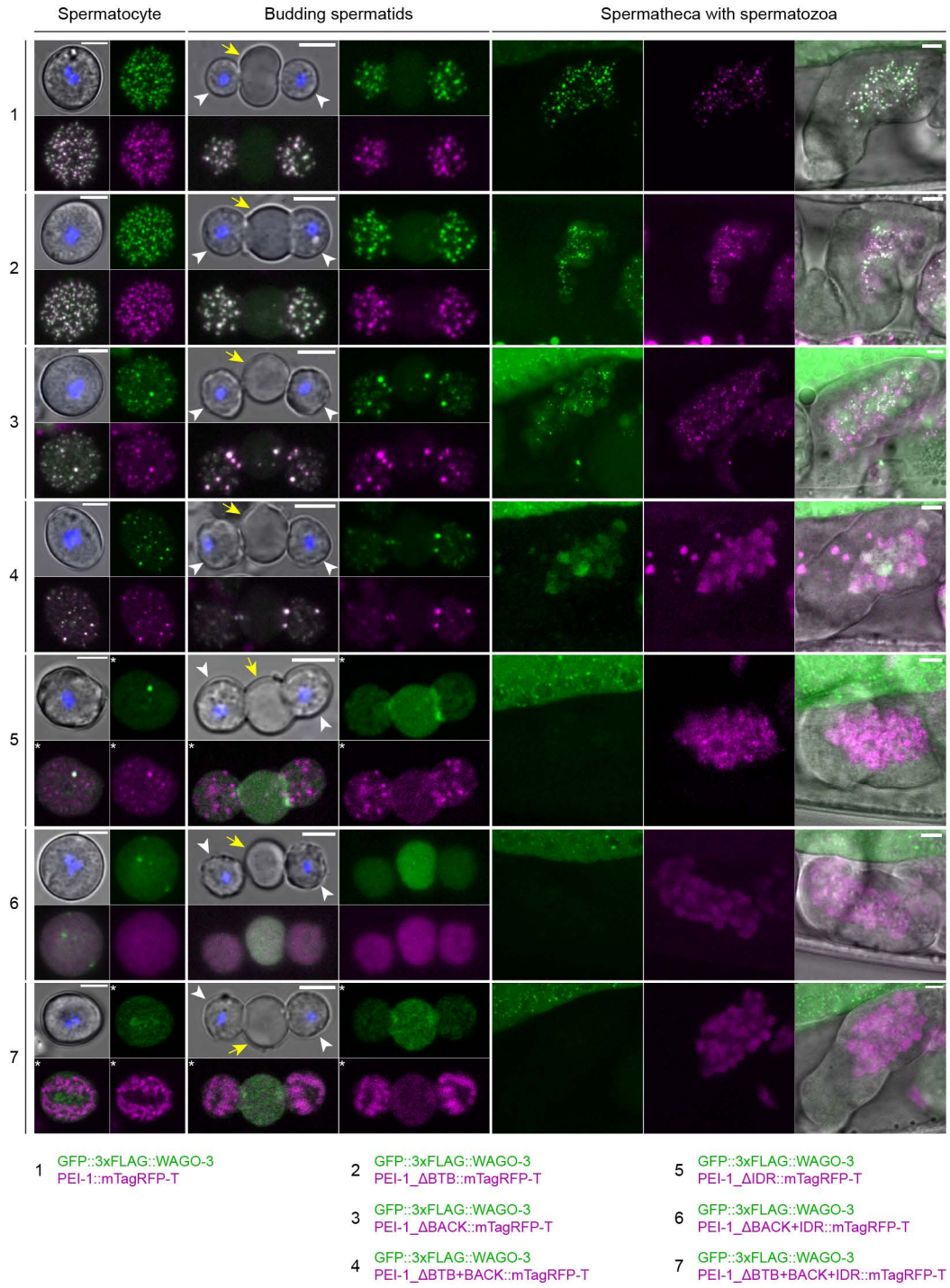

Figure 24 | PEI-1 recruits WAGO-3 and affects sperm foci formation. Confocal maximum intensity projections of isolated spermatocytes (male-derived), budding spermatids (male-derived) and spermatozoa within the spermatheca (hermaphrodite) expressing GFP::3xFLAG::WAGO-3 and indicated PEI-1::mTagRFP-T variants. White arrowheads mark budding spermatids, yellow arrows indicate residual bodies. Hoechst33342 was used to stain DNA. Asterisks indicate optical sections. Scale bars: 4 µm

Upon deletion of the intrinsically disordered region of PEI-1, GFP::3xFLAG::WAGO-3 was found to recapitulate its localization in *pei-1(ok1050)* mutant animals, namely diffuse distribution in spermatocytes, localization to residual bodies and absence in spermatozoa. Intriguingly, the remaining, structurally ordered part of PEI-1 did not accumulate in residual bodies, but displayed localization to faint foci in spermatocytes, budding spermatids and spermatozoa. Additional removal of the BACK domain did not further affect the subcellular localization of GFP::3xFLAG::WAGO-3. However, the remaining BTB::mTagRFP-T fusion-protein was found to no longer localize to cytoplasmic foci, but was evenly distributed between residual body and the budding spermatis. The last examined *pei-1* deletion removed almost the whole protein, leaving only 14 N-terminal and 6 C-terminal amino acids of PEI-1. To our very surprise, this fusion-protein was found to localize to unknown structures of defined shape throughout spermatogenesis. In addition, we observed that these structures were asymmetrically segregated into spermatids leaving no detectable signal in residual bodies (**Figure 24 and 25**). Strikingly, none of the examined PEI-1::mTagRFP-T variants were found to recapitulate the subcellular distribution of GFP::3xFLAG::WAGO-3 in *pei-1(ok1050)* mutants. In contrast, all six truncated PEI-1::mTagRFP-T proteins were detected within the spermatheca, indicating their presence in mature sperm.

Taken together, the structurally ordered part of PEI-1, represented by the BTB domain and BACK domain, is likely involved in forming and stabilizing PEI-1 foci throughout sperm maturation. While the BTB domain specifically stabilized PEI-1 foci after spermiogenesis, the BACK domain was found to play a role in forming and stabilizing PEI-1 foci during the entire process of spermatogenesis and in spermatozoa. The intrinsically disordered region of PEI-1, however, is crucial for WAGO-3 interaction and seemingly contributes to PEI-1 foci stabilization.

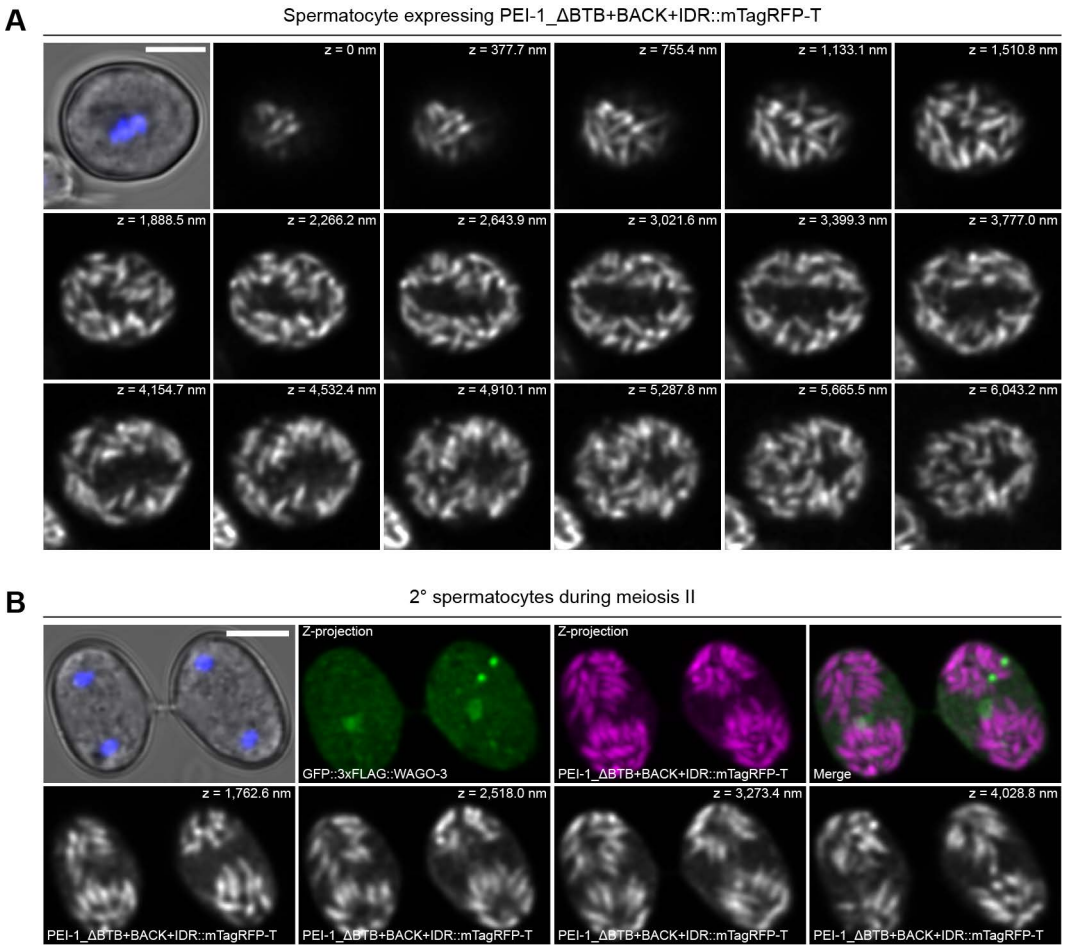

Figure 25 | PEI-1_ΔBTB+BACK+IDR::mTagRFP-T is asymmetrically segregated into spermatids. A, Confocal Z-stack of a male-derived spermatocyte expressing PEI-1_ΔBTB+BACK+IDR::mTagRFP-T as shown in Figure 24. B, Confocal maximum intensity projections and respective optical sections of two male-derived secondary spermatocytes during their second meiotic division. Cells are expressing GFP::3xFLAG::WAGO-3 and PEI-1_ΔBTB+BACK+IDR::mTagRFP-T. Z-sizes: 125.9 nm (A-B). Scale bars: 4 µm (A-B)

As we observed a variety of subcellular alterations when manipulating PEI-1, we wondered about the localization and segregation of a simple fluorescent protein during germ cell development, and in particular spermatogenesis. Therefore, we used the CRISPR/Cas9-mediated genome editing system to further edit the endogenous *wago-3(xf119)* locus, which encodes the GFP::3xFLAG::WAGO-3 fusion-protein. By introducing a defined deletion covering all expressed and intervening sequences of *wago-3*, we managed to generate a transcriptional GFP::3xFLAG reporter whose expression was still controlled by the endogenous *wago-3* locus (**Figure 26A**).

First, we performed confocal microscopy of hermaphrodites to determine the expression pattern of the transcriptional GFP::3xFLAG reporter. Similar to GFP::3xFLAG::WAGO-3, the transcriptional reporter was specifically and globally expressed throughout germline

development, but did not localize to any distinct foci in the cytoplasm or at the nuclear periphery (**Figure 26B**). Second, we isolated male-derived spermatocytes and budding spermatids to have a closer look at the subcellular localization and segregation of GFP::3xFLAG during spermatogenesis. We found that GFP::3xFLAG was evenly distributed in all cell types without showing any preference for either residual body or budding spermatid (**Figure 26C**), reminiscent of the symmetric segregation of PEI-1_ΔBACK+IDR::mTagRFP-T. Concordantly, we also detected diffuse GFP::3xFLAG signals within the spermatheca (**Figure 26B**), indicating the presence of GFP::3xFLAG in mature sperm. The fact that the asymmetric segregation into residual bodies was only detected for GFP::3xFLAG::WAGO-3 in *pei-1(ok1050)* mutants (or any truncated PEI-1::mTagRFP-T variant lacking the IDR), but not for free GFP::3xFLAG, indicates that the accumulation into the residual body may be driven by an active sorting process during meiosis II. Alternatively, non-PEI-1 bound WAGO-3 may be unstable in spermatocytes and spermatids.

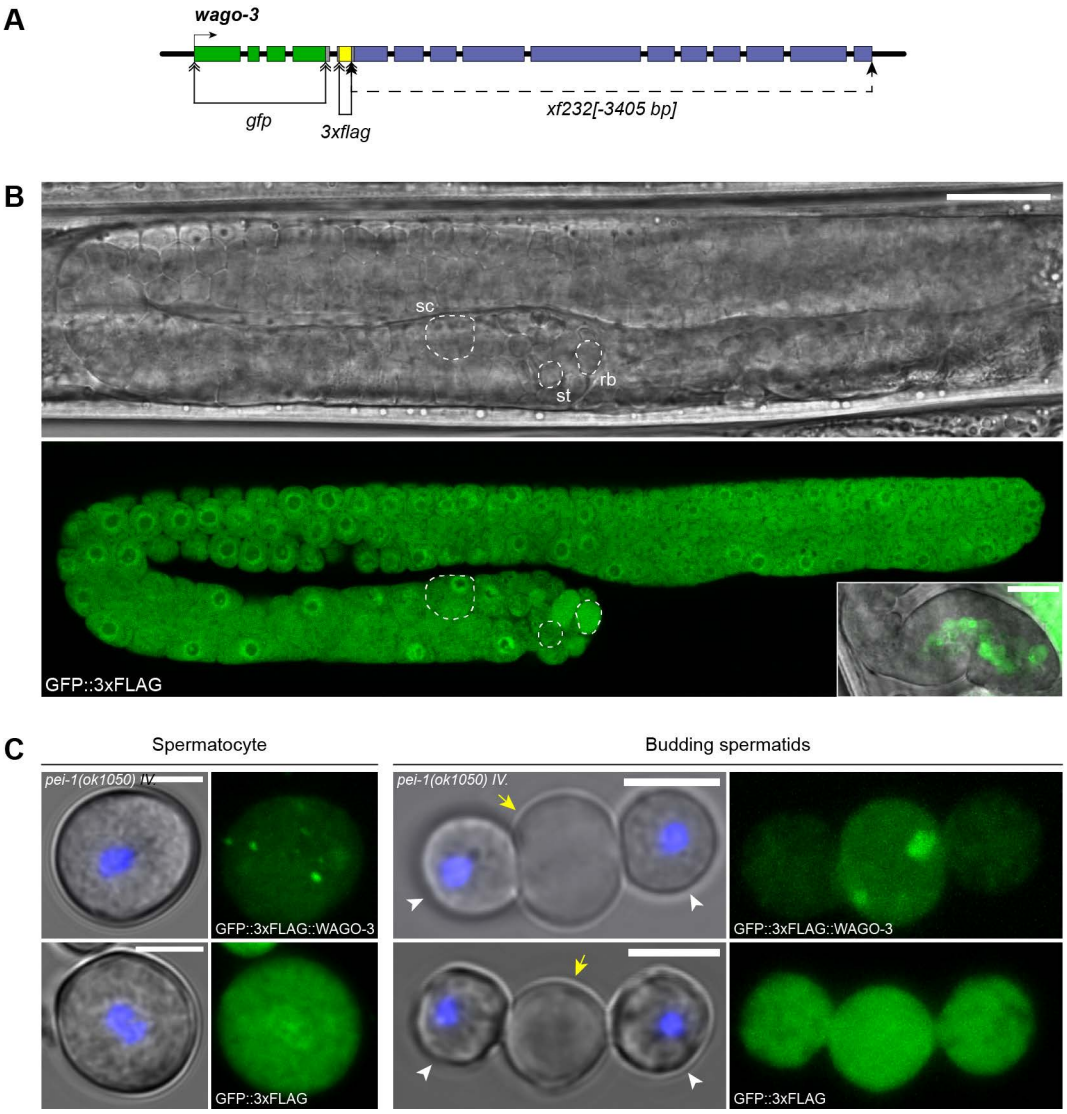

Figure 26 | A transcriptional GFP reporter from the *wago-3* locus is evenly distributed throughout spermatogenesis. A, Schematic representation of the *wago-3* locus. Double-headed arrows indicate inserted sequences, dashed arrows indicate a 3405 bp deletion, the single headed arrow marks the transcription start site and boxes represent exonic sequences (green; *gfp*, yellow; *flag*, blue; *wago-3*). B, Confocal micrographs of a L4 stage hermaphrodite expressing GFP::3xFLAG from the endogenous *wago-3* locus. Insert shows presence of GFP::3xFLAG within the spermatheca of an adult hermaphrodite. A representative spermatocyte (sc), spermatid (st) and residual body (rb) is outlined by a dashed line. C, Confocal maximum intensity projections of isolated male-derived spermatocytes and budding spermatids expressing indicated proteins. White arrowheads mark budding spermatids, yellow arrows indicate residual bodies. Hoechst33342 was used to stain DNA. Scale bars: 20 µm (B, gonad), 10 µm (B, spermatheca), 4 µm (C)

The specific feature of WAGO-3 enabling PEI-1 interaction remains elusive

The intrinsically disordered region of PEI-1 was found to be required for the interaction with WAGO-3. As such regions were often reported to interact with other intrinsically disordered regions (Cho et al., 2018; Chong et al., 2018; Sabari et al., 2018), we had a closer look at WAGO-3 in order to identify a certain peptide or region allowing PEI-1 to specifically recruit WAGO-3 to the described sperm foci. Using PONDR® algorithms, we found that WAGO-3 contains four predicted intrinsically disordered regions: one covering the first 78 amino acids, another two within the PAZ domain and the PIWI domain, respectively, and finally a fourth covering the last 14 amino acids (**Figure 27A**). Although the intrinsically disordered region covering the most N-terminal peptide of WAGO-3 is the most prominent in terms of PONDR® scores, we noticed this feature to be common among worm Argonaute proteins (**Figure 27, B-E**). Only two Argonaute proteins of *C. elegans*, namely RDE-1 and WAGO-5, were found to encode an N-terminal peptide that was not predicted to adopt an intrinsically disordered region. However, we also noticed differences, as only branch 1 WAGO proteins, except WAGO-5, exhibit a proline-rich low complexity region causing the predicted high degree of disorder (**Figure 27F**). We again used the CRISPR/Cas9-mediated genome editing system to specifically remove the first 50 amino acids of WAGO-3 within the GFP::3xFLAG::WAGO-3 fusion-protein. Surprisingly, we found that any in-frame deletion covering these amino acids resulted in acute sterility, even in a heteroallelic combination (data not shown), a phenotype that was never observed before for any mutant *wago-3* allele (de Albuquerque et al., 2015; Gu et al., 2009; Robert et al., 2005; Vastenhouw et al., 2003; Yigit et al., 2006). Thus far, this dominant sterility has prevented us from studying the relevance of the WAGO-3 N-terminus in its subcellular localization.

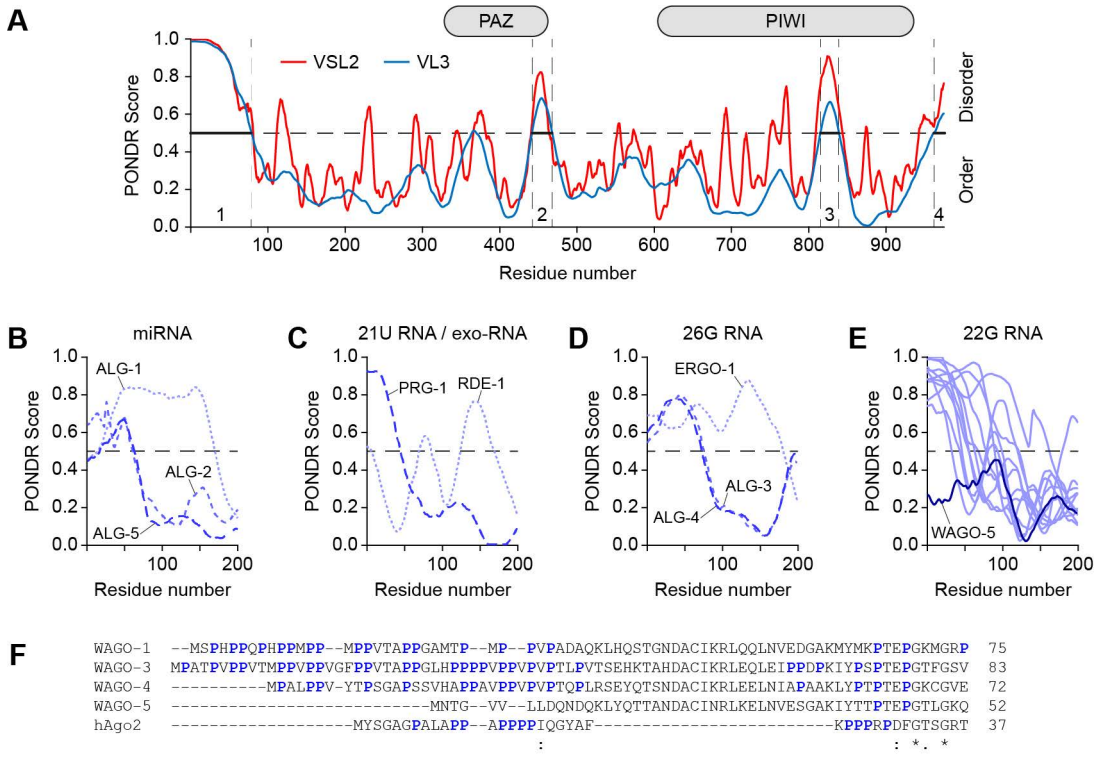

Figure 27 | WAGO-3 contains four intrinsically disordered regions. A, PONDR® predictions of intrinsically disordered regions in WAGO-3 using VSL2 and VL3 algorithms. Intrinsically disordered regions are marked by vertical dashed lines and numbered from one to four. Locations of the PAZ and PIWI domain are indicated above the diagram. B-E, PONDR® VL3 predictions of intrinsically disordered regions within the first 200 amino acids of all Argonaute proteins of *C. elegans*, sorted by the associated small RNAs. Pseudogenes were excluded from the analysis. F, Sequence alignment of branch 1 WAGO proteins and human Ago2. Only the most N-terminal amino acids are shown. Prolines are highlighted with bold blue letters. The sequence alignment was generated using Clustal Omega (Madeira et al., 2019).

The intrinsically disordered region within the PAZ domain as well as the most C-terminal peptide revealed no discernible characteristics with regard to the primary WAGO-3 protein structure when compared to other members of the Argonaute family. In contrast, the intrinsically disordered region within the PIWI domain is based on an intriguing peptide. We found that the PIWI domain of WAGO-3 contains a serine-rich low complexity region causing a high degree of predicted disorder according both PONDR® algorithms. These two characteristics could not be identified for human Ago2 (**Figure 28A**) or any other Argonaute protein of *C. elegans* (**Figure 28B**). We noticed, however, that WAGO-4 also contains a serine-rich low complexity region within the PIWI domain, but no prominent intrinsically disordered region was predicted to cover this peptide according to the VL3 predictor. RDE-1, on the other hand, was indeed predicted

to contain a prominent intrinsically disordered region within its PIWI domain, which, however, is not based on a serine-rich low complexity region.

Next, we used the *SWISS-MODEL Repository* to generate a homology model of WAGO-3 using the experimentally resolved protein structure of human Ago2 (template: 4z4f.1.A) (Bienert et al., 2017). Intriguingly, we found that the PIWI domain-located serine-rich low complexity region likely adopts a loop, which was predicted to be on the surface of WAGO-3 (**Figure 28C**). Since this structural feature seemed to be unique to WAGO-3, we removed a 22 amino acid long peptide containing every serine of this feature using the CRISPR/Cas9 system. Unfortunately, we found that the edited GFP::3xFLAG::WAGO-3 fusion-protein still localized to cytoplasmic foci during spermatogenesis (**Figure 28D**), suggesting that the serine-rich low complexity region is not required for sperm localization.

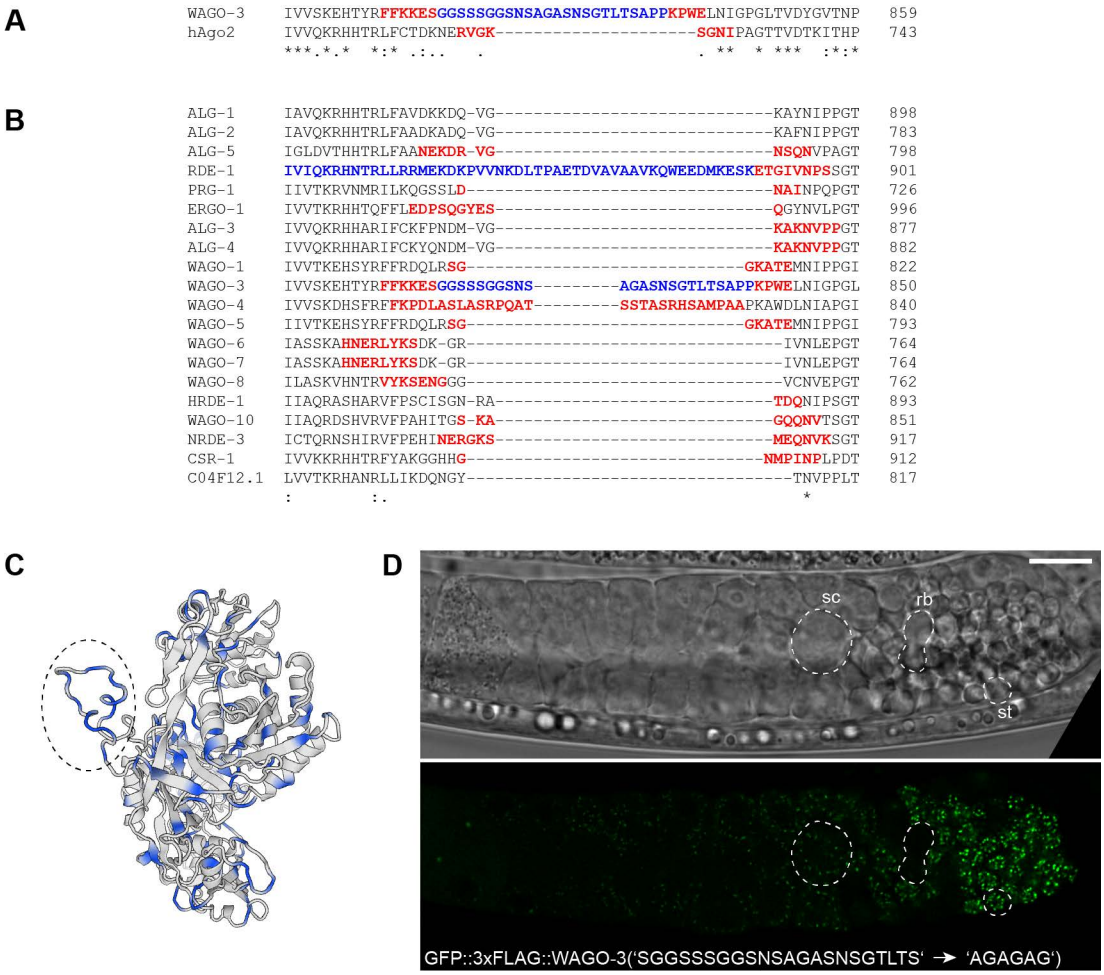

Figure 28 | The serine-rich low complexity region of WAGO-3 is not required for sperm localization. A-B, Sequence alignments of WAGO-3 and human Ago2 (A), and of all Argonaute proteins of *C. elegans* (B). Only the protein regions aligned to the serine-rich low complexity region of WAGO-3 are shown. PONDR® predictions of intrinsically disordered regions are highlighted with bold red and bold blue letters according to VSL2 and VL3 algorithms, respectively. Pseudogenes were excluded from the analysis. The sequence alignments were generated using Clustal Omega (Madeira et al., 2019). C, SWISS-MODEL of WAGO-3 using human Ago2 as template (4z4f.1.A) (Bienert et al., 2017). Serines and threonines are highlighted in blue. The serine-rich low complexity region is marked by a dashed oval. D, Confocal micrographs showing the proximal region of a spermatogenic gonad of a late-L4 stage hermaphrodite expressing GFP::3xFLAG::WAGO-3('SGGSSSGGSNSAGASNSGTLTS'-to-'AGAGAG'). A representative spermatocyte (sc), spermatid (st) and residual body (rb) is outlined by a dashed line. Scale bar: 10 µm (D)

PEI granules are independent condensates

In *C. elegans*, non-membranous compartments, like P granules and *Mutator* foci, are phase-separated condensates known to play crucial roles in germ cell biology as they, amongst other things, compartmentalize the biogenesis of 21U RNAs and 22G RNAs, respectively. In this context, we tested whether PEI-1::mTagRFP-T foci depend on any of these known, phase-separated condensates. To achieve this, we introduced the

mut-16(xf142) deletion allele in animals expressing PEI-1::mTagRFP-T. As described earlier, MUT-16 was shown to act as the nucleator triggering *Mutator* foci assembly (Phillips et al., 2012; Uebel et al., 2018). Similarly, we used the *deps-1(bn124)* mutant allele to disrupt P granule formation (Spike et al., 2008). We found that neither MUT-16 nor DEPS-1 was required for proper localization of PEI-1::mTagRFP-T during spermatogenesis (**Figure 29**), indicating that the assembly of PEI-1::mTagRFP-T foci does not depend on P granules or *Mutator* foci. Conversely to the effect of PEI-1 on GFP::3xFLAG::WAGO-3, we also found that loss of WAGO-3 did not affect PEI-1::mTagRFP-T localization during sperm maturation (**Figure 29**). Hence, PEI-1::mTagRFP-T foci represent an independent entity, which we will from here on refer to as PEI granules.

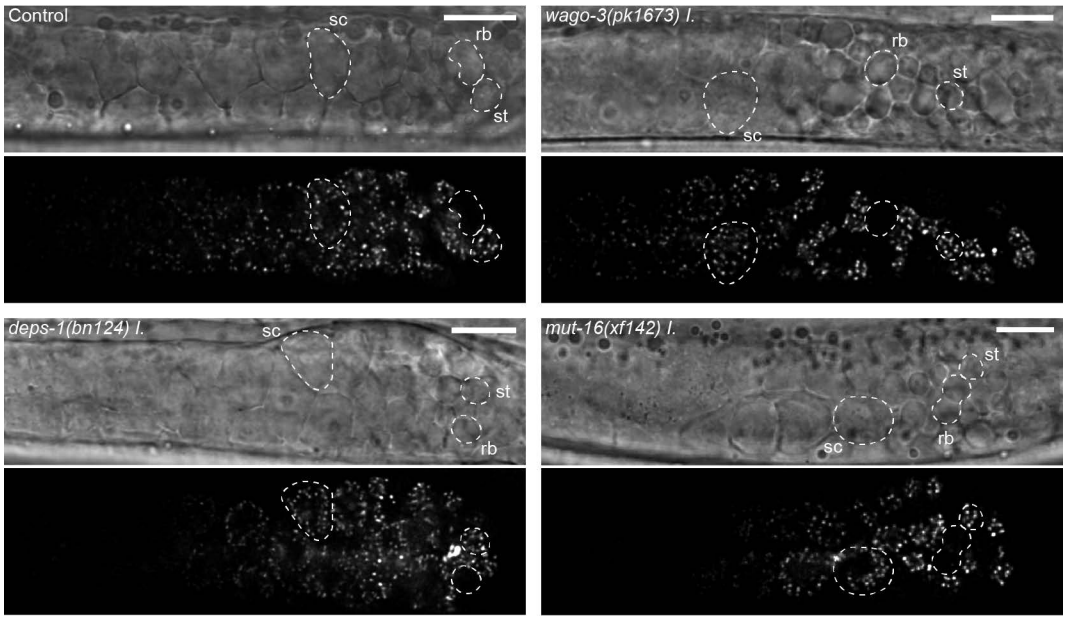

Figure 29 | PEI-1 foci formation is independent on P granules and *Mutator* foci. Confocal micrographs showing proximal regions of spermatogenic gonads of late-L4 stage hermaphrodites expressing PEI-1::mTagRFP-T in indicated mutants. Representative spermatocytes (sc), spermatids (st) and residual bodies (rb) are outlined by a dashed line. Scale bars: 10 µm

PEI granules retain WAGO-3 via hydrophobic interactions

Many physicochemical factors, either intrinsic to components of biomolecular condensates or defined by its environment, affect phase separation behavior. Various studies have demonstrated that phase separation can involve various types of intermolecular interaction including pi/pi, cation/pi, electrostatic and hydrophobic

interactions (Alberti et al., 2019; Hyman et al., 2014; Kroschwald et al., 2017; Wegmann et al., 2018).

In order to start characterizing the physical properties of PEI granules, we used 1,6-hexanediol, an aliphatic compound that was shown to disrupt weak hydrophobic interactions, and hence affect intermolecular interactions regulating phase separation (Kroschwald et al., 2017). 1,6-hexanediol is membrane permeable and easy to apply in *ex vivo* studies. Thus, we isolated male-derived spermatocytes and budding spermatids to monitor both GFP::3xFLAG::WAGO-3 and PEI-1::mTagRFP-T in the presence of different concentrations of 1,6-hexanediol. Notably, GFP::3xFLAG::WAGO-3 was found to be highly sensitive towards this treatment, as no localization to PEI granules was detected anymore in the presence of merely 1.25 % 1,6-hexanediol. Also, we did not detect any difference in WAGO-3 sensitivity between spermatocytes (**Figure 30A**) and budding spermatids (**Figure 30B**). These results indicate a major role for hydrophobic interactions in GFP::3xFLAG::WAGO-3 localization to PEI granules throughout spermatogenesis. We also noticed that GFP::3xFLAG::WAGO-3 preferentially localized to residual bodies upon 1,6-hexanediol treatment, which in turn substantiates the idea of a cellular process ensuring the accumulation of selected proteins and organelles into the residual body.

In contrast, PEI-1::mTagRFP-T was found to be more resistant towards the 1,6-hexanediol treatment. We observed a gradual tendency for PEI-1::mTagRFP-T to be more diffusely localized the more we increased the 1,6-hexanediol concentration. Notably, we found 1,6-hexanediol to differentially affect PEI-1::mTagRFP-T localization depending on the cell type. In spermatocytes, we could hardly detect any remaining PEI-1::mTagRFP-T foci in the presence of 5 % 1,6-hexanediol (**Figure 30A**). In striking contrast, PEI-1::mTagRFP-T foci were detectable in budding spermatids throughout our dilution series (**Figure 30B**). Even at a concentration of 5 % 1,6-hexanediol, PEI-1::mTagRFP-T was localizing to cytoplasmic foci in budding spermatids, although faint signals in residual bodies started to become apparent. Any further increase in the 1,6-hexanediol concentration caused cell death of both spermatocytes and budding spermatids.

Everything considered, PEI granules were found to retain GFP::3xFLAG::WAGO-3 via weak hydrophobic interactions, whereas PEI granules themselves seemingly depend on additional interactions or stronger hydrophobicity. Moreover, we observed that PEI granules show a reduced sensitivity towards the 1,6-hexanediol treatment in budding

spermatids compared to spermatocytes, suggesting changes in the physical properties of these condensates during sperm maturation.

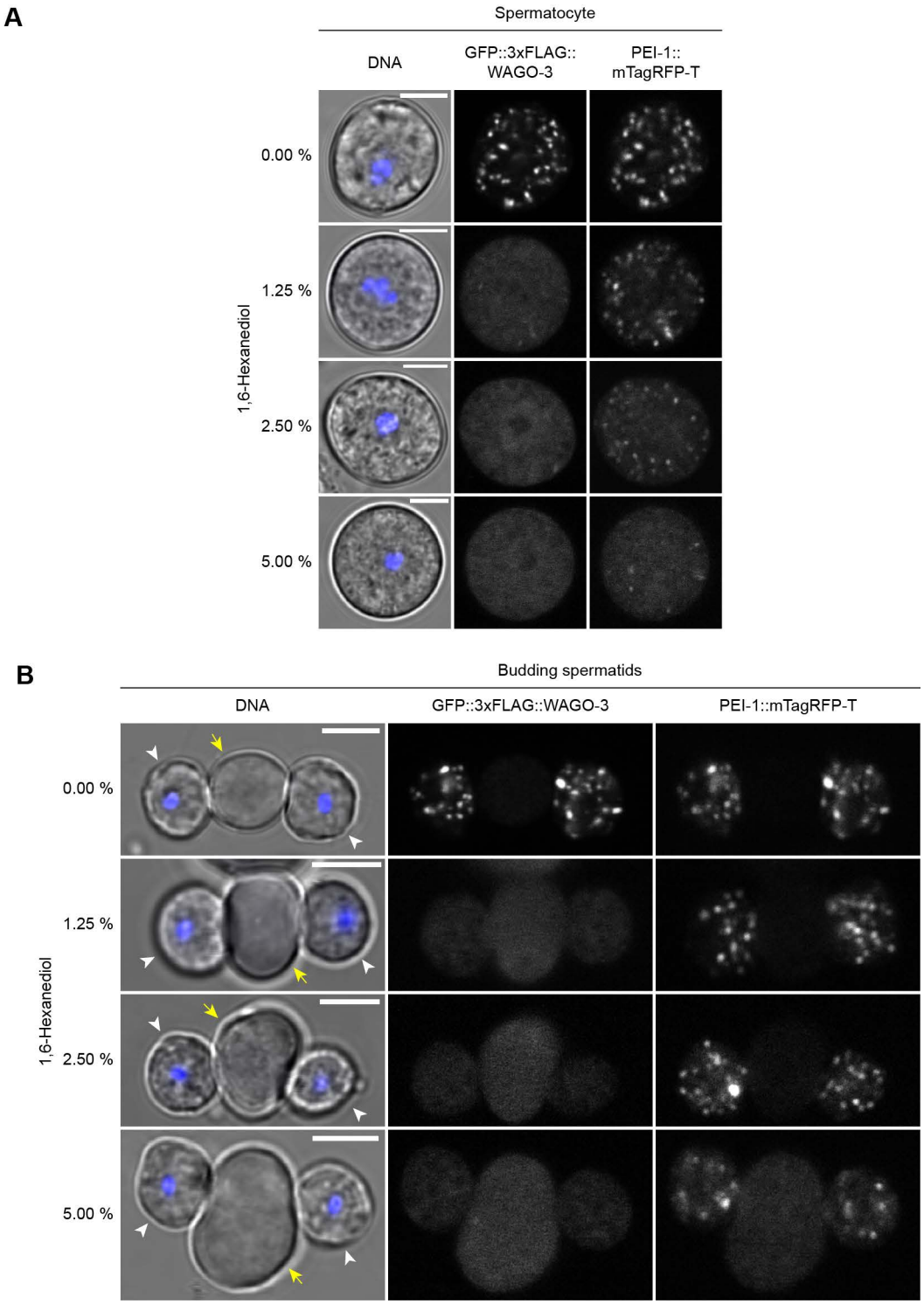

Figure 30 | PEI granules retain WAGO-3 via hydrophobic interactions. A-B, Confocal micrographs of isolated male-derived spermatocytes (A) and budding spermatids (B) after treatment with 1,6-hexanediol. White arrowheads mark budding spermatids and yellow arrows indicate residual bodies. Hoechst33342 was used to stain DNA. Scale bars: 4 µm (A-B)

PEI granules are liquid-like condensates of low mobility

We then addressed the dynamics of PEI granules to properly describe them as either liquid-like or solid-like condensates. Liquid-like condensates are characterized by their ability to fuse followed by a subsequent reversion to a spherical shape. In addition, liquid-like condensates exhibit internal rearrangements and show exchange dynamics with their environment, while constantly maintaining their spherical shape. Even though gel-like condensates can potentially keep the form of the liquid-like state they originated from, none of the above describes dynamics were found in condensates after extensive hardening (Hyman et al., 2014).

First, we addressed PEI granule mobility using a live-imaging approach. Therefore, we monitored isolated, male-derived spermatocytes expressing GFP::3xFLAG::WAGO-3. Surprisingly, we found that GFP::3xFLAG::WAGO-3 foci were rather static, as no major movements were observed within a period of one hour (**Figure 31A**). This feature obviously also prevented us from detecting any fusion or fission events between individual foci.

Next, we asked to which extent PEI granules exchange material with the surrounding cytoplasm. In order to compare obtained properties, we measured the fluorescence recovery after photobleaching (FRAP) of GFP::3xFLAG::WAGO-3 when localizing to either P granules in meiotic germ cells or PEI granules in male-derived budding spermatids. As previously reported, proteins localizing to the liquid phase of P granules exhibit high recovery rates (Brangwynne et al., 2009; Putnam et al., 2019; Sheth et al., 2010). Similarly, we found that GFP::3xFLAG::WAGO-3 also showed very rapid fluorescence recovery in P granules ($t_{½}$ = 3.2 +/- 1.5 s) (**Figure 31, B and C**). Strikingly, GFP::3xFLAG::WAGO-3 exhibited much lower exchange dynamics when localizing to PEI granules in budding spermatids ($t_{½}$ = 47.3 +/- 17.6 s) (**Figure 31, B and C**). The calculated half-time of the measured fluorescence recovery of GFP::3xFLAG::WAGO-3 thus differed by about one order of magnitude between P granules and PEI granules. Furthermore, we found that the mobile fraction of GFP::3xFLAG::WAGO-3 within the condensates was slightly reduced in PEI granules compared to P granules (**Figure 31C**).

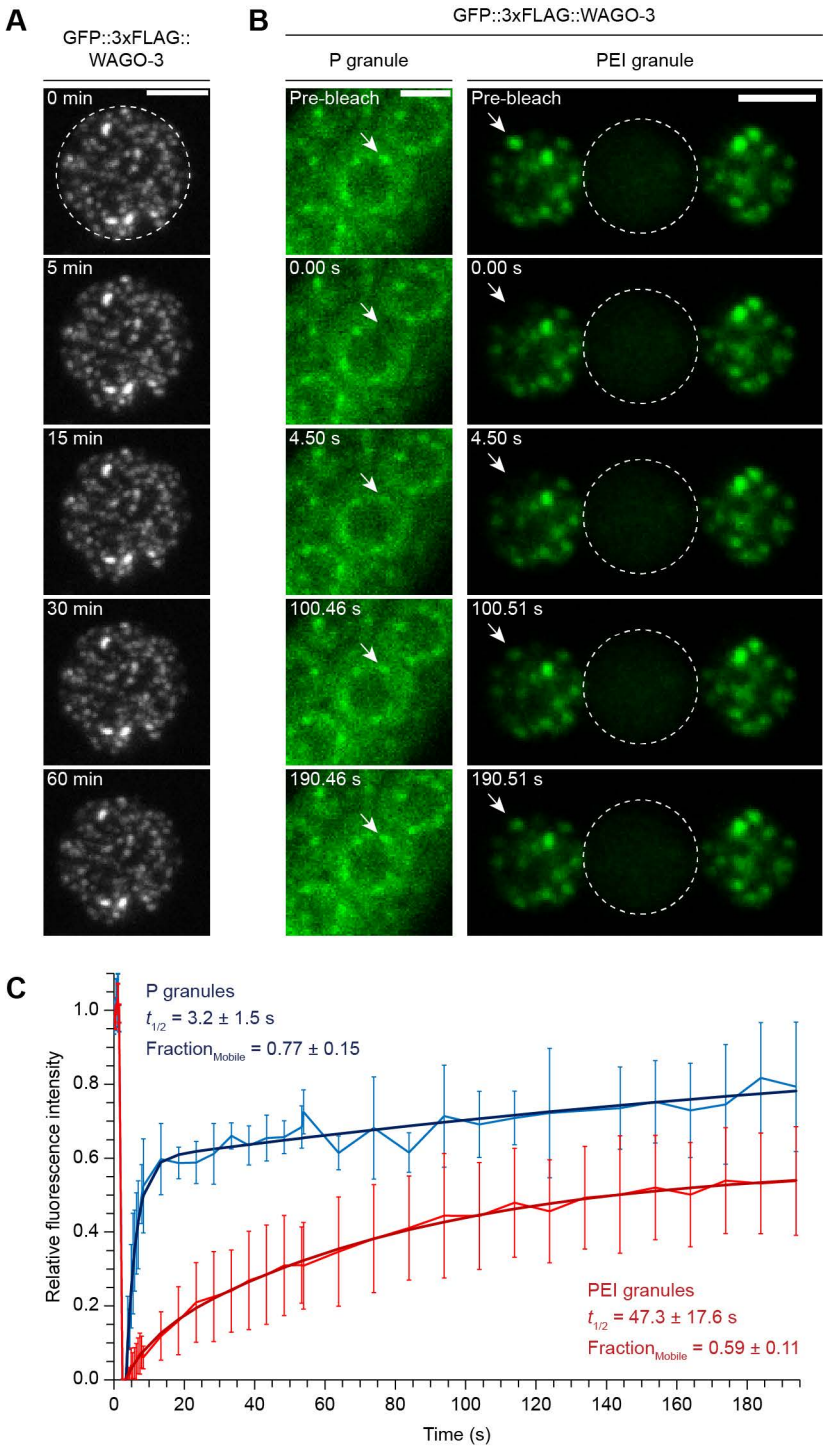

Figure 31 | PEI granules show exchange dynamics with the cytoplasm and low intracellular mobility. A, Time sequence of an isolated male-derived spermatocyte expressing GFP::3xFLAG::WAGO-3. Images are confocal maximum intensity projections. The spermatocyte is outlined by a dashed circle. B, Time sequence of naïve germ cells and isolated male-derived budding spermatids showing fluorescence recovery after photobleaching (FRAP) of GFP::3xFLAG::WAGO-3 localizing to P granules and PEI granules, respectively. White arrows mark bleached foci and dashed circles indicate the residual body. C, FRAP recovery curve of GFP::3xFLAG::WAGO-3. Normalized data is presented as mean +/- standard deviation, and was fitted to a double exponential curve (n = 4 granules). Scale bars: 4 µm (A-B)

Although the fluorescence recovery of GFP::3xFLAG::WAGO-3 was slower in PEI granules compared to P granules, the measured exchange dynamic was still faster than that typically found in gel-like assemblies (Putnam et al., 2019). Thus, we compared PEI-1 with proteins found in either the liquid or the gel-like phase of P granules. PGL-1 and PGL-3 were shown to localize to the liquid phase of P granules, where they affect P granule formation (Hanazawa et al., 2011; Kawasaki et al., 1998, 2004). In contrast, MEG-3 and MEG-4 were reported to form gel-like assemblies that associate with the liquid phase of P granules in the embryo (Putnam et al., 2019). As previously demonstrated, the prevalence of certain amino acids modulates the material property of phase-separated condensates (Wang et al., 2018). In particular, glycine residues were shown to maintain liquidity, while serine and glutamine residues promote hardening of condensates (**Figure 32A**). Thus, we analyzed the amino acid composition of the intrinsically disordered regions that were predicted for PEI-1, PGL-1, PGL-3, MEG-3 and MEG-4. In order to identify enrichments of certain residues, we compared the determined amino acid compositions with the SwissProt database (Bateman, 2019), which was shown to be closest to the distribution of amino acids in nature (Vacic et al., 2007).

We found that serine residues are significantly overrepresented in PEI-1 (**Figure 32B**), while both serine and glycine residues are enriched in PGL-1 and PGL-3 (**Figure 32, C and D**). In contrast, MEG-3 and MEG-4 revealed an enrichment in serine and asparagine residues, with MEG-3 additionally showing a compositional bias for glutamines (**Figure 32, E and F**). Although asparagine has not been shown to promote hardening of biomolecular condensates, its impact on phase separation is well described. Both asparagine and glutamine were characterized as aggregation-prone amino acids, which are commonly found in eukaryotic, amyloid-like aggregates, prion proteins and intrinsically disordered proteins like TDP-43 and hnRNPA1L2 (Alberti et al., 2009; Babinchak et al., 2019; Cascarina and Ross, 2019; French et al., 2019; Michelitsch and Weissman, 2000; Reijns et al., 2008; Wang et al., 2018a). Whether the enrichment of serine and asparagine/glutamine residues in combination with a deletion of glycines promotes the formation of the gel-like MEG phase remains to be determined.

Taken together, we found that PEI granules indeed exchange material with the surrounding cytoplasm. Considering the measured exchange dynamics as well as the mobile fraction of GFP::3xFLAG::WAGO-3, PEI granules clearly display characteristics of liquid-like condensates. Moreover, our results show that PEI granules retain WAGO-3 more efficiently than P granules. This observation may indicate an increased viscoelasticity of PEI granules, which is possibly driven by the prevalence of serine

residues in the intrinsically disordered region of PEI-1. The lack of intracellular mobility, however, may indicate an association of PEI granules to bigger subcellular structures, similar to P granule association with clusters of nuclear pore complexes on germ cell nuclei (Sheth et al., 2010).

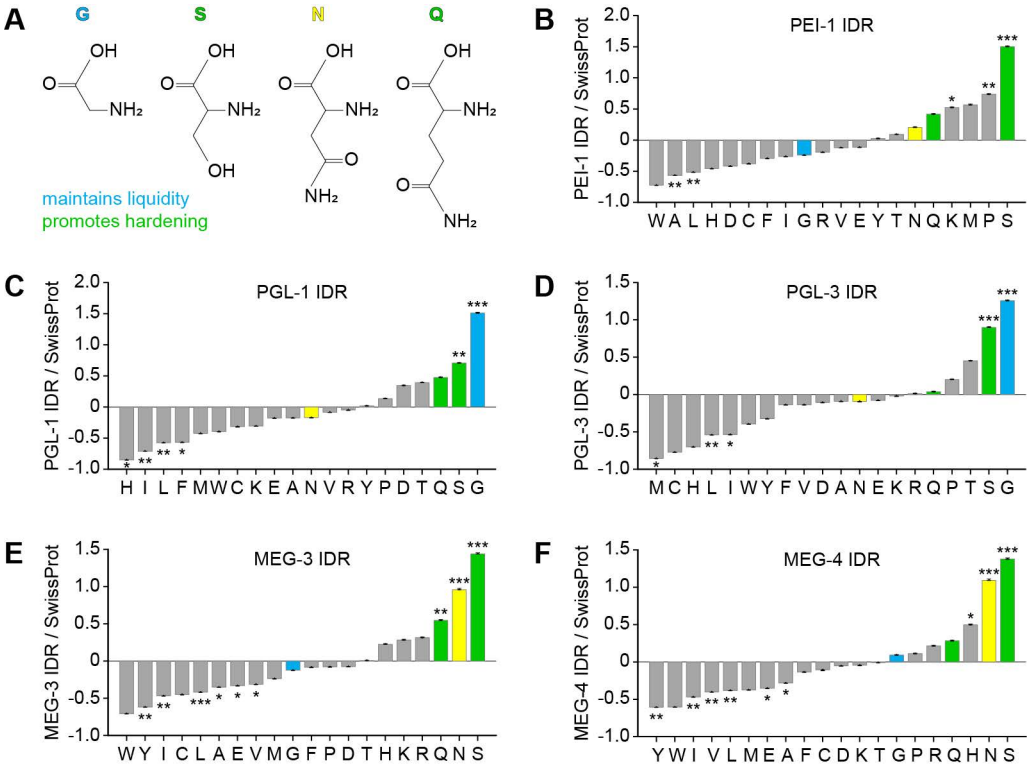

Figure 32 | The intrinsically disordered region of PEI-1 displays an amino acid composition that potentially promotes PEI granule hardening. A, Chemical structure of glycine, serine, asparagine and glutamine. B-F, Amino acid composition profiles of the intrinsically disordered regions of PEI-1 (B), PGL-1 (C), PGL-3 (D), MEG-3 (E) and MEG-4 (F). Bars representing serines/glutanimes, glycines and asparagines are highlighted in green, blue and yellow, respectively. The profiles were generated using Composition Profiler (Vacic et al., 2007). Sequences were analyzed against the SwissProt database (Bateman, 2019) using 10,000 bootstrap iterations. Statistical significance was tested using the two-sample t-test (Vacic et al., 2007). ***: $p \leq 0.001$, **: $p \leq 0.01$, *: $p \leq 0.05$

Immunoprecipitation of PEI co-enriched numerous mitochondrial proteins and a PEI-1 homolog

A substantial amount of cellular material, including free ribosomes, the endoplasmic reticulum and the Golgi apparatus, is asymmetrically segregated into residual bodies during the second meiotic division. Only a few organelles, like the nucleus, mitochondria and the sperm-specific fibrous body-membranous organelles (FB-MOs) are exclusively sorted into budding spermatids (Ellis and Stanfield, 2014). Given the very low mobility of PEI granules, we wondered whether they might be associated with one of these organelles, thereby ensuring their segregation into budding spermatids.

To address this issue, we performed immunoprecipitation experiments of PEI-1::3xMYC using whole-worm extracts of late-L4 stage hermaphrodites, followed by label-free quantitative mass spectrometry. These experiments identified 172 enriched proteins (**Figure 33A**), which we compared to proteomic studies describing either male-derived spermatids or purified mitochondria from *C. elegans* (Jing et al., 2009; Ma et al., 2014). As expected, the vast majority of the enriched proteins were also identified in the spermatid proteome (141/172; 82 %) (**Figure 33B**), leaving only a few proteins that might be present in spermatocytes, but absent in spermatids. A large number of proteins strikingly coincided with the published mitochondria proteome (110/172; 64 %) (**Figure 33B**). In addition, we also found numerous ribosomal proteins (43/172; 25 %) and major sperm protein (MSP), which is the major component of the fibrous body. Among all detected proteins, RBM-3.2 and R09A1.2 showed the highest enrichment scores upon PEI-1::3xMYC immunoprecipitation (**Figure 33A**). Both proteins were also identified in the spermatid, but not the mitochondria proteome. *RBM-3.2* encodes a germline-expressed protein of 9.4 kDa (85 aa), which solely contains an RNA binding motif (F4 - N82). Proteomic analyses indicate that RBM-3.2 is present in spermatids and spermatozoa (Kasimatis et al., 2018; Ma et al., 2014).

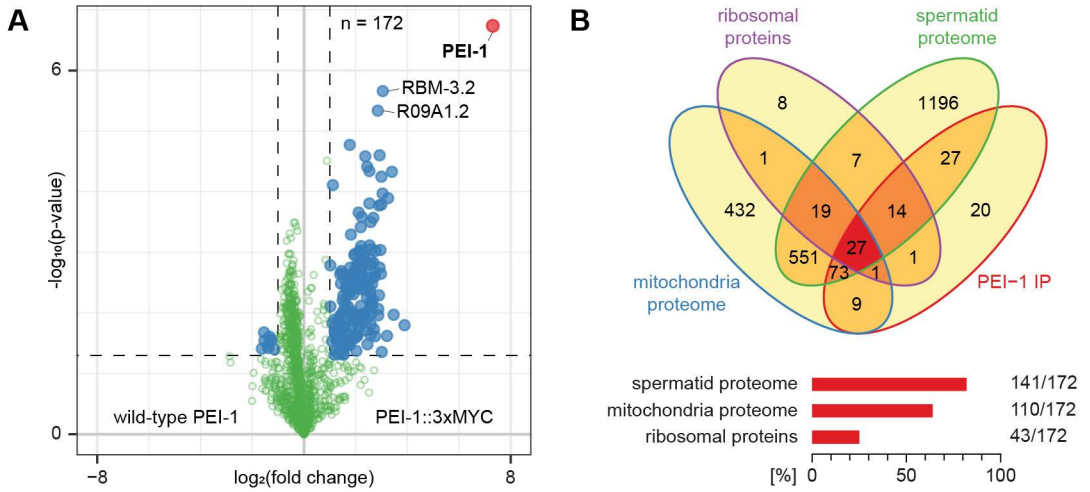

Figure 33 | PEI-1 immunoprecipitations co-enrich numerous mitochondrial proteins. A, Volcano plot representing label-free proteomic quantification of PEI-1::3xMYC immunoprecipitation experiments from late-L4 stage hermaphrodite extracts. The *X*-axis indicates the mean fold enrichment of individual proteins in the control (wild-type PEI-1) versus the genome-edited strain (PEI-1::3xMYC). The *Y*-axis represents $-\log_{10}$(p-value) of observed enrichments. Dashed lines show thresholds at P = 0.05 and twofold enrichment. Blue and green data points represent above and below threshold, respectively. PEI-1 is highlighted with a red data point. B, Venn diagramm and bar chart showing comparison of enriched proteins from (A) with ribosomal proteins and the proteomes of spermatids and mitochondria from *C. elegans*.

As PEI-1 evidently affects PEI granule formation, stabilization and composition, we were intrigued by the proteomic identification of R09A1.2, as it represents a PEI-1 homolog. In total, we found four *pei-1* paralogs to be encoded in the genome of *C. elegans*, of which *R09A1.2* is predicted to be the closest paralog to *pei-1* (**Figure 34A**). Notably, R09A1.2 was the only PEI-1 homolog identified in our PEI-1 IP-MS/MS experiments, while both R09A1.2 and C17H12.12 were identified in the proteomic analysis of isolated, male-derived spermatids (**Figure 34B**) (Ma et al., 2014). Even though *R09A1.2* encodes a smaller protein than *pei-1*, both proteins contain an annotated BTB domain, an HHpred-predicted BACK domain (**Figure 34C**) (Zimmermann et al., 2018) and a PONDR®-predicted intrinsically disordered region (**Figure 34, D and E**). The latter feature, however, is clearly different between both homologs, as R09A1.2 lacks the extent of the intrinsically disordered region found in PEI-1. Interestingly, R09A1.2 additionally contains a predicted intrinsically disordered region covering the first 15 amino acids. Using the NetPhos 3.1 server to predict potential serine, threonine or tyrosine phosphorylation sites, we found that both PEI-1 and R09A1.2 show a high potential to be regulated in a phosphorylation-dependent manner (Blom et al., 1999) (**Figure 34, F and G**).

Overall, our IP-MS/MS experiments clearly point towards an association of PEI granules with mitochondria, and possibly with FB-MOs. The identification of many ribosomal proteins is also consistent with the idea of mitochondria association, as previous proteomic and microscopic analyses identified and visualized cytosolic ribosomes on the surface of mitochondria, respectively (Gold et al., 2017; Jing et al., 2009). Moreover, our proteomic experiments identified two proteins, RBM-3.2 and R09A1.2, which potentially interact with PEI-1 and may function in PEI granule formation.

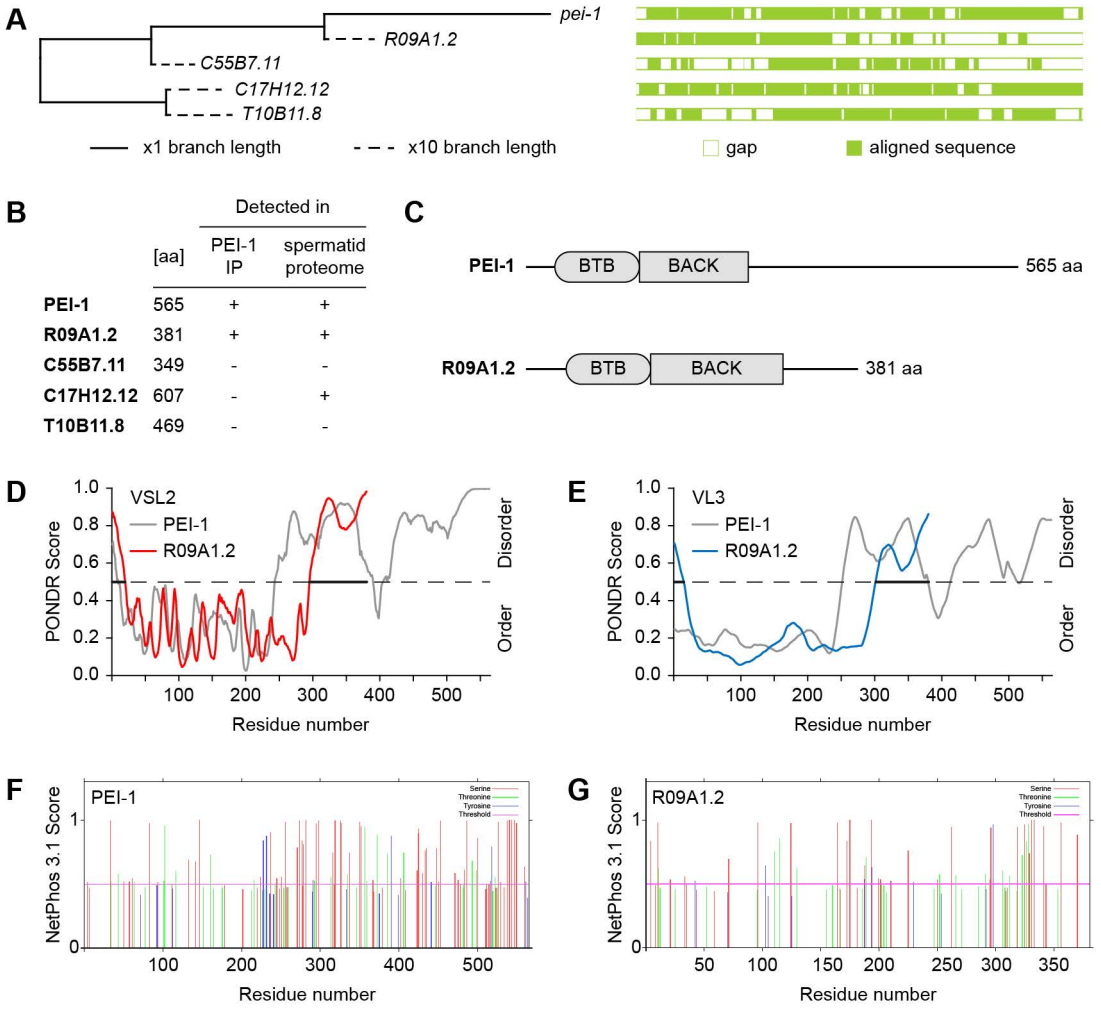

Figure 34 | *R09A1.2* is a *pei-1* paralog. A, Ensemble gene tree representing paralogs of *pei-1*. The tree was generated by the Gene Orthology/Paralogy prediction method pipeline (Yates et al., 2019). B, Only R09A1.2 was both co-enriched in PEI-1 IP-MS/MS experiments and identified in the spermatid proteome. C, Schematic representing protein domains of PEI-1 and R09A1.2. Domain annotations are based on InterPro (BTB) and HHpred (BACK) (Mitchell et al., 2019; Zimmermann et al., 2018). D-E, PONDR® predictions of intrinsically disordered regions in R09A1.2 using VSL2 (D) and VL3 (E) algorithms. PONDR® predictions for PEI-1 are shown in grey. F-G, Predictions of serine, threonine and tyrosine phosphorylation sites in PEI-1 (F) and R09A1.2 (G), generated by the NetPhos 3.1 server (Blom et al., 1999).

PEI granules localize next to mitochondria throughout spermatogenesis

As our proteomic experiments identified numerous mitochondrial proteins and MSP, we sought to determine the subcellular localization of mitochondria and FB-MOs in maturing sperm cells in relation to PEI granules. We found that PEI-1::mTagRFP-T foci always localized next to mitochondria in both male-derived spermatocytes and budding spermatids (**Figure 35A**). Throughout our microscopic analysis, we did not detect any co-localization of both signals. To probe for FB-MO association, we performed confocal microscopy on isolated, male-derived spermatids expressing GFP::3xFLAG::WAGO-3 and SPE-45::mCherry. SPE-45 has been reported to localize to membranous organelles of FB-MOs (Gleason et al., unpublished), which are found close to the cell membrane in spermatids (Ellis and Stanfield, 2014). Likewise, SPE-45::mCherry adopted a peripheral distribution. In contrast, GFP::3xFLAG::WAGO-3 foci were detected throughout the cytoplasm (**Figure 35B**), suggesting that PEI granules are not closely associated with FB-MO-derived membranous organelles in spermatids.

Finally, we also checked whether the structures visualized by PEI-1_ΔBTB+BACK+IDR::mTagRFP-T correspond to mitochondria. Simultaneous imaging of the truncated PEI-1_ΔBTB+BACK+IDR::mTagRFP-T variant and mitochondria revealed a mutually exclusive localization pattern in both spermatocytes and budding spermatids (**Figure 35, C and D**), suggesting that the earlier described unknown structures of defined shape are not mitochondria.

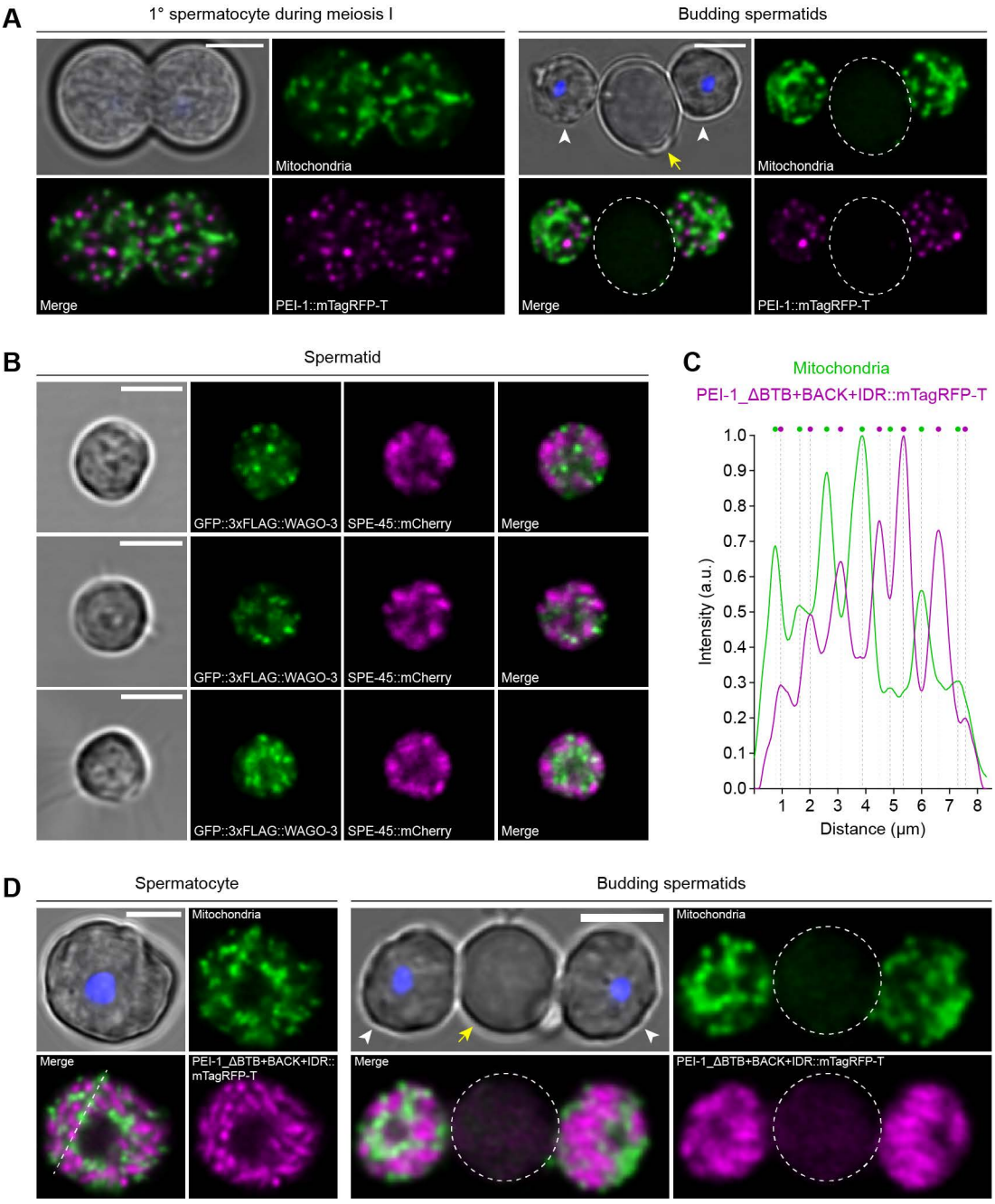

Figure 35 | PEI granules localize next to mitochondria without showing a peripheral distribution in spermatids. A, Confocal micrographs of isolated male-derived spermatocytes and budding spermatids showing the subcellular distribution of mitochondria and PEI-1::mTagRFP-T. White arrowheads mark budding spermatids, yellow arrows and dashed ovals indicate residual bodies. Hoechst 33342 was used to stain DNA. MitoTracker® Green FM was used to stain mitochondria. B, Confocal micrographs of isolated male-derived spermatids expressing GFP::3xFLAG::WAGO-3 and SPE-45::mCherry. C, Line profiles display fluorescence intensity for PEI-1_ΔBTB+BACK+IDR::mTagRFP-T (magenta) versus mitochondria (green) signals over indicated line (shown in D). Vertical lines and colored circles indicate fluorescence peaks. a.u. – arbitrary unit. D, Confocal micrographs of isolated male-derived spermatocytes and budding spermatids showing the subcellular distribution of mitochondria and PEI-1_ΔBTB+BACK+IDR::mTagRFP-T. White arrowheads mark budding spermatids, yellow arrows and dashed ovals indicate residual bodies. Hoechst 33342 was used to stain DNA. MitoTracker® Green FM was used to stain mitochondria. Scale bars: 4 µm (A, B, D)

Correct segregation of PEI granules depends on a myosin VI motor protein and requires S-palmitoylation

Our current results indicate that the asymmetric segregation of PEI granules is dependent on an association with mitochondria, and possibly FB-MOs. In order to substantiate this model, we used *spe* mutants to get a more detailed insight into molecular mechanisms that ensure proper PEI granule localization and segregation. *spe* mutants produce functionally defective spermatocytes, spermatids or spermatozoa, which causes a self-sterility phenotype (Nishimura and L'Hernault, 2010). Previous studies have demonstrated distinct roles of the myosin VI motor protein SPE-15 and the myosin II motor protein NMY-2 in spermatid differentiation. Both proteins were shown to be required for proper cytokinesis and hence residual body formation during meiosis II. Interestingly, loss of any of these two motor proteins causes both mitochondria and FB-MOs to be evenly distributed between budding spermatids and residual bodies (Hu et al., 2019; Kelleher et al., 2000). Thus, we asked whether the asymmetric sorting of PEI granules, and hence their presence in mature sperm, is subject to the same principle. Since *spe* mutant hermaphrodites produce very few progeny, we introduced mutant alleles of *him* genes during strain generation. The Him phenotype is characterized by a high incidence of males, which was beneficial to obtain male-derived spermatocytes and budding spermatids for confocal microscopy. In absence of SPE-15, we did not detect any differences in GFP::3xFLAG::WAGO-3 and PEI-1::mTagRFP-T localization within spermatocytes (**Figure 36A**). However, both proteins were symmetrically segregated into budding spermatids and residual body (**Figure 36A**). This observation reveals that their subcellular distribution is indeed dependent on SPE-15 and hence likely driven by the segregation of mitochondria, and possibly FB-MOs.

Next, we analyzed the impact of the sperm-specific palmitoyl transferase SPE-10 on PEI granule formation and segregation. S-palmitoylation describes the covalent attachment of palmitic acid to cysteine residues, while the less common O-palmitoylation targets serine or threonine residues. Both of these post-translational modifications serve as membrane anchor to guide protein localization, and typically occur at the Golgi complex or Golgi-derived membranes. In contrast to other common lipid modifications like N-myristoylation and prenylation, S-palmitoylation is a reversible process, which can also occur at internal residues (Charollais and Van Der Goot, 2009; Guan and Fierke, 2011; Tabaczar et al., 2017).

SPE-10 has been reported to localize to FB-MOs. It was shown to be required for the stable interaction between the fibrous body and the Golgi-derived membranous

organelle. In absence of SPE-10, defects of FB-MOs become apparent during the second meiotic division. Here, fibrous bodies dissociate prematurely from the membranous organelles, resulting in their accumulation in the residual body, where they frequently bud off in so-called FB cytoplasts (Gleason et al., 2006). Like residual bodies, FB cytoplasts are enucleated cells that are presumably phagocytosed by the gonadal sheath cells (Huang et al., 2012b).

Analogous to the *spe-15* analysis, we generated a *spe-10; him-5* double mutant strains expressing GFP::3xFLAG::WAGO-3 and PEI-1::mTagRFP-T. Following isolation of male-derived spermatocytes and budding spermatids, we found that the localization of both proteins was severely defective in *spe-10* mutant animals. Already during the first meiotic division, a stage well before *spe-10* defects were described, both GFP::3xFLAG::WAGO-3 and PEI-1::mTagRFP-T localized to irregularly shaped patches in spermatocytes (**Figure 36A**). Unlike the much smaller wild-type PEI granules, these patches were found to differ in size and were always arranged along the cell membrane. Similar to our previous live-imaging experiment, we did not observe any major, intracellular mobility resulting in either fusion or fission events between individual patches (**Figure 36B**). During the second meiotic division, the described patches accumulated in the residual body, leaving no detectable signal in budding spermatids (**Figure 36A**). Notably, no fluorescent signal was detected in any identified FB cytoplast, suggesting that the irregularly shaped patches in the residual body of *spe-10* mutants were not associated to fibrous bodies.

Intrigued by these findings, we used the prediction tool GPS-Lipid in order to identify potential lipid modification sites in PEI-1 (Xie et al., 2016). GPS-Lipid covers a variety of lipid modifications including S-palmitoylation, S-farnesylation (a type of prenylation), S-geranylgeranylation (a type of prenylation) and N-myristoylation. Indeed, GPS-Lipid predicted three potential S-palmitoylation sites, one in the BACK domain and two in the intrinsically disordered region (**Figure 36C**). No sites for any of the other lipid modifications were predicted for PEI-1. Interestingly, we found that R09A1.2 also contains a predicted S-palmitoylation site at position C6 (**Figure 36C**). An additional prediction tool, called CSS-Palm, confirmed all four predicted S-palmitoylation sites in PEI-1 and R09A1.2 (Ren et al., 2008), suggesting that the palmitoyl transferase activity of SPE-10 may act directly on any or both of the two homologs.

Taken together, we found that GFP::3xFLAG::WAGO-3 and PEI-1::mTagRFP-T still co-localized in absence of either SPE-15 or SPE-10, indicating that neither the myosin VI motor protein nor S-palmitoylation affects the interaction between both proteins. Our

observations rather show that the molecular function of SPE-10 is not restricted to FB-MO stabilization, but also affects both shape and segregation of PEI granules. Overall, we hypothesize that SPE-10-mediated S-palmitoylation ensures the association of PEI granules with mitochondria, ensuring their asymmetric segregation in a myosin VI-dependent manner.

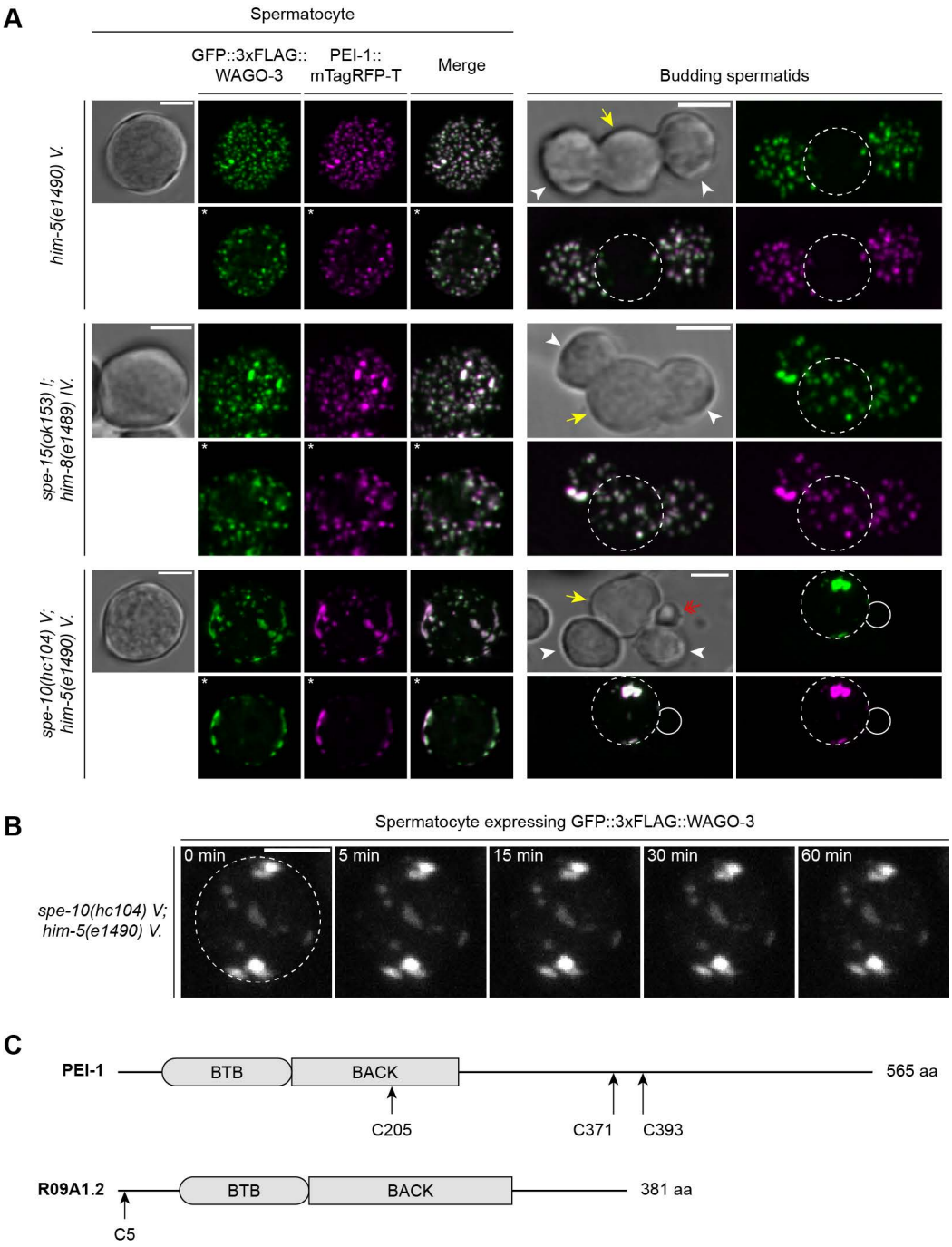

Figure 36 | Myosin VI activity and S-palmitoylation ensure asymmetric segregation of PEI granules. A, Confocal maximum intensity projections of isolated male-derived spermatocytes and budding spermatids expressing GFP::3xFLAG::WAGO-3 (green) and PEI-1::mTagRFP-T (magenta) in indicated mutants. White arrowheads mark budding spermatids, yellow arrows and dashed circles indicate residual bodies. The red double-headed arrow and solid circles mark the fibrous body (FB) cytoplast. Asterisks indicate optical sections. B, Time sequence of an isolated male-derived spermatocyte expressing GFP::3xFLAG::WAGO-3 in absence of SPE-10. Images are confocal maximum intensity projections. The spermatocyte is outlined by a dashed circle. C, Schematic representing protein domains and predicted S-palmitoylation sites of PEI-1 and R09A1.2. Domain annotations are based on InterPro (BTB) and HHpred (BACK) (Mitchell et al., 2019; Zimmermann et al., 2018). S-palmitoylation sites were predicted using CSS-Palm (v4.0) and GPS-Lipid (v1.0) (Ren et al., 2008; Xie et al., 2016). Scale bars: 4 µm (A-B)

PEI granules contain multiple proteins that are required for paternal epigenetic inheritance

Thus far, we identified PEI granules as sperm-specific condensates that are required for the proper subcellular concentration and segregation of WAGO-3 during spermatogenesis. *Are PEI granules home to other RNAi factors ensuring paternal 22G RNA-mediated TEI?* Although the PEI-1::3xMYC IP-MS/MS experiments provide a plethora of potential candidates, a collaborating laboratory at the Friedrich Miescher Institute in Basel identified yet another sperm-localized protein: DPF-3 (Gudipati et al., submitted). The gene *dpf-3* encodes a member of the dipeptidyl peptidase IV family, which was indeed detected in the proteomic analysis of male-derived spermatids (Ma et al., 2014). We performed confocal microscopy of male-derived spermatocytes, budding spermatids and hermaphroditic spermathecae using an endogenously edited allele of *dpf-3* expressing a DPF-3::GFP fusion-protein. Strikingly, we found that DPF-3::GFP co-localized with PEI-1::mTagRFP-T to cytoplasmic foci during spermatogenesis (**Figure 37A**), revealing a localization of DPF-3 to PEI granules. We observed, however, that DPF-3::GFP only partially co-localized with PEI-1::mTagRFP-T in spermatozoa. Here, we additionally detected individual foci that were either specific to DPF-3::GFP or PEI-1::mTagRFP-T (**Figure 37A**). Next, we investigated the effect of PEI-1 on the subcellular localization and segregation of DPF-3::GFP during spermatogenesis. Notably, DPF-3::GFP recapitulated the behavior of GFP::3xFLAG::WAGO-3 in *pei-1(ok1050)* mutant animals. We found DPF-3::GFP to be diffusely distributed in male-derived spermatocytes and to accumulate in residual bodies during meiosis II (**Figure 37B**). Conversely, loss of DPF-3 did not affect PEI-1 localization (**Figure 37, C and D**).

Given the PEI-1 dependent localization of DPF-3::GFP to PEI granules, we tested the role of DPF-3 in paternal 22G RNA-mediated TEI. We found that *dpf-3*, like *wago-3*, is a crucial factor for the paternal inheritance of gene silencing information, even in the presence of PEI-1 and 21U RNAs (**Figure 37E**). This finding suggests that DPF-3 likely acts on either WAGO-3 or components of the *Mutator* complex, responsible for the biogenesis of WAGO-3 associated 22G RNAs. We conclude that PEI-1 does not exclusively affect WAGO-3 localization, but also secures DPF-3 during spermatogenesis to ensure its presence in mature sperm. Hence, PEI granules comprise at least two proteins that are required for the paternal epigenetic memory of gene silencing information.

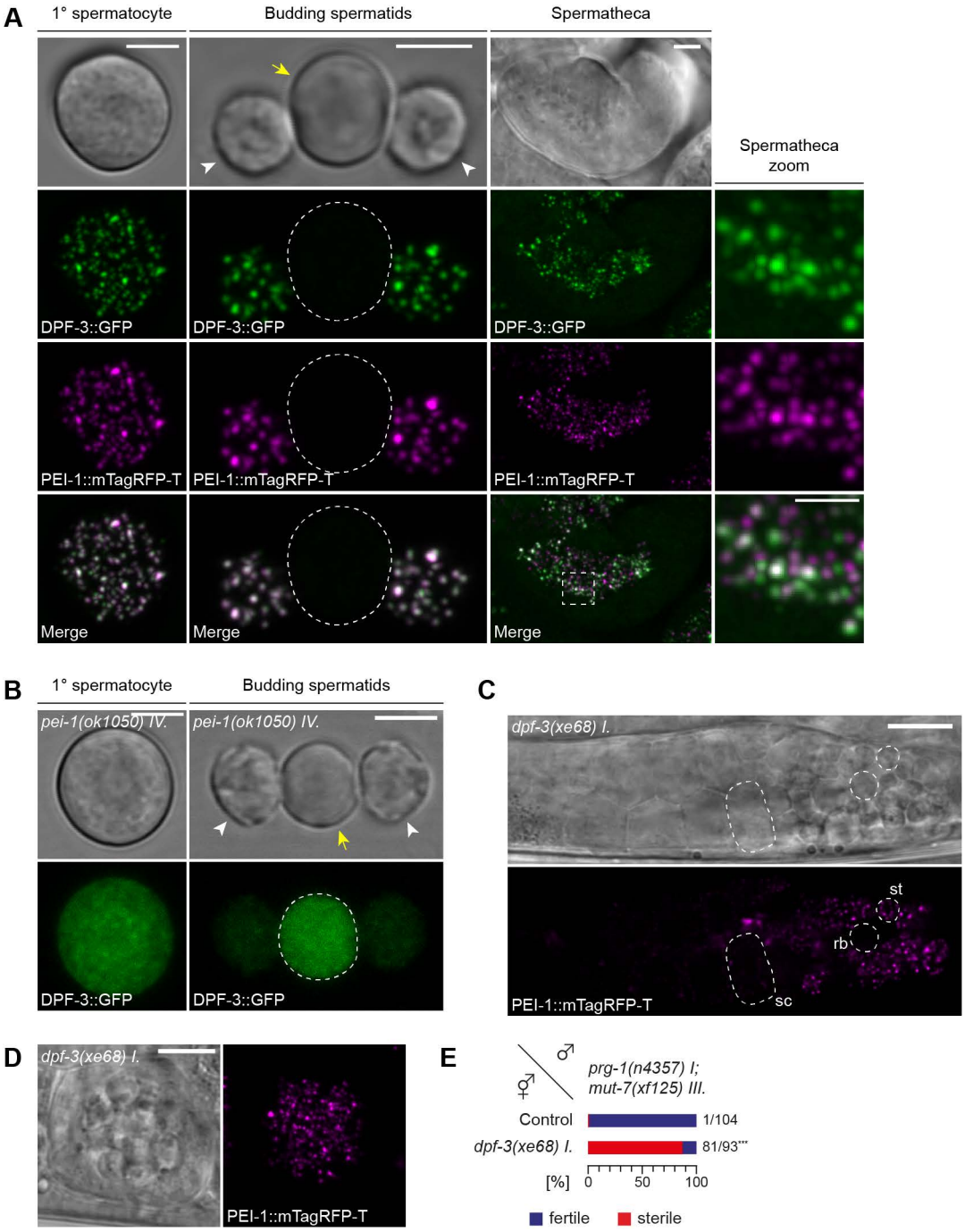

Figure 37 | The dipeptidyl peptidase DPF-3 also localizes to PEI granules and is required for paternal epigenetic inheritance. A-B, Confocal maximum intensity projections of isolated spermatocytes (male-derived), budding spermatids (male-derived) and spermatozoa within the spermatheca (hermaphrodite) expressing DPF-3::GFP either together with PEI-1::mTagRFP-T (A), or in absence of PEI-1 (B). Zoom shows partial co-localization of DPF-3::GFP and PEI-1::mTagRFP-T within the spermatheca (A). White arrowheads mark budding spermatids, yellow arrows and dashed ovals indicate residual bodies. C, Confocal micrograph showing the proximal region of a spermatogenic gonad of a late-L4 stage hermaphrodite expressing PEI-1::mTagRFP-T in absence of DPF-3. A representative spermatocyte (sc), spermatid (st) and residual body (rb) is outlined by a dashed line. D, Confocal maximum intensity projection showing PEI-1::mTagRFP-T foci within the spermatheca of a *dpf-3(xe68)* mutant adult hermaphrodite. E, Percentage of fertile F1 animals generated by indicated crosses like shown in Figure 22. Fertility indicates presence of paternal 22G RNA-mediated epigenetic inheritance.►

BTB domain-containing proteins with an intrinsically disordered region are commonly found in various kingdoms of life

How conserved is the molecular mechanism that we uncovered? Based on the primary protein structure, four independent phylogenetic analyses predicted PEI-1 to be merely conserved within the *Caenorhabditis* genus (**Figure 38A**) (Altenhoff et al., 2018; Huerta-Cepas et al., 2016b; Kriventseva et al., 2019; Sonnhammer and Östlund, 2015). However, we found that BTB domain-containing proteins with a predicted intrinsically disordered region are commonly found in metazoa, viridiplantae, fungi and viruses (Letunic and Bork, 2018; Letunic et al., 2015). The human genome encodes six proteins that closely resemble the domain organization of PEI-1 (**Figure 38B**). Intriguingly, all six of these proteins are expressed in testes and the mouse orthologs of BTBD18 and GMCL1 were recently characterized. BTBD18 was shown to localize to distinct nuclear foci occupying a subset of pachytene piRNA-producing loci during mouse spermatogenesis. Loss of BTBD18 in mice impairs piRNA biogenesis, spermiogenesis and male fertility (Zhou et al., 2017). GMCL1 (germ cell-less protein-like 1) is a non-integral, nuclear envelope protein with a suggested function during mammalian spermatogenesis (Kleiman et al., 2003; Nili et al., 2001). Interestingly, the mouse ortholog of human GMCL1, called mGCL-1, is required for sperm morphogenesis and male fertility (Kimura et al., 2003; Maekawa et al., 2004). Furthermore, mGCL-1 and GMCL1 were reported to modulate the nucleocytoplasmic transport by specifically affecting the subcellular localization of MDM2 and GAGE proteins, respectively (Gjerstorff et al., 2012; Masuhara et al., 2003). Notably, the recruitment of GAGE proteins to the nuclear envelop by GMCL1 is suggested to be mediated via interactions of their intrinsically disordered regions (Gjerstorff et al., 2012).

These reports in combination with our presented data suggest that BTB domain-containing proteins with an intrinsically disordered region may facilitate subcellular compartmentalization and organization by triggering and/or affecting the formation of biomolecular condensates.

► Sterility is caused by lack of every parental 22G RNA-mediated epigenetic inheritance, resulting in stochastic gene silencing in the F1 progeny. Scale bars: 4 µm (A-B), 2 µm (A, zoom), 10 µm (C), 7 µm (D). P-values were calculated with a chi-square test (C). ***: $p \leq 0.001$

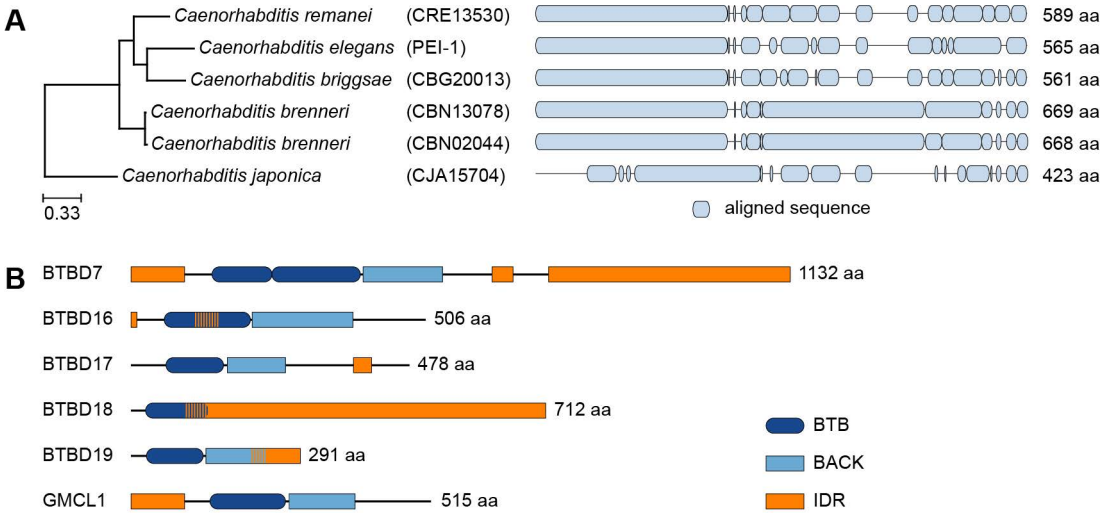

Figure 38 | BTB domain-containing proteins comprising IDRs are commonly found in eukaryota. A, Phylogenetic analysis showing PEI-1 conservation within the *Caenorhabditis* genus. The phylogenetic three was generated using EggNOG (v4.5.1) (Huerta-Cepas et al., 2016b). PEI-1 was defined as query and compared to all eukaryote entries. B, Protein length and domain composition of six human BTB domain-containing proteins that resemble PEI-1. All six human proteins are expressed in the testis.

Discussion

An increasing number of studies start to reveal molecular mechanisms driving transgenerational epigenetics based on small RNA inheritance in *C. elegans*. In particular, the contribution via the oocyte gained much knowledge in terms of novel factors and subcellular processes that ensure the inheritance of certain small RNA populations (Ishidate et al., 2018; Wan et al., 2018; Xu et al., 2018b). Although paternal epigenetic inheritance has been described as well (de Albuquerque et al., 2015; Alcazar et al., 2008; Lev et al., 2019; Phillips et al., 2015), it is largely based on phenomenology, with recent studies giving a first insight into chromatin-based mechanisms (Kaneshiro et al., 2019; Tabuchi et al., 2018). However, the existence of a cytoplasmic contribution in paternal epigenetic inheritance remains unknown. In this work, we identify WAGO-3 as a germline-specific Argonaute protein and describe how a defective *Mutator* complex affects WAGO-3 loading and subcellular localization. Furthermore, we provide evidence that WAGO-3 is required for germ cell development and transgenerational maintenance of RNAe-driven gene silencing. In particular, we characterize the role of WAGO-3 in paternal epigenetic inheritance and describe a novel, sperm-specific condensate, the PEI granule, which ensures the inheritance of WAGO-3 through sperm. Our results link the localization of this phase-separated structure to lipid modification and myosin-driven segregation of membranous organelles. Various aspects related to our findings will be discussed here.

The target repertoire of WAGO-3 may change during germ cell development

Many germline-expressed genes display specific, 3' UTR-driven expression patterns during germ cell development (Merritt et al., 2008). Especially the transcriptomes during oogenesis and spermatogenesis significantly differ from each other, with many genes showing sex-regulated expression (Ortiz et al., 2014; Reinke et al., 2004). Our presented data describes WAGO-3 target genes in adult hermaphrodites (**Figures 12-14 and Figure 21**). Thus, we may not have identified the whole target repertoire but rather a set of genes that is highly covered by WAGO-3 associated 22G RNAs in adults. Given that WAGO-3 is expressed throughout germline development and parentally deposited into embryos (**Figure 8**), it would be informative to identify WAGO-3 target genes, and their respective expression profiles, in animals of different developmental stages, early embryos, or isolated cells like oocytes, spermatocytes and spermatozoa. Thereby, we could address changes in the target repertoire during germ cell development. Possibly, WAGO-3, or WAGO proteins in general, target different sets of genes in different cell types, and this aspect has thus far been ignored by the field.

WAGO-3 loading requires shuttling between perinuclear condensates

Consistent with studies describing target genes of WAGO-1 and WAGO-4 (Gu et al., 2009; Xu et al., 2018b), we found that the vast majority of WAGO-3 associated 22G RNAs target protein-coding genes (**Figure 12A**). However, the target repertoire between WAGO-1/WAGO-3 and WAGO-4 is seemingly different. While WAGO-4 was reported to share a substantial amount of target genes with CSR-1 (Xu et al., 2018b), WAGO-1 and WAGO-3 are associated with a 22G RNA population that is distinct from CSR-1 bound 22G RNAs (**Figure 12H**) (Gu et al., 2009). *How is it possible that WAGO proteins associate with different 22G RNA populations?* The answer to this question may involve distinct biomolecular condensates, which compartmentalize small RNA biogenesis. On the one hand, *Mutator*-dependent 22G RNA biogenesis occurs in phase-separated condensates called *Mutator* foci, which are spatially separated from P granules and predominately fond at the nuclear periphery of mitotic germ cells (Phillips et al., 2012; Uebel et al., 2018; Wan et al., 2018). On the other hand, EGO-1 is required for the production of a distinct 22G RNA population, which associates with the Argonaute protein CSR-1 (Claycomb et al., 2009; Maniar and Fire, 2011; Smardon et al., 2000; van Wolfswinkel et al., 2009). Notably, EGO-1 localizes to P granules (Claycomb et al., 2009). Both 22G RNA populations share the same characteristics in terms of length, first nucleotide bias and chemical nature of both the 5' and 3' end. Thus, CSR-1 and WAGO proteins could potentially bind both 22G RNA populations. In fact, it remains elusive how WAGO proteins are loaded with 22G RNAs. *Do WAGO proteins enter Mutator foci in order to associate with 22G RNAs? Do Mutator foci merely represent a place of 22G RNA biogenesis without participating in WAGO loading?* These questions touch upon the possibility that WAGO proteins or 22G RNAs may shuttle between both condensates. While WAGO-1, WAGO-3 and WAGO-4 usually localize to P granules in naïve germ cells (**Figure 8A**) (Gu et al., 2009; Wan et al., 2018), we demonstrate that WAGO-3 localizes to *Mutator* foci in 22G RNA-defective animals, which were generated by loss of MUT-7 (**Figure 10B**). As previously described, loss of MUT-7 does not affect MUT-16 localization (Phillips et al., 2012). Thus, MUT-16 may still trigger the assembly of an incomplete *Mutator* complex by recruiting MUT-2, MUT-14, MUT-15, RRF-1 and RDE-2 (Uebel et al., 2018). In this scenario, WAGO-3 possibly enters *Mutator* foci without being properly loaded with 22G RNAs. To test this hypothesis, we mutated the PAZ domain of WAGO-3 to determine how small RNA loading affects WAGO-3 localization. In particular, we mutated tyrosine-685 and phenylalanine-686 to alanine residues. Both mutations were previously shown to abrogate small RNA binding by impairing the association of the PAZ domain with the 3' end of small RNAs (Guang et al., 2008; Ma et al., 2004). Strikingly, we found that these

mutations caused global destabilization of GFP::3xFLAG::WAGO-3, with localization to a few perinuclear foci in the distal gonad, reminiscent of the localization of GFP::3xFLAG::WAGO-3 in *mut-7* mutant animals (data not shown). However, further experiments inducing co-localization studies and small RNA sequencing of WAGO-3 associated 22G RNAs are required to confirm our hypothesis. Nonetheless, we provide the first results that suggest that WAGO-3 may migrate from *Mutator* foci to P granules. Our current knowledge points to a scenario where WAGO-3 localizes to *Mutator* foci in order to get loaded with *Mutator*-dependent 22G RNAs, and that this step serves as checkpoint to ensure properly loaded WAGO-3 to enter P granules (**Figure 39**). Thus, the association of WAGO proteins with distinct 22G RNA populations may require a controlled localization to specific condensates. Obviously, we would need to perform the same experiments with WAGO-4 to determine whether WAGO-4 loading is independent on the *Mutator* complex. Accordingly, WAGO-4 may associate with EGO-1 dependent 22G RNAs in P granules, which could potentially explain the high degree of shared target genes with CSR-1.

How does WAGO-3 shuttle between Mutator foci and P granules? A recent study describing ENRI proteins may provide an intriguing clue. ENRI proteins were shown to interact with the Argonaute protein NRDE-3, thereby regulating its function by preventing premature nuclear translocation (Lewis et al., 2020). Similarly, ENRI-like proteins may control the subcellular localization of other members of the WAGO family, for example their shuttling between *Mutator* foci and P granules. ENRI proteins are rather small proteins of 25-39 kDa, do not contain discernable domains, and are predicted to contain multiple intrinsically disordered regions. These characteristics also apply to W09B7.2 and F40A3.6, two proteins of unknown function, which were co-enriched in GFP::3xFLAG::WAGO-3 immunoprecipitation experiments (**Figure 15A**). Interestingly, F40A3.6 is similar to ENRI-1 (19 % identity, 30 % similarity), suggesting that they may represent members of a protein family. *How can ENRI-like or other proteins control the shuttling of WAGO proteins?* Intriguingly, Argonaute proteins are described to adopt specific conformations depending on their small RNA loading (Endo et al., 2013; Iki et al., 2010; Iwasaki et al., 2010, 2015; Miyoshi et al., 2010; Nakanishi, 2016; Tahbaz et al., 2001). These conformational changes are recognized by a chaperone machinery, which enables a specific interaction with unloaded Argonaute proteins. Similar mechanisms may also regulate the subcellular localization of WAGO proteins to either *Mutator* foci or P granules. In fact, we set out to identify WAGO-3 interacting proteins to shed light on the altered localization of GFP::3xFLAG::WAGO-3 in *mut-7* mutant animals. For this purpose, we performed immunoprecipitation experiments of GFP::3xFLAG::WAGO-3 in

mut-7 and *mut-16* mutant hermaphrodites. However, we used wild-type animals as control, which may have compromised our aim to identify WAGO-3 interacting proteins, as both *mut-7* and *mut-16* mutants are known to display transcriptional dysregulation. Thus, it is likely that the proteome of wild-type animals is a suboptimal choice for background normalization and proteomic quantification. It will be better to compare immunoprecipitation experiments of GFP::3xFLAG::WAGO-3 against the respective mutant background. Hence, we will need to repeat these experiments in order to properly assess GFP::3xFLAG::WAGO-3 co-enriched proteins via label-free quantitative mass spectrometry. In case the above described PAZ domain mutations really cause GFP::3xFLAG::WAGO-3 to recapitulate its localization in *mut-7* mutants, this WAGO-3 variant may prove beneficial for an additional proteomic approach to identify interacting proteins that may regulate the shuttling between *Mutator* foci and P granules.

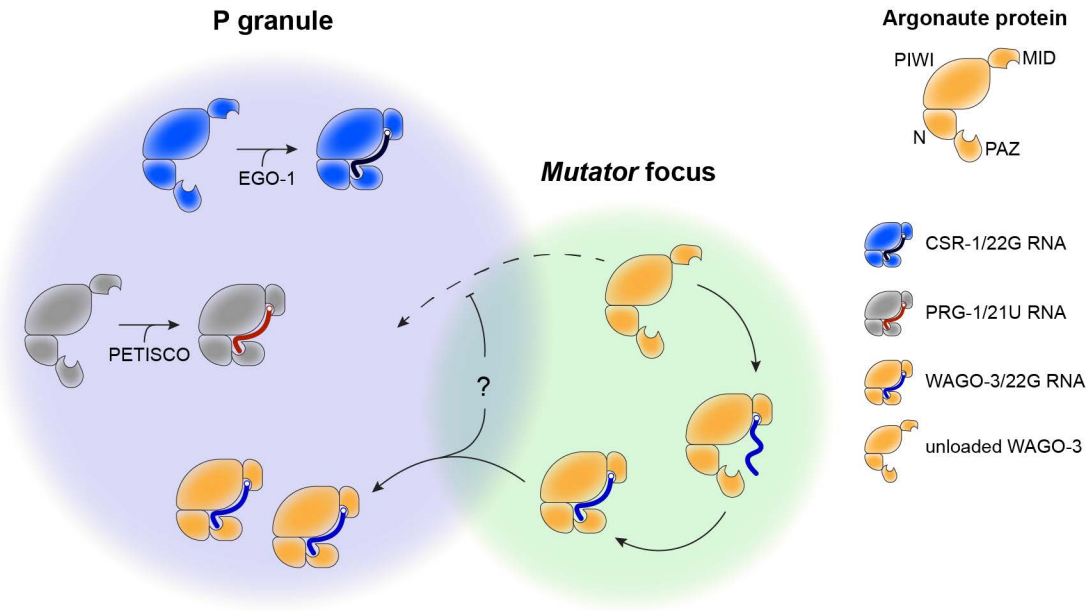

Figure 39 | Loading of WAGO-3 in *Mutator* foci may precede P granule localization. Schematic representation of how WAGO-3 proteins may associate with *Mutator*-dependent 22G RNAs in mitotic germ cells. Both the RNA-dependent RNA polymerase EGO-1 and the 21U RNA biogenesis machinery, governed by the PETISCO complex, localize to P granules. In contrast, *Mutator*-dependent 22G RNAs are generated in a distinct phase-separated condensate, the *Mutator* focus, which juxtaposes to P granules. In 22G RNA-defective animals, WAGO-3 localizes to *Mutator* foci, suggesting a certain regulatory mechanism, which ensures only properly loaded WAGO-3 to enter P granules.

WAGO-3 may be the only Argonaute protein present in mature sperm

Although a number of Argonaute proteins, namely PRG-1, ALG-3, WAGO-1, HRDE-1 and CSR-1 have been reported in spermatocytes, none of them have been described in spermatozoa (Batista et al., 2008; Buckley et al., 2012; Conine et al., 2010, 2013). In contrast, ALG-3 and HRDE-1 were shown to accumulate in residual bodies (Buckley et al., 2012; Conine et al., 2010) and immunofluorescence signals of PRG-1 were not detectable in male-derived spermatids (Batista et al., 2008). However, contradictory results have been reported for WAGO-1 and CSR-1. A study from 2010 demonstrated that a transgenic GFP::WAGO-1 fusion-protein localizes to cytoplasmic foci in isolated, male-derived spermatids, while also showing the accumulation of GFP::WAGO-1 in structures whose shape and position within the proximal gonad are possibly related to residual bodies (Conine et al., 2010). The presence of GFP::WAGO-1 in mature sperm remained questionable, since spermatozoa within the spermatheca were not investigated. Similarly, different localization patterns during sperm maturation have been reported for CSR-1. Two studies suggested either the presence (Conine et al., 2013) or the absence (Gerson-Gurwitz et al., 2016) of CSR-1 in mature sperm. Using tagged proteins expressed from endogenous loci, we could not detect WAGO-1 or CSR-1 in spermatids, but found that both Argonaute proteins were discarded into the residual body (**Figure 18, B and D**).

What could be the reasons for these discrepancies? The reported localization of WAGO-1 was based on a MosSCI transgene (Conine et al., 2010), which might not fully recapitulate the expression pattern of the endogenous gene. In fact, we found differences in expression pattern between endogenously tagged (PGL-1::mTagRFP-T) and ectopically expressed (PGL-1::mTagBFP) PGL-1 (data not shown). While PGL-1::mTagRFP-T was not detected after the spermatocyte stage, we found transgenic PGL-1::mTagBFP to localize to faint, cytoplasmic foci in maturing sperm, reminiscent of GFP::3xFLAG::WAGO-3. This observation indicates potential artefacts arising from transgenes, which may express at too high or too low levels, or at the wrong place in time. This may give a first explanation for the reported subcellular localization of WAGO-1.

On the one hand, CSR-1 has been described to localize to cytoplasmic foci in both spermatocytes and spermatids (Conine et al., 2013). This finding was based on immunofluorescence using antibodies against endogenous CSR-1. These antibodies possibly showed cross-reactivity with WAGO-3, which represents a homolog of CSR-1, and thus caused co-staining of PEI granules. We note that a control staining in animals lacking CSR-1 was not performed, and admittedly is difficult to do due to the strong

lethality of *csr-1* mutant embryos. On the other hand, published work (Gerson-Gurwitz et al., 2016) and our own results describing CSR-1 in residual bodies (**Figure 18D**) is based on N-terminally tagged CSR-1, and we cannot exclude that this tag interferes with localization of CSR-1 during spermatogenesis. Given that WAGO-3 is not affected by the same N-terminal tag, such an effect would be rather CSR-1 specific.

Finally, two more WAGO proteins need to be considered as potential sperm-residing Argonaute proteins. According to transcriptomic data, WAGO-5 and WAGO-10 are the only members of the WAGO family that display a spermatogenesis-enriched expression pattern (Ortiz et al., 2014). However, this likely results from ALG-3-like expression, i.e. being expressed in spermatocytes and discarded into residual bodies, as proteomic analysis did not identify WAGO-5 or WAGO-10 in male-derived spermatids (Ma et al., 2014). Overall, it appears that WAGO-3 may be the only Argonaute protein present in mature sperm, and as such may represent a crucial paternal inheritance factor.

PEI-1 may interact with R09A1.2 to promote PEI granule assembly

PEI-1 is specifically expressed during spermatogenesis and in spermatozoa, where it exclusively marks a novel biomolecular condensate: the PEI granule (**Figure 17 and Figure 19A**). We show that both the intrinsically disordered region and the structurally ordered region, comprising a BTB domain and a BACK domain, are able to form assemblies, and likely contribute to PEI granule formation (**Figure 24**). Both of these regions have an effect on PEI granule stability, whereas only the intrinsically disordered region seemingly specifies interactions with other proteins, such as WAGO-3 and possibly DPF-3 (**Figure 24 and Figure 37, A and B**). Interestingly, BTB domains are described to mediate both homo- and heteromeric oligomerization (Ahmad et al., 1998; Bardwell and Treisman, 1994; Collins et al., 2001; Katsani, 1999; Li et al., 1999; Melnick et al., 2000, 2002; Takenaga et al., 2003), which provides multivalency, a key property known to drive phase separation (Alberti, 2017; Banani et al., 2017; Shin and Brangwynne, 2017). In contrast, the molecular function of the BACK domain remains elusive and further experiments are needed to characterize this protein domain in detail (Stogios and Privé, 2004). The BTB and BACK domains of PEI-1, however, may function synergistically to stabilize PEI granules.

The BTB/BACK domain-driven oligomerization may also involve the PEI-1 homolog R09A1.2, which was found to be highly co-enriched in PEI-1 immunoprecipitation experiments (**Figure 33A**). Both proteins may interact via their BTB and BACK domains,

and possibly via their intrinsically disordered regions, to form a complex that is required for PEI granule formation. Although PEI-1 and R09A1.2 are highly similar, they differ in the extent of their intrinsically disordered region: the intrinsically disordered region of R09A1.2 is significantly shorter (**Figure 34, C-E**). Thus, R09A1.2 may only contribute to PEI granule formation, whereas the intrinsically disordered region of PEI-1 may have a dual function. The C-terminal extension of PEI-1 may be specifically required for the recruitment of additional proteins, like WAGO-3. Consistent with this idea, we did not detected R09A1.2 in our GFP::3xFLAG::WAGO-3 immunoprecipitation experiments and loss of PEI-1 is sufficient to abrogate WAGO-3 localization to PEI granules. Hence, PEI-1 and R09A1.2 may be responsible to form a certain "scaffold" to which "client" proteins, like WAGO-3, can be recruited (**Figure 40**). Further experiments of R09A1.2 will be required to test these hypotheses.

Another important aspect of PEI granule formation may be post-translational modifications. Previous studies on embryonic P granules highlighted the importance of phosphorylation, which promotes P granule dissolution, and dephosphorylation, which promotes P granule assembly (Gallo et al., 2010; Pellettieri et al., 2003; Quintin et al., 2003; Wang et al., 2014; Wippich et al., 2013). Interestingly, the NetPhos 3.1 server predicted many potential phosphorylation sites for both PEI-1 and R09A1.2 (**Figure 34, F and G**), suggesting that phosphorylation may also play a role in PEI granule assembly.

Our current knowledge is rather limited and further experiments are required to reveal specific steps in PEI granule formation and WAGO-3 recruitment. Especially *in vitro* experiments with recombinant proteins will enable a more detailed insight into protein-protein interactions, stoichiometry, and phase separation behaviors. Using recombinant proteins, the interaction of specific protein domains can be quantitatively assessed and intrinsic properties driving phase separation can be determined under controlled conditions (Alberti et al., 2019). Finally, a forward genetic approach based on EMS mutagenesis could potentially identify novel factors that are required for proper localization of WAGO-3 and/or PEI-1 during sperm maturation. Given the bright fluorescence of GFP::3xFLAG::WAGO-3 and PEI-1::mTagRFP-T in the easily recognizable spermatheca, such a screen would be rather straightforward to perform.

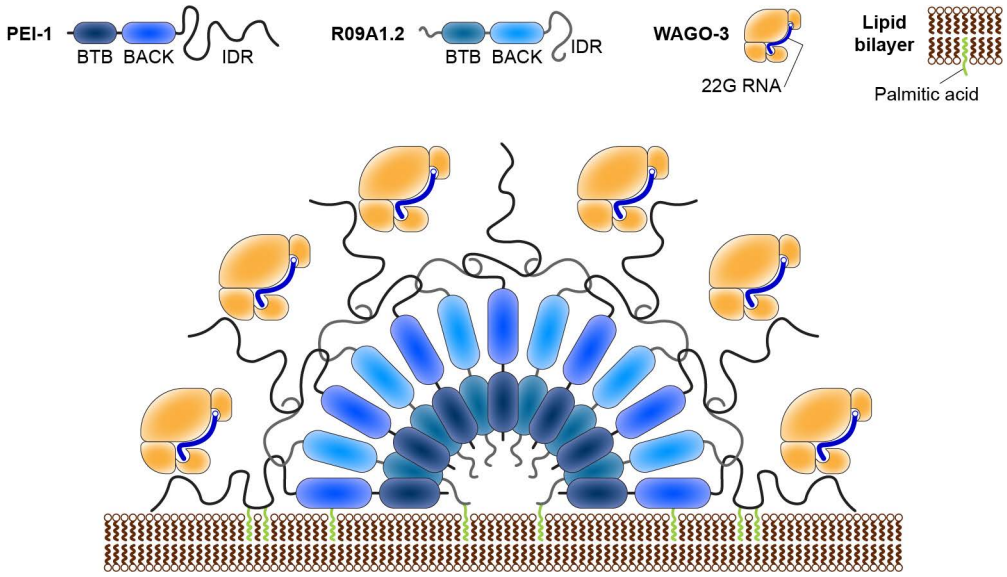

Figure 40 | Working model of PEI granule assembly. Schematic illustrating how PEI-1 and its homolog R09A1.2 may trigger PEI granule assembly. The respective BTB and BACK domains may mediate heteromeric oligomerization, which possibly stabilizes IDR-IDR interactions between individual PEI-1 and R09A1.2 proteins. The C-terminal IDR extension of PEI-1 is required for WAGO-3 recruitment. Membrane association is presumably mediated via S-palmitoylation of both PEI-1 and R09A1.2.

The intrinsically disordered region of PEI-1 acts as WAGO-3 hook

We demonstrate that the intrinsically disordered region of PEI-1 is responsible for WAGO-3 recruitment to PEI granules (**Figure 24**). However, the targeted WAGO-3 region remains unknown and multiple scenarios of how the intrinsically disordered region of PEI-1 interacts with WAGO-3 can be hypothesized (**Figure 41**).

First, intrinsically disordered regions were frequently reported to interact with other intrinsically disordered regions (Cho et al., 2018; Chong et al., 2018; Sabari et al., 2018). While we identified four such regions within WAGO-3 (**Figure 27A**), only the serine-rich low complexity region within the PIWI domain was analyzed in detail (**Figure 28**). Removal of this 22 amino acid peptide, however, did not result in WAGO-3 accumulation in residual bodies (**Figure 28D**). Possibly, any of the other three intrinsically disordered regions of WAGO-3 may be required for PEI-1 interaction.

Second, a previous study described a short, linear peptide motif within the intrinsically disordered region of yeast Tas3 and human TNRC6B that is necessary and sufficient for interaction with PIWI domains of distinct Argonaute proteins (Till et al., 2007). Similarly, a linear peptide motif within the intrinsically disordered region of PEI-1 may enable a peptide-mediated interaction with the PIWI domain, or another structurally ordered region, of WAGO-3 (Petsalaki and Russell, 2008).

Third, Argonaute proteins, like most proteins, can be post-translationally modified (Meister, 2013). Various modifications have been shown to affect Argonaute protein function. In particular, prolyl 4-hydroxylation was shown to regulate Argonaute protein stability (Qi et al., 2008), while the addition of poly(ADP-ribose) relieves Argonaute-mediated gene regulation (Leung et al., 2011). In addition, Argonaute proteins have been described to contain several phosphorylation sites, of which some were reported to affect small RNA association (Rüdel et al., 2011), mRNA binding (Quévillon Huberdeau et al., 2017) or Argonaute protein localization (Lopez-Orozco et al., 2015; Zeng et al., 2008). The latter studies might be especially relevant in this context. Phosphorylation of human Ago2 at either serine-387 or serine-798 was shown to facilitate its localization to specific phase-separated condensates: processing bodies and stress granules (Lopez-Orozco et al., 2015; Zeng et al., 2008). Similarly, a phosphorylation-dependent interaction of WAGO-3 with the intrinsically disordered region of PEI-1 may ensure WAGO-3 localization to PEI granules.

The fact that we found WAGO-1 to be co-enriched in GFP::3xFLAG::WAGO-3 immunoprecipitation experiments (**Figure 15A**) indicates a certain difference between both Argonaute proteins that specifically allows WAGO-3 to be secured during sperm maturation, while at other stages they are closely associated. Alternatively, WAGO-1 may contain features that actively prevent its association with PEI-1. Further experiments and in detail comparison with WAGO-1 are required to identify WAGO-1/-3 specific features that ensure WAGO-3 specific interaction with PEI-1.

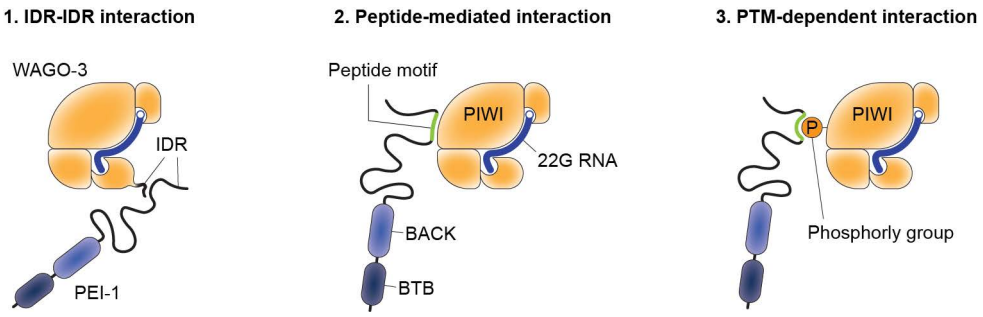

Figure 41 | Possible features that enable the interaction between PEI-1 and WAGO-3. Schematics summarizing three possible scenarios of how the interaction of PEI-1 and WAGO-3 could be mediated: i) interaction between two intrinsically disordered regions (IDRs), ii) peptide-mediated interaction based on a linear peptide motif within the intrinsically disordered region of PEI-1, iii) post-translational modification, e.g. phosphorylation, of WAGO-3.

PEI granules are liquid-like condensates with increased viscoelasticity

Our FRAP experiments demonstrate that PEI granules display liquid-like properties. However, the exchange dynamics of WAGO-3 indicate an increased viscoelasticity of PEI granules compared to P granules (**Figure 31**). This finding is supported by the amino acid composition, especially the frequency of serine and glycine residues, of the intrinsically disordered region of PEI-1, which is more similar to MEG proteins, which form gel-like condensates, than to PGL proteins, which form liquid condensates (**Figure 32**). However, our results also suggest that the material properties of PEI granules may change during sperm maturation. While the disruption of weak hydrophobic interactions causes PEI-1::mTagRFP-T foci to dissolve in spermatocytes, we noticed a reduced sensitivity towards the 1,6-hexanediol treatment in budding spermatids (**Figure 30**). *Do PEI granules become more viscous during sperm maturation?* In fact, previous *in vitro* studies demonstrated that liquid-like assemblies can display hardening over time, which can eventually result in the transition to a gel-like state (Kato et al., 2012; Wang et al., 2018a; Wegmann et al., 2018). Such changes in viscoelasticity without reaching a gel-like property may prove beneficial for PEI granule function. First, it needs to recruit cytoplasmic WAGO-3 that is no longer in P granules (**Figure 17, A and B**). This process may be facilitated by a relatively low viscoelasticity of PEI granules, allowing a rapid recruitment of WAGO-3, and possibly other "client" proteins like DPF-3. During the second meiotic division, however, PEI granules get asymmetrically segregated into budding spermatids. Increased viscoelasticity may enable robust transport of PEI granules as it may help to maintain condensate integrity. Further experiments addressing extrusion behavior, temperature sensitivity and internal rearrangements of PEI granules will provide a more detailed insight into the material property of PEI granules (Alberti et al., 2019; Putnam et al., 2019). In addition, systematic alterations of the amino acid composition may reveal the contribution of the intrinsically disordered region of PEI-1 to the material property of PEI granules.

Correct segregation of PEI granules is dependent on membranous structures

Alike mitochondria and FB-MOs, the asymmetric segregation of PEI granules to budding spermatids requires myosin VI-dependent intracellular trafficking (**Figure 36A**) (Hu et al., 2019; Kelleher et al., 2000). Our microscopic and proteomic data suggest that mitochondria are an important vector of transport for PEI granules (**Figure 33B, Figure 35A and Figure 36A**). Interestingly, association of RNAi-related pathways with

mitochondria has been described in various animals and include spermatogenic structures like pi-bodies, piP-bodies, chromatoid bodies and mitochondria-associated ER membranes (Aravin et al., 2009; Csordás et al., 2006; Eddy, 1974, 1976; N. Kotaja, 2007; Rizzuto, 1998; Wang et al., 2020, 2018b). Although these structures contain many proteins that are associated with the piRNA pathway, most studies have been describing the involvement of mitochondria in small RNA biogenesis (Aravin et al., 2009; Ge et al., 2019; Huang et al., 2011; Kuramochi-Miyagawa et al., 2010; Ma et al., 2009; Munafò et al., 2019; Shoji et al., 2009; Wang et al., 2020; Watanabe et al., 2011; Zhang et al., 2016). In addition to these reports, we demonstrate yet another function of mitochondria in small RNA transport and TEI (**Figure 42**).

However, we cannot exclude a potential function for FB-MOs in PEI granule segregation. As the FB-MO proteome is poorly understood, we cannot link any co-enriched protein of our PEI-1 immunoprecipitation experiments to FB-MO localization without further analyses. Among all known FB-MO-localized proteins, only MSP has been identified in our proteomic analysis. However, following segregation to spermatids, the membrane surrounding the fibrous body retracts and depolymerized MSP monomers/dimers can be found throughout the cytoplasm (King et al., 1992; Klass and Hirsh, 1981; Nishimura and L'Hernault, 2010; Smith and Ward, 1998). Notably, MSP was also identified on isolated mitochondria (Jing et al., 2009), suggesting a common contamination or possible interaction between both organelles.

S-palmitoylation anchors PEI granules to membranous structures

How are PEI granules associated with membranous structures? We demonstrate that SPE-10, an FB-MO-localized palmitoyl transferase, affects both shape and segregation of PEI granules, suggesting that anchoring of PEI granules may require lipid modification (**Figure 36A and Figure 42**). Interestingly, defects in PEI granule localization already occur in spermatocytes, suggesting that PEI granules may be *ab initio* attached to membranous structures in wild-type animals. The altered PEI granule shape in *spe-10* mutants, however, may represent a pleiotropic effect, without S-palmitoylation directly affecting PEI granule assembly. Anchoring of PEI granules to membranes may facilitate the formation of relatively small condensates by lowering intracellular mobility, thus preventing fusion of individual foci into larger assemblies. Membranous structures, like mitochondria, possibly contain certain regions that specify the distribution of PEI granules along the outer membrane. Although S-palmitoylation sites have been predicted for both PEI-1 and R09A1.2, it remains unknown whether any of these proteins

is targeted for lipid modification and further experiments are needed to test this hypothesis. However, a role for S-palmitoylation in relation to phase-separated condensates is by itself a novel, and intriguing finding that may find relevance in many other settings.

The subcellular localization of PEI-1_ΔBTB+BACK+IDR::mTagRFP-T may provide an intriguing clue regarding the question of whether FB-MOs are involved in PEI granule localization. Although only a few amino acids at both N- and C-termini are left, we detected localization to structures of defined shape, which are asymmetrically segregated in budding spermatids (**Figure 24 and Figure 25**). Since these structures are not mitochondria (**Figure 35, C and D**), by principle of exclusion, they might well be FM-MOs. The elongated shape indeed resembles FB-MO morphology as revealed by electron microscopy (Fabig et al., 2019). This would imply that the terminal PEI-1 residues mediate FB-MO localization, where PEI-1, or an associated protein, could serve as a substrate for SPE-10. Thus, PEI-1_ΔBTB+BACK+IDR::mTagRFP-T may visualize a normally transient association of PEI-1 with FB-MOs. How S-palmitoylation would lead to mitochondria association remains unknown, but we note that S-palmitoylation in general plays an important role in subcellular sorting of proteins, making this a non-PEI-1 specific problem. However, some *spe* mutants that affect FB-MOs also show defects of mitochondria (Kelleher et al., 2000; L'Hernault et al., 1993; Nishimura and L'Hernault, 2010; Shakes and Ward, 1989). It appears that mitochondria and FB-MOs may interact to ensure proper PEI granule assembly and localization. Further experiments including electron microscopy-based approaches will be required to reveal the involvement of membranous structures in PEI granule localization. Moreover, the combination of click-chemistry-based chemical probes, a catalytically inactive SPE-10 variant and CRISPR/Cas9-mediated mutagenesis of cysteine residues in PEI-1 and R09A1.2 may help to further dissect the S-palmitoylation-dependent anchoring of PEI granules to membranous structures (Gao and Hannoush, 2018).

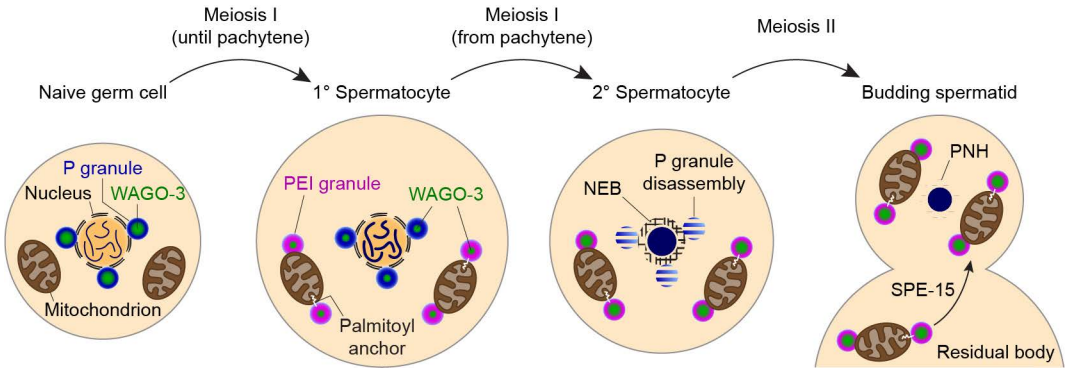

Figure 42 | Segregation of PEI granules is coupled to intracellular trafficking of mitochondria. Schematic representation of intracellular dynamics that ensure WAGO-3 maintenance in maturing sperm. In naïve germ cells, WAGO-3 localizes to P granules at the nuclear periphery. In spermatocytes, however, PEI-1 starts to be expressed and recruits WAGO-3 to PEI granules before the nuclear envelope breaks down and P granules dissolve. PEI granules are presumably anchored to mitochondria via S-palmitoylation, which ensures their asymmetric segregation in budding spermatids in a myosin VI-dependent manner. NEB – nuclear envelope breakdown, PNH – perinuclear halo.

PEI granules are required for WAGO-3 inheritance

Why are PEI granules required for paternal inheritance of a cytoplasmic 22G RNA population? In *C. elegans*, like in all nematodes except members of the Enoplida class, the nuclear envelope breaks down during spermatogenesis and sperm nuclei are devoid of a double membrane (Yushin and Malakhov, 2014). Instead, the highly condensed genome of spermatids and spermatozoa is surrounded by an electron-dense halo that contains both RNA and proteins (Browning and Strome, 1996; Ward et al., 1981; Wolf et al., 1978). Thus, P granules may not be able to act as a carrier of epigenetic information in sperm, as they seemingly rely on an association with the nuclear envelope. Indeed, proteins localizing to P granules are destabilized in spermatocytes or accumulate in the residual body (**Figure 17A and Figure 18, B-D**) (Updike and Strome, 2010). In contrast, we demonstrate that WAGO-3 is maintained during sperm maturation by localizing to PEI granules (**Figure 17 and Figure 19A**). In contrast to P granules, the stability of PEI granules is seemingly independent on the nuclear periphery. Furthermore, P granules serve multiple functions as they are home to the 21U RNA biogenesis machinery and many Argonaute proteins including PRG-1, ALG-3, WAGO-1, WAGO-3, WAGO-4 and CSR-1 (Batista et al., 2008; Conine et al., 2010; Cordeiro Rodrigues et al., 2019; Gu et al., 2009; Wan et al., 2018). Among them, only WAGO-3 was found to localize to mature sperm (**Figure 8A**). PEI granules may therefore provide a stable environment for only a selected set of proteins to ensure their segregation during spermatogenesis and

consequently their inheritance via spermatozoa. Thus, PEI granules likely represent a dedicated condensate for epigenetic inheritance (**Figure 42**).

How do PEI granules release WAGO-3 after fertilization? To function in epigenetic inheritance, WAGO-3 proteins, together with their associated 22G RNAs, have to be released from PEI granules to prime embryonic 22G RNA pathways. This step is of particular importance, since paternally deposited mitochondria and FB-MO-derived membranous organelles are degraded until the 16-cell stage of embryogenesis (Sato and Sato, 2011). Multiple, mutually non-exclusive scenarios of how this process may work can be hypothesized (**Figure 43**). First, although PEI granules display an increased viscoelasticity compared to P granules, our measurements do not support a transition to a gel-like state (**Figure 31**). Upon fertilization, paternally inherited factors are massively diluted due to the size difference between spermatozoon and oocyte. This may trigger PEI granule disassembly as concentrations drop below critical thresholds that are required for phase separation (Alberti, 2017). Second, maternally deposited enzymes may stimulate WAGO-3 release or even the dissolution of entire PEI granules by mediating post-translational protein modifications. Such modifications have been reported to regulate phase separation behavior and affect the material property of biomolecular condensates (Hofweber and Dormann, 2019). Relevant in this context, MBK-2-mediated phosphorylation of MEG proteins was shown to cause disassembly of embryonic P granules (Pellettieri et al., 2003; Quintin et al., 2003; Wang et al., 2014; Wippich et al., 2013). Given the prediction of several phosphorylation sites for PEI-1 and R09A1.2, a similar mechanism may promote a controlled dissolution of PEI granules in fertilized oocytes (**Figure 34, F and G**). Moreover, addition or removal of phosphoryl groups may disrupt weak hydrophobic interactions that are required for WAGO-3 localization to PEI granules, which may promote WAGO-3 release (**Figure 30**) (Lopez-Orozco et al., 2015; Zeng et al., 2008). Third, the reversible nature of S-palmitoylation raises the possibility that maternally inherited serine hydrolases may control membrane localization of PEI granules (Duncan and Gilman, 1998; Tomatis et al., 2010; Yeh et al., 1999). This process could possibly remove entire PEI granules from mitochondria. All of the scenarios may function synergistically to promote WAGO-3 release. However, additional experiments are required to test each hypothesis.

The PEI-1::mTagRFP-T fusion-protein may already provide an intriguing starting point to address this issue. *prg-1* mutant males expressing PEI-1::mTagRFP-T trigger the Mis phenotype (**Figure 22B**), although GFP::3xFLAG::WAGO-3 still localizes to PEI granules, which are properly segregated during the second meiotic division (data not shown). This may indicate a defect in WAGO-3-mediated priming of embryonic 22G RNA activity,

possibly driven by a steric hindrance due to the mTagRFP-T tag. It would be informative to determine whether the mTagRFP-T tag affects the retention of WAGO-3 in PEI granules and possibly prevents intermolecular interactions ensuring WAGO-3 release upon fertilization.

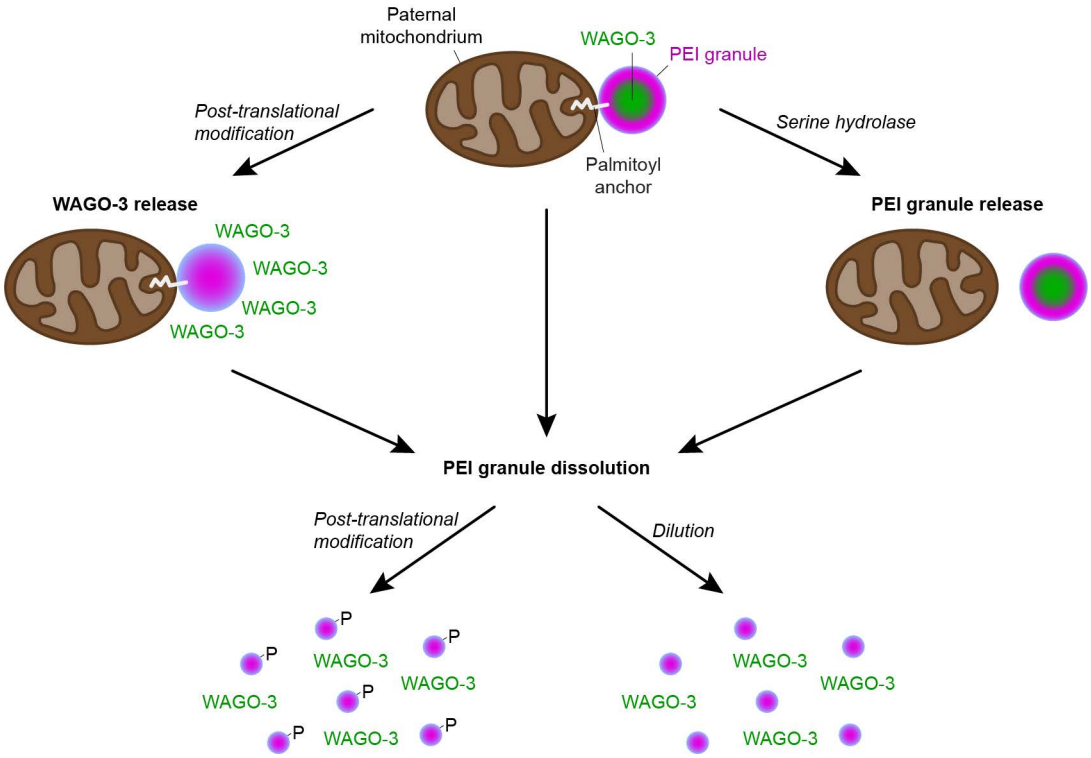

Figure 43 | Possible scenarios of WAGO-3 release after fertilization. WAGO-3 release might be dependent on maternally deposited enzymes. In this scenario, post-translational modification of WAGO-3 may result in WAGO-3 release from otherwise intact PEI granules. Alternatively, post-translational modification of other PEI granule components may promote PEI granule disassembly. The latter event, however, could also be triggered by the massive dilution of paternally inherited factors upon fertilization.

PEI granules, a specific feature of paternal mitochondria

Paternal mitochondria are selectively degraded until the 16-cell stage of embryonic development by a process called paternal mitochondria elimination (PME) (Sato and Sato, 2011). Even though novel factors involved in PME were previously identified (Sato and Sato, 2017), none of them has been reported to localize on the surface of mitochondria. In contrast, the endonuclease CPS-6 relocates from the inner mitochondrial membrane to the matrix where it plays a role in mitochondrial DNA degradation. This process promotes disorganization of the inner mitochondrial membrane structure and ensures PME to be completed until the 16-cell stage of embryogenesis (Zhou et al., 2016). In addition, damaged mitochondria are recognized by

PHB-2, another inner mitochondrial membrane protein, which is required for selective autophagy of paternally provided mitochondria (Hernando-Rodríguez and Artal-Sanz, 2018; Wei et al., 2017). These reports show that membrane disorganization of paternal mitochondria facilitates PME. However, it remains elusive how paternal mitochondria are specifically targeted during embryo development. PEI granules may play a role in this process. Upon fertilization, S-palmitoylation of certain PEI granule components may ensure remaining structures on the surface of paternal mitochondria. These PEI granule remnants could be targeted for ubiquitination, which is required for ALLO-1 localization on paternal mitochondria. Maternally deposited ALLO-1 functions as autophagy receptor and recruits LGG-1, which leads to local autophagosome formation (Sato et al., 2018). In this scenario, PEI granules may not only function in paternal inheritance of epigenetic information, but also play a role in paternal mitochondria elimination (**Figure 44**).

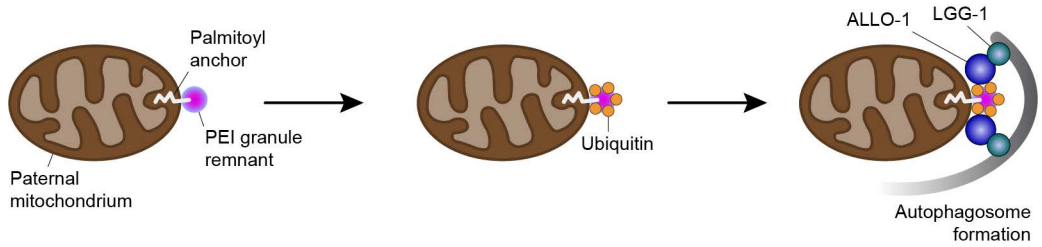

Figure 44 | PEI granule remnants may trigger paternal mitochondria elimination. After fertilization and WAGO-3 release, PEI granule remnants may still be anchored to paternal mitochondria via S-palmitoylation. These remaining structures may be targeted for ubiquitination and subsequent ALLO-1 recruitment, which in turn triggers LGG-1-driven autophagosome formation around paternal mitochondria.

PEI-1 independent functions of WAGO-3

Surprisingly, *pei-1* mutant males, which do not support cytoplasmic inheritance of WAGO-3, neither show a Mis nor Mrt phenotype when PRG-1 is present (**Figure 20A and Figure 22B**). This is in contrast to *wago-3* mutant males, which do show both phenotypes, even in presence of PRG-1 (**Figure 20A and Figure 22B**). This suggests that WAGO-3 affects these phenotypes not only via cytoplasmic inheritance, but also by additional mechanisms.

Besides the cytoplasmic aspect we describe here, epigenetic inheritance can also comprise nuclear processes. For instance, Susan Strome and colleagues recently revealed the importance of a paternal histone-based epigenetic memory for proper germ cell development in offspring (Kaneshiro et al., 2019; Kreher et al., 2018; Tabuchi et al., 2018). Consistently, our crosses addressing the Mis phenotype confirm the involvement of a nuclear RNAi pathway in paternal epigenetic inheritance, and this may at least partially explain the lack of a Mis phenotype in *pei-1* single mutant males. However, the nuclear Argonaute protein HRDE-1 does not seem to play a major role (**Figure 22B**), even though HRDE-1 is the main nuclear Argonaute protein known to act downstream of PRG-1. This result begs the following question: *How is WAGO-3 affecting nuclear RNAi?* In one possible scenario, WAGO-3-mediated gene silencing during spermatogenesis may also target genes that are involved in nuclear processes of epigenetic inheritance. Thus, loss of WAGO-3 may cause erroneous depositions of histone modifications, which in turn alter the paternal histone-based epigenetic memory. Alternatively, WAGO-3 may directly trigger nuclear RNAi. This putative function of WAGO-3 may be related to a co-enriched protein that was identified in our GFP::3xFLAG::WAGO-3 immunoprecipitation experiments: SET-27 (**Figure 15A**). SET-27 is a putative histone methyltransferase, which is predicted to mediate H3K4 or H3K36 specific methylation, which is typically associated with gene activation. However, H3K4 methylation was also shown to repress the expression of somatic genes in the germline (Robert et al., 2014). Interestingly, both chromatin marks have been implicated in transgenerational epigenetic inheritance and germline immortality (Arico et al., 2011; Greer et al., 2011, 2014; Katz et al., 2009; Kreher et al., 2018; Robert et al., 2014). In particular, the balance between activating and repressing histone modifications is proposed to ensure germ cell identify and genome integrity (Weiser et al., 2017). Further experiments are required to uncover a potential contribution of WAGO-3 in nuclear RNAi, which may explain its essential role in paternal epigenetic inheritance.

Another intriguing aspect of WAGO-3 is its global expression throughout germ cell development as well as its inheritance via the oocyte (**Figure 8 and Figure 19C**). Both aspects point to a maternal contribution of WAGO-3 in epigenetic inheritance. Yet, we did not find an effect of WAGO-3 from the maternal side in our crosses that addressed the Mis phenotype (**Figure 22C**). *How can that be explained?* Small RNA sequencing of sperm and oocytes revealed that both gametes contain 22G RNA populations that share most of their targets (**Figure 21A**) (Stoeckius et al., 2014). Assuming that WAGO-3 associated 22G RNAs may not significantly differ between both gametes, maternal inheritance of WAGO-3 may therefore certainly be of biological relevance. In contrast to sperm, however, WAGO-3 is not the only Argonaute protein to be inherited via the oocyte (Batista et al., 2008; Gu et al., 2009; Wan et al., 2018), and it seems likely that a combination of various Argonaute proteins including PRG-1, WAGO-1, WAGO-3 and WAGO-4 may ensure proper maternal inheritance of silencing information. WAGO-1, WAGO-3 and WAGO-4 are homologs, but we note that WAGO-1 and WAGO-3 share certain features that differ from WAGO-4. First, both WAGO-1 and WAGO-3 are associated with a 22G RNA population that is distinct from WAGO-4, whose target repertoire is similar to that of CSR-1 (**Figure 12H**) (Gu et al., 2009; Xu et al., 2018b). Second, WAGO-1 and WAGO-3 localize to P granules during oogenesis, while WAGO-4 is found in Z granules (Gu et al., 2009; Wan et al., 2018). Third, WAGO-1, but not WAGO-4, was found to be co-enriched in GFP::3xFLAG::WAGO-3 immunoprecipitation experiments, suggesting that WAGO-1 and WAGO-3 may be part of a common complex. Strikingly, neither loss of WAGO-3 nor WAGO-4 suspended the maternal RNAe memory (**Figure 22C**), suggesting that both 22G RNA populations may be required for the inheritance of RNAe-driven gene silencing. In this scenario, WAGO-1 may compensate loss of WAGO-3, as both Argonaute proteins are maternally inherited via P granules and may target a similar set of genes. Further experiments addressing all three WAGO proteins are needed to fully understand the impact of 22G RNA inheritance in maternal epigenetics. Here, the Mis phenotype and the 21U RNA sensor represent reliable approaches to assess the requirement of certain WAGO combinations for maternal epigenetic inheritance and transgenerational maintenance of RNAe-driven gene silencing, respectively.

N-terminal processing may regulate epigenetic inheritance

DPF-3 is one of seven proteins that belong to the dipeptidyl peptidase four family (DPF) of *C. elegans*. These enzymes process the N-termini of their substrates by removing dipeptides with penultimate proline or alanine, which in turn regulates substrate stability and function (Keane et al., 2011; Kieffer et al., 1995; Mentlein, 1999; Mentlein et al., 1993; Turk, 2006). Alike WAGO-3, DPF-3 localizes to PEI granules in a PEI-1 dependent manner, while DPF-3 itself is not needed for PEI granule assembly or segregation (**Figure 37, A-D**). Furthermore, DPF-3 is required for paternal epigenetic inheritance, even in the presence of a paternal 21U RNA pathway (**Figure 37E**). So far, this observation has only been described for WAGO-3 or proteins involved in *Mutator*-dependent 22G RNA biogenesis (**Figure 22B**) (de Albuquerque et al., 2015; Phillips et al., 2015), suggesting that DPF-3 may regulate several proteins that are involved in epigenetic inheritance. Interestingly, we found an N-terminal proline-rich low complexity region in WAGO-1, WAGO-3 and WAGO-4 (**Figure 27F**), which qualifies them as potential DPF-3 targets. Insertion of a *gfp::3xflag* sequence directly downstream of the endogenous start codon of *wago-3* or *wago-4* indeed generated hypomorphic alleles (**Figure 22B**) (Wan et al., 2018), possibly because the tag impairs N-terminal processing by DPF-3 and/or other proteases. Strikingly, additional removal of the first 50 amino acids of WAGO-3 caused dominant sterility, suggesting that N-terminal processing of WAGO-3 may be required to prevent transcriptional dysregulation during germ cell development. These finding possibly point to a novel mechanism that regulates Argonaute protein function during epigenetic inheritance.

List of references

Ade, C., Roy-Engel, A.M., and Deininger, P.L. (2013). Alu elements: an intrinsic source of human genome instability. Curr. Opin. Virol. *3*, 639–645.

Ahmad, K.F., Engel, C.K., and Privé, G.G. (1998). Crystal structure of the BTB domain from PLZF. Proc. Natl. Acad. Sci. U. S. A. *95*, 12123–12128.

Ahmad, K.F., Melnick, A., Lax, S., Bouchard, D., Liu, J., Kiang, C.L., Mayer, S., Takahashi, S., Licht, J.D., and Privé, G.G. (2003). Mechanism of SMRT Corepressor Recruitment by the BCL6 BTB Domain. Mol. Cell *12*, 1551–1564.

Akay, A., Di Domenico, T., Suen, K.M., Nabih, A., Parada, G.E., Larance, M., Medhi, R., Berkyurek, A.C., Zhang, X., Wedeles, C.J., et al. (2017). The Helicase Aquarius/EMB-4 Is Required to Overcome Intronic Barriers to Allow Nuclear RNAi Pathways to Heritably Silence Transcription. Dev. Cell *42*, 241-255.e6.

Alberti, S. (2017). Phase separation in biology. Curr. Biol. *27*, R1097–R1102.

Alberti, S., Halfmann, R., King, O., Kapila, A., and Lindquist, S. (2009). A Systematic Survey Identifies Prions and Illuminates Sequence Features of Prionogenic Proteins. Cell *137*, 146–158.

Alberti, S., Gladfelter, A., and Mittag, T. (2019). Considerations and Challenges in Studying Liquid-Liquid Phase Separation and Biomolecular Condensates. Cell *176*, 419–434.

Albertson, D.G., and Thomson, J.N. (1982). The kinetochores of Caenorhabditis elegans. Chromosoma *86*, 409–428.

Albertson, D.G., and Thomson, J.N. (1993). Segregation of holocentric chromosomes at meiosis in the nematode,Caenorhabditis elegans. Chromosom. Res. *1*, 15–26.

de Albuquerque, B.F.M., Luteijn, M.J., Cordeiro Rodrigues, R.J., van Bergeijk, P., Waaijers, S., Kaaij, L.J.T., Klein, H., Boxem, M., and Ketting, R.F. (2014). PID-1 is a novel factor that operates during 21U-RNA biogenesis in Caenorhabditis elegans. Genes Dev. *28*, 683–688.

de Albuquerque, B.F.M., Placentino, M., and Ketting, R.F. (2015). Maternal piRNAs Are Essential for Germline Development following De Novo Establishment of Endo-siRNAs in Caenorhabditis elegans. Dev. Cell *34*, 448–456.

Alcazar, R.M., Lin, R., and Fire, A.Z. (2008). Transmission dynamics of heritable silencing induced by double-stranded RNA in Caenorhabditis elegans. Genetics *180*, 1275–1288.

Almeida, M.V., Dietz, S., Redl, S., Karaulanov, E., Hildebrandt, A., Renz, C., Ulrich, H.D., König, J., Butter, F., and Ketting, R.F. (2018). GTSF -1 is required for formation of a functional RNA -dependent RNA Polymerase complex in Caenorhabditis elegans. EMBO J. *37*, 1–18.

Altenhoff, A.M., Glover, N.M., Train, C.-M., Kaleb, K., Warwick Vesztrocy, A., Dylus, D., de Farias, T.M., Zile, K., Stevenson, C., Long, J., et al. (2018). The OMA orthology database in 2018: retrieving evolutionary relationships among all domains of life through richer web and programmatic interfaces. Nucleic Acids Res. *46*, D477–D485.

Anders, S., Pyl, P.T., and Huber, W. (2015). HTSeq-A Python framework to work with high-throughput sequencing data. Bioinformatics *31*, 166–169.

Anderson, P., and Kedersha, N. (2009). RNA granules: post-transcriptional and epigenetic modulators of gene expression. Nat. Rev. Mol. Cell Biol. *10*, 430–436.

Anderson, J.L., Morran, L.T., and Phillips, P.C. (2010). Outcrossing and the Maintenance of Males within C. elegans Populations. J. Hered. *101*, S62–S74.

Aravin, A.A., van der Heijden, G.W., Castañeda, J., Vagin, V. V., Hannon, G.J., and Bortvin, A. (2009). Cytoplasmic Compartmentalization of the Fetal piRNA Pathway in Mice. PLoS Genet. *5*, e1000764.

Arduengo, P.M., Appleberry, O.K., Chuang, P., and L'Hernault, S.W. (1998). The presenilin protein family member SPE-4 localizes to an ER/Golgi derived organelle and is required for proper cytoplasmic partitioning during Caenorhabditis elegans spermatogenesis. J. Cell Sci. *111 (Pt 2*, 3645–3654.

Arico, J.K., Katz, D.J., van der Vlag, J., and Kelly, W.G. (2011). Epigenetic Patterns Maintained in Early Caenorhabditis elegans Embryos Can Be Established by Gene Activity in the Parental Germ Cells. PLoS Genet. *7*, e1001391.

Arkhipova, I.R. (2017). Using bioinformatic and phylogenetic approaches to classify transposable elements and understand their complex evolutionary histories. Mob. DNA *8*, 19.

Arribere, J.A., Bell, R.T., Fu, B.X.H., Artiles, K.L., Hartman, P.S., and Fire, A.Z. (2014). Efficient marker-free recovery of custom genetic modifications with CRISPR/Cas9 in caenorhabditis elegans. Genetics *198*, 837–846.

Arur, S., Ohmachi, M., Nayak, S., Hayes, M., Miranda, A., Hay, A., Golden, A., and Schedl, T. (2009). Multiple ERK substrates execute single biological processes in Caenorhabditis elegans germ-line development. Proc. Natl. Acad. Sci. *106*, 4776–4781.

Ashe, A., Sapetschnig, A., Weick, E.M., Mitchell, J., Bagijn, M.P., Cording, A.C., Doebley, A.L., Goldstein, L.D., Lehrbach, N.J., Le Pen, J., et al. (2012). PiRNAs can trigger a multigenerational epigenetic memory in the germline of C. elegans. Cell *150*, 88–99.

Babinchak, W.M., Haider, R., Dumm, B.K., Sarkar, P., Surewicz, K., Choi, J.-K., and Surewicz, W.K. (2019). The role of liquid–liquid phase separation in aggregation of the TDP-43 low-complexity domain. J. Biol. Chem. *294*, 6306–6317.

Bagijn, M.P., Goldstein, L.D., Sapetschnig, A., Weick, E., Bouasker, S., Lehrbach, N.J., Simard, M.J., and Miska, E.A. (2012). Function, targets, and evolution of Caenorhabditis elegans piRNAs. Science (80-.). *337*, 574–578.

Balagopal, V., and Parker, R. (2009). Polysomes, P bodies and stress granules: states and fates of eukaryotic mRNAs. Curr. Opin. Cell Biol. *21*, 403–408.

Banani, S.F., Lee, H.O., Hyman, A.A., and Rosen, M.K. (2017). Biomolecular condensates: Organizers of cellular biochemistry. Nat. Rev. Mol. Cell Biol. *18*, 285–298.

Bardwell, V.J., and Treisman, R. (1994). The POZ domain: A conserved protein-protein interaction motif. Genes Dev. *8*, 1664–1677.

Barnes, T.M., Kohara, Y., Coulson, A., and Hekimi, S. (1995). Meiotic recombination, noncoding DNA and genomic organization in Caenorhabditis elegans. Genetics *141*, 159–179.

Barucci, G., Cornes, E., Singh, M., Li, B., Ugolini, M., Samolygo, A., Didier, C., Dingli, F., Loew, D., Quarato, P., et al. (2020). Small RNA-mediated transgenerational silencing of histone genes impairs fertility in piRNA mutants. Nat. Cell Biol. *22*.

Bateman, A. (2019). UniProt: A worldwide hub of protein knowledge. Nucleic Acids Res. *47*, D506–D515.

Batista, P.J., Ruby, J.G., Claycomb, J.M., Chiang, R., Fahlgren, N., Kasschau, K.D., Chaves, D.A., Gu, W., Vasale, J.J., Duan, S., et al. (2008). PRG-1 and 21U-RNAs Interact to Form the piRNA Complex Required for Fertility in C. elegans. Mol. Cell *31*, 67–78.

Beltran, T., Barroso, C., Birkle, T.Y., Stevens, L., Schwartz, H.T., Sternberg, P.W., Fradin, H., Gunsalus, K., Piano, F., Sharma, G., et al. (2019). Comparative Epigenomics Reveals that RNA Polymerase II Pausing and Chromatin Domain Organization Control Nematode piRNA Biogenesis. Dev. Cell *48*, 793-810.e6.

Bennetzen, J.L., and Wang, H. (2014). The Contributions of Transposable Elements to the Structure, Function, and Evolution of Plant Genomes. Annu. Rev. Plant Biol. *65*, 505–530.

Benyshek, D.C., Johnston, C.S., and Martin, J.F. (2006). Glucose metabolism is altered in the adequately-nourished grand-offspring (F3 generation) of rats malnourished during gestation and perinatal life. Diabetologia *49*, 1117–1119.

Berrens, R. V., Andrews, S., Spensberger, D., Santos, F., Dean, W., Gould, P., Sharif, J., Olova, N., Chandra, T., Koseki, H., et al. (2017). An endosiRNA-Based Repression Mechanism Counteracts Transposon Activation during Global DNA Demethylation in Embryonic Stem Cells. Cell Stem Cell *21*, 694-703.e7.

Berry, J., Weber, S.C., Vaidya, N., Haataja, M., and Brangwynne, C.P. (2015). RNA transcription modulates phase transition-driven nuclear body assembly. Proc. Natl. Acad. Sci. *112*, E5237–E5245.

Bienert, S., Waterhouse, A., De Beer, T.A.P., Tauriello, G., Studer, G., Bordoli, L., and Schwede, T. (2017). The SWISS-MODEL Repository-new features and functionality. Nucleic Acids Res. *45*, D313–D319.

Billi, A.C., Alessi, A.F., Khivansara, V., Han, T., Freeberg, M., Mitani, S., and Kim, J.K. (2012). The Caenorhabditis elegans HEN1 Ortholog, HENN-1, Methylates and Stabilizes Select Subclasses of Germline Small RNAs. PLoS Genet. *8*, e1002617.

Billi, A.C., Freeberg, M.A., Day, A.M., Chun, S.Y., Khivansara, V., and Kim, J.K. (2013). A Conserved Upstream Motif Orchestrates Autonomous, Germline-Enriched Expression of Caenorhabditis elegans piRNAs. PLoS Genet. *9*, e1003392.

Blom, N., Gammeltoft, S., and Brunak, S. (1999). Sequence and structure-based prediction of eukaryotic protein phosphorylation sites. J. Mol. Biol. *294*, 1351–1362.

Bluhm, A., Casas-Vila, N., Scheibe, M., and Butter, F. (2016). Reader interactome of epigenetic histone marks in birds. Proteomics *16*, 427–436.

Boeke, J.D., Garfinkel, D.J., Styles, C.A., and Fink, G.R. (1985). Ty elements transpose through an RNA intermediate. Cell *40*, 491–500.

Boland, A., Tritschler, F., Heimstädt, S., Izaurralde, E., and Weichenrieder, O. (2010). Crystal structure and ligand binding of the MID domain of a eukaryotic Argonaute protein. EMBO Rep. *11*, 522–527.

Bošković, A., and Rando, O.J. (2018). Transgenerational epigenetic inheritance. Annu. Rev. Genet. *52*, 21–41.

Bourque, G., Burns, K.H., Gehring, M., Gorbunova, V., Seluanov, A., Hammell, M., Imbeault, M., Izsvák, Z., Levin, H.L., Macfarlan, T.S., et al. (2018). Ten things you should know about transposable elements. Genome Biol. *19*, 199.

Brangwynne, C.P., Eckmann, C.R., Courson, D.S., Rybarska, A., Hoege, C., Gharakhani, J., Jülicher, F., and Hyman, A.A. (2009). Germline P granules are liquid droplets that localize by controlled dissolution/condensation. Science (80-.). *324*, 1729–1732.

Brennecke, J., Malone, C.D., Aravin, A.A., Sachidanandam, R., Stark, A., and Hannon, G.J. (2008). An Epigenetic Role for Maternally Inherited piRNAs in Transposon Silencing. Science (80-.). *322*, 1387–1392.

Brenner, S. (1974). The genetics of Caenorhabditis elegans. Genetics *77*, 71–94.

Brink, R.A. (1956). A Genetic Change Associated with the R Locus in Maize Which Is Directed and Potentially Reversible. Genetics *41*, 872–889.

Brown, K.C., Svendsen, J.M., Tucci, R.M., Montgomery, B.E., and Montgomery, T.A. (2017). ALG-5 is a miRNA-associated Argonaute required for proper developmental timing in the Caenorhabditis elegans germline. Nucleic Acids Res. *45*, 9093–9107.

Browning, H., and Strome, S. (1996). A sperm-supplied factor required for embryogenesis in C. elegans. Development *122*, 391–404.

Buckley, B.A., Burkhart, K.B., Gu, S.G., Spracklin, G., Kershner, A., Fritz, H., Kimble, J., Fire, A., and Kennedy, S. (2012). A nuclear Argonaute promotes multigenerational epigenetic inheritance and germline immortality. Nature *489*, 447–451.

Burkhart, K.B., Guang, S., Buckley, B.A., Wong, L., Bochner, A.F., and Kennedy, S. (2011). A pre-mrna-associating factor links endogenous sirnas to chromatin regulation. PLoS Genet. *7*.

Burton, N.O., Burkhart, K.B., and Kennedy, S. (2011). Nuclear RNAi maintains heritable gene silencing in Caenorhabditis elegans. Proc. Natl. Acad. Sci. *108*, 19683–19688.

Camacho, C., Coulouris, G., Avagyan, V., Ma, N., Papadopoulos, J., Bealer, K., and Madden, T.L. (2009). BLAST+: Architecture and applications. BMC Bioinformatics *10*, 1–9.

Carvalho, C.M.B., and Lupski, J.R. (2016). Mechanisms underlying structural variant formation in genomic disorders. Nat. Rev. Genet. *17*, 224–238.

Cascarina, S.M., and Ross, E.D. (2019). Aggregation and degradation scales for prion-like domains: sequence features and context weigh in. Curr. Genet. *65*, 387–392.

Castel, S.E., and Martienssen, R.A. (2013). RNA interference in the nucleus: Roles for small RNAs in transcription, epigenetics and beyond. Nat. Rev. Genet. *14*, 100–112.

Charollais, J., and Van Der Goot, F.G. (2009). Palmitoylation of membrane proteins (Review). Mol. Membr. Biol. *26*, 55–66.

Chasnov, J.R., and Chow, K.L. (2002). Why are there males in the hermaphroditic species Caenorhabditis elegans? Genetics *160*, 983–994.

Chatterjee, I., Richmond, A., Putiri, E., Shakes, D.C., and Singson, A. (2005). The Caenorhabditis elegans spe-38 gene encodes a novel four-pass integral membrane protein required for sperm function at fertilization. Development *132*, 2795–2808.

Chen, B., Gilbert, L.A., Cimini, B.A., Schnitzbauer, J., Zhang, W., Li, G.W., Park, J., Blackburn, E.H., Weissman, J.S., Qi, L.S., et al. (2013). Dynamic imaging of genomic loci in living human cells by an optimized CRISPR/Cas system. Cell *155*, 1479–1491.

Chen, Q., Yan, M., Cao, Z., Li, X., Zhang, Y., Shi, J., Feng, G.H., Peng, H., Zhang, X., Zhang, Y., et al. (2016). Sperm tsRNAs contribute to intergenerational inheritance of an acquired metabolic disorder. Science (80-.). *351*, 397–400.

Chiu, J., March, P.E., Lee, R., and Tillett, D. (2004). Site-directed, Ligase-Independent Mutagenesis (SLIM): a single-tube methodology approaching 100% efficiency in 4 h. Nucleic Acids Res. *32*.

Chiu, J., Tillett, D., Dawes, I.W., and March, P.E. (2008). Site-directed, Ligase-Independent Mutagenesis (SLIM) for highly efficient mutagenesis of plasmids greater than 8kb. J. Microbiol. Methods *73*, 195–198.

Cho, W.-K., Spille, J.-H., Hecht, M., Lee, C., Li, C., Grube, V., and Cisse, I.I. (2018). Mediator and RNA polymerase II clusters associate in transcription-dependent condensates. Science (80-.). *361*, 412–415.

Chong, S., Dugast-Darzacq, C., Liu, Z., Dong, P., Dailey, G.M., Cattoglio, C., Heckert, A., Banala, S., Lavis, L., Darzacq, X., et al. (2018). Imaging dynamic and selective low-complexity domain interactions that control gene transcription. Science (80-.). *361*, eaar2555.

Chuong, E.B., Elde, N.C., and Feschotte, C. (2017). Regulatory activities of transposable elements: from conflicts to benefits. Nat. Rev. Genet. *18*, 71–86.

Church, D.L., Guan, K.L., and Lambie, E.J. (1995). Three genes of the MAP kinase cascade, mek-2, mpk-1/sur-1 and let-60 ras, are required for meiotic cell cycle progression in Caenorhabditis elegans. Development *121*, 2525–2535.

Claycomb, J.M., Batista, P.J., Pang, K.M., Gu, W., Vasale, J.J., van Wolfswinkel, J.C., Chaves, D.A., Shirayama, M., Mitani, S., Ketting, R.F., et al. (2009). The Argonaute CSR-1 and Its 22G-RNA Cofactors Are Required for Holocentric Chromosome Segregation. Cell *139*, 123–134.

Collins, T., Stone, J.R., and Williams, A.J. (2001). All in the Family: the BTB/POZ, KRAB, and SCAN Domains. Mol. Cell. Biol. *21*, 3609–3615.

Conine, C.C., Batista, P.J., Gu, W., Claycomb, J.M., Chaves, D.A., Shirayama, M., and Mello, C.C. (2010). Argonautes ALG-3 and ALG-4 are required for spermatogenesis-specific 26G-RNAs and thermotolerant sperm in Caenorhabditis elegans. Proc. Natl. Acad. Sci. U. S. A. *107*, 3588–3593.

Conine, C.C., Moresco, J.J., Gu, W., Shirayama, M., Conte, D., Yates, J.R., and Mello, C.C. (2013). Argonautes promote male fertility and provide a paternal memory of germline gene expression in C. Elegans. Cell *155*, 1532–1544.

Cordeiro Rodrigues, R.J., de Jesus Domingues, A.M., Hellmann, S., Dietz, S., de Albuquerque, B.F.M., Renz, C., Ulrich, H.D., Sarkies, P., Butter, F., and Ketting, R.F. (2019). PETISCO is a novel protein complex required for 21U RNA biogenesis and embryonic viability. Genes Dev. *33*, 857–870.

Cox, J., and Mann, M. (2008). MaxQuant enables high peptide identification rates, individualized p.p.b.-range mass accuracies and proteome-wide protein quantification. Nat. Biotechnol. *26*, 1367–1372.

Cox, D.N., Chao, A., Baker, J., Chang, L., Qiao, D., and Lin, H. (1998). A novel class of evolutionarily conserved genes defined by. Genes Dev. *12*, 3715–3727.

Crivat, G., and Taraska, J.W. (2012). Imaging proteins inside cells with fluorescent tags. Trends Biotechnol. *30*, 8–16.

Cropley, J.E., Eaton, S.A., Aiken, A., Young, P.E., Giannoulatou, E., Ho, J.W.K., Buckland, M.E., Keam, S.P., Hutvagner, G., Humphreys, D.T., et al. (2016). Male-lineage transmission of an acquired metabolic phenotype induced by grand-paternal obesity. Mol. Metab. *5*, 699–708.

Csordás, G., Renken, C., Várnai, P., Walter, L., Weaver, D., Buttle, K.F., Balla, T., Mannella, C.A., and Hajnóczky, G. (2006). Structural and functional features and significance of the physical linkage between ER and mitochondria. J. Cell Biol. *174*, 915–921.

Daniel, C., Behm, M., and Öhman, M. (2015). The role of Alu elements in the cis-regulation of RNA processing. Cell. Mol. Life Sci. *72*, 4063–4076.

Das, P.P., Bagijn, M.P., Goldstein, L.D., Woolford, J.R., Lehrbach, N.J., Sapetschnig, A., Buhecha, H.R., Gilchrist, M.J., Howe, K.L., Stark, R., et al. (2008). Piwi and piRNAs Act Upstream of an Endogenous siRNA Pathway to Suppress Tc3 Transposon Mobility in the Caenorhabditis elegans Germline. Mol. Cell *31*, 79–90.

Deininger, P.L., Moran, J. V., Batzer, M.A., and Kazazian, H.H. (2003). Mobile elements and mammalian genome evolution. Curr. Opin. Genet. Dev. *13*, 651–658.

Derrien, B., Baumberger, N., Schepetilnikov, M., Viotti, C., De Cillia, J., Ziegler-Graff, V., Isono, E., Schumacher, K., and Genschik, P. (2012). Degradation of the antiviral component ARGONAUTE1 by the autophagy pathway. Proc. Natl. Acad. Sci. U. S. A. *109*, 15942–15946.

Dewannieux, M., Esnault, C., and Heidmann, T. (2003). LINE-mediated retrotransposition of marked Alu sequences. Nat. Genet. *35*, 41–48.

Dias, B.G., and Ressler, K.J. (2014). Parental olfactory experience influences behavior and neural structure in subsequent generations. Nat. Neurosci. *17*, 89–96.

Dickinson, D.J., Ward, J.D., Reiner, D.J., and Goldstein, B. (2013). Engineering the Caenorhabditis elegans genome using Cas9-triggered homologous recombination. Nat. Methods *10*, 1028–1034.

Dickinson, D.J., Pani, A.M., Heppert, J.K., Higgins, C.D., and Goldstein, B. (2015). Streamlined genome engineering with a self-excising drug selection cassette. Genetics *200*, 1035–1049.

Dodson, A.E., and Kennedy, S. (2019). Germ Granules Coordinate RNA-Based Epigenetic Inheritance Pathways. Dev. Cell *50*, 704-715.e4.

Drozdetskiy, A., Cole, C., Procter, J., and Barton, G.J. (2015). JPred4: a protein secondary structure prediction server. Nucleic Acids Res. *43*, W389–W394.

Duchaine, T.F., Wohlschlegel, J.A., Kennedy, S., Bei, Y., Conte, D., Pang, K., Brownell, D.R., Harding, S., Mitani, S., Ruvkun, G., et al. (2006). Functional Proteomics Reveals the Biochemical Niche of C. elegans DCR-1 in Multiple Small-RNA-Mediated Pathways. Cell *124*, 343–354.

Duncan, J.A., and Gilman, A.G. (1998). A Cytoplasmic Acyl-Protein Thioesterase That Removes Palmitate from G Protein α Subunits and p21 RAS. J. Biol. Chem. *273*, 15830–15837.

Eddy, E.M. (1974). Fine structural observations on the form and distribution of nuage in germ cells of the rat. Anat. Rec. *178*, 731–757.

Eddy, E.M. (1976). Germ Plasm and the Differentiation of the Germ Cell Line. In International Review of Cytology, pp. 229–280.

El-Gebali, S., Mistry, J., Bateman, A., Eddy, S.R., Luciani, A., Potter, S.C., Qureshi, M., Richardson, L.J., Salazar, G.A., Smart, A., et al. (2019). The Pfam protein families database in 2019. Nucleic Acids Res. *47*, D427–D432.

Elbarbary, R.A., Lucas, B.A., and Maquat, L.E. (2016). Retrotransposons as regulators of gene expression. Science (80-.). *351*, aac7247–aac7247.

Ellis, R.E., and Stanfield, G.M. (2014). The regulation of spermatogenesis and sperm function in nematodes. Semin. Cell Dev. Biol. *29*, 17–30.

Endo, Y., Iwakawa, H., and Tomari, Y. (2013). Arabidopsis ARGONAUTE7 selects miR390 through multiple checkpoints during RISC assembly. EMBO Rep. *14*, 652–658.

Engels, W.R., Johnson-Schlitz, D.M., Eggleston, W.B., and Sved, J. (1990). High-frequency P element loss in Drosophila is homolog dependent. Cell *62*, 515–525.

Fabig, G., Schwarz, A., Striese, C., Laue, M., and Müller-Reichert, T. (2019). In situ analysis of male meiosis in C. elegans. In Methods in Cell Biology, pp. 119–134.

Faehnle, C.R., Elkayam, E., Haase, A.D., Hannon, G.J., and Joshua-Tor, L. (2013). The Making of a Slicer: Activation of Human Argonaute-1. Cell Rep. *3*, 1901–1909.

Félix, M.-A., and Wang, D. (2019). Natural Viruses of Caenorhabditis Nematodes. Annu. Rev. Genet. *53*, 313–326.

Félix, M.-A., Ashe, A., Piffaretti, J., Wu, G., Nuez, I., Bélicard, T., Jiang, Y., Zhao, G., Franz, C.J., Goldstein, L.D., et al. (2011). Natural and Experimental Infection of Caenorhabditis Nematodes by Novel Viruses Related to Nodaviruses. PLoS Biol. *9*, e1000586.

Feric, M., Vaidya, N., Harmon, T.S., Mitrea, D.M., Zhu, L., Richardson, T.M., Kriwacki, R.W., Pappu, R. V., and Brangwynne, C.P. (2016). Coexisting Liquid Phases Underlie Nucleolar Subcompartments. Cell *165*, 1686–1697.

Fernandez, A.G. (2005). New genes with roles in the C. elegans embryo revealed using RNAi of ovary-enriched ORFeome clones. Genome Res. *15*, 250–259.

Feschotte, C. (2008). Transposable elements and the evolution of regulatory networks. Nat. Rev. Genet. *9*, 397–405.

Feschotte, C., and Pritham, E.J. (2007). DNA Transposons and the Evolution of Eukaryotic Genomes. Annu. Rev. Genet. *41*, 331–368.

Fire, A., Xu, S., Montgomery, M.K., Kostas, S.A., Driver, S.E., and Mello, C.C. (1998). Potent and specific genetic interference by double-stranded RNA in Caenorhabditis elegans. Nature *391*, 806–811.

Fischer, S.E.J., Montgomery, T.A., Zhang, C., Fahlgren, N., Breen, P.C., Hwang, A., Sullivan, C.M., Carrington, J.C., and Ruvkun, G. (2011). The ERI-6/7 Helicase Acts at the First Stage of an siRNA Amplification Pathway That Targets Recent Gene Duplications. PLoS Genet. *7*, e1002369.

Frank, F., Sonenberg, N., and Nagar, B. (2010). Structural basis for 5′-nucleotide base-specific recognition of guide RNA by human AGO2. Nature *465*, 818–822.

Frank, F., Hauver, J., Sonenberg, N., and Nagar, B. (2012). Arabidopsis Argonaute MID domains use their nucleotide specificity loop to sort small RNAs. EMBO J. *31*, 3588–3595.

French, R.L., Grese, Z.R., Aligireddy, H., Dhavale, D.D., Reeb, A.N., Kedia, N., Kotzbauer, P.T., Bieschke, J., and Ayala, Y.M. (2019). Detection of TAR DNA-binding protein 43 (TDP-43) oligomers as initial intermediate species during aggregate formation. J. Biol. Chem. *294*, 6696–6709.

Frøkjær-Jensen, C., Wayne Davis, M., Hopkins, C.E., Newman, B.J., Thummel, J.M., Olesen, S.P., Grunnet, M., and Jorgensen, E.M. (2008). Single-copy insertion of transgenes in Caenorhabditis elegans. Nat. Genet. *40*, 1375–1383.

Frøkjær-Jensen, C., Davis, M.W., Ailion, M., and Jorgensen, E.M. (2012). Improved Mos1-mediated transgenesis in C. elegans. Nat. Methods *9*, 117–118.

Gallo, C.M., Wang, J.T., Motegi, F., and Seydoux, G. (2010). Cytoplasmic Partitioning of P Granule Components Is Not Required to Specify the Germline in C. elegans. Science (80-.). *330*, 1685–1689.

Gao, X., and Hannoush, R.N. (2018). A Decade of Click Chemistry in Protein Palmitoylation: Impact on Discovery and New Biology. Cell Chem. Biol. *25*, 236–246.

Ge, D.T., Wang, W., Tipping, C., Gainetdinov, I., Weng, Z., and Zamore, P.D. (2019). The RNA-Binding ATPase, Armitage, Couples piRNA Amplification in Nuage to Phased piRNA Production on Mitochondria. Mol. Cell *74*, 982-995.e6.

Gent, J.I., Schvarzstein, M., Villeneuve, A.M., Gu, S.G., Jantsch, V., Fire, A.Z., and Baudrimont, A. (2009). A Caenorhabditis elegans RNA-directed RNA polymerase in sperm development and endogenous RNA interference. Genetics *183*, 1297–1314.

Gent, J.I., Lamm, A.T., Pavelec, D.M., Maniar, J.M., Parameswaran, P., Tao, L., Kennedy, S., and Fire, A.Z. (2010). Distinct Phases of siRNA Synthesis in an Endogenous RNAi Pathway in C. elegans Soma. Mol. Cell *37*, 679–689.

Gerson-Gurwitz, A., Wang, S., Sathe, S., Green, R., Yeo, G.W., Oegema, K., and Desai, A. (2016). A Small RNA-Catalytic Argonaute Pathway Tunes Germline Transcript Levels to Ensure Embryonic Divisions. Cell *165*, 396–409.

Ghildiyal, M., and Zamore, P.D. (2009). Small silencing RNAs: An expanding universe. Nat. Rev. Genet. *10*, 94–108.

Gjerstorff, M.F., Rösner, H.I., Pedersen, C.B., Greve, K.B. V., Schmidt, S., Wilson, K.L., Mollenhauer, J., Besir, H., Poulsen, F.M., Møllegaard, N.E., et al. (2012). GAGE Cancer-Germline Antigens Are Recruited to the Nuclear Envelope by Germ Cell-Less (GCL). PLoS One *7*, e45819.

Gleason, E.J., Lindsey, W.C., Kroft, T.L., Singson, A.W., and L'Hernault, S.W. (2006). Spe-10 encodes a DHHC-CRD zinc-finger membrane protein required for endoplasmic reticulum/golgi membrane morphogenesis during Caenorhabditis elegans spermatogenesis. Genetics *172*, 145–158.

Goh, W.S.S., Seah, J.W.E., Harrison, E.J., Chen, C., Hammell, C.M., and Hannon, G.J. (2014). A genome-wide RNAi screen identifies factors required for distinct stages of C. elegans piRNA biogenesis. Genes Dev. *28*, 797–807.

Gold, V.A., Chroscicki, P., Bragoszewski, P., and Chacinska, A. (2017). Visualization of cytosolic ribosomes on the surface of mitochondria by electron cryo-tomography. EMBO Rep. *18*, 1786–1800.

Gong, C., and Maquat, L.E. (2011). lncRNAs transactivate STAU1-mediated mRNA decay by duplexing with 3′ UTRs via Alu elements. Nature *470*, 284–288.

Goodier, J.L. (2016). Restricting retrotransposons: a review. Mob. DNA *7*, 16.

Govindan, J.A., Nadarajan, S., Kim, S., Starich, T.A., and Greenstein, D. (2009). Somatic cAMP signaling regulates MSP-dependent oocyte growth and meiotic maturation in C. elegans. Development *136*, 2211–2221.

Grant, B., and Hirsh, D. (1999). Receptor-mediated Endocytosis in the Caenorhabditis elegans Oocyte. Mol. Biol. Cell *10*, 4311–4326.

Greenblatt, I.M., and Alexander Brink, R. (1963). Transpositions of Modulator in Maize into Divided and Undivided Chromosome Segments. Nature *197*, 412–413.

Greenblatt, I.M., and Brink, R.A. (1962). Twin Mutations in Medium Variegated Pericarp Maize. Genetics *47*, 489–501.

Greer, E.L., Maures, T.J., Ucar, D., Hauswirth, A.G., Mancini, E., Lim, J.P., Benayoun, B.A., Shi, Y., and Brunet, A. (2011). Transgenerational epigenetic inheritance of longevity in Caenorhabditis elegans. Nature *479*, 365–371.

Greer, E.L., Beese-Sims, S.E., Brookes, E., Spadafora, R., Zhu, Y., Rothbart, S.B., Aristizábal-Corrales, D., Chen, S., Badeaux, A.I., Jin, Q., et al. (2014). A Histone Methylation Network Regulates Transgenerational Epigenetic Memory in C. elegans. Cell Rep. *7*, 113–126.

Greer, E.L., Becker, B., Latza, C., Antebi, A., and Shi, Y. (2016). Mutation of C. elegans demethylase spr-5 extends transgenerational longevity. Cell Res. *26*, 229–238.

Gregory, T.R., and Johnston, J.S. (2008). Genome size diversity in the family Drosophilidae. Heredity (Edinb). *101*, 228–238.

Grishok, A., Tabara, H., and Mello, C.C. (2000). Genetic requirements for inheritance of RNAi in C. elegans. Science (80-.). *287*, 2494–2497.

Gu, S.G., Pak, J., Guang, S., Maniar, J.M., Kennedy, S., and Fire, A. (2012a). Amplification of siRNA in Caenorhabditis elegans generates a transgenerational sequence-targeted histone H3 lysine 9 methylation footprint. Nat. Genet. *44*, 157–164.

Gu, W., Shirayama, M., Conte, D., Vasale, J., Batista, P.J., Claycomb, J.M., Moresco, J.J., Youngman, E.M., Keys, J., Stoltz, M.J., et al. (2009). Distinct Argonaute-Mediated 22G-RNA Pathways Direct Genome Surveillance in the C. elegans Germline. Mol. Cell *36*, 231–244.

Gu, W., Lee, H.-C., Chaves, D., Youngman, E.M., Pazour, G.J., Conte, D., and Mello, C.C. (2012b). CapSeq and CIP-TAP Identify Pol II Start Sites and Reveal Capped Small RNAs as C. elegans piRNA Precursors. Cell *151*, 1488–1500.

Guan, X., and Fierke, C.A. (2011). Understanding protein palmitoylation: Biological significance and enzymology. Sci. China Chem. *54*, 1888–1897.

Guang, S., Bochner, A.F., Pavelec, D.M., Burkhart, K.B., Harding, S., Lachowiec, J., and Kennedy, S. (2008). An Argonaute Transports siRNAs from the Cytoplasm to the Nucleus. Science (80-.). *321*, 537–541.

Guang, S., Bochner, A.F., Burkhart, K.B., Burton, N., Pavelec, D.M., and Kennedy, S. (2010). Small regulatory RNAs inhibit RNA polymerase II during the elongation phase of transcription. Nature *465*, 1097–1101.

Gumienny, T.L., Lambie, E., Hartwieg, E., Horvitz, H.R., and Hengartner, M.O. (1999). Genetic control of programmed cell death in the Caenorhabditis elegans hermaphrodite germline. Development *126*, 1011–1022.

Habchi, J., Tompa, P., Longhi, S., and Uversky, V.N. (2014). Introducing Protein Intrinsic Disorder. Chem. Rev. *114*, 6561–6588.

Haeussler, M., Schönig, K., Eckert, H., Eschstruth, A., Mianné, J., Renaud, J.-B., Schneider-Maunoury, S., Shkumatava, A., Teboul, L., Kent, J., et al. (2016). Evaluation of off-target and on-target scoring algorithms and integration into the guide RNA selection tool CRISPOR. Genome Biol. *17*, 148.

Hall, D.H., Winfrey, V.P., Blaeuer, G., Hoffman, L.H., Furuta, T., Rose, K.L., Hobert, O., and Greenstein, D. (1999). Ultrastructural Features of the Adult Hermaphrodite Gonad of Caenorhabditis elegans: Relations between the Germ Line and Soma. Dev. Biol. *212*, 101–123.

Han, K., Lee, J., Meyer, T.J., Remedios, P., Goodwin, L., and Batzer, M.A. (2008). L1 recombination-associated deletions generate human genomic variation. Proc. Natl. Acad. Sci. *105*, 19366–19371.

Han, T., Manoharan, A.P., Harkins, T.T., Bouffard, P., Fitzpatrick, C., Chu, D.S., Thierry-Mieg, D., Thierry-Mieg, J., and Kim, J.K. (2009). 26G endo-siRNAs regulate spermatogenic and zygotic gene expression in Caenorhabditis elegans. Proc. Natl. Acad. Sci. *106*, 18674–18679.

Hanazawa, M., Yonetani, M., and Sugimoto, A. (2011). PGL proteins self associate and bind RNPs to mediate germ granule assembly in C. elegans. J. Cell Biol. *192*, 929–937.

Hancks, D.C., and Kazazian, H.H. (2016). Roles for retrotransposon insertions in human disease. Mob. DNA *7*, 9.

Hauptmann, J., Dueck, A., Harlander, S., Pfaff, J., Merkl, R., and Meister, G. (2013). Turning catalytically inactive human Argonaute proteins into active slicer enzymes. Nat. Struct. Mol. Biol. *20*, 814–817.

Hernando-Rodríguez, B., and Artal-Sanz, M. (2018). Mitochondrial Quality Control Mechanisms and the PHB (Prohibitin) Complex. Cells *7*, 238.

Hirsh, D., Oppenheim, D., and Klass, M. (1976). Development of the reproductive system of Caenorhabditis elegans. Dev. Biol. *49*, 200–219.

Höck, J., and Meister, G. (2008). The Argonaute protein family. Genome Biol. *9*.

Hodgkin, J. (1983). Male Phenotypes and Mating Efficiency in CAENORHABDITIS ELEGANS. Genetics *103*, 43–64.

Hofweber, M., and Dormann, D. (2019). Friend or foe-Post-translational modifications as regulators of phase separation and RNP granule dynamics. J. Biol. Chem. *294*, 7137–7150.

Horváth, V., Merenciano, M., and González, J. (2017). Revisiting the Relationship between Transposable Elements and the Eukaryotic Stress Response. Trends Genet. *33*, 832–841.

Hu, J., Cheng, S., Wang, H., Li, X., Liu, S., Wu, M., Liu, Y., and Wang, X. (2019). Distinct roles of two myosins in C. Elegans spermatid differentiation.

Hu, S.-B., Xiang, J.-F., Li, X., Xu, Y., Xue, W., Huang, M., Wong, C.C., Sagum, C.A., Bedford, M.T., Yang, L., et al. (2015). Protein arginine methyltransferase CARM1 attenuates the paraspeckle-mediated nuclear retention of mRNAs containing IR Alu s. Genes Dev. *29*, 630–645.

Huang, C.R.L., Burns, K.H., and Boeke, J.D. (2012a). Active Transposition in Genomes. Annu. Rev. Genet. *46*, 651–675.

Huang, H., Gao, Q., Peng, X., Choi, S.-Y., Sarma, K., Ren, H., Morris, A.J., and Frohman, M.A. (2011). piRNA-Associated Germline Nuage Formation and Spermatogenesis Require MitoPLD Profusogenic Mitochondrial-Surface Lipid Signaling. Dev. Cell *20*, 376–387.

Huang, J., Wang, H., Chen, Y., Wang, X., and Zhang, H. (2012b). Residual body removal during spermatogenesis in C. elegans requires genes that mediate cell corpse clearance. Development *139*, 4613–4622.

Huang, S., Tao, X., Yuan, S., Zhang, Y., Li, P., Beilinson, H.A., Zhang, Y., Yu, W., Pontarotti, P., Escriva, H., et al. (2016). Discovery of an Active RAG Transposon Illuminates the Origins of V(D)J Recombination. Cell *166*, 102–114.

Huelgas-Morales, G., and Greenstein, D. (2018). Control of oocyte meiotic maturation in C. elegans. Semin. Cell Dev. Biol. *84*, 90–99.

Huerta-Cepas, J., Serra, F., and Bork, P. (2016a). ETE 3: Reconstruction, Analysis, and Visualization of Phylogenomic Data. Mol. Biol. Evol. *33*, 1635–1638.

Huerta-Cepas, J., Szklarczyk, D., Forslund, K., Cook, H., Heller, D., Walter, M.C., Rattei, T., Mende, D.R., Sunagawa, S., Kuhn, M., et al. (2016b). eggNOG 4.5: a hierarchical orthology framework with improved functional annotations for eukaryotic, prokaryotic and viral sequences. Nucleic Acids Res. *44*, D286–D293.

Hutvagner, G., and Simard, M.J. (2008). Argonaute proteins: Key players in RNA silencing. Nat. Rev. Mol. Cell Biol. *9*, 22–32.

Hyman, A.A., Weber, C.A., and Jülicher, F. (2014). Liquid-Liquid Phase Separation in Biology. Annu. Rev. Cell Dev. Biol. *30*, 39–58.

Iki, T., Yoshikawa, M., Nishikiori, M., Jaudal, M.C., Matsumoto-Yokoyama, E., Mitsuhara, I., Meshi, T., and Ishikawa, M. (2010). In Vitro Assembly of Plant RNA-Induced Silencing Complexes Facilitated by Molecular Chaperone HSP90. Mol. Cell *39*, 282–291.

Imbeault, M., Helleboid, P.-Y., and Trono, D. (2017). KRAB zinc-finger proteins contribute to the evolution of gene regulatory networks. Nature *543*, 550–554.

Ishidate, T., Ozturk, A.R., Durning, D.J., Sharma, R., Shen, E., Chen, H., Seth, M., Shirayama, M., and Mello, C.C. (2018). ZNFX-1 Functions within Perinuclear Nuage to Balance Epigenetic Signals. Mol. Cell *70*, 639-649.e6.

Iwasaki, S., Kobayashi, M., Yoda, M., Sakaguchi, Y., Katsuma, S., Suzuki, T., and Tomari, Y. (2010). Hsc70/Hsp90 Chaperone Machinery Mediates ATP-Dependent RISC Loading of Small RNA Duplexes. Mol. Cell *39*, 292–299.

Iwasaki, S., Sasaki, H.M., Sakaguchi, Y., Suzuki, T., Tadakuma, H., and Tomari, Y. (2015). Defining fundamental steps in the assembly of the Drosophila RNAi enzyme complex. Nature *521*, 533–536.

Jangam, D., Feschotte, C., and Betrán, E. (2017). Transposable Element Domestication As an Adaptation to Evolutionary Conflicts. Trends Genet. *33*, 817–831.

Jinek, M., and Doudna, J.A. (2009). A three-dimensional view of the molecular machinery of RNA interference. Nature *457*, 405–412.

Jing, L., Tanxi, C., Peng, W., Ziyou, C., Xiulan, C., Junjie, H., Zhensheng, X., Peng, X., Linan, S., Pingsheng, L., et al. (2009). Proteomic analysis of mitochondria from Caenorhabditis elegans. Proteomics *9*, 4539–4553.

Johnston, M., Geoffroy, M.C., Sobala, A., Hay, R., and Hutvagner, G. (2010). HSP90 protein stabilizes unloaded argonaute complexes and microscopic P-bodies in human cells. Mol. Biol. Cell *21*, 1462–1469.

Joly-Lopez, Z., and Bureau, T.E. (2018). Exaptation of transposable element coding sequences. Curr. Opin. Genet. Dev. *49*, 34–42.

Kajikawa, M., and Okada, N. (2002). LINEs Mobilize SINEs in the Eel through a Shared 3′ Sequence. Cell *111*, 433–444.

Kamminga, L.M., van Wolfswinkel, J.C., Luteijn, M.J., Kaaij, L.J.T., Bagijn, M.P., Sapetschnig, A., Miska, E.A., Berezikov, E., and Ketting, R.F. (2012). Differential impact of the HEN1 homolog HENN-1 on 21U and 26G RNAs in the germline of Caenorhabditis elegans. PLoS Genet. *8*.

Kaneshiro, K.R., Rechtsteiner, A., and Strome, S. (2019). Sperm-inherited H3K27me3 impacts offspring transcription and development in C. elegans. Nat. Commun. *10*, 1–9.

Kapitonov, V. V., and Jurka, J. (2001). Rolling-circle transposons in eukaryotes. Proc. Natl. Acad. Sci. *98*, 8714–8719.

Kapitonov, V. V., and Koonin, E. V. (2015). Evolution of the RAG1-RAG2 locus: both proteins came from the same transposon. Biol. Direct *10*, 20.

Kappei, D., Butter, F., Benda, C., Scheibe, M., Draškovič, I., Stevense, M., Novo, C.L., Basquin, C., Araki, M., Araki, K., et al. (2013). HOT1 is a mammalian direct telomere repeat-binding protein contributing to telomerase recruitment. EMBO J. *32*, 1681–1701.

Kapusta, A., Suh, A., and Feschotte, C. (2017). Dynamics of genome size evolution in birds and mammals. Proc. Natl. Acad. Sci. *114*, E1460–E1469.

Kasimatis, K.R., Moerdyk-Schauwecker, M.J., Timmermeyer, N., and Phillips, P.C. (2018). Proteomic and evolutionary analyses of sperm activation identify uncharacterized genes in Caenorhabditis nematodes. BMC Genomics *19*, 1–13.

Kaspar, D., Hastreiter, S., Irmler, M., Hrabé de Angelis, M., and Beckers, J. (2020). Nutrition and its role in epigenetic inheritance of obesity and diabetes across generations. Mamm. Genome.

Kasper, D.M., Wang, G., Gardner, K.E., Johnstone, T.G., and Reinke, V. (2014). The C. elegans SNAPc Component SNPC-4 Coats piRNA Domains and Is Globally Required for piRNA Abundance. Dev. Cell *31*, 145–158.

Kato, M., Han, T.W., Xie, S., Shi, K., Du, X., Wu, L.C., Mirzaei, H., Goldsmith, E.J., Longgood, J., Pei, J., et al. (2012). Cell-free Formation of RNA Granules: Low Complexity Sequence Domains Form Dynamic Fibers within Hydrogels. Cell *149*, 753–767.

Katsani, K.R. (1999). Co-operative DNA binding by GAGA transcription factor requires the conserved BTB/POZ domain and reorganizes promoter topology. EMBO J. *18*, 698–708.

Katz, D.J., Edwards, T.M., Reinke, V., and Kelly, W.G. (2009). A C. elegans LSD1 Demethylase Contributes to Germline Immortality by Reprogramming Epigenetic Memory. Cell *137*, 308–320.

Kawasaki, I., Shim, Y.H., Kirchner, J., Kaminker, J., Wood, W.B., and Strome, S. (1998). PGL-1, a predicted RNA-binding component of germ granules, is essential for fertility in C. elegans. Cell *94*, 635–645.

Kawasaki, I., Amiri, A., Fan, Y., Meyer, N., Dunkelbarger, S., Motohashi, T., Karashima, T., Bossinger, O., and Strome, S. (2004). The PGL family proteins associate with germ granules and function redundantly in Caenorhabditis elegans germline development. Genetics *167*, 645–661.

Keane, F.M., Nadvi, N.A., Yao, T.-W., and Gorrell, M.D. (2011). Neuropeptide Y, B-type natriuretic peptide, substance P and peptide YY are novel substrates of fibroblast activation protein-α. FEBS J. *278*, 1316–1332.

Kelleher, J.F., Mandell, M.A., Moulder, G., Hill, K.L., L'Hernault, S.W., Barstead, R., and Titus, M.A. (2000). Myosin VI is required for asymmetric segregation of cellular components during C. elegans spermatogenesis. Curr. Biol. *10*, 1489–1496.

Ketting, R.F. (2001). Dicer functions in RNA interference and in synthesis of small RNA involved in developmental timing in C. elegans. Genes Dev. *15*, 2654–2659.

Ketting, R.F. (2011). The Many Faces of RNAi. Dev. Cell *20*, 148–161.

Ketting, R.F., Haverkamp, T.H.A., Van Luenen, H.G.A.M., and Plasterk, R.H.A. (1999). mut-7 of C. elegans, required for transposon silencing and RNA interference, is a homolog of werner syndrome helicase and RNaseD. Cell *99*, 133–141.

Khan, A., and Mathelier, A. (2017). Intervene: A tool for intersection and visualization of multiple gene or genomic region sets. BMC Bioinformatics *18*, 1–8.

Kieffer, T.J., McIntosh, C.H., and Pederson, R.A. (1995). Degradation of glucose-dependent insulinotropic polypeptide and truncated glucagon-like peptide 1 in vitro and in vivo by dipeptidyl peptidase IV. Endocrinology *136*, 3585–3596.

Kim, S., Spike, C., and Greenstein, D. (2013). Control of Oocyte Growth and Meiotic Maturation in Caenorhabditis elegans. In Advances in Experimental Medicine and Biology, T. Schedl, ed. (New York, NY: Springer New York), pp. 277–320.

Kimble, J., and Hirsh, D. (1979). The postembryonic cell lineages of the hermaphrodite and male gonads in Caenorhabditis elegans. Dev. Biol. *70*, 396–417.

Kimble, J.E., and White, J.G. (1981). On the control of germ cell development in Caenorhabditis elegans. Dev. Biol. *81*, 208–219.

Kimura, T., Ito, C., Watanabe, S., Takahashi, T., Ikawa, M., Yomogida, K., Fujita, Y., Ikeuchi, M., Asada, N., Matsumiya, K., et al. (2003). Mouse Germ Cell-Less as an Essential Component for Nuclear Integrity. Mol. Cell. Biol. *23*, 1304–1315.

King, M. Lou, and Zhou, Y. (2004). Sending RNAs into the Future: RNA Localization and Germ Cell Fate. IUBMB Life (International Union Biochem. Mol. Biol. Life) *56*, 19–27.

King, S.E., and Skinner, M.K. (2020). Epigenetic Transgenerational Inheritance of Obesity Susceptibility. Trends Endocrinol. Metab. *31*, 478–494.

King, K.L., Stewart, M., Roberts, T.M., and Seavy, M. (1992). Structure and macro molecular assembly of two isoforms of the major sperm protein (MSP) from the amoeboid sperm of the nematode, Ascaris suum. J. Cell Sci. *101*, 847–857.

Kishimoto, S., Uno, M., and Nishida, E. (2018). Molecular mechanisms regulating lifespan and environmental stress responses. Inflamm. Regen. *38*, 1–7.

Klass, M.R., and Hirsh, D. (1981). Sperm isolation and biochemical analysis of the major sperm protein from Caenorhabditis elegans. Dev. Biol. *84*, 299–312.

Klass, M., Wolf, N., and Hirsh, D. (1976). Development of the male reproductive system and sexual transformation in the nematode Caenorhabditis elegans. Dev. Biol. *52*, 1–18.

Kleiman, S.E., Yogev, L., Gal-Yam, E.N., Hauser, R., Gamzu, R., Botchan, A., Paz, G., Yavetz, H., Maymon, B.B.S., Schreiber, L., et al. (2003). Reduced Human Germ Cell-Less (HGCL) Expression in Azoospermic Men with Severe Germinal Cell Impairment. J. Androl. *24*, 670–675.

Klosin, A., Casas, E., Hidalgo-Carcedo, C., Vavouri, T., and Lehner, B. (2017). Transgenerational transmission of environmental information in C. elegans. Science (80-.). *356*, 320–323.

Knutson, K.A., Egelhofer, T., Rechtsteiner, A., and Strome, S. (2017). Germ granules prevent accumulation of somatic transcripts in the adult. Genetics *206*, 163–178.

Kobayashi, H., Shoji, K., Kiyokawa, K., Negishi, L., and Tomari, Y. (2019a). Iruka Eliminates Dysfunctional Argonaute by Selective Ubiquitination of Its Empty State. Mol. Cell *73*, 119-129.e5.

Kobayashi, H., Shoji, K., Kiyokawa, K., Negishi, L., and Tomari, Y. (2019b). VCP Machinery Mediates Autophagic Degradation of Empty Argonaute. Cell Rep. *28*, 1144-1153.e4.

Koulouras, G., Panagopoulos, A., Rapsomaniki, M.A., Giakoumakis, N.N., Taraviras, S., and Lygerou, Z. (2018). EasyFRAP-web: A web-based tool for the analysis of fluorescence recovery after photobleaching data. Nucleic Acids Res. *46*, W467–W472.

Kourtidis, A., and Anastasiadis, P.Z. (2018). Close encounters of the RNAi kind: the silencing life of the adherens junctions. Curr. Opin. Cell Biol. *54*, 30–36.

Kourtidis, A., Ngok, S.P., Pulimeno, P., Feathers, R.W., Carpio, L.R., Baker, T.R., Carr, J.M., Yan, I.K., Borges, S., Perez, E.A., et al. (2015). Distinct E-cadherin-based complexes regulate cell behaviour through miRNA processing or Src and p120 catenin activity. Nat. Cell Biol. *17*, 1145–1157.

Kourtidis, A., Necela, B., Lin, W.-H., Lu, R., Feathers, R.W., Asmann, Y.W., Thompson, E.A., and Anastasiadis, P.Z. (2017). Cadherin complexes recruit mRNAs and RISC to regulate epithelial cell signaling. J. Cell Biol. *216*, 3073–3085.

Kramerov, D., and Vassetzky, N. (2005). Short Retroposons in Eukaryotic Genomes. Int. Rev. Cytol. *247*, 165–221.

Kreher, J., Takasaki, T., Cockrum, C., Sidoli, S., Garcia, B.A., Jensen, O.N., and Strome, S. (2018). Distinct roles of two histone methyltransferases in transmitting h3k36me3-based epigenetic memory across generations in caenorhabditis elegans. Genetics *210*, 969–982.

Kriventseva, E. V., Kuznetsov, D., Tegenfeldt, F., Manni, M., Dias, R., Simão, F.A., and Zdobnov, E.M. (2019). OrthoDB v10: sampling the diversity of animal, plant, fungal, protist, bacterial and viral genomes for evolutionary and functional annotations of orthologs. Nucleic Acids Res. *47*, D807–D811.

Kroft, T.L., Gleason, E.J., and L'Hernault, S.W. (2005). The spe-42 gene is required for sperm–egg interactions during C. elegans fertilization and encodes a sperm-specific transmembrane protein. Dev. Biol. *286*, 169–181.

Kroschwald, S., Maharana, S., and Simon, A. (2017). Hexanediol: a chemical probe to investigate the material properties of membrane-less compartments. Matters 1–7.

Kuramochi-Miyagawa, S., Watanabe, T., Gotoh, K., Takamatsu, K., Chuma, S., Kojima-Kita, K., Shiromoto, Y., Asada, N., Toyoda, A., Fujiyama, A., et al. (2010). MVH in piRNA processing and gene silencing of retrotransposons. Genes Dev. *24*, 887–892.

Kuzmenko, A., Oguienko, A., Esyunina, D., Yudin, D., Petrova, M., Kudinova, A., Maslova, O., Ninova, M., Ryazansky, S., Leach, D., et al. (2020). DNA targeting and interference by a bacterial Argonaute nuclease. Nature.

Kwak, P.B., and Tomari, Y. (2012). The N domain of Argonaute drives duplex unwinding during RISC assembly. Nat. Struct. Mol. Biol. *19*, 145–151.

L'Hernault, S.W. (2009). The genetics and cell biology of spermatogenesis in the nematode C. elegans. Mol. Cell. Endocrinol. *306*, 59–65.

L'Hernault, S.W., and Arduengo, P.M. (1992). Mutation of a putative sperm membrane protein in Caenorhabditis elegans prevents sperm differentiation but not its associated meiotic divisions. J. Cell Biol. *119*, 55–68.

L'Hernault, S.W., Benian, G.M., and Emmons, R.B. (1993). Genetic and molecular characterization of the Caenorhabditis elegans spermatogenesis-defective gene spe-17. Genetics *134*, 769–780.

Lamesch, P., Milstein, S., Hao, T., Rosenberg, J., Li, N., Sequerra, R., Bosak, S., Doucette-Stamm, L., Vandenhaute, J., Hill, D.E., et al. (2004). C. elegans ORFeome version 3.1: Increasing the coverage of ORFeome resources with improved gene predictions. Genome Res. *14*, 2064–2069.

Lampe, D.J., Akerley, B.J., Rubin, E.J., Mekalanos, J.J., and Robertson, H.M. (1999). Hyperactive transposase mutants of the Himar1 mariner transposon. Proc. Natl. Acad. Sci. *96*, 11428–11433.

LaMunyon, C.W., and Ward, S. (1995). Sperm predence in a hermaphroditic nematode (Caenorhabditis elegans) is due to competitive superiority of male sperm. Experientia *51*, 817–823.

LaMunyon, C.W., and Ward, S. (1998). Larger sperm outcompete smaller sperm in the nematode Caenorhabditis elegans. Proc. R. Soc. London. Ser. B Biol. Sci. *265*, 1997–2002.

Lanciano, S., and Mirouze, M. (2018). Transposable elements: all mobile, all different, some stress responsive, some adaptive? Curr. Opin. Genet. Dev. *49*, 106–114.

Langmead, B., Trapnell, C., Pop, M., and Salzberg, S.L. (2009). Ultrafast and memory-efficient alignment of short DNA sequences to the human genome. Genome Biol. *10*.

Laricchia, K.M., Zdraljevic, S., Cook, D.E., and Andersen, E.C. (2017). Natural Variation in the Distribution and Abundance of Transposable Elements Across the Caenorhabditis elegans Species. Mol. Biol. Evol. *34*, 2187–2202.

Lee, C.-Y.S., Putnam, A., Lu, T., He, S., Ouyang, J.P.T., and Seydoux, G. (2020). Recruitment of mRNAs to P granules by condensation with intrinsically-disordered proteins. Elife *9*, 1–31.

Lee, H.C., Gu, W., Shirayama, M., Youngman, E., Conte, D., and Mello, C.C. (2012). C. elegans piRNAs mediate the genome-wide surveillance of germline transcripts. Cell *150*, 78–87.

Lee, J.A., Carvalho, C.M.B., and Lupski, J.R. (2007a). A DNA Replication Mechanism for Generating Nonrecurrent Rearrangements Associated with Genomic Disorders. Cell *131*, 1235–1247.

Lee, M.-H., Ohmachi, M., Arur, S., Nayak, S., Francis, R., Church, D., Lambie, E., and Schedl, T. (2007b). Multiple Functions and Dynamic Activation of MPK-1 Extracellular Signal-Regulated Kinase Signaling in Caenorhabditis elegans Germline Development. Genetics *177*, 2039–2062.

Lehtiniemi, T., and Kotaja, N. (2018). Germ granule-mediated RNA regulation in male germ cells. Reproduction *155*, R77–R91.

Letunic, I., and Bork, P. (2018). 20 years of the SMART protein domain annotation resource. Nucleic Acids Res. *46*, D493–D496.

Letunic, I., Doerks, T., and Bork, P. (2015). SMART: recent updates, new developments and status in 2015. Nucleic Acids Res. *43*, D257–D260.

Leung, A.K.L., Vyas, S., Rood, J.E., Bhutkar, A., Sharp, P.A., and Chang, P. (2011). Poly(ADP-Ribose) Regulates Stress Responses and MicroRNA Activity in the Cytoplasm. Mol. Cell *42*, 489–499.

Lev, I., Seroussi, U., Gingold, H., Bril, R., Anava, S., and Rechavi, O. (2017). MET-2-Dependent H3K9 Methylation Suppresses Transgenerational Small RNA Inheritance. Curr. Biol. *27*, 1138–1147.

Lev, I., Toker, I.A., Mor, Y., Nitzan, A., Weintraub, G., Antonova, O., Bhonkar, O., Ben Shushan, I., Seroussi, U., Claycomb, J.M., et al. (2019). Germ Granules Govern Small RNA Inheritance. Curr. Biol. *29*, 2880-2891.e4.

Lewis, A., Berkyurek, A.C., Greiner, A., Sawh, A.N., Vashisht, A., Merrett, S., Flamand, M.N., Wohlschlegel, J., Sarov, M., Miska, E.A., et al. (2020). A Family of Argonaute-Interacting Proteins Gates Nuclear RNAi. Mol. Cell *78*, 862-875.e8.

Li, H., Handsaker, B., Wysoker, A., Fennell, T., Ruan, J., Homer, N., Marth, G., Abecasis, G., and Durbin, R. (2009). The Sequence Alignment/Map format and SAMtools. Bioinformatics *25*, 2078–2079.

Li, X., Peng, H., Schultz, D.C., Lopez-Guisa, J.M., Rauscher, F.J., and Marmorstein, R. (1999). Structure-function studies of the BTB/POZ transcriptional repression domain from the promyelocytic leukemia zinc finger oncoprotein. Cancer Res. *59*, 5275–5282.

Lin, Y., Protter, D.S.W., Rosen, M.K., and Parker, R. (2015). Formation and Maturation of Phase-Separated Liquid Droplets by RNA-Binding Proteins. Mol. Cell *60*, 208–219.

Lingel, A., Simon, B., Izaurralde, E., and Sattler, M. (2004). Nucleic acid 3′-end recognition by the Argonaute2 PAZ domain. Nat. Struct. Mol. Biol. *11*, 576–577.

Lohe, A.R., and Hartl, D.L. (1996). Autoregulation of mariner transposase activity by overproduction and dominant-negative complementation. Mol. Biol. Evol. *13*, 549–555.

Lopez-Orozco, J., Pare, J.M., Holme, A.L., Chaulk, S.G., Fahlman, R.P., and Hobman, T.C. (2015). Functional analyses of phosphorylation events in human Argonaute 2. RNA *21*, 2030–2038.

Love, M.I., Huber, W., and Anders, S. (2014). Moderated estimation of fold change and dispersion for RNA-seq data with DESeq2. Genome Biol. *15*, 1–21.

Luan, D.D., Korman, M.H., Jakubczak, J.L., and Eickbush, T.H. (1993). Reverse transcription of R2Bm RNA is primed by a nick at the chromosomal target site: A mechanism for non-LTR retrotransposition. Cell *72*, 595–605.

Luteijn, M.J., Van Bergeijk, P., Kaaij, L.J.T., Almeida, M.V., Roovers, E.F., Berezikov, E., and Ketting, R.F. (2012). Extremely stable Piwi-induced gene silencing in Caenorhabditis elegans. EMBO J. *31*, 3422–3430.

Ma, J.B., Ye, K., and Patel, D.J. (2004). Structural basis for overhang-specific small interfering RNA recognition by the PAZ domain. Nature *429*, 318–322.

Ma, L., Buchold, G.M., Greenbaum, M.P., Roy, A., Burns, K.H., Zhu, H., Han, D.Y., Harris, R.A., Coarfa, C., Gunaratne, P.H., et al. (2009). GASZ Is Essential for Male Meiosis and Suppression of Retrotransposon Expression in the Male Germline. PLoS Genet. *5*, e1000635.

Ma, X., Zhu, Y., Li, C., Xue, P., Zhao, Y., Chen, S., Yang, F., and Miao, L. (2014). Characterisation of Caenorhabditis elegans sperm transcriptome and proteome. BMC Genomics *15*, 1–13.

Ben Maamar, M., Sadler-Riggleman, I., Beck, D., McBirney, M., Nilsson, E., Klukovich, R., Xie, Y., Tang, C., Yan, W., and Skinner, M.K. (2018). Alterations in sperm DNA methylation, non-coding RNA expression, and histone retention mediate vinclozolin-induced epigenetic transgenerational inheritance of disease. Environ. Epigenetics *4*, 1–19.

Madeira, F., Park, Y.M., Lee, J., Buso, N., Gur, T., Madhusoodanan, N., Basutkar, P., Tivey, A.R.N., Potter, S.C., Finn, R.D., et al. (2019). The EMBL-EBI search and sequence analysis tools APIs in 2019. Nucleic Acids Res. *47*, W636–W641.

Maekawa, M., Ito, C., Toyama, Y., Suzuki-Toyota, F., Kimura, T., Nakano, T., and Toshimori, K. (2004). Stage-specific expression of mouse germ cell-less-1 (mGCL-1), and multiple deformations during mgcl-1 deficient spermatogenesis leading to reduced fertility. Arch. Histol. Cytol. *67*, 335–347.

Makarova, K.S., Wolf, Y.I., van der Oost, J., and Koonin, E. V. (2009). Prokaryotic homologs of Argonaute proteins are predicted to function as key components of a novel system of defense against mobile genetic elements. Biol. Direct *4*, 29.

Maniar, J.M., and Fire, A.Z. (2011). EGO-1, a C. elegans RdRP, Modulates Gene Expression via Production of mRNA-Templated Short Antisense RNAs. Curr. Biol. *21*, 449–459.

Mao, H., Zhu, C., Zong, D., Weng, C., Yang, X., Huang, H., Liu, D., Feng, X., and Guang, S. (2015). The Nrde Pathway Mediates Small-RNA-Directed Histone H3 Lysine 27 Trimethylation in Caenorhabditis elegans. Curr. Biol. *25*, 2398–2403.

Marnik, E.A., and Updike, D.L. (2019). Membraneless organelles: P granules in Caenorhabditis elegans. Traffic *20*, 373–379.

Martin, M. (2011). Cutadapt removes adapter sequences from high-throughput sequencing reads. EMBnet.Journal *17*, 10.

Martinez, N.J., and Gregory, R.I. (2013). Argonaute2 expression is post-transcriptionally coupled to microRNA abundance. Rna *19*, 605–612.

Masuhara, M., Nagao, K., Nishikawa, M., Kimura, T., and Nakano, T. (2003). Enhanced degradation of MDM2 by a nuclear envelope component, mouse germ cell-less. Biochem. Biophys. Res. Commun. *308*, 927–932.

Mátés, L., Chuah, M.K.L., Belay, E., Jerchow, B., Manoj, N., Acosta-Sanchez, A., Grzela, D.P., Schmitt, A., Becker, K., Matrai, J., et al. (2009). Molecular evolution of a novel hyperactive Sleeping Beauty transposase enables robust stable gene transfer in vertebrates. Nat. Genet. *41*, 753–761.

McClintock, B. (1951). Chromosome organization and genic expression. Cold Spring Harb. Symp. Quant. Biol. *16*, 13–47.

McClintock, B. (1956). Controlling Elements and the Gene. Cold Spring Harb. Symp. Quant. Biol. *21*, 197–216.

McCue, A.D., and Slotkin, R.K. (2012). Transposable element small RNAs as regulators of gene expression. Trends Genet. *28*, 616–623.

Meister, G. (2013). Argonaute proteins: functional insights and emerging roles. Nat. Rev. Genet. *14*, 447–459.

Melnick, A., Ahmad, K.F., Arai, S., Polinger, A., Ball, H., Borden, K.L., Carlile, G.W., Prive, G.G., and Licht, J.D. (2000). In-Depth Mutational Analysis of the Promyelocytic Leukemia Zinc Finger BTB/POZ Domain Reveals Motifs and Residues Required for Biological and Transcriptional Functions. Mol. Cell. Biol. *20*, 6550–6567.

Melnick, A., Carlile, G., Ahmad, K.F., Kiang, C.-L., Corcoran, C., Bardwell, V., Prive, G.G., and Licht, J.D. (2002). Critical Residues within the BTB Domain of PLZF and Bcl-6 Modulate Interaction with Corepressors. Mol. Cell. Biol. *22*, 1804–1818.

Mentlein, R. (1999). Dipeptidyl-peptidase IV (CD26)-role in the inactivation of regulatory peptides. Regul. Pept. *85*, 9–24.

Mentlein, R., Gallwitz, B., and Schmidt, W.E. (1993). Dipeptidyl-peptidase IV hydrolyses gastric inhibitory polypeptide, glucagon-like peptide-1(7-36)amide, peptide histidine methionine and is responsible for their degradation in human serum. Eur. J. Biochem. *214*, 829–835.

Merritt, C., Rasoloson, D., Ko, D., and Seydoux, G. (2008). 3′ UTRs Are the Primary Regulators of Gene Expression in the C. elegans Germline. Curr. Biol. *18*, 1476–1482.

Michelitsch, M.D., and Weissman, J.S. (2000). A census of glutamine/asparagine-rich regions: Implications for their conserved function and the prediction of novel prions. Proc. Natl. Acad. Sci. *97*, 11910–11915.

Miller, M.A., Nguyen, V.Q., Lee, M.H., Kosinski, M., Schedl, T., Caprioli, R.M., and Greenstein, D. (2001). A sperm cytoskeletal protein that signals oocyte meiotic maturation and ovulation. Science (80-.). *291*, 2144–2147.

Miller, M.A., Ruest, P.J., Kosinski, M., Hanks, S.K., and Greenstein, D. (2003). An Eph receptor sperm-sensing control mechanism for oocyte meiotic maturation in Caenorhabditis elegans. Genes Dev. *17*, 187–200.

Mitchell, A.L., Attwood, T.K., Babbitt, P.C., Blum, M., Bork, P., Bridge, A., Brown, S.D., Chang, H.Y., El-Gebali, S., Fraser, M.I., et al. (2019). InterPro in 2019: Improving coverage, classification and access to protein sequence annotations. Nucleic Acids Res. *47*, D351–D360.

Miyoshi, T., Takeuchi, A., Siomi, H., and Siomi, M.C. (2010). A direct role for Hsp90 in pre-RISC formation in Drosophila. Nat. Struct. Mol. Biol. *17*, 1024–1026.

Molaro, A., and Malik, H.S. (2016). Hide and seek: how chromatin-based pathways silence retroelements in the mammalian germline. Curr. Opin. Genet. Dev. *37*, 51–58.

Montgomery, T.A., Rim, Y.-S., Zhang, C., Dowen, R.H., Phillips, C.M., Fischer, S.E.J., and Ruvkun, G. (2012). PIWI Associated siRNAs and piRNAs Specifically Require the Caenorhabditis elegans HEN1 Ortholog henn-1. PLoS Genet. *8*, e1002616.

El Mouridi, S., Lecroisey, C., Tardy, P., Mercier, M., Leclercq-Blondel, A., Zariohi, N., and Boulin, T. (2017). Reliable CRISPR/Cas9 genome engineering in Caenorhabditis elegans using a single efficient sgRNA and an easily recognizable phenotype. G3 Genes, Genomes, Genet. *7*, 1429–1437.

Munafò, M., Manelli, V., Falconio, F.A., Sawle, A., Kneuss, E., Eastwood, E.L., Seah, J.W.E., Czech, B., and Hannon, G.J. (2019). Daedalus and gasz recruit armitage to mitochondria, bringing piRNA precursors to the biogenesis machinery. Genes Dev. *33*, 844–856.

N. Kotaja, P.S.-C. (2007). The chromatoid body: a germ-cell-specific RNA-processing centre. Nat. Rev. Mol. Cell Biol. *8*, 85–90.

Nadarajan, S., Govindan, J.A., McGovern, M., Hubbard, E.J.A., and Greenstein, D. (2009). MSP and GLP-1/Notch signaling coordinately regulate actomyosin-dependent cytoplasmic streaming and oocyte growth in C. elegans. Development *136*, 2223–2234.

Nakanishi, K. (2016). Anatomy of RISC: how do small RNAs and chaperones activate Argonaute proteins? Wiley Interdiscip. Rev. RNA *7*, 637–660.

Nakanishi, K., Weinberg, D.E., Bartel, D.P., and Patel, D.J. (2012). Structure of yeast Argonaute with guide RNA. Nature *486*, 368–374.

Nassif, N., Penney, J., Pal, S., Engels, W.R., and Gloor, G.B. (1994). Efficient copying of nonhomologous sequences from ectopic sites via P-element-induced gap repair. Mol. Cell. Biol. *14*, 1613–1625.

Naville, M., Warren, I.A., Haftek-Terreau, Z., Chalopin, D., Brunet, F., Levin, P., Galiana, D., and Volff, J.-N. (2016). Not so bad after all: retroviruses and long terminal repeat retrotransposons as a source of new genes in vertebrates. Clin. Microbiol. Infect. *22*, 312–323.

Nelson, G.A., and Ward, S. (1980). Vesicle fusion, pseudopod extension and amoeboid motility are induced in nematode spermatids by the ionophore monensin. Cell *19*, 457–464.

Newman, M.A., Ji, F., Fischer, S.E.J., Anselmo, A., Sadreyev, R.I., and Ruvkun, G. (2018). The surveillance of pre-mRNA splicing is an early step in C. Elegans RNAi of endogenous genes. Genes Dev. *32*, 670–681.

Nigon, V. (1949). Les modalités de la reproduction et le déterminisme due sexe chez quelques nematodes libres. Ann. Sci. Nat. Zool. Biol. Anim. *11*, 1–132.

Nili, E., Cojocaru, G.S., Kalma, Y., Ginsberg, D., Copeland, N.G., Gilbert, D.J., Jenkins, N.A., Berger, R., Shaklai, S., Amariglio, N., et al. (2001). Nuclear membrane protein LAP2β mediates transcriptional repression alone and together with its binding partner GCL (germ-cell-less). J. Cell Sci. *114*, 3297–3307.

Nishimura, H., and L'Hernault, S.W. (2010). Spermatogenesis-defective (spe) mutants of the nematode Caenorhabditis elegans provide clues to solve the puzzle of male germline functions during reproduction. Dev. Dyn. *239*, 1502–1514.

Olovnikov, I., Chan, K., Sachidanandam, R., Newman, D.K., and Aravin, A.A. (2013). Bacterial Argonaute Samples the Transcriptome to Identify Foreign DNA. Mol. Cell *51*, 594–605.

Ortiz, M.A., Noble, D., Sorokin, E.P., and Kimble, J. (2014). A New Dataset of Spermatogenic vs . Oogenic Transcriptomes in the Nematode Caenorhabditis elegans. G3 Genes, Genomes, Genet. *4*, 1765–1772.

Öst, A., Lempradl, A., Casas, E., Weigert, M., Tiko, T., Deniz, M., Pantano, L., Boenisch, U., Itskov, P.M., Stoeckius, M., et al. (2014). Paternal Diet Defines Offspring Chromatin State and Intergenerational Obesity. Cell *159*, 1352–1364.

Ouyang, J.P.T., Folkmann, A., Bernard, L., Lee, C., Seroussi, U., Charlesworth, A.G., Claycomb, J.M., and Seydoux, G. (2019). P Granules Protect RNA Interference Genes from Silencing by piRNAs. Dev. Cell *50*, 716-728.e6.

Ozata, D.M., Gainetdinov, I., Zoch, A., O'Carroll, D., and Zamore, P.D. (2019). PIWI-interacting RNAs: small RNAs with big functions. Nat. Rev. Genet. *20*, 89–108.

Paix, A., Wang, Y., Smith, H.E., Lee, C.Y.S., Calidas, D., Lu, T., Smith, J., Schmidt, H., Krause, M.W., and Seydoux, G. (2014). Scalable and versatile genome editing using linear DNAs with microhomology to Cas9 sites in Caenorhabditis elegans. Genetics *198*, 1347–1356.

Paix, A., Schmidt, H., and Seydoux, G. (2016). Cas9-assisted recombineering in C. elegans: Genome editing using in vivo assembly of linear DNAs. Nucleic Acids Res. *44*, e128.

Pak, J., and Fire, A. (2007). Distinct Populations of Primary and Secondary Effectors During RNAi in C. elegans. Science (80-.). *315*, 241–244.

Parker, J.S. (2010). How to slice: Snapshots of Argonaute in action. Silence *1*, 1–10.

Parker, G.S., Eckert, D.M., and Bass, B.L. (2006). RDE-4 preferentially binds long dsRNA and its dimerization is necessary for cleavage of dsRNA to siRNA. RNA *12*, 807–818.

Parker, J.S., Roe, S.M., and Barford, D. (2004). Crystal structure of a PIWI protein suggests mechanisms for siRNA recognition and slicer activity. EMBO J. *23*, 4727–4737.

Pavelec, D.M., Lachowiec, J., Duchaine, T.F., Smith, H.E., and Kennedy, S. (2009). Requirement for the ERI/DICER complex in endogenous RNA interference and sperm development in Caenorhabditis elegans. Genetics *183*, 1283–1295.

Pellettieri, J., Reinke, V., Kim, S.K., and Seydoux, G. (2003). Coordinate Activation of Maternal Protein Degradation during the Egg-to-Embryo Transition in C. elegans. Dev. Cell *5*, 451–462.

Pellicer, J., Kelly, L.J., Leitch, I.J., Zomlefer, W.B., and Fay, M.F. (2014). A universe of dwarfs and giants: genome size and chromosome evolution in the monocot family Melanthiaceae. New Phytol. *201*, 1484–1497.

Perez-Riverol, Y., Csordas, A., Bai, J., Bernal-Llinares, M., Hewapathirana, S., Kundu, D.J., Inuganti, A., Griss, J., Mayer, G., Eisenacher, M., et al. (2019). The PRIDE database and related tools and resources in 2019: Improving support for quantification data. Nucleic Acids Res. *47*, D442–D450.

Perez, M.F., and Lehner, B. (2019). Intergenerational and transgenerational epigenetic inheritance in animals. Nat. Cell Biol. *21*, 143–151.

Peters, L., and Meister, G. (2007). Argonaute Proteins: Mediators of RNA Silencing. Mol. Cell *26*, 611–623.

Petsalaki, E., and Russell, R.B. (2008). Peptide-mediated interactions in biological systems: new discoveries and applications. Curr. Opin. Biotechnol. *19*, 344–350.

Phillips, C.M., Montgomery, T.A., Breen, P.C., and Ruvkun, G. (2012). MUT-16 promotes formation of perinuclear Mutator foci required for RNA silencing in the C. elegans germline. Genes Dev. *26*, 1433–1444.

Phillips, C.M., Montgomery, B.E., Breen, P.C., Roovers, E.F., Rim, Y.S., Ohsumi, T.K., Newman, M.A., Van Wolfswinkel, J.C., Ketting, R.F., Ruvkun, G., et al. (2014). MUT-14 and SMUT-1 DEAD box RNA helicases have overlapping roles in germline RNAi and endogenous siRNA formation. Curr. Biol. *24*, 839–844.

Phillips, C.M., Brown, K.C., Montgomery, B.E., Ruvkun, G., and Montgomery, T.A. (2015). PiRNAs and piRNA-Dependent siRNAs Protect Conserved and Essential C. elegans Genes from Misrouting into the RNAi Pathway. Dev. Cell *34*, 457–465.

Piovesan, D., Tabaro, F., Paladin, L., Necci, M., Mičetić, I., Camilloni, C., Davey, N., Dosztányi, Z., Mészáros, B., Monzon, A.M., et al. (2018). MobiDB 3.0: More annotations for intrinsic disorder, conformational diversity and interactions in proteins. Nucleic Acids Res. *46*, D471–D476.

Piriyapongsa, J., Mariño-Ramírez, L., and Jordan, I.K. (2007). Origin and Evolution of Human microRNAs From Transposable Elements. Genetics *176*, 1323–1337.

Pitt, J.N., Schisa, J.A., and Priess, J.R. (2000). P Granules in the Germ Cells of Caenorhabditis elegans Adults Are Associated with Clusters of Nuclear Pores and Contain RNA. Dev. Biol. *219*, 315–333.

Price, M.N., Dehal, P.S., and Arkin, A.P. (2009). FastTree: Computing Large Minimum Evolution Trees with Profiles instead of a Distance Matrix. Mol. Biol. Evol. *26*, 1641–1650.

Putiri, E., Zannoni, S., Kadandale, P., and Singson, A. (2004). Functional domains and temperature-sensitive mutations in SPE-9, an EGF repeat-containing protein required for fertility in Caenorhabditis elegans. Dev. Biol. *272*, 448–459.

Putnam, A., Cassani, M., Smith, J., and Seydoux, G. (2019). A gel phase promotes condensation of liquid P granules in Caenorhabditis elegans embryos. Nat. Struct. Mol. Biol. *26*, 220–226.

Qi, H.H., Ongusaha, P.P., Myllyharju, J., Cheng, D., Pakkanen, O., Shi, Y., Lee, S.W., Peng, J., and Shi, Y. (2008). Prolyl 4-hydroxylation regulates Argonaute 2 stability. Nature *455*, 421–424.

Quévillon Huberdeau, M., Zeitler, D.M., Hauptmann, J., Bruckmann, A., Fressigné, L., Danner, J., Piquet, S., Strieder, N., Engelmann, J.C., Jannot, G., et al. (2017). Phosphorylation of Argonaute proteins affects mRNA binding and is essential for micro RNA -guided gene silencing in vivo. EMBO J. *36*, 2088–2106.

Quinlan, A.R., and Hall, I.M. (2010). BEDTools: A flexible suite of utilities for comparing genomic features. Bioinformatics *26*, 841–842.

Quintin, S., Mains, P.E., Zinke, A., and Hyman, A.A. (2003). The mbk-2 kinase is required for inactivation of MEI-1/katanin in the one-cell Caenorhabditis elegans embryo. EMBO Rep. *4*, 1175–1181.

Ramírez, F., Dündar, F., Diehl, S., Grüning, B.A., and Manke, T. (2014). DeepTools: A flexible platform for exploring deep-sequencing data. Nucleic Acids Res. *42*, 187–191.

Rappsilber, J., Mann, M., and Ishihama, Y. (2007). Protocol for micro-purification, enrichment, pre-fractionation and storage of peptides for proteomics using StageTips. Nat. Protoc. *2*, 1896–1906.

Rassoulzadegan, M., Grandjean, V., Gounon, P., Vincent, S., Gillot, I., and Cuzin, F. (2006). RNA-mediated non-mendelian inheritance of an epigenetic change in the mouse. Nature *441*, 469–474.

Rechavi, O., and Lev, I. (2017). Principles of Transgenerational Small RNA Inheritance in Caenorhabditis elegans. Curr. Biol. *27*, R720–R730.

Rechavi, O., Houri-Ze'evi, L., Anava, S., Goh, W.S.S., Kerk, S.Y., Hannon, G.J., and Hobert, O. (2014). Starvation-Induced Transgenerational Inheritance of Small RNAs in C. elegans. Cell *158*, 277–287.

Reed, K.J., Svendsen, J.M., Brown, K.C., Montgomery, B.E., Marks, T.N., Vijayasarathy, T., Parker, D.M., Nishimura, E.O., Updike, D.L., and Montgomery, T.A. (2019). Widespread roles for piRNAs and WAGO-class siRNAs in shaping the germline transcriptome of Caenorhabditis elegans. Nucleic Acids Res. 1–17.

Reijns, M.A.M., Alexander, R.D., Spiller, M.P., and Beggs, J.D. (2008). A role for Q/N-rich aggregation-prone regions in P-body localization. J. Cell Sci. *121*, 2463–2472.

Reinke, V., Gil, I.S., Ward, S., and Kazmer, K. (2004). Genome-wide germline-enriched and sex-biased expression profiles in Caenorhabditis elegans. Development *131*, 311–323.

Ren, J., Wen, L., Gao, X., Jin, C., Xue, Y., and Yao, X. (2008). CSS-Palm 2.0: An updated software for palmitoylation sites prediction. Protein Eng. Des. Sel. *21*, 639–644.

Rizzuto, R. (1998). Close Contacts with the Endoplasmic Reticulum as Determinants of Mitochondrial Ca2+ Responses. Science (80-.). *280*, 1763–1766.

Robert, V.J., Mercier, M.G., Bedet, C., Janczarski, S., Merlet, J., Garvis, S., Ciosk, R., and Palladino, F. (2014). The SET-2/SET1 Histone H3K4 Methyltransferase Maintains Pluripotency in the Caenorhabditis elegans Germline. Cell Rep. *9*, 443–450.

Robert, V.P. V, Sijen, T., van Wolfswinkel, J., and Plasterk, R.H.A. (2005). Chromatin and RNAi factors protect the C. elegans germline against repetitive sequences. Genes Dev. *19*, 782–787.

Roberts, T.M. (1983). Crawling caenorhabditis elegans spermatozoa contact the substrate only by their pseudopods and contain 2-nm filaments. Cell Motil. *3*, 333–347.

Roberts, T.M., and Stewart, M. (1997). Nematode sperm: Amoeboid movement without actin. Trends Cell Biol. *7*, 368–373.

Roberts, T.M., Pavalko, F.M., and Ward, S. (1986). Membrane and cytoplasmic proteins are transported in the same organelle complex during nematode spermatogenesis. J. Cell Biol. *102*, 1787–1796.

Rockman, M. V., and Kruglyak, L. (2009). Recombinational Landscape and Population Genomics of Caenorhabditis elegans. PLoS Genet. *5*, e1000419.

Ros, F., and Kunze, R. (2001). Regulation of activator/dissociation transposition by replication and DNA methylation. Genetics *157*, 1723–1733.

Ruby, J.G., Jan, C., Player, C., Axtell, M.J., Lee, W., Nusbaum, C., Ge, H., and Bartel, D.P. (2006). Large-Scale Sequencing Reveals 21U-RNAs and Additional MicroRNAs and Endogenous siRNAs in C. elegans. Cell *127*, 1193–1207.

Rüdel, S., Wang, Y., Lenobel, R., Körner, R., Hsiao, H.H., Urlaub, H., Patel, D., and Meister, G. (2011). Phosphorylation of human Argonaute proteins affects small RNA binding. Nucleic Acids Res. *39*, 2330–2343.

Sabari, B.R., Dall'Agnese, A., Boija, A., Klein, I.A., Coffey, E.L., Shrinivas, K., Abraham, B.J., Hannett, N.M., Zamudio, A. V., Manteiga, J.C., et al. (2018). Coactivator condensation at super-enhancers links phase separation and gene control. Science (80-.). *361*, eaar3958.

Saha, A., Mitchell, J.A., Nishida, Y., Hildreth, J.E., Ariberre, J.A., Gilbert, W. V., and Garfinkel, D.J. (2015). A trans -Dominant Form of Gag Restricts Ty1 Retrotransposition and Mediates Copy Number Control. J. Virol. *89*, 3922–3938.

Sakaguchi, A., Sarkies, P., Simon, M., Doebley, A.-L., Goldstein, L.D., Hedges, A., Ikegami, K., Alvares, S.M., Yang, L., LaRocque, J.R., et al. (2014). Caenorhabditis elegans RSD-2 and RSD-6 promote germ cell immortality by maintaining small interfering RNA populations. Proc. Natl. Acad. Sci. *111*, E4323–E4331.

Sapetschnig, A., Sarkies, P., Lehrbach, N.J., and Miska, E.A. (2015). Tertiary siRNAs Mediate Paramutation in C. elegans. PLoS Genet. *11*, 1–23.

Sasaki, H.M., and Tomari, Y. (2012). The true core of RNA silencing revealed. Nat. Struct. Mol. Biol. *19*, 657–660.

Sato, K., and Sato, M. (2017). Multiple ways to prevent transmission of paternal mitochondrial DNA for maternal inheritance in animals. J. Biochem. *162*, 247–253.

Sato, M., and Sato, K. (2011). Degradation of Paternal Mitochondria by Fertilization-Triggered Autophagy in C. elegans Embryos. Science (80-.). *334*, 1141–1144.

Sato, M., Sato, K., Tomura, K., Kosako, H., and Sato, K. (2018). The autophagy receptor ALLO-1 and the IKKE-1 kinase control clearance of paternal mitochondria in Caenorhabditis elegans. Nat. Cell Biol. *20*, 81–91.

Schedl, T. (1997). Developmental Genetics of the Germ Line. In C. Elegans II, pp. 241–269.

Schuster, A., Skinner, M.K., and Yan, W. (2016). Ancestral vinclozolin exposure alters the epigenetic transgenerational inheritance of sperm small noncoding RNAs. Environ. Epigenetics *2*, dvw001.

Schweinsberg, P.J., and Grant, B.D. (2013). C. elegans gene transformation by microparticle bombardment. In WormBook, pp. 1–10.

Seth, M., Shirayama, M., Gu, W., Ishidate, T., Conte, D., and Mello, C.C. (2013). The C. elegans CSR-1 argonaute pathway counteracts epigenetic silencing to promote germline gene expression. Dev. Cell *27*, 656–663.

Seth, M., Shirayama, M., Tang, W., Shen, E.Z., Tu, S., Lee, H.C., Weng, Z., and Mello, C.C. (2018). The Coding Regions of Germline mRNAs Confer Sensitivity to Argonaute Regulation in C. elegans. Cell Rep. *22*, 2254–2264.

Seydoux, G., and Braun, R.E. (2006). Pathway to Totipotency: Lessons from Germ Cells. Cell *127*, 891–904.

Seydoux, G., and Dunn, M.A. (1997). Transcriptionally repressed germ cells lack a subpopulation of phosphorylated RNA polymerase II in early embryos of Caenorhabditis elegans and Drosophila melanogaster. Development *124*, 2191–2201.

Seydoux, G., Mello, C.C., Pettitt, J., Wood, W.B., Priess, J.R., and Fire, A. (1996). Repression of gene expression in the embryonic germ lineage of C. elegans. Nature *382*, 713–716.

Shakes, D.C., and Ward, S. (1989). Mutations that disrupt the morphogenesis and localization of a sperm-specific organelle in Caenorhabditis elegans. Dev. Biol. *134*, 307–316.

Sharma, U. (2019). Paternal Contributions to Offspring Health: Role of Sperm Small RNAs in Intergenerational Transmission of Epigenetic Information. Front. Cell Dev. Biol. *7*, 1–15.

Sharma, U., Conine, C.C., Shea, J.M., Boskovic, A., Derr, A.G., Bing, X.Y., Belleannee, C., Kucukural, A., Serra, R.W., Sun, F., et al. (2016). Biogenesis and function of tRNA fragments during sperm maturation and fertilization in mammals. Science (80-.). *351*, 391–396.

Shen, E.-Z., Chen, H., Ozturk, A.R., Tu, S., Shirayama, M., Tang, W., Ding, Y.-H., Dai, S.-Y., Weng, Z., and Mello, C.C. (2018). Identification of piRNA Binding Sites Reveals the Argonaute Regulatory Landscape of the C. elegans Germline. Cell *172*, 937-951.e18.

Shen, S., Lin, L., Cai, J.J., Jiang, P., Kenkel, E.J., Stroik, M.R., Sato, S., Davidson, B.L., and Xing, Y. (2011). Widespread establishment and regulatory impact of Alu exons in human genes. Proc. Natl. Acad. Sci. *108*, 2837–2842.

Sheth, U., Pitt, J., Dennis, S., and Priess, J.R. (2010). Perinuclear P granules are the principal sites of mRNA export in adult C. elegans germ cells. Development *137*, 1305–1314.

Sheu-Gruttadauria, J., and MacRae, I.J. (2017). Structural Foundations of RNA Silencing by Argonaute. J. Mol. Biol. *429*, 2619–2639.

Sheu-Gruttadauria, J., and MacRae, I.J. (2018). Phase Transitions in the Assembly and Function of Human miRISC. Cell *173*, 946-957.e16.

Shevchenko, A., Tomas, H., Havliš, J., Olsen, J. V., and Mann, M. (2007). In-gel digestion for mass spectrometric characterization of proteins and proteomes. Nat. Protoc. *1*, 2856–2860.

Shin, Y., and Brangwynne, C.P. (2017). Liquid phase condensation in cell physiology and disease. Science (80-.). *357*.

Shirayama, M., Seth, M., Lee, H.C., Gu, W., Ishidate, T., Conte, D., and Mello, C.C. (2012). PiRNAs initiate an epigenetic memory of nonself RNA in the C. elegans germline. Cell *150*, 65–77.

Shirayama, M., Stanney, W., Gu, W., Seth, M., and Mello, C.C. (2014). The Vasa homolog RDE-12 engages target mRNA and multiple argonaute proteins to promote RNAi in C. elegans. Curr. Biol. *24*, 845–851.

Shoji, M., Tanaka, T., Hosokawa, M., Reuter, M., Stark, A., Kato, Y., Kondoh, G., Okawa, K., Chujo, T., Suzuki, T., et al. (2009). The TDRD9-MIWI2 Complex Is Essential for piRNA-Mediated Retrotransposon Silencing in the Mouse Male Germline. Dev. Cell *17*, 775–787.

Shukla, A., Yan, J., Pagano, D.J., Dodson, A.E., Fei, Y., Gorham, J., Seidman, J.G., Wickens, M., and Kennedy, S. (2020). poly(UG)-tailed RNAs in genome protection and epigenetic inheritance. Nature *582*, 283–288.

Sijen, T., Fleenor, J., Simmer, F., Thijssen, K.L., Parrish, S., Timmons, L., Plasterk, R.H.A., and Fire, A. (2001). On the Role of RNA Amplification in dsRNA-Triggered Gene Silencing. Cell *107*, 465–476.

Sijen, T., Steiner, F.A., Thijssen, K.L., and Plasterk, R.H.A. (2007). Secondary siRNAs result from unprimed RNA synthesis and form a distinct class. Science (80-.). *315*, 244–247.

Simon, B., Kirkpatrick, J.P., Eckhardt, S., Reuter, M., Rocha, E.A., Andrade-Navarro, M.A., Sehr, P., Pillai, R.S., and Carlomagno, T. (2011). Recognition of 2′-o-methylated 3′-end of piRNA by the PAZ domain of a Piwi protein. Structure *19*, 172–180.

Simon, M., Sarkies, P., Ikegami, K., Doebley, A.-L., Goldstein, L.D., Mitchell, J., Sakaguchi, A., Miska, E.A., and Ahmed, S. (2014). Reduced Insulin/IGF-1 Signaling Restores Germ Cell Immortality to Caenorhabditis elegans Piwi Mutants. Cell Rep. *7*, 762–773.

Skinner, M.K., Ben Maamar, M., Sadler-Riggleman, I., Beck, D., Nilsson, E., McBirney, M., Klukovich, R., Xie, Y., Tang, C., and Yan, W. (2018). Alterations in sperm DNA methylation, non-coding RNA and histone retention associate with DDT-induced epigenetic transgenerational inheritance of disease. Epigenetics Chromatin *11*, 8.

Skvortsova, K., Iovino, N., and Bogdanović, O. (2018). Functions and mechanisms of epigenetic inheritance in animals. Nat. Rev. Mol. Cell Biol. *19*, 774–790.

Smardon, A., Spoerke, J.M., Stacey, S.C., Klein, M.E., Mackin, N., and Maine, E.M. (2000). EGO-1 is related to RNA-directed RNA polymerase and functions in germ-line development and RNA interference in C. elegans. Curr. Biol. *10*, 169–178.

Smibert, P., Yang, J.S., Azzam, G., Liu, J.L., and Lai, E.C. (2013). Homeostatic control of Argonaute stability by microRNA availability. Nat. Struct. Mol. Biol. *20*, 789–795.

Smith, H.E., and Ward, S. (1998). Identification of Protein-Protein interactions of the major sperm protein (MSP) of Caenorhabditis elegans. J. Mol. Biol. *279*, 605–619.

Song, J.-J., Smith, S.K., Hannon, G.J., and Joshua-Tor, L. (2004). Crystal Structure of Argonaute and Its Implications for RISC Slicer Activity. Science (80-.). *305*, 1434–1437.

Song, J., Song, J., Mo, B., and Chen, X. (2015). Uridylation and adenylation of RNAs. Sci. China Life Sci. *58*, 1057–1066.

Sonnhammer, E.L.L., and Östlund, G. (2015). InParanoid 8: orthology analysis between 273 proteomes, mostly eukaryotic. Nucleic Acids Res. *43*, D234–D239.

Spencer, W.C., Zeller, G., Watson, J.D., Henz, S.R., Watkins, K.L., McWhirter, R.D., Petersen, S., Sreedharan, V.T., Widmer, C., Jo, J., et al. (2011). A spatial and temporal map of C. elegans gene expression. Genome Res. *21*, 325–341.

Spieth, J., Brooke, G., Kuersten, S., Lea, K., and Blumenthal, T. (1993). Operons in C. elegans: Polycistronic mRNA precursors are processed by trans-splicing of SL2 to downstream coding regions. Cell *73*, 521–532.

Spike, C.A., Bader, J., Reinke, V., and Strome, S. (2008). DEPS-1 promotes P-granule assembly and RNA interference in C. elegans germ cells. Development *135*, 983–993.

Spracklin, G., Fields, B., Wan, G., Becker, D., Wallig, A., Shukla, A., and Kennedy, S. (2017). The RNAi Inheritance Machinery of Caenorhabditis elegans. Genetics *206*, 1403–1416.

Steiner, F.A., Okihara, K.L., Hoogstrate, S.W., Sijen, T., and Ketting, R.F. (2009). RDE-1 slicer activity is required only for passenger-strand cleavage during RNAi in Caenorhabditis elegans. Nat. Struct. Mol. Biol. *16*, 207–211.

Stoeckius, M., Grün, D., and Rajewsky, N. (2014). Paternal RNA contributions in the Caenorhabditis elegans zygote. EMBO J. *33*, 1740–1750.

Stogios, P.J., and Privé, G.G. (2004). The BACK domain in BTB-kelch proteins. Trends Biochem. Sci. *29*, 634–637.

Strome, S., and Updike, D. (2015). Specifying and protecting germ cell fate. Nat. Rev. Mol. Cell Biol. *16*, 406–416.

Sulston, J.E., Schierenberg, E., White, J.G., and Thomson, J.N. (1983). The embryonic cell lineage of the nematode Caenorhabditis elegans. Dev. Biol. *100*, 64–119.

Sultana, T., Zamborlini, A., Cristofari, G., and Lesage, P. (2017). Integration site selection by retroviruses and transposable elements in eukaryotes. Nat. Rev. Genet. *18*, 292–308.

Suzuki, Y., Minami, M., Suzuki, M., Abe, K., Zenno, S., Tsujimoto, M., Matsumoto, K., and Minami, Y. (2009). The Hsp90 inhibitor geldanamycin abrogates colocalization of eIF4E and eIF4E-transporter into stress granules and association of eIF4E with eIF4G. J. Biol. Chem. *284*, 35597–35604.

Svendsen, J.M., Reed, K.J., Vijayasarathy, T., Montgomery, B.E., Tucci, R.M., Brown, K.C., Marks, T.N., Nguyen, D.A.H., Phillips, C.M., and Montgomery, T.A. (2019). henn-1/HEN1 Promotes Germline Immortality in Caenorhabditis elegans. Cell Rep. *29*, 3187-3199.e4.

Swarts, D.C., Makarova, K., Wang, Y., Nakanishi, K., Ketting, R.F., Koonin, E. V., Patel, D.J., and Van Der Oost, J. (2014a). The evolutionary journey of Argonaute proteins. Nat. Struct. Mol. Biol. *21*, 743–753.

Swarts, D.C., Jore, M.M., Westra, E.R., Zhu, Y., Janssen, J.H., Snijders, A.P., Wang, Y., Patel, D.J., Berenguer, J., Brouns, S.J.J., et al. (2014b). DNA-guided DNA interference by a prokaryotic Argonaute. Nature *507*, 258–261.

Tabaczar, S., Czogalla, A., Podkalicka, J., Biernatowska, A., and Sikorski, A.F. (2017). Protein palmitoylation: Palmitoyltransferases and their specificity. Exp. Biol. Med. *242*, 1150–1157.

Tabara, H., Sarkissian, M., Kelly, W.G., Fleenor, J., Grishok, A., Timmons, L., Fire, A., and Mello, C.C. (1999). The rde-1 Gene, RNA Interference, and Transposon Silencing in C. elegans. Cell *99*, 123–132.

Tabara, H., Yigit, E., Siomi, H., and Mello, C.C. (2002). The dsRNA Binding Protein RDE-4 Interacts with RDE-1, DCR-1, and a DExH-Box Helicase to Direct RNAi in C. elegans. Cell *109*, 861–871.

Tabuchi, T.M., Rechtsteiner, A., Jeffers, T.E., Egelhofer, T.A., Murphy, C.T., and Strome, S. (2018). Caenorhabditis elegans sperm carry a histone-based epigenetic memory of both spermatogenesis and oogenesis. Nat. Commun. *9*, 1–11.

Tahbaz, N., Carmichael, J.B., and Hobman, T.C. (2001). GERp95 Belongs to a Family of Signal-transducing Proteins and Requires Hsp90 Activity for Stability and Golgi Localization. J. Biol. Chem. *276*, 43294–43299.

Takenaga, M., Hatano, M., Takamori, M., Yamashita, Y., Okada, S., Kuroda, Y., and Tokuhisa, T. (2003). Bcl6-dependent transcriptional repression by BAZF. Biochem. Biophys. Res. Commun. *303*, 600–608.

Tang, W., Tu, S., Lee, H.C., Weng, Z., and Mello, C.C. (2016). The RNase PARN-1 Trims piRNA 3′ Ends to Promote Transcriptome Surveillance in C. elegans. Cell *164*, 974–984.

Tang, W., Seth, M., Tu, S., Shen, E.Z., Li, Q., Shirayama, M., Weng, Z., and Mello, C.C. (2018). A Sex Chromosome piRNA Promotes Robust Dosage Compensation and Sex Determination in C. elegans. Dev. Cell *44*, 762-770.e3.

The C. elegans Sequencing Consortium (1998). Genome sequence of the nematode C. elegans: A platform for investigating biology. Science (80-.). *282*, 2012–2018.

Thivierge, C., Makil, N., Flamand, M., Vasale, J.J., Mello, C.C., Wohlschlegel, J., Conte, D., and Duchaine, T.F. (2012). Tudor domain ERI-5 tethers an RNA-dependent RNA polymerase to DCR-1 to potentiate endo-RNAi. Nat. Struct. Mol. Biol. *19*, 90–97.

Thybert, D., Roller, M., Navarro, F.C.P., Fiddes, I., Streeter, I., Feig, C., Martin-Galvez, D., Kolmogorov, M., Janoušek, V., Akanni, W., et al. (2018). Repeat associated mechanisms of genome evolution and function revealed by the Mus caroli and Mus pahari genomes. Genome Res. *28*, 448–459.

Tijsterman, M., Okihara, K.L., Thijssen, K., and Plasterk, R.H.A. (2002). PPW-1, a PAZ/PIWI protein required for efficient germline RNAi, is defective in a natural isolate of C. elegans. Curr. Biol. *12*, 1535–1540.

Till, S., Lejeune, E., Thermann, R., Bortfeld, M., Hothorn, M., Enderle, D., Heinrich, C., Hentze, M.W., and Ladurner, A.G. (2007). A conserved motif in Argonaute-interacting proteins mediates functional interactions through the Argonaute PIWI domain. Nat. Struct. Mol. Biol. *14*, 897–903.

Tomatis, V.M., Trenchi, A., Gomez, G.A., and Daniotti, J.L. (2010). Acyl-Protein Thioesterase 2 Catalizes the Deacylation of Peripheral Membrane-Associated GAP-43. PLoS One *5*, e15045.

Tsai, H.Y., Chen, C.C.G., Conte, D., Moresco, J.J., Chaves, D.A., Mitani, S., Yates, J.R., Tsai, M.D., and Mello, C.C. (2015). A ribonuclease coordinates siRNA amplification and mRNA Cleavage during NAi. Cell *160*, 407–419.

Turk, B. (2006). Targeting proteases: successes, failures and future prospects. Nat. Rev. Drug Discov. *5*, 785–799.

Tyc, K.M., Nabih, A., Wu, M.Z., Wedeles, C.J., Sobotka, J.A., and Claycomb, J.M. (2017). The Conserved Intron Binding Protein EMB-4 Plays Differential Roles in Germline Small RNA Pathways of C. elegans. Dev. Cell *42*, 256-270.e6.

Tyebji, S., Hannan, A.J., and Tonkin, C.J. (2020). Pathogenic Infection in Male Mice Changes Sperm Small RNA Profiles and Transgenerationally Alters Offspring Behavior. Cell Rep. *31*, 107573.

Uebel, C.J., Anderson, D.C., Mandarino, L.M., Manage, K.I., Aynaszyan, S., and Phillips, C.M. (2018). Distinct regions of the intrinsically disordered protein MUT-16 mediate assembly of a small RNA amplification complex and promote phase separation of Mutator foci. PLoS Genet. *14*, 1–22.

Untergasser, A., Cutcutache, I., Koressaar, T., Ye, J., Faircloth, B.C., Remm, M., and Rozen, S.G. (2012). Primer3—new capabilities and interfaces. Nucleic Acids Res. *40*, e115–e115.

Updike, D., and Strome, S. (2010). P granule assembly and function in Caenorhabditis elegans germ cells. J. Androl. *31*, 53–60.

Updike, D.L., Knutson, A.K., Egelhofer, T.A., Campbell, A.C., and Strome, S. (2014). Germ-Granule Components Prevent Somatic Development in the C. elegans Germline. Curr. Biol. *24*, 970–975.

Vacic, V., Uversky, V.N., Dunker, A.K., and Lonardi, S. (2007). Composition Profiler: a tool for discovery and visualization of amino acid composition differences. BMC Bioinformatics *8*, 211.

Varkey, J.P., Jansma, P.L., Minniti, A.N., and Ward, S. (1993). The Caenorhabditis elegans spe-6 gene is required for major sperm protein assembly and shows second site non-complementation with an unlinked deficiency. Genetics *133*, 79–86.

Vasale, J.J., Gu, W., Thivierge, C., Batista, P.J., Claycomb, J.M., Youngman, E.M., Duchaine, T.F., Mello, C.C., and Conte, D. (2010). Sequential rounds of RNA-dependent RNA transcription drive endogenous small-RNA biogenesis in the ERGO-1/Argonaute pathway. Proc. Natl. Acad. Sci. *107*, 3582–3587.

Vastenhouw, N.L., Fischer, S.E.J., Robert, V.J.P., Thijssen, K.L., Fraser, A.G., Kamath, R.S., Ahringer, J., and Plasterk, R.H.A. (2003). A genome-wide screen identifies 27 genes involved in transposon silencing in C. elegans. Curr. Biol. *13*, 1311–1316.

Voronina, E., Seydoux, G., Sassone-Corsi, P., and Nagamori, I. (2011). RNA granules in germ cells. Cold Spring Harb. Perspect. Biol. *3*.

Wan, G., Fields, B.D., Spracklin, G., Shukla, A., Phillips, C.M., and Kennedy, S. (2018). Spatiotemporal regulation of liquid-like condensates in epigenetic inheritance. Nature *557*, 679–683.

Wang, G., and Reinke, V. (2008). A C. elegans Piwi, PRG-1, Regulates 21U-RNAs during Spermatogenesis. Curr. Biol. *18*, 861–867.

Wang, J.T., and Seydoux, G. (2014). P granules. Curr. Biol. *24*, 637–638.

Wang, Lv, Guo, and Yuan (2020). Mitochondria Associated Germinal Structures in Spermatogenesis: piRNA Pathway Regulation and Beyond. Cells *9*, 399.

Wang, J., Choi, J.-M., Holehouse, A.S., Lee, H.O., Zhang, X., Jahnel, M., Maharana, S., Lemaitre, R., Pozniakovsky, A., Drechsel, D., et al. (2018a). A Molecular Grammar Governing the Driving Forces for Phase Separation of Prion-like RNA Binding Proteins. Cell *174*, 688-699.e16.

Wang, J.T., Smith, J., Chen, B.-C., Schmidt, H., Rasoloson, D., Paix, A., Lambrus, B.G., Calidas, D., Betzig, E., and Seydoux, G. (2014). Regulation of RNA granule dynamics by phosphorylation of serine-rich, intrinsically disordered proteins in C. elegans. Elife *3*, 1–23.

Wang, X., Wen, Y., Dong, J., Cao, C., and Yuan, S. (2018b). Systematic In-Depth Proteomic Analysis of Mitochondria-Associated Endoplasmic Reticulum Membranes in Mouse and Human Testes. Proteomics *18*, 1700478.

Ward, J.D. (2014). Rapid and precise engineering of the caenorhabditis elegans genome with lethal mutation co-conversion and inactivation of NHEJ repair. Genetics *199*, 363–377.

Ward, S., and Carrel, J.S. (1979). Fertilization and sperm competition in the nematodeCaenorhabditis elegans. Dev. Biol. *73*, 304–321.

Ward, S., and Klass, M. (1982). The location of the major protein in Caenorhabditis elegans sperm and spermatocytes. Dev. Biol. *92*, 203–208.

Ward, S., Argon, Y., and Nelson, G.A. (1981). Sperm morphogenesis in wild-type and fertilization-defective mutants of Caenorhabditis elegans. J. Cell Biol. *91*, 26–44.

Washington, N.L., and Ward, S. (2006). FER-1 regulates Ca2+-mediated membrane fusion during C. elegans spermatogenesis. J. Cell Sci. *119*, 2552–2562.

Watanabe, T., Chuma, S., Yamamoto, Y., Kuramochi-Miyagawa, S., Totoki, Y., Toyoda, A., Hoki, Y., Fujiyama, A., Shibata, T., Sado, T., et al. (2011). MITOPLD Is a Mitochondrial Protein Essential for Nuage Formation and piRNA Biogenesis in the Mouse Germline. Dev. Cell *20*, 364–375.

Waterston, R., and Sulston, J. (1995). The genome of Caenorhabditis elegans. Proc. Natl. Acad. Sci. *92*, 10836–10840.

Wedeles, C., Wu, M., and Claycomb, J. (2014). Silent no more: Endogenous small RNA pathways promote gene expression. Worm *3*, e28641.

Wedeles, C.J., Wu, M.Z., and Claycomb, J.M. (2013). Protection of germline gene expression by the C. elegans argonaute CSR-1. Dev. Cell *27*, 664–671.

Wegmann, S., Eftekharzadeh, B., Tepper, K., Zoltowska, K.M., Bennett, R.E., Dujardin, S., Laskowski, P.R., MacKenzie, D., Kamath, T., Commins, C., et al. (2018). Tau protein liquid–liquid phase separation can initiate tau aggregation. EMBO J. *37*, 1–21.

Wei, Y., Chiang, W., Sumpter, R., Mishra, P., and Levine, B. (2017). Prohibitin 2 Is an Inner Mitochondrial Membrane Mitophagy Receptor. Cell *168*, 224–238.

Weick, E.-M., Sarkies, P., Silva, N., Chen, R.A., Moss, S.M.M., Cording, A.C., Ahringer, J., Martinez-Perez, E., and Miska, E.A. (2014). PRDE-1 is a nuclear factor essential for the biogenesis of Ruby motif-dependent piRNAs in C. elegans. Genes Dev. *28*, 783–796.

Weiser, N.E., and Kim, J.K. (2019). Multigenerational Regulation of the Caenorhabditis elegans Chromatin Landscape by Germline Small RNAs. Annu. Rev. Genet. *53*, 289–311.

Weiser, N.E., Yang, D.X., Feng, S., Kalinava, N., Brown, K.C., Khanikar, J., Freeberg, M.A., Snyder, M.J., Csankovszki, G., Chan, R.C., et al. (2017). MORC-1 Integrates Nuclear RNAi and Transgenerational Chromatin Architecture to Promote Germline Immortality. Dev. Cell *41*, 408-423.e7.

Welker, N.C., Maity, T.S., Ye, X., Aruscavage, P.J., Krauchuk, A.A., Liu, Q., and Bass, B.L. (2011). Dicer's Helicase Domain Discriminates dsRNA Termini to Promote an Altered Reaction Mode. Mol. Cell *41*, 589–599.

Weng, C., Kosalka, J., Berkyurek, A.C., Stempor, P., Feng, X., Mao, H., Zeng, C., Li, W.-J., Yan, Y.-H., Dong, M.-Q., et al. (2019). The USTC co-opts an ancient machinery to drive piRNA transcription in C. elegans. Genes Dev. *33*, 90–102.

Wicker, T., Sabot, F., Hua-Van, A., Bennetzen, J.L., Capy, P., Chalhoub, B., Flavell, A., Leroy, P., Morgante, M., Panaud, O., et al. (2007). A unified classification system for eukaryotic transposable elements. Nat. Rev. Genet. *8*, 973–982.

Wippich, F., Bodenmiller, B., Trajkovska, M.G., Wanka, S., Aebersold, R., and Pelkmans, L. (2013). Dual Specificity Kinase DYRK3 Couples Stress Granule Condensation/Dissolution to mTORC1 Signaling. Cell *152*, 791–805.

Wolf, N., Hirsh, D., and McIntosh, J.R. (1978). Spermatogenesis in males of the free-living nematode, Caenorhabditis elegans. J. Ultrasructure Res. *63*, 155–169.

van Wolfswinkel, J.C., Claycomb, J.M., Batista, P.J., Mello, C.C., Berezikov, E., and Ketting, R.F. (2009). CDE-1 Affects Chromosome Segregation through Uridylation of CSR-1-Bound siRNAs. Cell *139*, 135–148.

Wolke, U., Jezuit, E.A., and Priess, J.R. (2007). Actin-dependent cytoplasmic streaming in C. elegans oogenesis. Development *134*, 2227–2236.

Woodhouse, R.M., and Ashe, A. (2020). How do histone modifications contribute to transgenerational epigenetic inheritance in C. elegans? Biochem. Soc. Trans. 1–16.

Wu, X., Cai, Q., Feng, Z., and Zhang, M. (2020). Liquid-Liquid Phase Separation in Neuronal Development and Synaptic Signaling. Dev. Cell 1–12.

Xiao, Y., Bedet, C., Robert, V.J.P., Simonet, T., Dunkelbarger, S., Rakotomalala, C., Soete, G., Korswagen, H.C., Strome, S., and Palladino, F. (2011). Caenorhabditis elegans chromatin-associated proteins SET-2 and ASH-2 are differentially required for histone H3 Lys 4 methylation in embryos and adult germ cells. Proc. Natl. Acad. Sci. *108*, 8305–8310.

Xie, Y., Zheng, Y., Li, H., Luo, X., He, Z., Cao, S., Shi, Y., Zhao, Q., Xue, Y., Zuo, Z., et al. (2016). GPS-Lipid: a robust tool for the prediction of multiple lipid modification sites. Sci. Rep. *6*, 28249.

Xu, X.-Z.S., and Sternberg, P.W. (2003). A C. elegans Sperm TRP Protein Required for Sperm-Egg Interactions during Fertilization. Cell *114*, 285–297.

Xu, F., Guang, S., and Feng, X. (2018a). Distinct nuclear and cytoplasmic machineries cooperatively promote the inheritance of RNAi in Caenorhabditis elegans. Biol. Cell *110*, 217–224.

Xu, F., Feng, X., Chen, X., Weng, C., Yan, Q., Xu, T., Hong, M., and Guang, S. (2018b). A Cytoplasmic Argonaute Protein Promotes the Inheritance of RNAi. Cell Rep. *23*, 2482–2494.

Yang, H., Zhang, Y., Vallandingham, J., Li, H., Florens, L., and Mak, H.Y. (2012). The RDE-10/RDE-11 complex triggers RNAi-induced mRNA degradation by association with target mRNA in C. elegans. Genes Dev. *26*, 846–856.

Yang, H., Vallandingham, J., Shiu, P., Li, H., Hunter, C.P., and Mak, H.Y. (2014). The DEAD box helicase RDE-12 promotes amplification of RNAi in cytoplasmic foci in C. Elegans. Curr. Biol. *24*, 832–838.

Yang, P., Wang, Y., and Macfarlan, T.S. (2017). The Role of KRAB-ZFPs in Transposable Element Repression and Mammalian Evolution. Trends Genet. *33*, 871–881.

Yates, A.D., Achuthan, P., Akanni, W., Allen, J., Allen, J., Alvarez-Jarreta, J., Amode, M.R., Armean, I.M., Azov, A.G., Bennett, R., et al. (2019). Ensembl 2020. Nucleic Acids Res. *48*, D682–D688.

Yeh, D.C., Duncan, J.A., Yamashita, S., and Michel, T. (1999). Depalmitoylation of endothelial nitric-oxide synthase by acyl-protein thioesterase 1 is potentiated by Ca2+-calmodulin. J. Biol. Chem. *274*, 33148–33154.

Yigit, E., Batista, P.J., Bei, Y., Pang, K.M., Chen, C.-C.G., Tolia, N.H., Joshua-Tor, L., Mitani, S., Simard, M.J., and Mello, C.C. (2006). Analysis of the C. elegans Argonaute Family Reveals that Distinct Argonautes Act Sequentially during RNAi. Cell *127*, 747–757.

Yushin, V. V., and Malakhov, V. V. (2014). The origin of nematode sperm: Progenesis at the cellular level. Russ. J. Mar. Biol. *40*, 71–81.

Zeng, Y., Sankala, H., Zhang, X., and Graves, P.R. (2008). Phosphorylation of Argonaute 2 at serine-387 facilitates its localization to processing bodies. Biochem. J. *413*, 429–436.

Zhang, C., Montgomery, T.A., Gabel, H.W., Fischer, S.E.J., Phillips, C.M., Fahlgren, N., Sullivan, C.M., Carrington, J.C., and Ruvkun, G. (2011). mut-16 and other mutator class genes modulate 22G and 26G siRNA pathways in Caenorhabditis elegans. Proc. Natl. Acad. Sci. U. S. A. *108*, 1201–1208.

Zhang, C., Montgomery, T.A., Fischer, S.E.J., Garcia, S.M.D.A., Riedel, C.G., Fahlgren, N., Sullivan, C.M., Carrington, J.C., and Ruvkun, G. (2012). The Caenorhabditis elegans RDE-10/RDE-11 Complex Regulates RNAi by Promoting Secondary siRNA Amplification. Curr. Biol. *22*, 881–890.

Zhang, D., Tu, S., Stubna, M., Wu, W.S., Huang, W.C., Weng, Z., and Lee, H.C. (2018). The piRNA targeting rules and the resistance to piRNA silencing in endogenous genes. Science (80-.). *359*, 587–592.

Zhang, J., Wang, Q., Wang, M., Jiang, M., Wang, Y., Sun, Y., Wang, J., Xie, T., Tang, C., Tang, N., et al. (2016). GASZ and mitofusin-mediated mitochondrial functions are crucial for spermatogenesis . EMBO Rep. *17*, 220–234.

Zhao, Y.G., and Zhang, H. (2020). Phase Separation in Membrane Biology: The Interplay between Membrane-Bound Organelles and Membraneless Condensates. Dev. Cell 1–15.

Zhou, L., Canagarajah, B., Zhao, Y., Baibakov, B., Tokuhiro, K., Maric, D., and Dean, J. (2017). BTBD18 Regulates a Subset of piRNA-Generating Loci through Transcription Elongation in Mice. Dev. Cell *40*, 453-466.e5.

Zhou, Q., Li, H., Li, H., Nakagawa, A., Lin, J.L.J., Lee, E.-S., Harry, B.L., Skeen-Gaar, R.R., Suehiro, Y., William, D., et al. (2016). Mitochondrial endonuclease G mediates breakdown of paternal mitochondria upon fertilization. Science (80-.). *353*, 394–399.

Zhou, X., Xu, F., Mao, H., Ji, J., Yin, M., Feng, X., and Guang, S. (2014). Nuclear RNAi Contributes to the Silencing of Off-Target Genes and Repetitive Sequences in Caenorhabditis elegans. Genetics *197*, 121–132.

Zhu, G.D., and L'Hernault, S.W. (2003). The Caenorhabditis elegans spe-39 gene is required for intracellular membrane reorganization during spermatogenesis. Genetics *165*, 145–157.

Zhu, G., Salazar, G., Zlatic, S.A., Fiza, B., Doucette, M.M., Heilman, C.J., Levey, A.I., Faundez, V., and L'Hernault, S.W. (2009). SPE-39 Family Proteins Interact with the HOPS Complex and Function in Lysosomal Delivery. Mol. Biol. Cell *20*, 1223–1240.

Zimmermann, L., Stephens, A., Nam, S.-Z., Rau, D., Kübler, J., Lozajic, M., Gabler, F., Söding, J., Lupas, A.N., and Alva, V. (2018). A Completely Reimplemented MPI Bioinformatics Toolkit with a New HHpred Server at its Core. J. Mol. Biol. *430*, 2237–2243.

Zorio, D.A.R., Cheng, N.N., Blumenthal, T., and Spieth, J. (1994). Operons as a common form of chromosomal organization in C. elegans. Nature *372*, 270–272.